THE DIAGENESIS AND PALAEOMAGNETISM OF PERMIAN AND TRIASSIC SEDIMENTS FROM CENTRAL SPAIN.

VOL I

AMANDA ROSE TURNER

Doctor of Philosophy

THE UNIVERSITY OF ASTON IN BIRMINGHAM

Cctober 1988

The University of Aston in Birmingham

THE DIAGENESIS AND PALAEOMAGNETISM OF PERMIAN AND TRIASSIC SEDIMENTS FROM CENTRAL SPAIN.

Amanda Rose Turner
Doctor of Philosophy
1988

SUMMARY OF THESIS

Detailed diagenetic and palaeomagnetic studies have been made of Permian and Triassic rocks from the Iberian Cordillera, Spain. Five stratigraphical units comprising the Autunian, Saxonian, Buntsandstein, Muschelkalk, and Keuper have been studied in a number of sections which have been well documented sedimentologically. Autunian rocks have a characteristic remanence which is exclusively reversed and corresponds to the Kiaman Interval. The pole position identified is consistent with previous studies, which indicate the rotation of Iberia in post-Triassic times. The Saxonian facies show complex multicomponent magnetizations; no polarity zonation can be resolved. The Buntsandstein is remarkable in that much of it is remagnetised in a direction similar to the present-day local geomagnetic field direction. The secondary remanence is carried by fine-grained haematite which has been formed as a result of carbonate dissolution associated with structural inversion of the Iberian Cordillera. Dating of diagenetic events associated with this remagnetization is also possible. Fragments of primary remanence are preserved in some fine-grained lithologies of the Buntsandstein. These indicate that normal and reversed zones of magnetization were originally present. The magnetization of the Muschelkalk and Keuper carbonates is also complex; secondary components similar to those of the Buntsandstein are present but there is evidence that primary components were predominantly normal during Karnian times.

DIAGENESIS, PALAEOMAGNETISM, RED BEDS, PERMO-TRIASSIC, SPAIN.

Dedicated to My Parents

ACKNOWLEDGEMENTS

I wish to thank my supervisor, Dr. Peter Turner who originally suggested and arranged the project, for his continuous encouragement, advice, constructive criticism and enthusiasm throughout the project.

The research was funded by an award from the University of Aston in Birmingham, for which I am very grateful.

For work carried out in Spain I wish to thank Dr's Amparo Ramos, Alfonso Sopena, Alfredo Arche and Martha Perez-Alucea for their helpful comments and suggestions whilst in the field.

I also wish to thank the research students and the staff of the Geology Department at Aston who did much to help me during the course of my research. Special thanks is also given to Dr. Adrian Hartley and Dr. Geraldine Lennon, with whom I had many constructive conversations.

I am grateful to all the members of the drafting department at Mobil North Sea Limited for their excellent work in the preparation of the plates and diagrams for this thesis.

Thanks are also given to many colleagues and friends at Mobil, for their help and encouragement throughout the writing of the project, especially Ian Mitchell, who read parts of the manuscript and made many constructive criticisms.

I wish to thank Marjorie Bruce, Amanda Humble and Vivienne Moriarty for their much appreciated help in the preparation and typing of this manuscript.

I am also very grateful to my family for all the support they have given me during the course of the research. For his, continuous encouragement, understanding and patience I wish to express a very special thank you to Michael Chapman.

Finally I wish to thank Richard Hodgkinson and Jan Lasocki for devoting so much time and effort in helping me with the completion of this thesis.

LIST OF CONTENTS
VOLUME I

Page No

VOLUME II

LIST OF TABLES

LIST OF FIGURES

LIST OF PLATES

CHAPTER ONE

INTRODUCTION

1.1 OBJECTIVES

The principal aims of the current research are as follows:

- To present a critical review of the current literature available on topics covered by this research.

- To describe the sedimentology, detrital mineralogy, textural characteristics and diagenetic mineralogy of Permo-Triassic sediments from Central Spain and thus deduce their diagenetic history.

- To identify individual components of magnetization present in the sediments, using thermal, alternating field and chemical demagnetization techniques and to compare these with previously described results from Iberia and 'Stable Europe'.

- To establish a magnetostratigraphy for the Permian and Triassic in this part of Central Spain.

- To identify any relationships which exist between diagenesis and palaeomagnetism in the sediments studied.

1.2 LAYOUT OF THESIS

The thesis is divided into eight chapters. Chapter One, the introduction describes the principal objectives of the research and the methods used to achieve these objectives. It also contains a literature review which embraces topics relating to this research. A brief summary of the geological history of the area is included and the chapter concludes with a description of the most common magnetic minerals.

In the final chapter, the main conclusions of the research are presented and areas of interest for future research suggested.

The remaining six chapters, two to seven, contain the results of the research and are set out in chronological order i.e. from the Lower Permian (Chapter Two) to the Upper Triassic, Muschelkalk and Keuper facies (Chapter Seven).

Each of these chapters follows a similar pattern; a brief introduction is followed by a description of the stratigraphy and sedimentology of the deposits. A section on diagenesis follows, this includes a detailed account of the magnetic mineralogy. In the second half of each chapter the palaeomagnetic results are presented. Natural remanent magnetization (N.R.M.), isothermal remanent magnetization (I.R.M.) and demagnetization results are described in turn.

Every chapter concludes with a discussion of any relationships identified between diagenesis and palaeomagnetism.

1.3 METHODS AND TECHNIQUES

1.3.1 Introduction

A variety of sedimentological and palaeomagnetic techniques have been employed, both in the field and in the laboratory, during the course of this research. Various statistical and presentation techniques have also been used to express and illustrate the results attained in the best manner.

The principal methods and techniques used are described in the following section. For the purpose of simplicity and brevity, the reader is directed to accounts in the literature for a more comprehensive description of a particular technique used. Appendix I, contains a table showing the techniques used on each of the samples.

1.3.2 Field Techniques

A total of 156 hand samples of approximately 20x10x10cm were collected during two field seasons (July 1982 and May/June 1984) from Permo-Triassic rocks of the Iberian Cordillera in Central Spain (Fig. 1.1).

The samples were orientated using both sun compass (Appendix II) and magnetic compass. The exact stratigraphic horizon from which the samples were taken was noted using detailed sedimentological logs drawn up by Ramos (1979), Sopena (1979) and Perez-Arlucea (1985).


Aston University
Illustration removed for copyright restrictions

The Permo-Triassic sediments of this area are predominantly clastic (although carbonates dominate in the Upper Triassic) and range in grain size from mudstones to conglomerates. For consistency of sample and for the purpose of attaining detailed diagenetic descriptions, sandstones and coarse siltstones were selected in preference to conglomerates or mudstones.

In the carbonate rich Upper Triassic, samples were selected, whenever possible, at regular depth intervals.

1.3.3 Laboratory Techniques

A minimum of six, 2.2cm long by 2.5cm diameter specimen cores were prepared for palaeomagnetic measurements. The remainder of the hand sample was used for the preparation of thin and polished sections and for scanning electron microscope (S.E.M.) and X-ray diffraction (X.R.D.) studies.

1.3.3.1 Sedimentological Techniques

(a) Thin section transmitted light analysis: Thin sections (7.5 cm long by 5 cm wide by 30 μm thick) were made for the majority of samples. Impregnation with blue epoxy resin was carried out, in order to identify porosity and to prevent friable sands from disintegrating. In addition, all thin sections were stained using a combined stain (Alizarin Red S and Potassium ferricyanide) (Appendix III) to test for carbonate minerals. The mineralogy and diagenesis were then described and each sandstone sample was assigned a name using Dott's (1964) rock classification system (Appendix IV). Point counting of each suitable thin section was also performed, with a minimum of 500 points counted for each sample.

(b) Reflected light analysis: Polished blocks and polished thin sections were made for many of the samples. Examination under reflected light microscope enabled detailed descriptions of the magnetic mineralogy. Best results were achieved using a x40 lens with immersion oil.

(c) Scanning Electron Microscope (S.E.M.) analysis: An S.E.M. equipped with an X-ray energy dispersive analyser was used to study the detrital and diagenetic mineralogy and morphology of the deposits. Sample preparation consisted of splutter coating with gold and/or spraying the sample with a conductive spray and mounting on an aluminium chip.

(d) X-ray Diffraction Analysis: This method was used for the identification of clay minerals. Sample preparation involved crushing the samples by hand with a mortar and pestle to gently disaggregate the clays. Less than 2 micron (<2 μm) clay fraction samples were prepared using the "Suction-onto-ceramic tile method" (Shaw, 1972) (Appendix V). A tube producing Co Kα radiation was used throughout. Each sample disk was run four times: air dried, after glycolation, after heating for one hour to 180°C and after heating for one hour to 580°C. The diffractograms produced cover the range 3°-41° 2θ. The clay minerals present were identified from diffractogram peaks (see Appendix V for key to peak identification). Semi-quantitative analysis, using the method described by Griffin (1971) was also attempted for each sample.

1.3.3.2 Palaeomagnetic Techniques

(a) Palaeomagnetic Measurements The majority of specimens were measured using the "Cryogenic Magnetometer" (or SQUID: Superconducting Quantum Interference Device) at the Nuffield Palaeomagnetic Laboratory, Close House, approximately 18 km west of Newcastle-Upon-Tyne. This magnetometer is described by Goree and Fuller (1977) and Collinson (1983). Its main advantage over other magnetometers is its greater sensitivity, with a reproducibility below 0.1 mAm^{-1}. It is also faster to use, and hence, more amenable to repeat measurements which will tend to improve accuracy.

A small proportion of the cores were measured using a "Digico Balanced Fluxgate Magnetometer" (Molyneux, 1971; Collinson, 1983) in the department of Geological Sciences at Aston University in Birmingham. This has a sensitivity lower than that of the cryogenic magnetometer, although reproducibility down to a magnetic intensity of around 0.1 mAm^{-1} to 0.2 mAm^{-1} may be achieved.

(b) Isothermal Remanent Magnetization (I.R.M.) Measurements I.R.M. acquisition curves have been constructed for selected samples by magnetizing them in increasing fields of up to 1.4 Tesla (T) and measuring the intensity of the acquired remanence. Each sample in turn was placed in the magnetic field for approximately five seconds before measurement using a Digico magnetometer. The field was increased progressively and the samples remeasured after each field increment. Reverse-field I.R.M. measurements were also taken until each sample reached zero intensity.

This method of analysis is useful in distinguishing between high coercivity minerals, such as haematite, which only saturates in fields much greater than 1.4T, and low coercivity minerals such as magnetite, which saturates in much weaker fields than haematite (<0.25T) (Tarling, 1983).

For an explanation of isothermal remanent magnetization and other types of magnetic remanence see Appendix VI.

(c) Thermal Demagnetization Procedures: After N.R.M. measurements were obtained for all specimens, one representative 'pilot' specimen was selected for thermal demagnetization. These specimens were then placed in a furnace, heated in a stepwise fashion and allowed to cool in 'field free' space (actually ±10 nT). This technique is well known and used routinely in palaeomagnetic studies (see McElhinny (1973) for a detailed description). After each increment of heating and cooling the specimens were remeasured. During the thermal demagnetization process, the low-field susceptibility was measured prior to each reheating using an inductance bridge (Collinson and Molyneux, 1967).

This enabled monitoring of any mineralogical changes, which might occur as a result of heating. Based on the results of partial thermal demagnetization of the pilot specimens, temperatures at which to demagnetize the remaining specimens, were selected.

(d) Alternating Field Demagnetization (A.F.): If pilot specimens did not respond well to thermal demagnetization then a second specimen was chosen to undergo alternating field demagnetization (see Irving et al., 1961) using a demagnetizer with a "3 axis" tumbler. In general, however, samples which did not respond well to thermal magnetization did not respond well to A.F. demagnetization. This was due, in most instances, to the low intensities of remanence exhibited by such samples.

(e) Chemical Demagnetization: Seven specimens were selected for demagnetization by means of acid leaching. The technique consists of allowing dilute HCl acid to soak into the specimens, which preferentially leaches away the haematite pigment. After a specified period of time, the rock is removed from the acid, thoroughly rinsed and dried, and the magnetization measured.

To prevent re-deposition of iron inside the specimen during drying, water was forced through the sample to remove all iron in solution. These rinsed specimens were then left to dry in magnetic 'field free space'.

For a more detailed description of chemical demagnetization techniques see Collinson (1967) and Park (1970).

1.3.4 Statistical Techniques and Methods of Presentation

1.3.4.1 Sedimentology

(a) Point Count Analysis: A minimum of 500 points per thin section were counted. The results were then recalculated as percentages and tabulated (Appendix VII). Quartz, feldspar and rock fragments were also recalculated to one hundred percent for each sample and plotted on a ternary diagram. A rock name was then assigned to each sample using Dott's (1964) classification system. The relative amounts and different types of porosity and iron oxide were also noted in many cases.

1.3.4.2 Palaeomagnetism

(a) Statistics: A statistical model was developed by Fisher (1953) to define a Gaussian distribution of equal weighted points on a sphere by which palaeomagnetic results could be analysed. The cone of confidence, α_{95}, is one of the most widely used statistical parameters derived from this analysis:

$$\text{where } \alpha_{95} = \arccos\left[1 - \frac{N-R}{R}\left(P^{-1/(N-1)} - 1\right)\right]$$

Where N = Number of directions.
R = Vectoral sum of directions.
P = Probability = 0.05 i.e. there is a 95% probability that the true mean direction lies within α_{95} degrees of the observed mean direction.

The behaviour of pilot specimens can be used to give an objective estimate of stability over different temperature (or magnetic field) ranges. The index used in this study is that given by Tarling and Symons (1967) and is defined as:
Stability Index, S.I. = max (Range$^{\frac{1}{2}}$/circular standard deviation);

for three or more observations of the direction after two or more successive increases in temperature (or magnetic field) (see Appendix VIII for comparison of Stability Index and a subjective classification).

The Stability Index was used in conjunction with visual inspections of the intensity, susceptibility and directional changes to select an appropriate demagnetization temperature for the remaining specimens of each sample.

Directions which pass the 10° linearity test are also recorded in this study. These represent linear segments between two successive temperature increments, that lie within 10° of each other (Kirschvink, 1980).

The fold test (Perry, 1979) is also useful and involves the comparison of direction groupings, before and after correction for the angle of bedding. If the scatter is best when tilt-corrected, then the magnetization is essentially pre-folding; if it is least when field-corrected, the magnetization has a predominantly post-folding age.

(b) Data Presentation: Palaeomagnetic results are presented using stereographic projections, normalised intensity and susceptibility decay curves and orthogonal vector plots (Zijderveld diagrams) (As, 1960).

Stereographic projections constructed using an equal angle stereonet are used to plot individual declinations (measured clockwise from north) and inclinations (measured from the equator which represents the horizontal). Conventionally, the projection is of the lower hemisphere i.e. downward inclinations are plotted as solid symbols and upward negative inclinations, are plotted as hollow symbols.

On normalised intensity and susceptibility curves the x axis is a measure of temperature (or magnetic field) and the y axis represents the normalised intensity (M/M_o) or susceptibility (X/X_o) values.

Orthogonal vector plots, allow components of the remanence to be plotted so that both intensity and directions of a vector may be plotted as the specimen is progressively demagnetized. The components chosen are vertical and horizontal. Individual components are represented by linear segments whose slopes are simply related to the declination, inclination and intensity of the resolved component.

Palaeomagnetic pole positions are also useful to plot. The magnetic vectors in the samples can be used to calculate the position of their corresponding pole (Tarling, 1983). The distribution of these pole positions can then be displayed on a stereographic projection in a similar manner to magnetic directions. Latitudes are plotted in the same way as inclinations and longitudes are plotted as declinations.

(c) Magnetic Units: Sommerfeld SI (Systeme International) units are used throughout this thesis. The magnetic field (F) of a material and its intensity of magnetization (J) are both measured in amperes per metre (Am^{-1}) and are related to magnetic induction (B) in a magnetic medium by

$$B = \mu_o (F+J)$$

which is measured in tesla (T).

Magnetic fields are, therefore, expressed in terms of tesla (T) and the intensity of magnetization per unit volume is expressed in terms of Am^{-1}.

1.4 GEOLOGICAL BACKGROUND

1.4.1 Geographical Situation

Geographically, the study region lies within the provinces of Guadalajara and Teruel in Central Spain (Fig. 1.1).

The main structural highs in this area are the northwest-southeast (Alpine) trending sierras of Aragoncillo, Vetosa, Santa Maria del Espino, Calderos, Menera and Albaracin. These consist predominantly of Ordovician and Silurian aged rocks and have an average height of between 1,200 and 1,500m. The highest point in this area lies in the sierra Albaracin (1,920m).

The principal rivers are (in the northwest) the Henares with its tributaries, Sorbe, Bornoba, Canamares and Salado. The Palmaces reservoir is situated over the source of the Canemares. Further southeast the rivers of Tajo, Gallo and Cabrillas are important. The principal town in this area is Molina de Aragon, which is the centre of commerce for the region. Other towns of lesser importance include Corduente, Mazarete,

Riba de Saelices, Maranchon, Alcolea del Pina, Tamajon, Palmaces de Jadraque, Imon and Cincovillas. The population is, however, generally sparce.

1.4.2 Geological Situation

The area studied is located in the Rama Castella branch of the Iberian Cordillera (Fig. 1.2). It is limited to the west by the Central System and to the north by Quaternary deposits of the Rio Jiloca basin. To the south and east Mesozoic deposits of the Serrania de Cuenca mark the limits of the study region.

The oldest deposits in the area are of Lower Palaeozoic age. They are commonly exposed as horst blocks and consist, predominantly, of Ordovician and Silurian material (Riba, 1983). In the western part, Devonian age deposits are also seen.

Unconformable over this older material are isolated areas of volcanic and volcaniclastic rocks (thought to be of Lowermost Permian age) and/or detrital red sediments of the Saxonian facies (Upper Permian) and Buntsandstein (Uppermost Permian-Middle Triassic) facies.

These Triassic deposits are similar in type to those seen in the Mediterranian areas and in Germany. The continental red beds of the Buntsandstein are overlain by carbonates and mudstones of the Muschelkalk facies. The sequence is capped by evaporites of the Keuper facies. The 'Dolomias tableadas de Imon' marks the Triassic-Jurassic boundary in this area, Riba (1983), assigned this unit to the Rhaetian.

The Jurassic is very well exposed throughout the region, extending from Hettangian to Kimmeridgian in age (Riba, 1983). The Cretaceous is poorly represented, existing in only a few isolated sections.

Tertiary deposits are present in certain areas, such as in the Tajo basin and are Palaeogene to Miocene in age.

Finally, Quaternary deposits are very extensive in the northern part of the zone studied and consist predominantly of alluvium.


Aston University
Illustration removed for copyright restrictions

1.4.3 Geological History

Towards the end of the Hercynian orogeny (Late Carboniferous-Early Permian), the Iberian Peninsula suffered an episode of complex wrench faulting. Two main east-west structural systems developed (the northern Pyrenean-Bay of Biscay system and the Gibraltar system). In the interior of the Iberian Plate important northwest-southeast and northeast-southwest trending fault systems were created. Sedimentary basins controlled by these faults, developed and were filled with continental sediments and associated volcanic rocks (Autunian deposits). These Lower Permian rocks rest unconformably on Hercynian basement and are covered, also unconformably, by Saxonian or Buntsandstein red beds. Sedimentation began with volcanoclastic tuffs (ash flows and ignimbrites, Munoz et al., 1983). Abundant plant remains are found within these deposits. As volcanic activity decreased, thinly bedded siltstones were laid down in a lacustrine environment.

Tectonic movements and subsequent erosion greatly modified the regional palaeotopography. Continental red beds of the Saxonian facies, consisting mainly of red mudstones with intercalated breccias of quartzite, sandstones, conglomerates and thin carbonate beds of mainly alluvial origin, indicate a climatic change to more arid conditions. A number of small alluvial fans were formed at this time but distinction between proximal and distal facies is not possible. No biostratigraphical data is available for the Saxonian facies, which reaches a maximum thickness of about 45m in this area.

Buntsandstein sediments unconformably overlie all previous rocks. They represent a period of extensive continental sedimentation. Traditionally, the basal unconformity was taken as the Palaeozoic-Mesozoic boundary, but the age of the lowest sediments is variable, ranging from Late Permian to Middle or Late Triassic. A Thuringian microflora has been recovered in the study area, from the lowest Buntsandstein unit (Ramos and Doubinger, 1979). During the Buntsandstein sedimentation was closely related to tectonics movements. A series of horsts and graben and associated with these, areas of major subsidence, developed. In these areas the Buntsandstein facies reached thicknesses in excess of 500m.

The Buntsandstein facies have been subdivided into six units (Ramos, 1979), ranging in age from Thuringian to Ladinian and consisting predominantly of red bed conglomerates and sandstones.

The lower four units comprise a siliciclastic complex which is closely related to tectonic events (Ramos et al., 1986). Alluvial deposits in the lower-most unit (Conglomerados de la Hoz de Gallo) were controlled by Late Hercynian faults which were active during the sedimentation. The overlying units, "Areniscas de Rillo de Gallo", "Nivel de Prados" and "Areniscas del Rio Arandilla", accumulated as a result of braided fluvial systems. Transverse or linguoid bars change upwards into channel fill deposits (Ramos et al., 1986). The upper two Buntsandstein units, "Lutites y Areniscas de Rillo" and "Lutites y Areniscas de Abigarradas de Torete" display evidence of evolution from a distal fluvial environment to one of tidal influence. Palynological evidence (Ramos, 1979), suggests that this probably occurred during the late Anisian and marks the beginning of the Tethys transgression over this part of Western Europe.

The highest Buntsandstein unit ("Lutites y Areniscas de Abigarradas de Torete") contains several palynological assemblages of Ladinian age. These show clear evidence of deposition within a supratidal environment in a semi-arid climate. Algal lamination and evaporite deposits are also common.

The Muschelkalk facies comprises carbonate deposits laid down in a marine environment. This facies is much more homogeneous than the underlying Buntsandstein and occurs over a much wider area.

1.5 PREVIOUS RESEARCH

1.5.1 The 'Red Bed' Debate

The term 'diagenesis' has a number of definitions (Larsen and Chilingar, 1979) but for the purposes of this work it can be described as "a collective term for all those processes which take place after the deposition of a sediment. These include physical and chemical processes which affect the detrital mineral grains and also the changes which take place in the chemistry of the interstitial connate fluids" (Turner, 1980).

The diagenesis of sandstones in general has been discussed in detail by a number of authors including Pettijohn (1957), Larsen and Chilingar (1967), Folk (1968), Pettijohn et al. (1973) and Burley et al. (1985).

The majority of the Permian and Triassic deposits studied during the course of this research are red sandstones and siltstones of continental origin (continental red beds).

At the present time, and also in the stratigraphical record, red beds occur in two main associations (Turner, 1980):

1. An arid climate association, with fluvial and aeolian sandstones and evaporites.

2. A moist climate association, with interdigitated coal bearing strata.

There has been considerable debate regarding the origin of haematite in both these red bed associations, since it is finely disseminated haematite (Fe_2O_3) which gives these rocks their red colouration. Krynine (1949) believed that red beds could form by direct derivation of haematite from red tropical soils (latosols). Van Houten (1961, 1964, 1973) believed that the haematite could form diagenetically by the *in situ* dehydration of yellow or brown iron hydroxides derived from deeply weathered soils but not necessarily latosols. Research carried out on first-cycle arkosic desert alluvium in the southwestern USA and northwestern New Mexico, however, led Walker (1967, 1976) and Walker *et al.* (1978), to argue that red beds in both arid and warm, moist climatic associations form as a result of authigenesis of haematite which has formed diagenetically due to the *in situ* alteration of detrital silicate minerals.

Glennie *et al.* (1978), Kessler (1978), Waugh (1978) and Turner (1980) support the idea that diagenetic processes are important in the reddening of sediments. This places little emphasis on the source area climate. If a special type of climate is important, it is in the depositional area not the source area (Walker and Honea, 1969). They concluded that "all sediments, regardless of source area climate or parental material, contain enough iron to produce bright red sedimentary rock, if the interstitial environment is favourable".

For more detailed reviews of red bed diagenesis, Glennie (1970) summarises the long history of controversy regarding the origin of reddening in sediments, and Turner (1980), provides an overview of red beds and red bed diagenesis.

1.5.2 Palaeomagnetic Studies on Red Beds

Continental red beds were the first sedimentary rocks to be studied in any detail and red sandstones and siltstones were amongst the first consolidated rocks to be studied palaeomagnetically, e.g. Runcorn (1956a,b), Irving (1957), Clegg *et al.* (1954a,b, 1956, 1957, 1958) Creer (1957) and still provide one of the main sources of palaeomagnetic data.

The origin of remanence in red beds has, for many years been a highly controversial issue (Helsley and Steiner, 1974; Baag and Helsley, 1974; Walker, 1976; Elston and Purucker, 1979; Walker et al. 1981). Many workers think that the remanence closely reflects the geomagnetic field at the time of deposition and can thus be used in palaeopole calculations, in recording secular variations and in detailing polarity reversals (Helsley, 1969; Helsley and Steiner, 1974; Khramov, 1967; Van den Ende, 1970). It is assumed by many authors that acquisition of the remanence occurred at the time of deposition and therefore a sequence of polarity reversals can be used to establish time lines for the chronological correlation of sedimentary facies, (Helsley, 1969; Helsley and Steiner, 1974; Shoemaker et al., 1973; Shoemaker and Purucker, 1974; Steiner and Helsley 1974a,b; Turner and Ixer, 1977; Elston and Purucker, 1979) i.e. red bed magnetostratigraphy.

Abundant data available in the literature indicate however, that red beds tend to be variably affected by magnetization acquired subsequent to deposition i.e. secondary magnetization (Chamalaun and Creer, 1964; Al-Khafaji and Vincerz, 1971; Roy and Park, 1972; Steiner and Helsley, 1972; McGlynn et al., 1974; Hoblitt et al., 1974; Larsen and Walker, 1975; Walker 1976; Turner and Archer 1975; Johnson, 1976; Turner, 1979, 1980, Turner et al., 1984 and Elmore et al., 1985). The results of these studies suggest that red bed magnetization is frequently, not the result of a simple process that occurs during or soon after deposition but rather one that may affect the sediments both non-uniformly and repeatedly at any time during their entire post depositional history. The data, therefore, is of little use for stratigraphic purposes.

The time of remanence acquisition is the crucial issue and therefore the heart of the controversy centres on the origin of the haematite (the principal magnetic carrier in red beds) which carries the remanence.

In the Triassic red beds of North America, Greenland and Europe a number of zones of approximately antiparallel reversely and normally magnetized rocks can be identified (Burek, 1968; Baag and Helsley, 1974; Reeve et al., 1974; Turner and Ixer, 1977; Elston and Purucker, 1979). In the case of the Moenkopi Formation, this feature and the preservation of apparent secular variation (Baag and Helsley, 1974), has been taken to indicate that the rocks were magnetized very shortly after deposition. This conflicts with detailed studies of the diagenesis, however, which indicate that long-term in situ alterations involving haematite

authigenesis (Walker, 1976; Walker et al., 1981) were important. The magnetostratigraphy of the Moenkopi Formation was established by Helsley (1969) and Helsley and Steiner (1974), who identified five normal and five reverse magnetozones. These magnetozones were analyzed by Baag and Helsley (1974). They argued that the small scale directional variations and the geomagnetic transition closely compared with present-day secular variations of the Earth's magnetic field and that consequently the Moenkopi Formation must have been magnetized penecontemporaneously. More recently, Elston and Purucker (1979), have argued that the magnetization of the Moenkopi is of detrital origin and based their conclusions partly on chemical demagnetization studies. This conclusion is not supported by studies of the diagenesis of iron oxides in the Moenkopi Formation (Walker 1976; Walker et al., 1981) which reveal authigenic haematite in a wide range of grain sizes and textural sites. The disagreement over interpretation of the Moenkopi palaeomagnetic results is of fundamental importance in palaeomagnetism.

1.5.3 Previous Spanish Research

1.5.3.1 Diagenetic Studies on the Permo-Triassic of Central Spain

The stratigraphy and sedimentology of the Permo-Triassic deposits of Central Spain have been the object of numerous studies for over a century (e.g. Jacquot, 1866; Calderon, 1898; Tricalinos, 1928; Sacher, 1966; Virgili, 1954; Riba, 1959; Ramos, 1979; Sopena, 1979; Perez-Arlucea, 1985). It is only in the last twenty years, however, that work of any detail has been published on the diagenesis of these deposits.

The relationship between colour and mineralogy in the Buntsandstein red beds was examined by Marfil et al., (1971). They identified a number of iron minerals including goethite, haematite, turite, pyrite, magnetite and lepidocrocite and concluded that "redness has a secondary origin".

A study by Hernando and Hernando (1976), suggested that heavy minerals may be used as a means of differentiating between the Permian and Triassic. Their results showed, for example, that tourmaline is much more common in the Buntsandstein than in the Saxonian facies.

Results from a detailed geochemical and mineralogical study of the Triassic sediments in the Castillian branch of the Iberian range were published by Garcia-Palacios and Lucas (1977). Their study included work on the clay mineralogy of the deposits and illite crystallinity. From the results attained, they attempted a geochemical, sedimentary and diagenetic

reconstruction of the evolution of the basin. In the same year Marfil et al. (1977), published a report on diagenetic processes in the Buntsandstein of the Iberian Cordillera. The main conclusions of this report are presented below:

1. The most important diagenetic processes to have occurred were:
   a. growth of authigenic quartz and feldspar.
   b. the creation of secondary matrix.
   c. the precipitation of a dolomitic cement.

2. The creation of secondary matrix resulted in 'greywackitisation' of the deposits.

3. The authigenic mineral sequence (deduced by textural relationships) is: goethite-haematite, quartz, feldspar, dolomite-barite, opal, calcite-limonite.

4. The precipitation of goethite and haematite in the sediments, and hence acquisition of their red colouration occurred during early diagenesis.

In 1980, Raffiella Marfil along with various co-workers, published a series of papers concerning the diagenesis of Permo-Triassic deposits from Central Spain. These included a study on the diagenetic evolution of Permo-Triassic sediments from a borehole in Siguenza (Marfil and Buendia, 1980). They concluded that "diagenesis was mainly controlled by depositional environment, original composition and textural characteristics, rather than by burial history". In addition to these findings, Marfil and Pena (1980), emphasised how clean arenites diagenetically change into wackes and concluded that diagenesis was strongly influenced by depositional conditions and climatic evolution during the Permian. Furthermore, they also suggested that evidence for pH-Eh variation exists in these rocks and that the Autunian facies formed under acid and reducing diagenetic conditions whereas the Saxonian formed under alkaline and oxidising conditions.

The application of scanning electron microscopy to the study of diagenetic processes was carried out by Marfil et al., (1980), on volcaniclastic rocks of Permian age. This study reached similar conclusions to the previous two with the presence of two very distinct types of diagenetic mineralogy corresponding to two different depositional

physiochemical conditions: An acid-reducing environment, characterised by kaolinite, siderite, pyrite, and organic material and a strongly alkaline environment with an arid to semi-arid climate, characterised by haematite smectite, zeolites, silica, gypsum, magnesite, dolomite and illite.

Results of a petrological study on the Saxonian and Buntsandstein facies of the "El Pobo de Duenas" zone of the Iberian Cordillera were published by Sentchordi and Marfil in 1983. Their study was to define the provenance of the deposits using quartz type and heavy mineral analysis. They found that the Saxonian has a low-middle rank metamorphic provenance with a secondary igneous influence and the Bunter has a more complex provenance ranging from low-middle rank metamorphic to high rank gneiss.

They also reported that illite crystallinity and vitrinite reflectance data suggests burial to the Mesodiagenetic Mature 'B' stage of diagenesis of Schmidt and McDonald (1979).

Marfil et al. (1984), returned to the problem of diagenesis in the Lower Permian, Autunian deposits of the Iberian Cordillera. They concluded that these lacustrine sediments underwent early dolomitisation in a hypersaline environment, the source of the magnesium probably being the surrounding volcanic rocks. Zeolites also formed at this time as a result of reactions between the tuffs and trapped lake water.

More recently, porosities of the Triassic sandstones from the Aragonesa branch of the Iberian Cordillia have been discussed by Arribas and Soriano, (1984). They concluded that the dissolution of potassium feldspar, carbonate and barite cement was related to meteoric pore-water flowing through the deposits and that fracture porosity was probably created during Tertiary tectonics in the Iberian range. They suggested that the amount of secondary porosity was related to the original composition of the sediments and also to the geochemistry of the sedimentary environment which controlled the first diagenetic stages (eodiagenesis).

1.5.3.2 Palaeomagnetic Research on the Permo-Triassic of Iberia

Several palaeomagnetic investigations on Spanish Permo-Triassic rocks have been carried out in the past . Clegg et al., (1957) were the first to publish palaeomagnetic results from the Spanish Meseta. They

reported magnetic directions approximately parallel to the recent local geomagnetic field from Triassic redbeds of northwest and central Spain. Van der Lingen (1960) was the first to find stable remanence in Permo-Triassic rocks from the Central Pyrenees and a few years later Schwarz (1962) published his results on andesites and redbeds from the adjoining region. Both found pole positions diverging from those found for stable Europe. Van Dongen (1967) reported similar results from Triassic redbeds in the eastern Pyrenees.

Van der Voo (1967, 1968) published two studies on Triassic red beds from the Spanish Meseta. The first analysed red bed samples from Alcazar de San Juan on the eastern margin of the Meseta. This yielded a mean direction with D = 359.5° and I = +23°. The second study, described the palaeomagnetism of red bed samples from Atienzar on the northeastern margin of the Meseta. The magnetic directions obtained were in agreement with those found by Clegg and his co-workers (Clegg et al., 1957) i.e. only secondary magnetizations were revealed by the analysis of N.R.M.

Girdler (1968) described directions of magnetization for Upper Triassic and Lower Jurassic volcanic rocks from the Northern Pyrenees. He found directions consistent with those for stable Europe. He compared these results with previous results from Spain and found that the axes of magnetization are consistent with other results from north of the Pyrenees but not consistent with results from Spain (south of the Pyrenees).

In 1969, Van der Voo published the results of a palaeomagnetic investigation on igneous and sedimentary rocks from Portugal and Spain. The age of the formations varied from Ordovician to Eocene. He compared palaeomagnetic results from the Spanish Meseta and Spanish Pyrenees with those from Africa and other European Countries. His aim was to investigate the theory that the Iberian peninsula has undergone an anticlockwise rotation relative to the rest of 'stable' Europe.

The rotation of Spain had been proposed earlier by Du Toit (1937), and Carey (1958), using geological arguments. Bullard et al., (1965), found their computer fit of the continents around the Atlantic was greatly improved if Spain was rotated, closing up the Bay of Biscay. Van der Voo (1969), concluded that there has been an anticlockwise rotation of the Iberian Peninsular of approximately 35° relative to that part of Europe north of the Alpine fold belts.

He also suggested that the pivot point of this rotation lay in the western Pyrenees and that rotation must have been of post-Permian age. Vandenberg (1980), went further, stating that the rotation was of Lower Cretaceous age and occurred between Barremian-Aptian and Maastrichtian times.

Hernando et al., (1980), published the results of a combined stratigraphic, palaeomagnetic study to find the age of the andesites and interbedded sediments of Atienza, Central Spain. They found the most likely age of the deposits to be Uppermost Carboniferous-Lower Permian (indicating a primary origin of the magnetic remanence).

More recently Turner et al., (in press), show palaeomagnetic results from the Triassic of the Molina de Aragon area Central Spain (Fig. 1.3) which suggest that the remanence is carried by more than one magnetic component and that original palaeomagnetic directions may be 'overprinted' by more recent directions, only revealed after demagnetization of the rocks.

1.6 MAGNETIC MINERALS

1.6.1 Introduction

A variety of remanence carrying minerals contribute to the N.R.M. of red sandstones. Other iron containing minerals are paramagnetic and do not carry a remanence, only contributing to the bulk magnetic properties. These minerals, their main magnetic properties and relative importance in red sandstones are described below. Tarling (1983), gives a more detailed description of magnetic minerals found in terrestrial and extraterrestrial materials:-

1.6.2 Titanomagnetites ($Fe_{3-x}\ Ti_x\ O_4$ for $0 > x > 1$)

This group of minerals have a cubic (spinel) structure at room temperature and forms a solid-solution series at temperatures above 800°C between end members magnetite (Fe_3O_4) and ulvospinel (Fe_2TiO_4). Magnetite is ferromagnetic with a spontaneous magnetization of $92 Am^2 Kg^{-1}$ and a Curie temperature of 575°C. Where as ulvospinel is only weakly ferrimagnetic with a Neel temperature of -153°C.

Most naturally occurring titanomagnetites show a certain degree of oxidation and are correctly termed as titanomagnetites. These minerals represent the most important group of magnetic minerals. They account for the magnetic remanence of igneous rocks and are also important magnetization carriers in some sediments. In the latter, titanomagnetites are rarely found in an unaltered state. Magnetite in red beds undergoes a process of oxidation known as martitization to form haematite.

1.6.3 Titanohaematites ($Fe_{2-x}\ Ti_x\ O_3$ for $0< x <1$)

This solid solution series, with a rhombohedral (corundum) crystal structure, consists of varying proportions of the end members, haematite ($Fe_2\ O_3$) and ilmenite ($FeTiO_3$) where $0< x <1$. There is a steady increase in Curie temperature with increasing ilmenite content (Wescott-Lewis and Parry, 1971) throughout the series. The magnetic behaviour, however, differs drastically with composition (Collinson, 1983).

Ilmenite is paramagnetic above -213°C and therefore in its pure form cannot retain a remanent magnetization. It will, however, contribute to the bulk magnetic properties.

Haematite:- The magnetic properties of haematite, despite considerable attention, are still not fully understood. The specific magnetic properties are strongly dependent on grain size impurities and also temperature. On cooling to -10°C haematite becomes a near perfect anti-ferromagnetic mineral with no spontaneous magnetization. The Neel temperature of haematite is generally reported as 675°C with a lower value for impure haematite.

In the sedimentary environment, haematite is the most important iron oxide. In red beds, magnetic evidence indicates that haematite is the principal magnetization carrier and is largely responsible for the bulk magnetic properties (Collinson, 1968). Much debate over the origin of haematite in red beds has taken place, it is generally agreed, however, that besides detrital grains, haematite forms from the in situ oxidation of magnetite, the pseudomorphing of iron silicates and also by the production of authigenic haematite overgrowths.

1.6.4 Iron Hydroxides, Carbonates etc.

Four basic crystal structures of iron hydroxide can exist, all loosely termed limonite and mainly associated with weathered rocks, soils and sediments. The most important of these is goethite (FeOOH) which is anti-ferromagnetic with a Neel temperature between 60°C and 170°C and is generally reported as 110°C.

Goethite is unstable on heating in air and converts to true haematite via an intermediary (proto haematite) on heating to higher temperatures. In addition to its association with weathered rocks and soils, goethite may also form by direct precipitation from iron-bearing solutions.

Limonite is strictly a complex iron hydroxide mineral consisting of a mixture of goethite and lepidocrocite, with goethite predominating and is thus magnetic. It is this mineral that accounts for much of the red and brown staining in weathered rocks and soils.

Iron is a common component of many other minerals, such as many of the carbonates. Siderite ($FeCO_2$) and ankerite ($Ca,Mg,FeCO_3$) for example are common constituents of sedimentary rocks. All such minerals are paramagnetic at room temperature and do not, therefore, contribute to the magnetic properties of rocks. They do, however, provide an important source of iron oxide if they are broken down by either weathering or other diagenetic or metamorphic processes.

1.6.5 Pyrrhotite (FeS_{1+x} for $0< x <1$)

Iron sulphides can vary in composition from troilite (FeS) to pyrite (FeS_2). Only the latter, however, is common in sediments especially associated with fossilized organic material. Pyrite has a cubic structure and is paramagnetic at room temperature.

1.6.6 Silicate Minerals

Most rock forming minerals which compose the greater part of red sandstones are either paramagnetic or diamagnetic depending on the presence or absence of magnetic ions such as Fe^{2+}, $Fe3+$, Mn^{2+} etc. in the crystal structure. Ferrous and ferric iron containing clay minerals (most commonly illite and montmorillonite in red sandstones) and silicates such as biotite and feldspars (both found in red sandstones) will contribute to the bulk magnetic properties of the rocks. They are paramagnetic in the pure form and unlikely to contribute to the N.R.M. (Collinson, 1969).

CHAPTER TWO

THE AUTUNIAN OF RILLO DE GALLO

2.1 INTRODUCTION

Two major Permian associations have been recognised in Central Spain, a lower grey facies, "Autunian" type and a younger red facies, "Saxonian" type (Sacher, 1966; Sopena et al., 1977; Fig. 2.1).

The sediments were deposited in a number of isolated fault bounded basins initiated towards the end of the Hercynian orogeny (Virgili et al., 1980).

Rocks of the Lower Permian, Autunian facies were sampled at two localities, Rillo de Gallo and Palmaces, both of which lie in the Province of Guadalajara (Fig. 2.2). The Rillo de Gallo section is situated approximately 6 km northwest of the town of Molina de Aragon, (1° 55' 12" W, 40° 55' 12"N). It has a total thickness of 262m. The sediments dip gently towards the south or southeast with inclinations of between 6° and 26°.

2.2 STRATIGRAPHY AND SEDIMENTOLOGY

Fifteen samples were collected from the cliff section at Rillo de Gallo which is exposed along the road between Rillo de Gallo and Pardos and in a nearby stream section (Fig. 2.3 and Plate 2.1a). The sequence unconformably overlies Ordovician quartzites and is unconformably overlain itself by the Saxonian facies. Sacher (1966), named the grey Autunian facies of this area the "Capas de la Ermita". He distinguished three subunits within it, E1, E2 and E3 (Fig. 2.4). The lowest subunit of the Rillo de Gallo section, E1, consists of 58m of white and green volcaniclastic sandstones with some thin conglomerates. Abundant floral remains are present including fossil wood and ferns (Ramos, 1979). Samples RG1 to RG4 were collected from this subunit.

Fig. 2.1 Schematic diagram showing the main characteristics of the lithostratigraphic units recognised in the Permian of Spain and their relationship with the Permian of Western Europe. Adapted from Sopena et al. (1977).

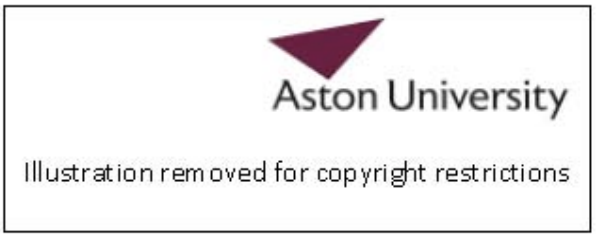
Aston University
Illustration removed for copyright restrictions

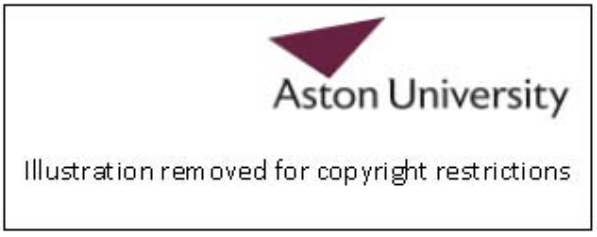

Fig. 2.3 Simplified geological sketch map, showing the location of the Rillo de Gallo section.

Fig. 2.4 Sedimentological column compiled by Ramos (1979) showing horizons from which RG samples were taken, Autunian of Rillo de Gallo section.

Subunit E2 is thick and is composed of interbedded volcanic siltstones and mudstones, some containing carbonate nodules (Plate 2.1b). The volcanic rich levels are found mainly in the lower part and are yellow, green or red in colour. In the upper part of E2, the rocks are predominantly grey and black and rich in floral remains. The microflora association present is typical of that found in the Autunian of other parts of Spain and W. Europe (Ramos, 1979). Samples RG5 to RG15 were taken from this subunit.

Subunit E3 is approximately 21m thick and consists of well bedded, siliceous dolomites with interbedded mudstones and siltstones. This subunit was not sampled.

Ramos (1979), interprets the sediments of the Capas de la Ermita as representing lacustrine deposits with fluvial episodes, corresponding, possibly with the marginal zones of the lacustrine system. Ramos (1979) also envisages deposition in a fairly humid climate with drier seasons in which desiccation occurred and horizons of carbonate nodules and possibly evaporites were formed.

2.3 DIAGENESIS

2.3.1 Introduction

All fifteen samples collected at Rillo de Gallo are very fine grained or cryptocrystalline rocks and most are considerably altered, making classification and diagenetic description of the samples difficult.

Petrographic studies indicate that an almost complete gradation exists between fine grained siltstones or mudstones (with only a negligible volcanic fraction) and rhyodacitic tuffs. The tuffs are cross-laminated in places indicating that they were water lain.

The mineralogy of these rocks consists predominantly of quartz, feldspar, micas and clay minerals with smaller amounts of carbonate, heavy minerals (including opaques) and zeolites. Visible porosities in all samples are very low (<2%) and are predominantly in the form of small fractures or dissolution voids.

2.3.2 Diagenetic Transformations

Silica comprises the greatest proportion of the rocks (up to 80%). It occurs both in the matrix (Plate 2.2a) and as larger individual quartz grains (up to 1 mm.). These grains are generally angular to subrounded. The quartz is usually quite fresh but many grains show corroded or embayed margins (Plate 2.2b). In RG13 the presence of numerous spherulites is evidence of the devitrification of a once glassy siliceous tuff (Plate 2.2c).

Authigenic overgrowths of quartz are occasionally present. These also show corroded margins. One particular type of authigenic quartz has been identified using the S.E.M.. It occurs as six-pointed "flower like" overgrowths. These unusual overgrowths have also been described by Marfil and Buendia (1980), from the Autunian of this area.

Authigenic quartz is also found infilling small fractures within the rocks. This phase of quartz must have been precipitated subsequent to lithification of the rock.

Both potassium (orthoclase and microcline) and plagioclase feldspars are present in the samples studied. Plagioclase, however, is only found in very small amounts (<2%). All feldspars show considerable replacement by clay minerals. This replacement is usually marginal, but sometimes the grain core shows preferential replacement (Plate 2.2d). Less commonly, quartz grains show alteration to fine grained siliceous material and clays.

Muscovite and biotite micas are abundant in these rocks. Muscovite often shows replacement by kaolinite (Plate 2.2e) and biotite laths sometimes show partial replacement by iron oxide.

Clay minerals account for up to 50% of the total composition of these deposits. Most are formed diagenetically by the replacement of framework minerals or the breakdown of the glassy matrix. X-ray diffraction studies on RG2 and RG5 (Figs. 2.5 and 2.6), show that, in order of abundance; illite, kaolinite, smectite (montmorillonite) and chlorite are the major clays present.

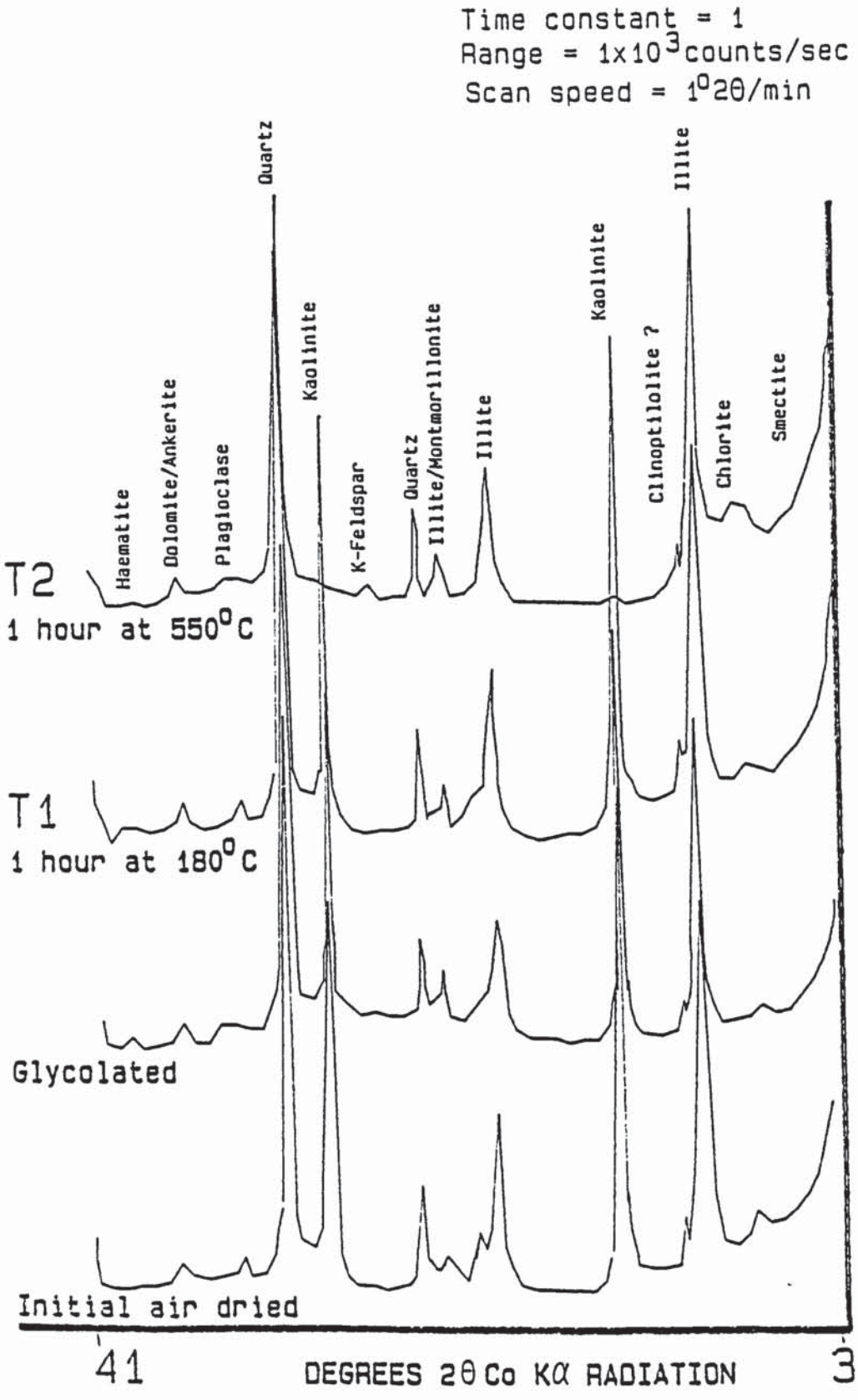

Fig. 2.5 X-ray diffractograms for the <2μm clay fraction of Sample RG2.

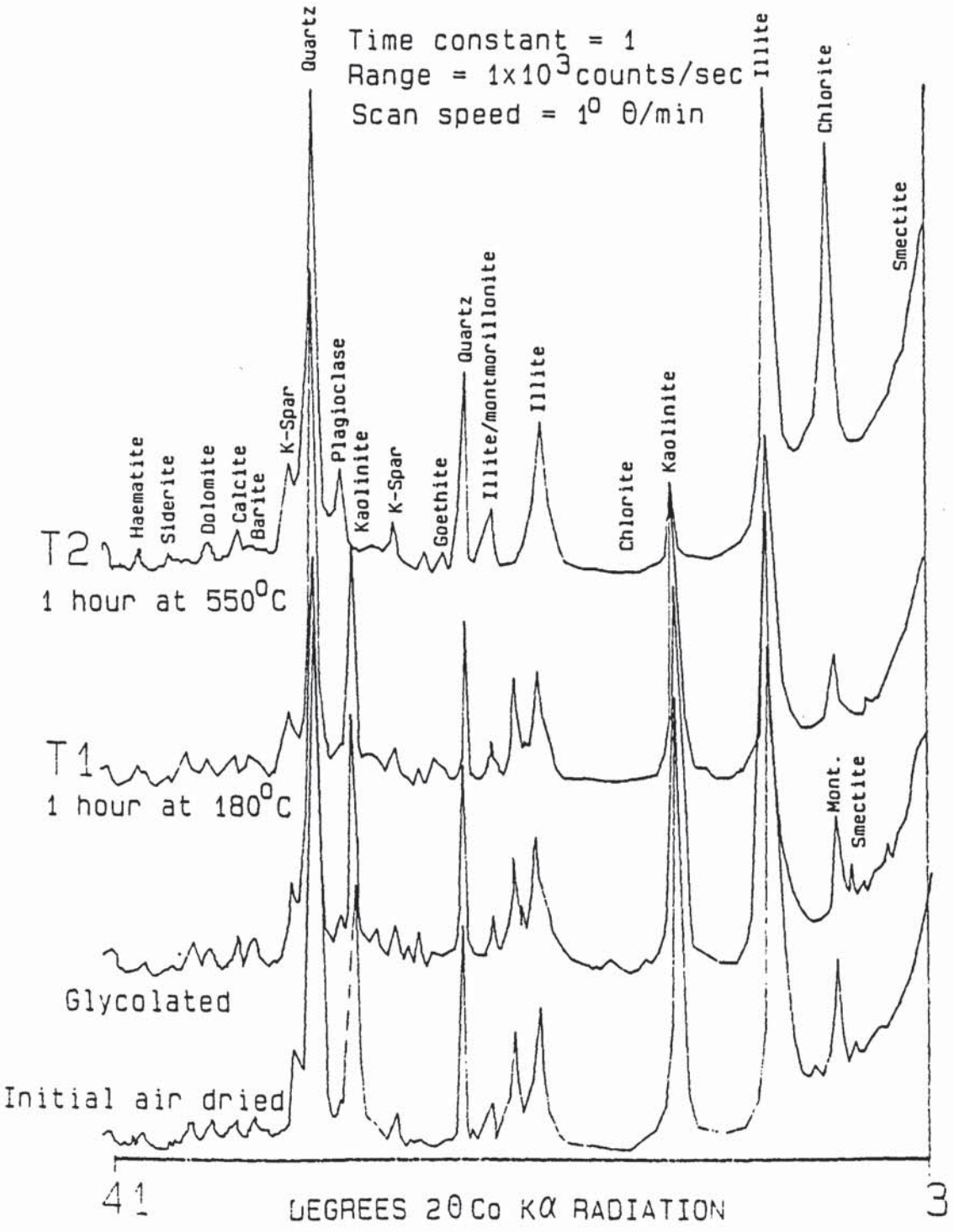

Fig. 2.6 X-ray diffractograms for the <2μm clay fraction of Sample RG5.

Table 2.1, shows the results of semi-quantitative analyses conducted on the two samples using the method described by Griffin (1971). The results are expressed as percentages.

Table 2.1 Results of semi-quantitative analysis carried out on the <2μm fraction of clays from the Autunian of Rillo de Gallo

	Illite	Kaolinite	Mont	Chlorite	Total
RG2	59	31	6	4	100%
RG5	64	23	5	8	100%

The two samples have a fairly similar clay assemblage. RG2 contains a greater proportion of kaolinite than RG5 but contains relatively less chlorite. In addition to the four clays previously mentioned, X-Ray diffraction peaks for haematite, pyrite, goethite, ilmenite, dolomite, calcite, potassium feldspar, plagioclase and quartz can also be readily identified for both samples. Diffractogram peaks at 8.9Å from untreated and glycolated samples indicate the presence of the alkali zeolite, clinoptilolite in RG2 (Fig. 2.5). Small peaks for mixed-layer chlorite-montmorillonite, barite and siderite are also present on the RG5 diffractogram (Fig. 2.6).

Although a small proportion of the clays are undoubtedly of detrital origin, the vast majority are authigenic and formed by a variety of diagenetic transformations. Some of these transformations have already been noted, such as the replacement of feldspars and micas by kaolinite and/or illite. Other transformations include, the replacement of micas by chlorite, that of volcanic detritus by smectite, mixed-layer illite-smectites and chlorite and the replacement of illite by kaolinite.

Carbonate cement is present in small amounts in most samples. It is patchy in nature and has an irregular distribution. Ferroan dolomite, and less commonly, non-ferroan dolomite are found in addition to non-ferroan

calcite. In all samples, calcite post-dates the dolomite cement. Strong evidence for dedolomitization exists in RG6, where irregular shaped patches of calcite cement contain disseminated haematite (Plate 2.2f). Rhombic outlines of the original dolomite crystals are also preserved in many places and some are clearly defined by the fine grained ironoxide (Plate 2.3a). Relict ferroan dolomite is occasionally present, but unlike the calcite, is not associated with any haematite.

Secondary porosity occurs in the form of large subhedral voids (Plate 2.3b). These are frequently lined by fine grained haematite. Occasionally small amounts of relict dolomite are also present within these voids.

Carbonaceous material is common in these deposits and is partly responsible for their dark colouration. Thin bifurcating veinlets, composed of iron-oxide stained organic material, cut through the rocks in certain horizons. These probably represent ancient rootlets.

2.3.3 Magnetic mineralogy

The total iron oxide content of these sediments is low (<2%). However, several distinct types of iron (and iron-titanium) oxide have been identified:-

Coarse detrital iron oxide: This is very rare, but rounded grains of detrital specularite are occasionally found within the matrix (Plate 2.3c). Magnetite is not found in any of the samples studied.

Iron-titanium oxide: Ilmenite is more common than haematite in these deposits. It occurs as euhedral laths within the matrix. Many show alteration to leucoxene (amorphous titanium-oxide). Authigenic ilmenite is also found within the cleavages of detrital micas (Plate 2.3d).

Fine grained aggregates of haematite: Framboidal aggregates of haematite (Plate 2.3e) and euhedral (cubic) haematite clusters are disseminated throughout these sediments. The textural habit of this haematite suggests that it is probably a pseudomorph after pyrite. Most samples contain some haematite of this type but it is especially common in RG10 and RG15.

Haematite associated with secondary porosity and carbonates: Fine grained haematite ,found in association with dissolution porosity is common in these deposits. This authigenic phase of haematite lines or infills subhedral (often rhombic shaped) voids (Plate 2.3f). It is also found in close association with non-ferroan calcite cement (Plate 2.2f). This type of haematite is very common in RG6.

Iron hydroxides: Goethite is present in many of the samples. It is particularly abundant in RG1 occurring as fine grained aggregates and a replacement for haematite.

2.3.4 Paragenesis

The earliest diagenetic transformation to have occurred in the Autunian of Rillo de Gallo was most probably, the devitrification of the tuffs. In the volcaniclastic deposits, many of the volcanic rock fragments were progressively replaced by smectite, chlorite and mixed-layer clays during early diagenesis. This resulted in the creation of an epimatrix which reduced the overall porosity and permeability of the rocks.

Zeolite formation also occurred at this time. Many studies (e.g. Hay, 1966; Surdam and Sheppard, 1978) indicate that saline, lacustrine environments, receiving glassy volcanics (as in the Rillo de Gallo area during the Autunian), are ideal sites for the formation of zeolites. The presence of the silica rich, alkali zeolite, clinoptilolite further suggests that the sequence was never deeply buried, since only low silica zeolites are found in deeply buried sediments (Iijima, 1970, 1975; Boles and Coombs, 1975).

In the highly saline, reducing conditions of the lacustrine environment, Fe^{2+} from decomposing detrital ferromagnesian minerals would have probably combined with free H_2S to form pyrite (Berner, 1984).

Below the sulphate reduction zone, however, sulphide ions would not have been available to combine with ferrous iron and the Fe^{2+} ions would have been free to go into ferroan dolomite cements. The high pH conditions being ideal for the promotion of early dolomitization (Chillingar and Bissell, 1963).

The replacement of feldspars and muscovite micas by illite would be favoured by the high pH values and hence these diagenetic transformations probably occurred at the same time as dolomitization of the sediments.

Ramos (1979), envisaged a humid but seasonal climate during the Autunian, with alternating wet and dry periods. During the wetter periods increased rainfall would result in large amounts of fresh, meteoric water flowing through the deposits. The pH would drop, and oxidising conditions would prevail. This would lead to pyrite oxidation, which in turn would enhance the process of dedolomitization (Chilingar et al., 1979) as:-

$$FeS_2 + 7/2\ O_2 + H_2O = Fe^{2+} + 2SO_4^{2-} + 2H^+$$

and $$Fe^{2+} + 1/4O_2 + 5/2\ H_2O = Fe(OH)_2 + 2H^+$$

The resultant acidification of pore waters would promote the reaction:

$$CaMg(CO_3)_2 + 2H^+ = CaCo_3 + Mg^{2+} + CO_2 + H_2O$$

Iron intrinsic to ferroan dolomite, has been omitted from the above equation for the sake of simplicity. During dedolomitisation, any iron present in the original dolomite would be released and, if suitable pH and Eh conditions existed, would precipitate near its source as fine grained haematite or as a precursor hydrated oxide (Walker, 1967), as seen in these Autunian deposits.

The dissolution of carbonate cement due to the circulation of meteoric water through the sediments is also known to promote kaolinite precipitation (Curtis, 1983) and hence, the replacement of feldspars, muscovite and illite by kaolinite would probably have occurred at this time.

Uplift of the sequence at some later stage again brought acid, oxidising waters in contact with the deposits promoting further kaolinite precipitation and the partial replacement of haematite by goethite.

2.4 PALAEOMAGNETISM

2.4.1 Natural Remanent Magnetization Results

The results of palaeomagnetic analyses carried out prior to demagnetization of the samples from Rillo de Gallo are summarized in Table 2.2.

The mean intensity of N.R.M. for the Rillo de Gallo site was 0.64 mAm^{-1}. Average N.R.M. intensities from individual samples were generally very low ranging from 0.02 mAm^{-1} up to 0.87 mAm^{-1}. Sample RG6 was the only exception, having an intensity of 5.07 mAm^{-1}. Mean initial susceptibility values for Rillo de Gallo samples ranged between 1.6 $mAm^{-1}nT^{-1}$ and 359.4 $mAm^{-1}nT^{-1}$ with an average of 117 $mAm^{-1}nT^{-1}$. There is a positive correlation between initial susceptibility and initial intensity values in these samples i.e. samples with low initial intensities also have low initial susceptibilities and those with high intensities have high susceptibilities.

The mean N.R.M. directions for the Rillo de Gallo samples lie predominantly in the SE quadrant when plotted on a stereogram (Fig. 2.7). They show a streaking effect from fairly shallow positive directions in the SE quadrant towards steeper positive directions in the NE quadrant. Field corrected directions are generally steeper than those corrected by both field and bedding. The site mean bedding corrected direction for the Autunian of Rillo de Gallo is D=165.5° I=22.7°, α_{95} = 6.0°, N = 9. Within site scatter is generally quite high with α_{95} values ranging from 4.6 (RG5) up to 25.8 (RG4). There also appears to be an inverse relationship between scatter (α_{95}) and initial intensity, i.e. samples with the lowest intensities have the largest scatter and those with high intensities have low scatter.

2.4.2. Isothermal Remanent Magnetization (I.R.M) Results

I.R.M. curves have been drawn for samples RG1 and RG5 (Fig. 2.8). The two samples show essentially similar behaviour. They reach 80% to 90% of their saturation values by 0.35T. Initially the curves approximate a straight line with RG5 having a steeper gradient than RG1. Gradually the curves become concave upwards and above 1T are almost horizontal. Neither of the two samples, however, quite reaches full saturation. Reverse field demagnetization curves for both RG samples are steep, falling to zero intensity by 0.14T. The magnitude of the maximum I.R.M. reached by RG1 is 175 mAm^{-1} and that of RG5 is 270 mAm^{-1}.

TABLE 2.2 N.R.M. RESULTS FOR THE AUTUNIAN OF RILLO DE GALLO

Sample	Height (m)	F Dec(°)	F Inc(°)	P Dec(°)	P Inc(°)	Pole Long(°)	Pole Lat(°)	N	R	α95(°)	α95(°) Pole	Intensity (mAm^{-1})	Susceptibility ($mAm^{-1}nT^{-1}$)
RG1	12	30.0	75.6	73.5	75.2	33.6	42.6	6	5.60	19.6	32.5	0.27	109.16
RG2	18	69.4	45.9	79.2	44.0	73.2	24.7	6	5.85	11.7	10.3	0.03	1.59
RG3	26	99.5	49.2	109.1	41.5	4.6	55.3	8	6.27	22.3	25.0	0.04	4.30
RG4	38	66.1	45.7	75.9	41.7	76.8	26.3	7	6.07	25.8	29.4	0.02	-
RG5	112	137.3	61.8	138.0	50.8	33.2	-7.8	7	6.96	4.6	5.6	0.87	293.93
RG6	121	167.3	34.4	165.6	22.7	15.5	-35.5	6	5.96	6.0	4.6	5.07	359.41
RG7	127	155.0	16.4	155.0	4.5	31.6	-40.7	8	7.8	10.9	11.2	0.14	125.95
RG11	189	133.0	38.4	139.7	27.5	41.0	-20.4	6	5.57	20.4	18.2	0.07	36.97
RG13	197	42.5	71.8	102.0	83.6	13.8	39.3	6	5.80	13.5	24.1	0.15	61.60
RG14	202	162.5	26.8	166.4	16.6	25.6	-38.7	8	7.75	10.7	8.9	0.15	46.18
RG15	218	66.5	79.4	128.1	81.5	13.0	32.0	8	7.5	15.8	27.7	0.21	131.62

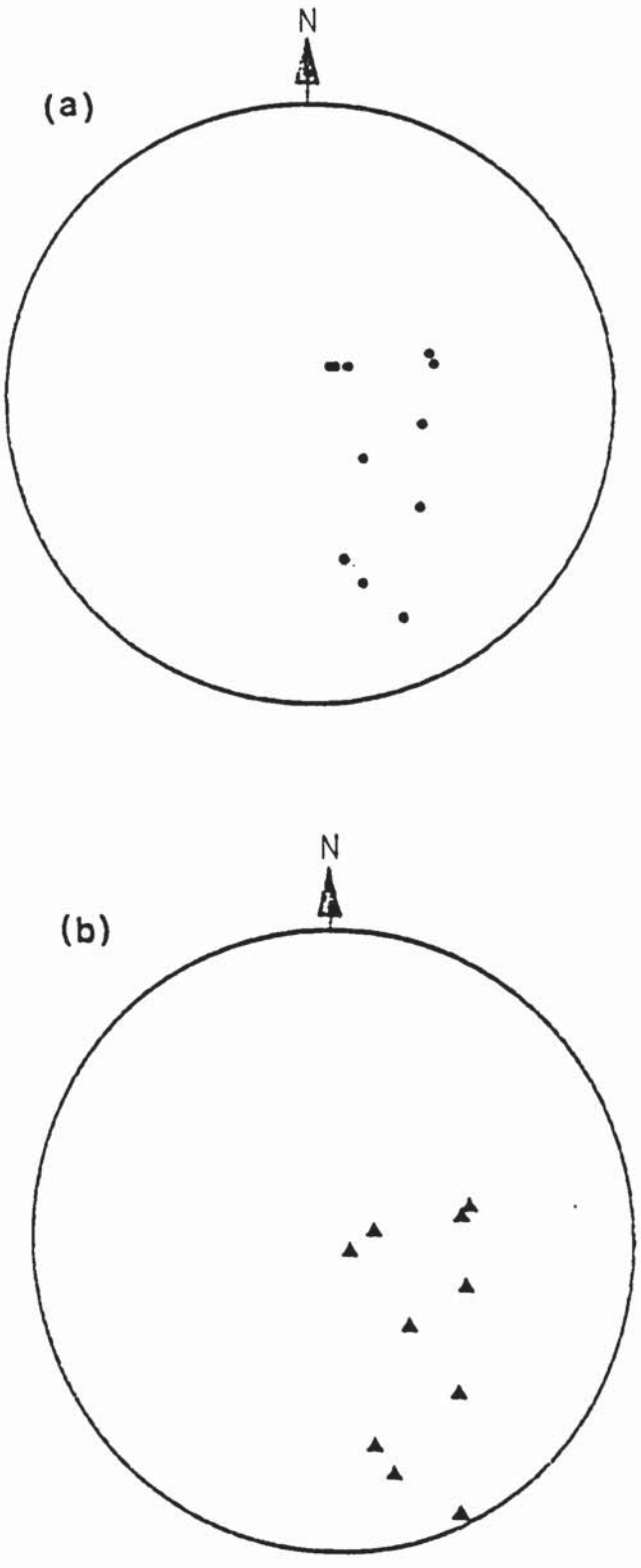

Fig. 2.7 Initial mean N.R.M. directions for the Autunian of Rillo de Gallo (a) before and (b) after correction for bedding.

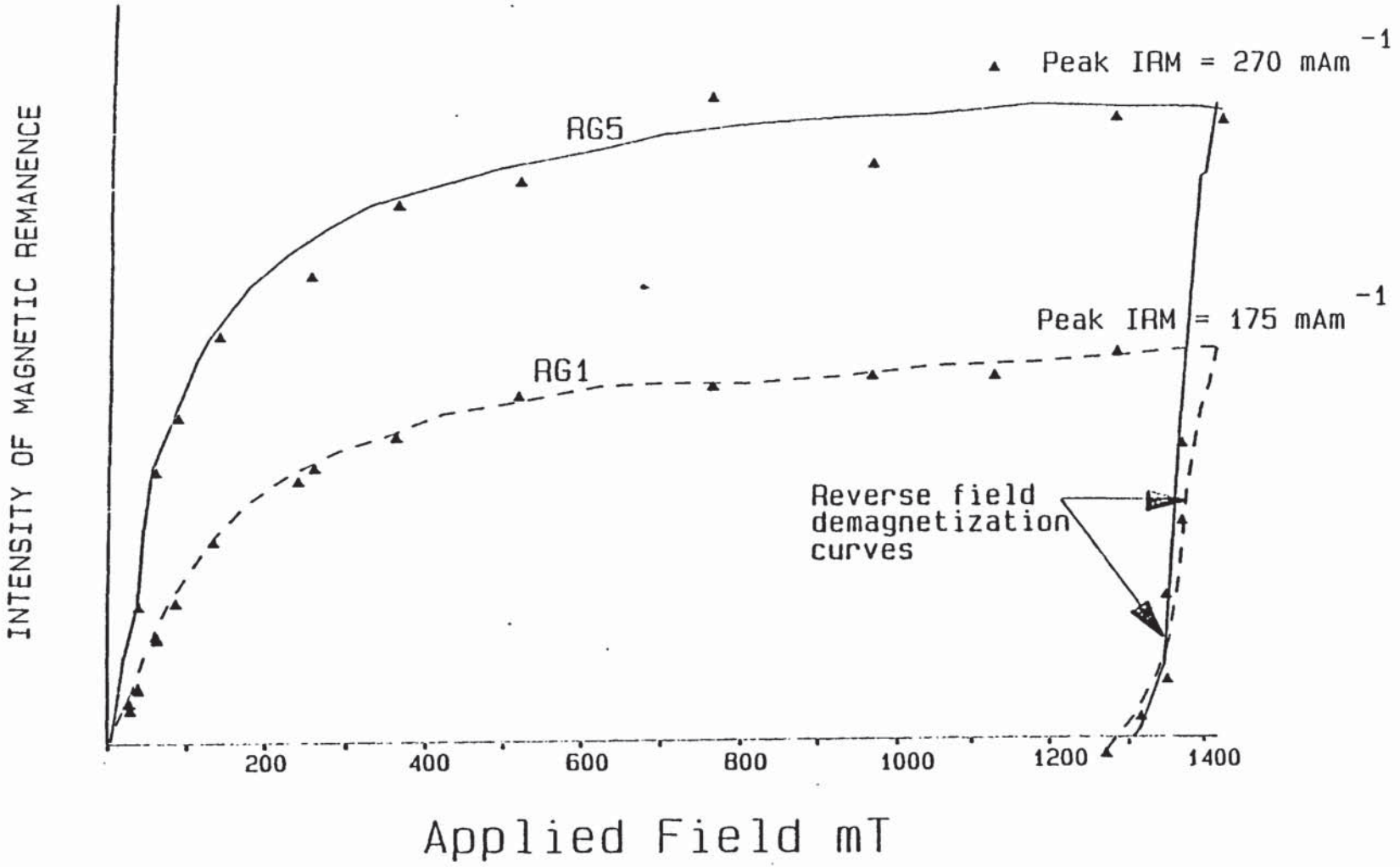

Fig. 2.8 I.R.M. acquisition and reverse field curves for the Autunian of Rillo de Gallo.

The above results suggest that the magnetic mineralogy of samples RG1 and RG5 probably consists of at least two minerals; one with a high coercivity since full saturation is not reached (probably haematite) and one or more, with a lower coercivity. This is suggested by the rapid acquisition of remanence at low field. This mineral is possibly poorly crystalline, fine grained haematite, goethite or pyrite or perhaps a mixture of any or all of these.

2.4.3 Thermal Demagnetization Results

2.4.3.1 Intensity and Susceptibility Changes

The normalized intensity and susceptibility decay curves from room temperature to 630°C are shown for specimens from Rillo de Gallo in Fig. 2.9.

Although there are exceptions, a general trend for the majority of the specimens can be identified from both intensity and susceptibility graphs.

The normalized intensity decay curves are quite variable. Most however, exhibit a slight drop in intensity between room temperature and 100°C. Between 100°C and 200°C a rapid drop in intensity is recorded by many specimens (the intensity of RG1 at 200°C is less than 5% of its original value). This drop in intensity is followed by a more stable intensity plateau between 200°C to 300°C. RG2 and RG11 are notable exceptions, both showing a sharp increase in intensity between these temperatures. Another drop in intensity occurs in the majority of specimens at temperatures above 300°C as the rocks gradually become demagnetized. This usually occurs over the temperature range 500°C to 650°C. Some specimens show a large increase in intensity at about 400°C, e.g. RG6.3.1, RG11.3.1, RG13.2.1, RG14.2.3, RG15.2.1.

The normalized susceptibility curves for the Rillo de Gallo specimens are less variable than those for intensity, especially at temperatures below 300°C. 70% of the specimens show a drop in susceptibility between room temperature and 100°C to between 65% and 80% of there original values. Susceptibilities then remain fairly constant between 100°C to 300°C. Between 350°C and 500°C specimens RG3.5.1, RG5.4.2, RG7.4.3, RG11.3.1, RG13.2.1. RG14.2.3, and RG15.2.1 all show a sharp increase in susceptibility.

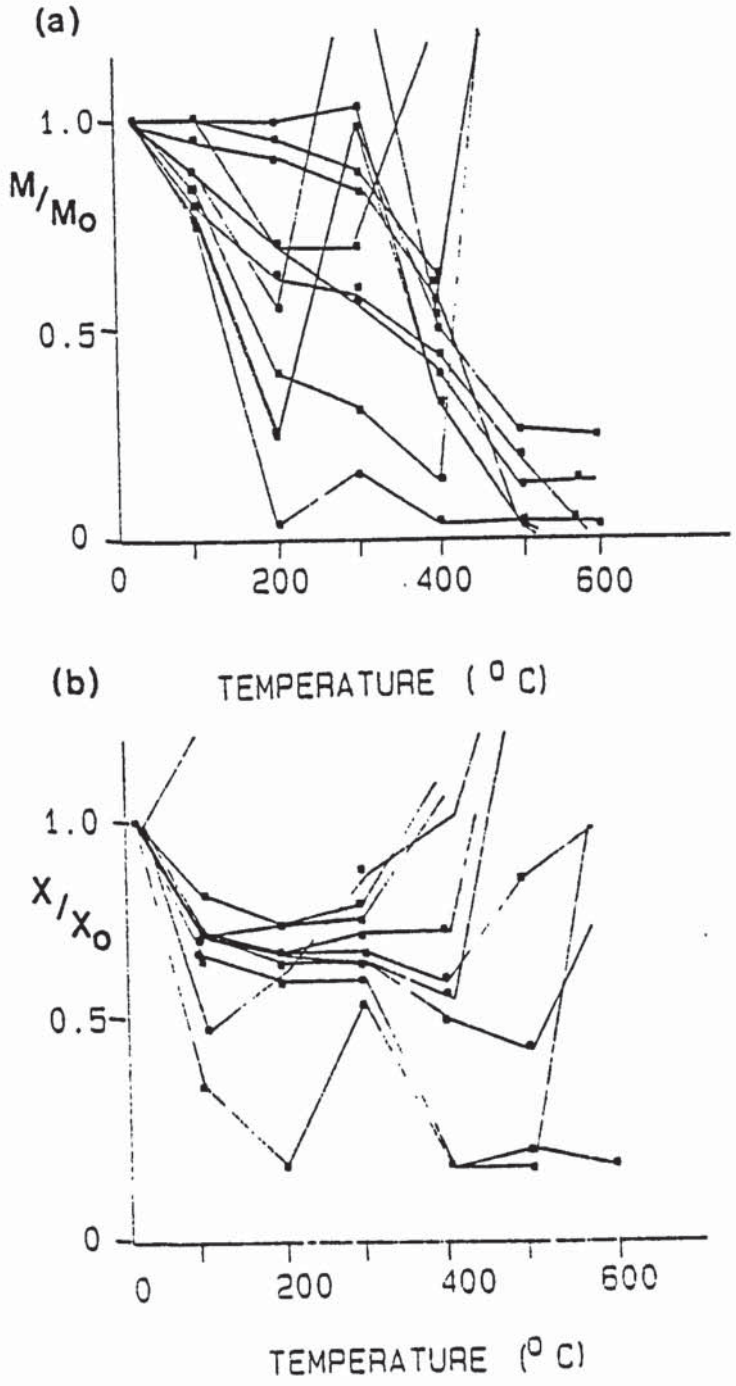

Fig. 2.9 Normalized intensity (a) and susceptibility (b) decay curves for the Autunian of Rillo de Gallo.

2.4.3.2 Discussion of Intensity and Susceptibility Results

Despite the non-uniform nature of the intensity and susceptibility curves for the Autunian of Rillo de Gallo, the results, when taken together with I.R.M. measurements, give useful information on the magnetic mineralogy of these sediments.

The rapid drop in intensity recorded by most specimens between 100°C and 200°C represents the removal of a viscous remanence probably carried by goethite. The I.R.M. curves for RG1 and RG5 (Fig. 2.8) also suggest the presence of a low coercivity mineral such a goethite.

The sharp increase in susceptibility between 350°C and 550°C in specimens RG3.5.1, RG5.4.2, RG6.3.1, RG7.4.3, RG11.3.1, RG13.2.1, RG14.2.3, and RG15.2.1 almost certainly represents the conversion of pyrite to magnetite. Increases in intensity also occur over this temperature range in many samples as a result of pyrite to magnetite conversion. At 575°C, the blocking temperature for magnetite, intensities drop rapidly as the magnetite is demagnetized. Specimens which still show a remanence at temperatures above 580°C almost certainly contain haematite.

In conclusion, the most likely magnetic mineralogy of these Autunian deposits in goethite, pyrite and haematite.

2.4.3.3 Directional Changes

One representative specimen was chosen as a pilot from each of the RG samples and subjected to partial thermal demagnetization.

The thermal demagnetization of these Autunian rocks reveals three fundamentally different types of behaviour.

The first type of behaviour is exhibited by RG6.3.1, RG7.4.3 and RG14.2.3 and is well demonstrated by RG6.3.1. In this example little directional change takes placed upon heating. The stereographic projection (Fig. 2.10a) shows an initial direction (corrected for field and bedding) with shallow positive dip and southeasterly declination. Above 100°C the direction moves southwards to an even shallower position with a negative dip. Between 200°C and 400°C this direction remains fairly constant but above 400°C moves back to a positive southeasterly direction. At temperatures above 500°C, the remanence becomes unstable and the directions are unreliable.

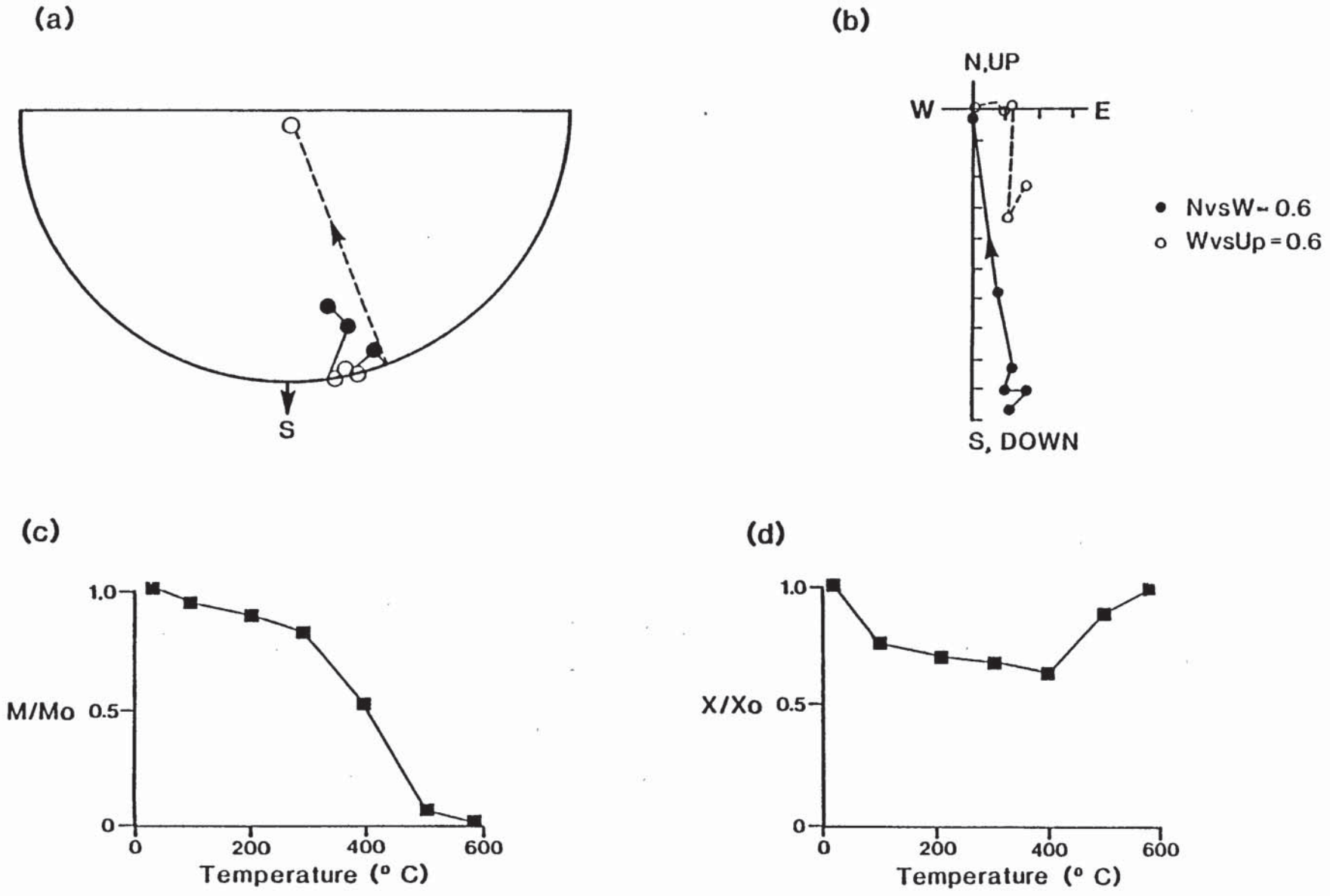

Fig. 2.10 Palaeomagnetic behaviour demonstrated by specimen RG6.3.1 during partial thermal demagnetization. (a) Stereographic projection, (b) Orthogonal vector plot, (c) Normalized intensity decay curve, (d) Normalized susceptibility decay curve.

The orthogonal vector plot for RG6.3.1 (Fig. 2.10b) shows the existence of one major component of magnetization which is present over the range 200°C to 500°C. A second, weaker component also apparently exists between room temperature and 200°C.

The normalised intensity versus temperature graph for this specimen (Fig. 2.10c) show that the predominant component of magnetization has a blocking temperature of approximately 400°C to 500°C. The rise in susceptibility above 400°C (Fig. 2.10d) suggests the presence of pyrite, which converts to magnetite at this temperature.

The most stable direction of magnetization (S.I. = 6.8) occurs over the range 200°C to 400°C and has a bedding corrected direction of D = 169.5°, I = -2.1°C, α_{95} = 3.1 with a pole position of 49°N, 154°W.

The second type of behaviour is shown by specimens RG1.3.1, RG2.4.1, RG11.3.1 and RG13. It is well demonstrated by RG1.3.1 (Fig. 2.11). The stereographic projection (Fig. 2.11a) shows that directions are steeper than those of the previous groups. Between room temperature and 100°C, bedding corrected directions lie in the northeast sector and have a fairly steep downward dip. Above 100°C the direction moves to a southward position but remains fairly steep (>50°). At temperature above 300°C the remanence is very low (0.01 mA m^{-1}) and directions are considered unreliable. The orthogonal vector plot (Fig. 2.11b) shows that the remanence is almost completely removed by 200°C.

The normalized intensity versus temperature graph (Fig. 2.11C) also demonstrates this rapid drop in remanence between room temperature and 200°C. Above 300°C the intensity falls to near zero as this component is apparently removed. Normalized changes in initial susceptibility versus temperature are shown in Fig. 2.11d. The curve shows an initial drop in susceptibility between room temperature and 200°C to 0.6 of its original value. Between 200°C and 300°C the susceptibility remains stable but at temperatures above 300°C another sharp drop is witnessed (possibly due to small amounts of maghaemite inverting to haematite?).

The final type of behaviour is exhibited by specimens RG3.5.1, RG5.4.2 and RG15.2.1. These show features characteristic of both the previously mentioned types.

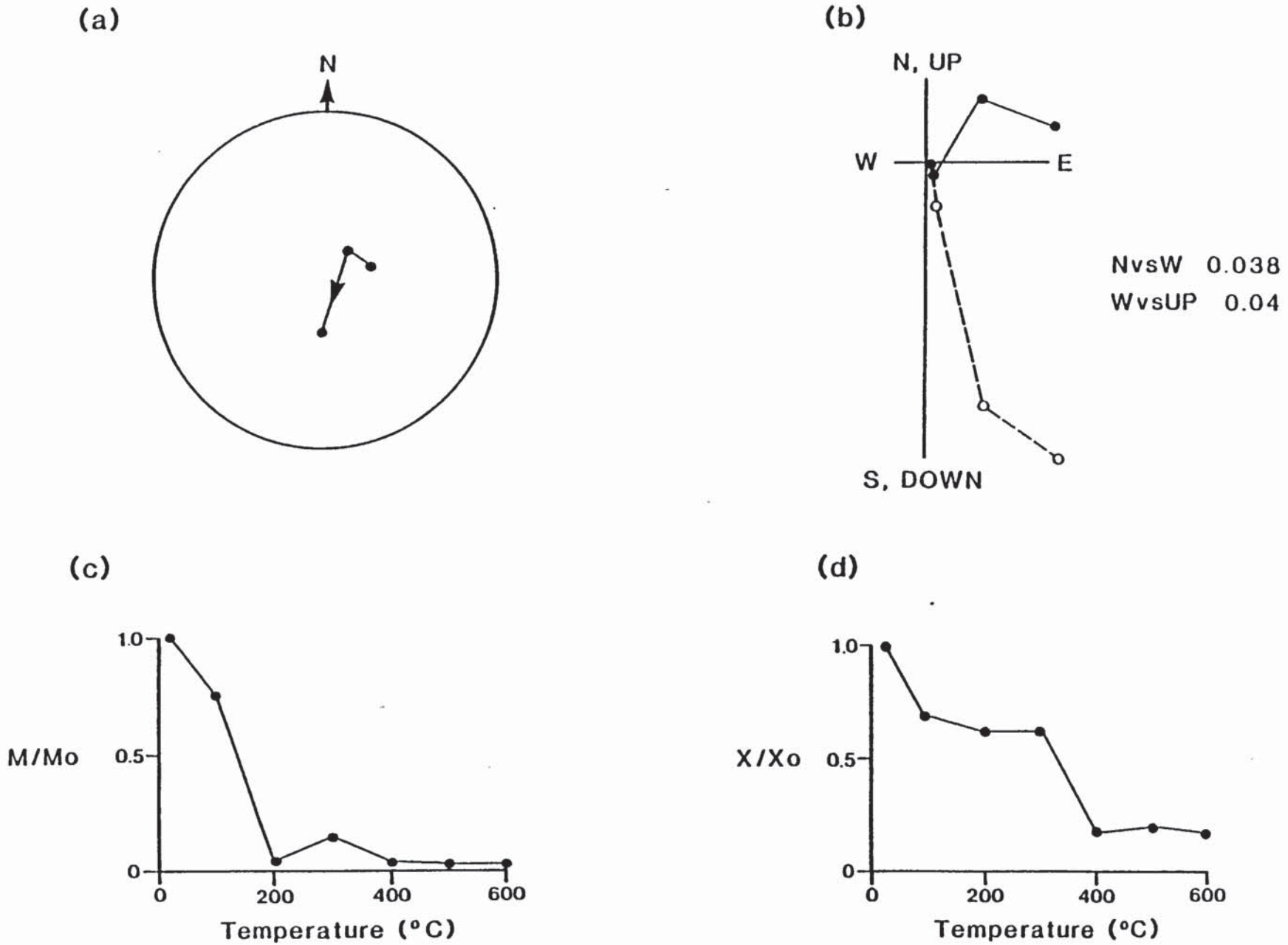

Fig. 2.11 Palaeomagnetic behaviour demonstrated by specimen RG1.3.1 during partial thermal demagnetization. (a) Stereographic projection, (b) Orthogonal vector plot, (c) Normalized intensity decay curve, (d) Normalized susceptibility decay curve.

RG5.4.2 is an example showing this type of behaviour. The stereographic projection (Fig. 2.12a) shows an initially steep downward dipping direction in the SE quadrant. Upon heating to 200°C the direction moves southwards to a shallow upward dipping position which remains stable to 400°C. Over the range 200°C to 400°C the bedding corrected direction is D = 162.5°, I = -6.7° with α_{95} = 5.3. Above 400°C, the direction remains shallow but becomes more easterly. Above 500°C, the remanence is very low and the upward dipping direction in the NW quadrant is unlikely to be reliable.

The orthogonal vector plot for RG5.4.2 (Fig. 2.12b) demonstrates the removal of one component of magnetization between room temperature and 200°C (see also the normalized intensity verses temperature curve, Fig. 2.12c). The removal of another component above approximately 300°C is also deduced from these plots.

The normalized susceptibility verses temperature curve (Fig. 2.12d) shows a drop between 20°C and 200°C and also between 300°C and 500°C indicating that changes in magnetic mineralogy are probably occurring over these temperature ranges. A sharp rise in susceptibility was is also noted above 500°C, again, probably due to changes in magnetic mineralogy.

2.4.3.4 Thermal Demagnetization Summary

The results of thermal demagnetization of the Autunian facies of Rillo de Gallo are summarised in Table 2.3. The results suggest the presence of at least two components of magnetization. Figure 2.13 shows the most stable directions of remanence isolated during thermal cleaning with their respective α_{95} values represented as circles. Figure 2.13a shows the directions in the field position and Figure 2.13b, after correction for bedding.

Two groupings can be clearly identified in both sterograms, A and B.
Group A: steep downward dipping directions.
Group B: shallow upward dipping directions in the southeast quadrant.

Mean α_{95} values from group A directions are generally larger (α_{95} = 15.6) than those from group B (α_{95} = 6.2). Stabilities in group A are lower (S.I. = 0.8 to 3.1) than those in group B (S.I. = 1.3 to 8.7).

The component of magnetization represented by group A directions is removed by heating to temperatures in excess of 200°C. Group B directions

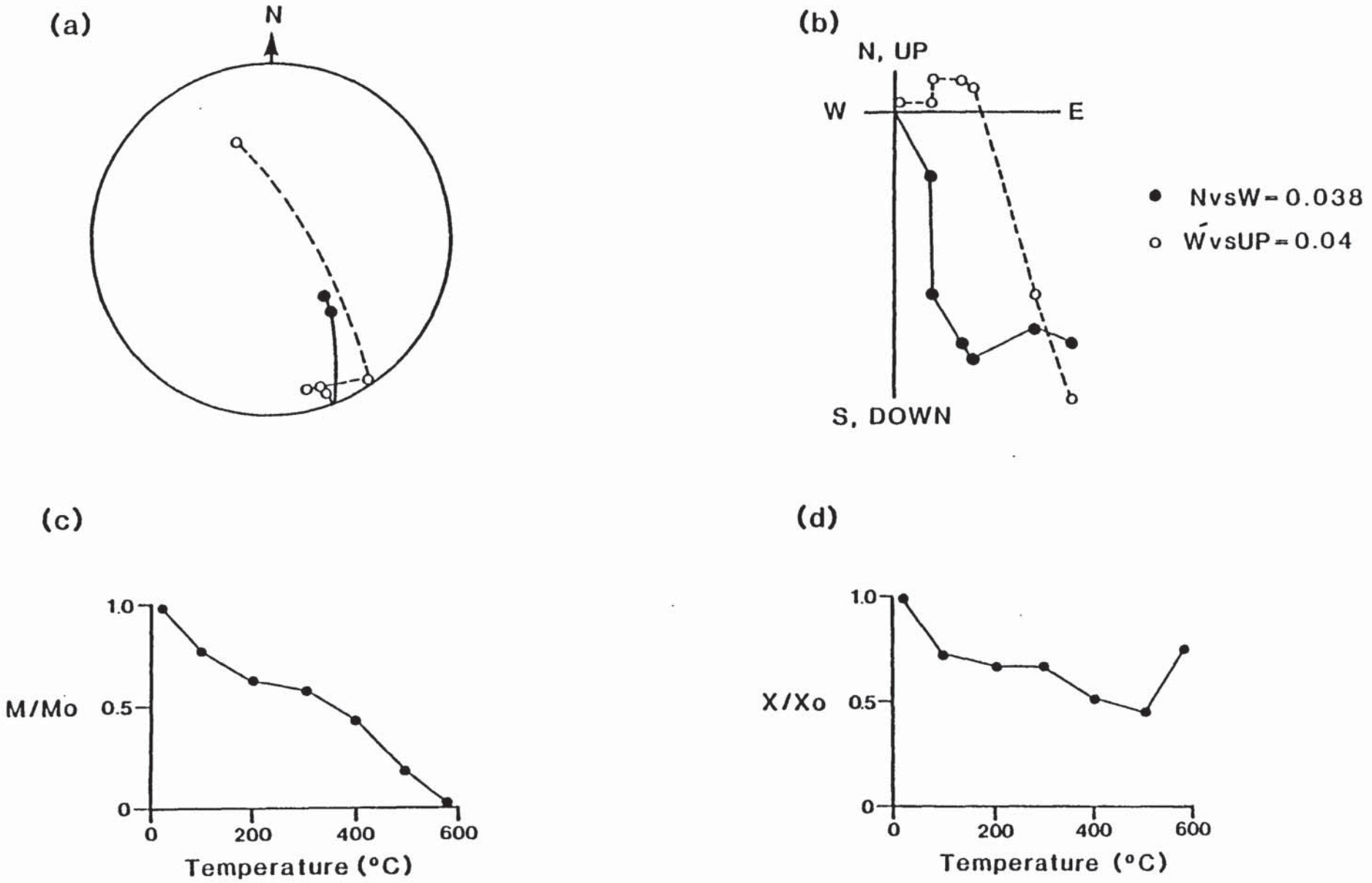

Fig. 2.12 Palaeomagnetic behaviour demonstrated by specimen RG5.4.2 during partial thermal demagnetization. (a) Stereographic projection, (b) Orthogonal vector plot, (c) Normalized intensity decay curve, (d) Normalized susceptibility decay curve.

TABLE 2.3 STEPWISE THERMAL DEMAGNETIZATION RESULTS FOR THE AUTUNIAN OF RILLO DE GALLO

		Most stable directions				Pole					Range	Directions passing 10° linearity test				
		F		P									F		P	
Specimen	S.I.	Dec(°)	Inc(°)	Dec(°)	Inc(°)	Long(°)	Lat(°)	N	R	α95(°)	(°C)	Range(°C)	Dec(°)	Inc(°)	Dec(°)	Inc(°)
RG1.3.1	0.8	11.4	86.3	133.5	75.5	18.8	20.1	6	5.46	23.3	20-500	300-500	159.9	73.1	152.4	62.5
												100-300	19.5	60.2	39.2	64.2
RG2.4.1	1.0	60.4	55.2	75.0	55.2	66.9	32.8	4	3.86	20.1	20-300	None				
RG3.5.1	1.3	184.1	31.4	180.3	23.2	357.8	-37.9	3	2.96	16.7	200-400	20-200	32.5	45.9	44.1	48.1
												300-580	162.0	2.9	162.1	7.3
RG5.4.2	4.1	162.3	3.5	162.5	-6.7	25.5	-49.2	3	3.00	5.3	200-400	200-400	147.4	11.2	147.2	0.3
RG6.3.1	6.8	169.7	9.3	169.5	-2.1	14.2	-49.0	3	3.00	3.1	200-400	400-580	170.8	9.2	170.3	-2.2
RG7.4.3	8.7	173.2	8.1	173.2	-3.1	8.7	-50.2	3	3.00	2.5	200-400	300-580	171.9	8.3	171.7	-3.0
												200-500	173.7	10.1	173.4	-1.1
RG11.3.1	1.4	89.9	67.0	121.3	62.7	36.6	10.1	4	3.93	13.8	20-300	None				
RG13.2.1	3.7	16.8	63.0	9.8	78.8	5.7	62.0	4	3.99	5.1	20-300	100-500	16.8	63.0	9.8	78.8
RG14.2.3	4.5	186.3	1.0	185.8	-12.0	348.0	-54.8	3	3.00	4.8	200-400	200-580	177.2	0.8	176.6	-11.2
												20-200	90.4	75.3	145.9	75.2
RG15.2.1	4.6	175.1	15.1	175.8	5.9	4.1	-46.0	3	3.00	4.7	200-400	200-580	239.7	-51.3	250.0	-58.2
												20-200	265.8	80.6	231.1	73.9

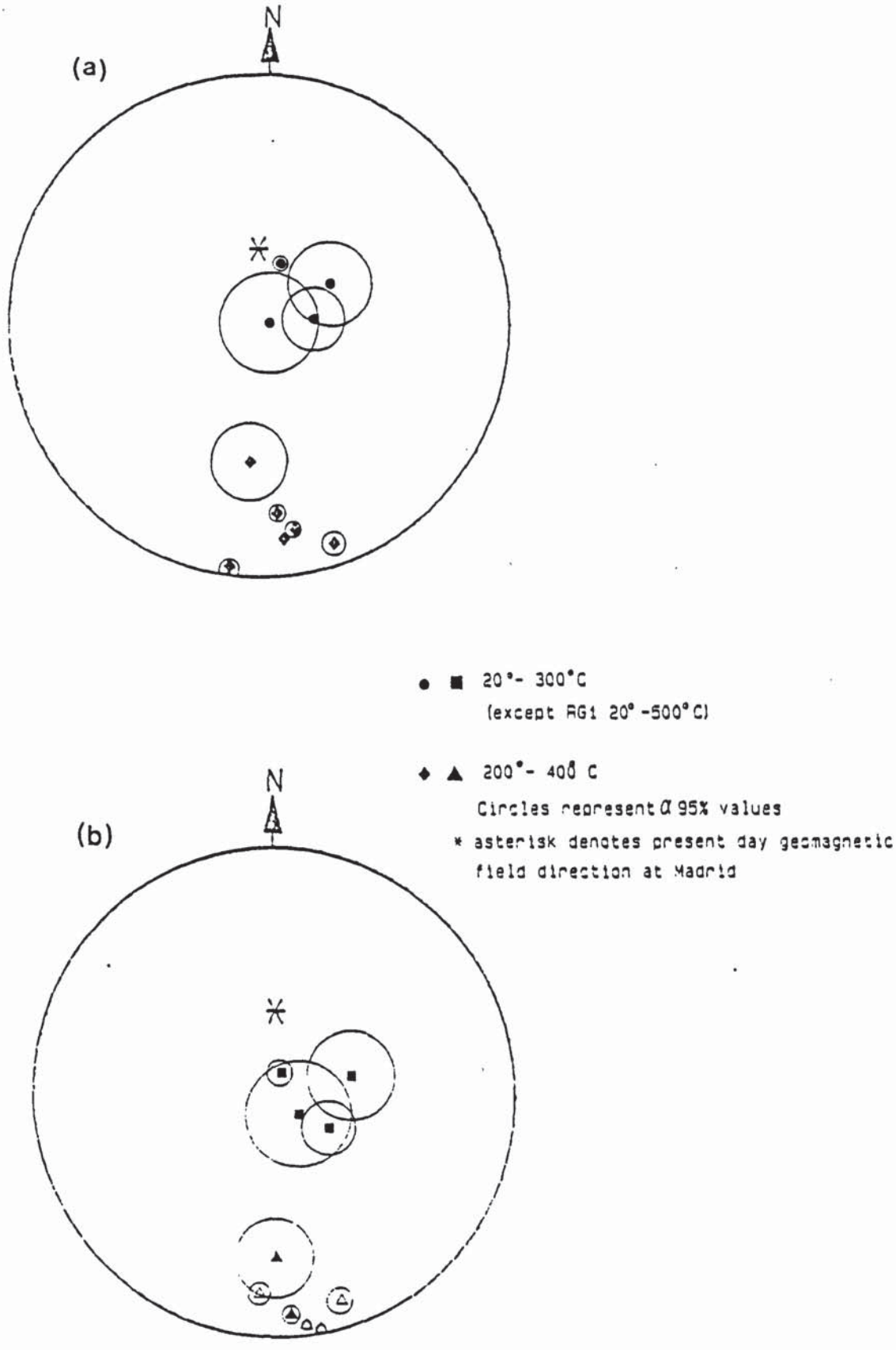

Fig. 2.13 Most stable directions isolated during partial thermal demagnetization for the Autunian of Rillo de Gallo (a) before and (b) after correction for bedding.

represent a second component of magnetization. This component is particularly stable between 200°C and 400°C and is apparently removed above 500°C.

Directions which pass the 10° linearity test are shown in Fig. 2.14. Fig. 2.14a shows field corrected directions and Fig. 2.14b, directions corrected for field and bedding. These show essentially similar results to the most stable directions shown in Fig. 2.13 i.e. two groupings one with steep downward dipping directions, stable at low temperatures and a second group demonstrating shallow upward dipping directions, stable between 200°C and 400°C.

2.4.3.5. Bulk Demagnetization Results

Bulk demagnetization results of the Autunian deposits of Rillo de Gallo are shown in Table 2.4 and Fig. 2.15. After thermal demagnetization of the pilot specimens, a temperature of 400°C was selected to demagnetize the remaining specimens.

Unfortunately, only two samples appeared to show reliable directions after heating to these temperatures (RG5 and RG6). Both of these samples revealed thermally cleaned directions lying in the southeast quadrant with fairly shallow upward dipping inclinations. The majority of the Rillo de Gallo samples demonstrated shallow bulk magnetic directions in the southwest quadrant. Their intensities were generally very low (predominantly $<0.1 mAm^{-1}$) which is at the detection limit of the magnetometer and thus well may be unreliable results incurred through instrumental error.

2.4.4 Discussion of Palaeomagnetic Results

Natural remanent intensities of magnetization for the Autunian deposits of Rillo de Gallo are low (generally less than $1 mAm^{-1}$) suggesting that they contain only very small amounts of magnetic minerals. N.R.M. directions show quite a large scatter, although two basic groups of directions can be identified.

A streaking of directions between the two groups is also seen. The first direction is steep and normal (close to the present-day geomagnetic field direction for Spain (Van der Voo, 1967)). The second is shallow and lies in the southeast quadrant (Fig. 2.7).

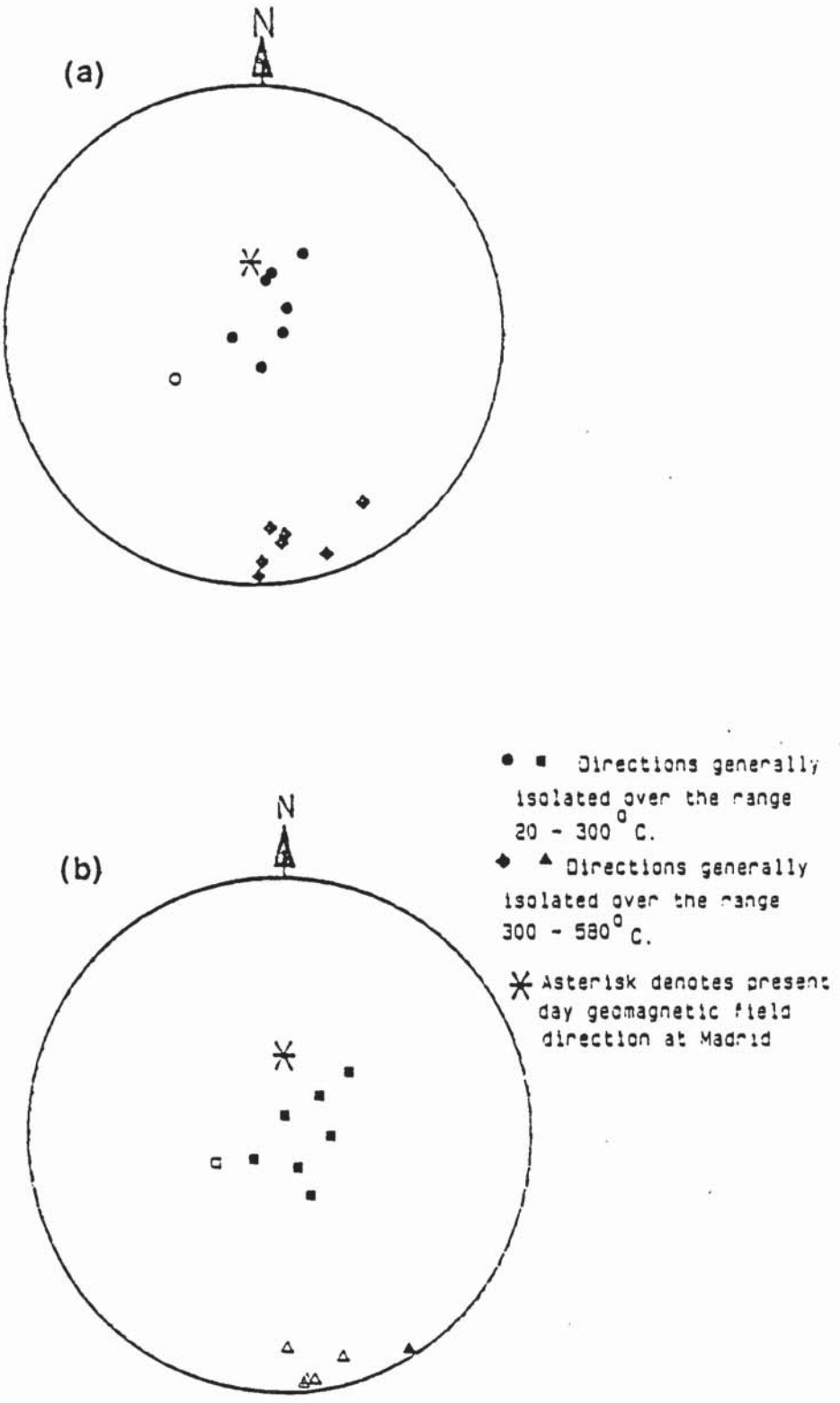

Fig. 2.14 Directions passing 10° linearity test for the Autunian of Rillo de Gallo (a) before and (b) after correction for bedding.

During thermal cleaning, the specimens exhibit one of three different types of behaviour.

1). Shallow directions in the southeast quadrant, which remained virtually unmoved upon heating e.g. RG6.3.1, RG7.4.3, RG14.2.3.

2) Steeply dipping normal directions close to the present-day geomagnetic field position for Madrid. This component was removed by heating to temperatures above 200°C to 300°C, but no significant movement took place upon further heating e.g. RG1.3.1, RG2.4.1, RG11.3.1 and RG13.2.1.

3). Two components of magnetization were identified in some specimens, one steep and normal, which is removed at temperatures above 200°C to 300°C revealing a second, shallow component, which lies in the southeast quadrant e.g. RG3.5.1, RG5.4.2, RG15.2.1.

The steep normal directions found in types (2) and (3) above, do not coincide exactly with the present-day geomagnetic field for Madrid (they lie further east). This is probably due to the influence of the Permian component of magnetization.

Intensity and susceptibility decay curves which accompany these demagnetization results show a rapid drop in intensity between 100°C to 200°C. This probably represents the removal of a viscous component of magnetization acquired recently. It may be carried by an iron hydroxide such goethite. A relatively stable remanence is shown by most specimens between 200°C to 300°C, but above 300°C the rocks gradually become demagnetised. A few specimens are not completely demagnetized until temperatures in excess of 650°C are reached, indicating that haematite is the magnetic mineral carrying this particular component of magnetization.

Large increases in intensity shown by some specimens above 400°C reflect changes in their magnetic mineralogy. The most likely explanation is the conversion of pyrite into magnetite.

TABLE 2.4 BULK DEMAGNETIZATION RESULTS FOR THE AUTUNIAN OF RILLO DE GALLO

Sample	Height (m)	F Dec(°)	F Inc(°)	P Dec(°)	P Inc(°)	Pole Long(°)	Pole Lat(°)	N	R	α95(°)	α95(°) Pole	Intensity (mAm^{-1})	Susceptibility ($mAm^{-1}nT^{-1}$)	Temp (°C)
RG1	12	230.8	1.8	230.5	1.9	297.2	2.8	4	3.99	5.1	4.8	0.07	19.50	400
RG2	18	245.6	1.0	254.4	1.3	296.1	27.3	4	3.80	24.7	27.3	0.06	12.50	400
RG3	26	238.2	1.5	237.8	3.0	292.1	-22.6	7	6.90	8.0	9.5	0.06	0.80	400
RG5	112	161.7	-11.7	163.0	-21.9	29.1	-55.7	7	6.71	13.5	12.6	0.16	153.70	400
RG6	121	168.9	8.3	168.8	-3.1	15.5	-49.4	6	5.99	3.6	2.9	4.37	220.60	400
RG7	127	212.7	8.3	211.7	2.3	316.8	-38.2	7	6.81	10.9	11.2	0.17	90.30	400
RG13	197	161.4	79.7	162.7	79.7	4	22.8	5	3.93	45.8	60.4	0.05	49.52	300
RG14	202	205.2	6.5	205.2	-7.5	323.0	-44.9	8	7.63	13.1	14.9	0.13	25.85	400
RG15	218	222.6	13.1	222.0	4.0	308.9	-30.8	8	7.38	17.3	21.8	0.06	347.90	400

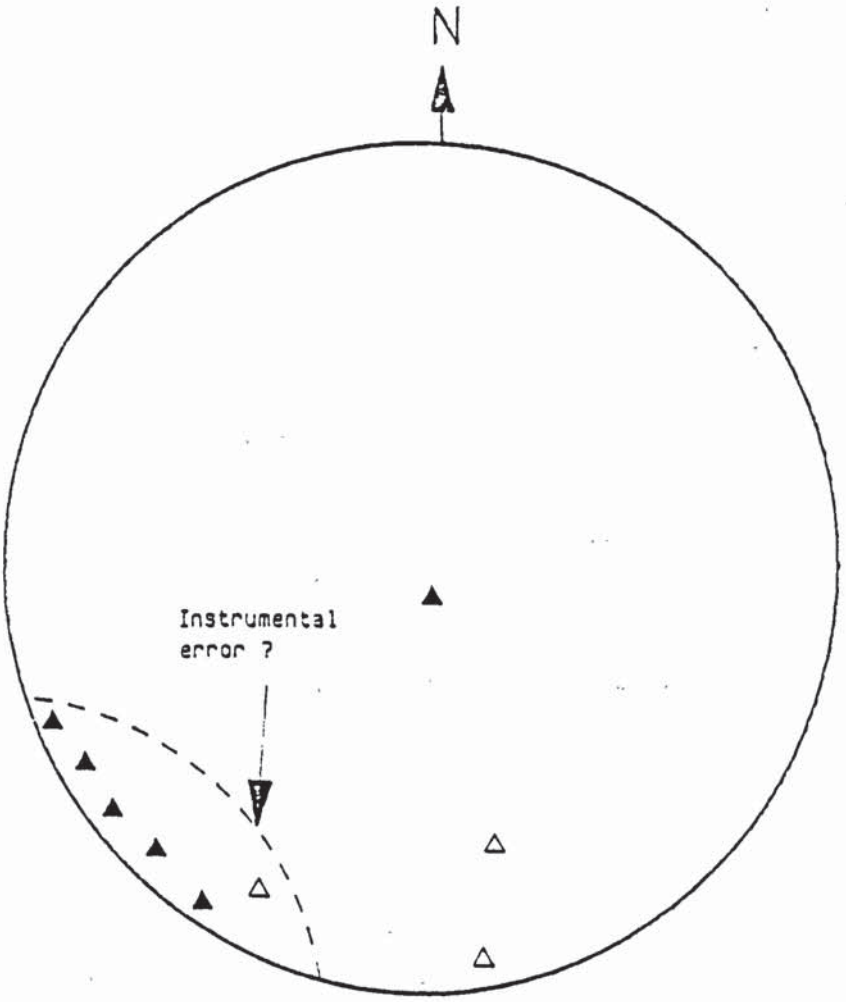

Fig. 2.15 Mean bedding corrected directions isolated during bulk thermal demagnetization of Autunian samples from Rillo de Gallo.

Previous palaeomagnetic studies on the Permian of the Iberian Peninsular date back to 1960 when Van der Lingen published results on andesites and sandstones from the Central Pyrenees. Since that time, a number of other workers have published their results of palaeomagnetic studies carried out on Permian rocks (Table 2.5, Figs. 2.16 and 17).

Figure 2.16 shows previously published palaeo-directions for Iberian rocks of Permian age (No's. 1-8). Directions for Permian rocks from 'Stable Europe' (Letters A-C) are also shown. The Rillo de Gallo samples exhibit directions very close to those previously published for the Spanish rocks (Mean: D = 174.5°, I = 1°) and are consistently different to those of Stable Europe.

Palaeopole positions are shown in Figure 2.17. Again, the Rillo de Gallo samples lie close to previously published Permian pole positions for Spain (Mean pole position for Rillo de Gallo is 47.5°N, 173.5°W).

These results are further evidence for the rotation of Iberia during the Mesozoic (see section 1.5.3.2)

2.5 RELATIONSHIP BETWEEN DIAGENESIS AND PALAEOMAGNETISM

A number of relationships have been noted between the detrital and diagenetic mineralogy of these deposits and their palaeomagnetic results:-

1. The very low initial intensities shown by most samples (Table 2.2) is due to the presence of only small amounts of magnetic minerals found in these deposits. This is due, in turn, to the mineralogy of the source rock and depositional environment.

2. Permian directions of magnetization have been isolated for most Rillo de Gallo samples (see Table 2.5 & Fig. 2.16). RG6, RG7 and RG14 have the highest intensities and most stable Permian directions. The samples are not fully demagnetized until temperatures in excess of 600°C are reached, suggesting that haematite is the principal remanence carrier.

3. Diagenetic studies reveal the presence of only very small amounts of detrital haematite in these deposits. Furthermore, samples with the

TABLE 2.5 PREVIOUSLY PUBLISHED PERMIAN DIRECTIONS AND POLES FOR STABLE EUROPE AND IBERIA TOGETHER WITH THOSE FOUND FOR THE AUTUNIAN OF RILLO DE GALLO

Letter/ No.	Locality (formation)	D(°)	I(°)	N	α95(°)	Lat	Long	Reference
STABLE EUROPE								
A	Exeter, England (Volcanics)	198	-25	23	7°	49.5°N	148.5°E	Zijderveld (1967)
B_1	Nahe region Germany (Volcanics)	196	-18	34	8°	48°N	168°E	Nijenhuis (1961)
B_2	Nahe region Germany (Volcanics)	201	-9	28	4°	42°N	163°E	Nijenhuis (1961)
C	Nideck region France (Volcanics)	192.5	-12.5	37	5°	47°N	169°E	Roche et al. (1962)
IBERIA								
1	Rio Aragon C.Pyrenees (Andesites)	152	-22.5	14	6°	51°N	133°W	Schwarz (1962)
2	Anayet C.Pyrenees (Andesites and Sandstones)	164	-14	11	10°	52°N	154°W	Van der Lingen (1960)
3	Serra del Cadi E.Pyrenees (Andesites)	169.5	-3	41	4°	48.5°N	163°W	Van Dongen (1967)
4	Borges Catelan Coast (Granodiorites)	168	-4	-	-	-	-	Banda et al. (in press)
5	Atienza C.Spain (Andesites)	165	+6.5	25	2°	-	-	Hernando et al. (1980)
6	Viar Sevilla (Dikes and Sills)	155.5	+10.5	14	4°	41°N	152°W	Van der Voo (1969)
7	Viar Sevilla (Redbeds)	151	+2	8	4.5°	42.5°N	144°W	Van der Voo (1969)
8	Bacaco Coimbra Portugal (Redbeds)	149	+11	17	5°	35.5°N	148.5°W	Van der Voo (1969)
RG3	Rillo de Gallo, C.Spain (Volcaniclastics)	180	+23	3	17°	38°N	178°E	This study
RG5	Rillo de Gallo, C.Spain (Volcaniclastics)	163	-7	3	5°	49°N	154°W	This study
RG6	Rillo de Gallo, C.Spain (Volcaniclastics)	169.5	-2	3	3°	49°N	166°W	This study
RG7	Rillo de Gallo, C.Spain (Volcaniclastics)	173	-3	3	2.5°	50°N	171°W	This study
RG14	Rillo de Gallo, C.Spain (Volcaniclastics)	186	-12	3	5°	55°N	168°W	This study
RG15	Rillo de Gallo, C.Spain (Volcaniclastics)	176	+6	3	5°	46°N	176°W	This study
Mean	Rillo de Gallo, C.Spain (Volcaniclastics)	174.5	+1	6	12.5°	47.5°N	173.5°W	This study

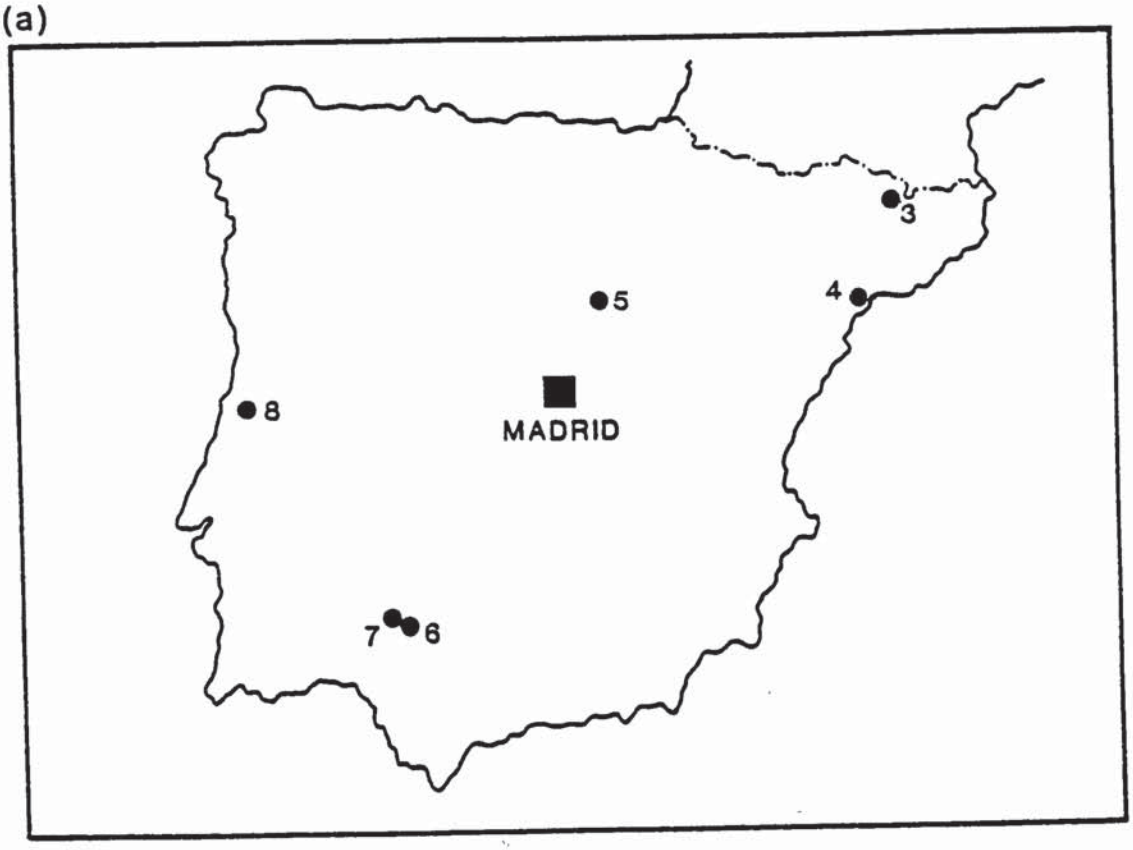

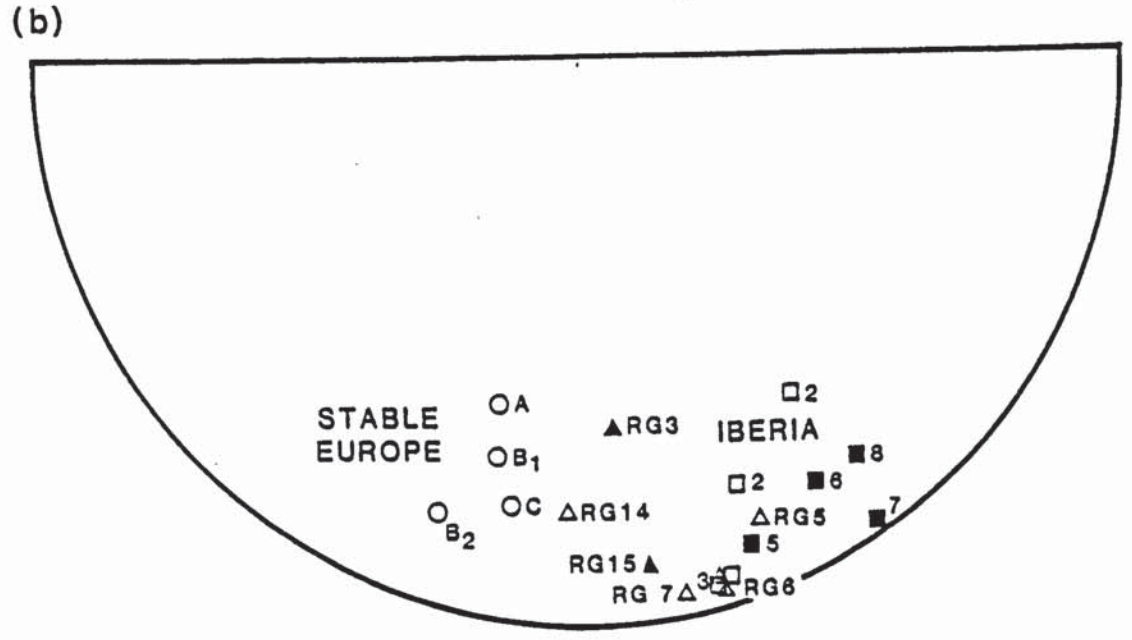

Fig. 2.16(a) Sketch map of the Iberian Peninsula showing previous Permian sampling sites (numbers refer to Table 2.5).
(b) Some Permian directions for Stable Europe and Iberia compared with mean stable directions for Rillo de Gallo .

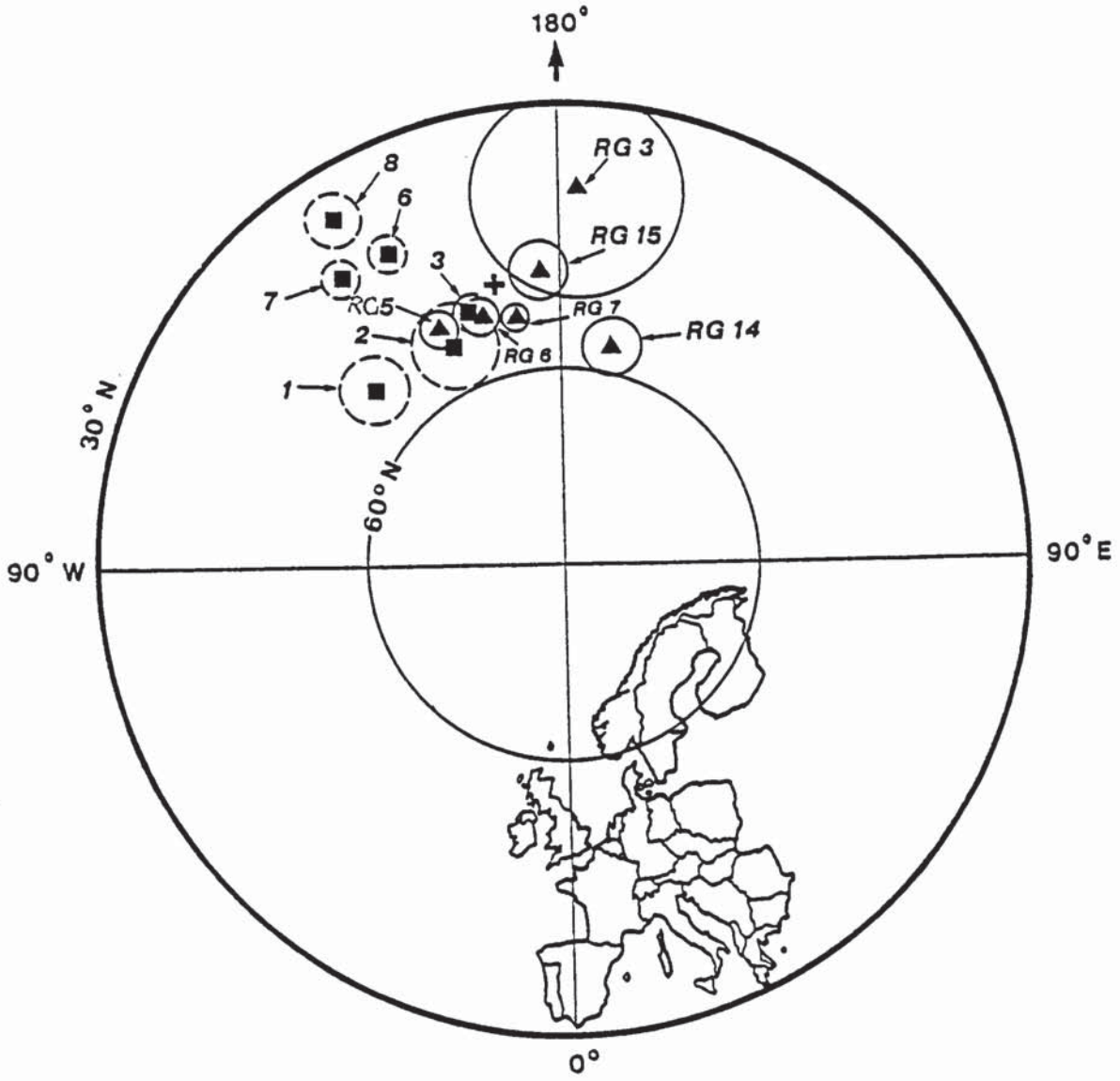

Fig. 2.17 Palaeopole positions for the Permian of Iberia.
■ Previously described Permian pole positions from Iberia (Numbers refer to Table 2.5).
▲ Palaeopole positions obtained from the Autunian of Rillo de Gallo (200-400°C).
+ Mean pole position for most stable RG directions.
N.B. Circles represent α_{95} values.

highest initial intensities contain no more detrital haematite than is found in those having significantly lower intensities (Table 2.3). This suggests that detrital haematite is not responsible for the Permian directions shown by RG6, RG7 and RG14.

These samples do, however, contain irregular patches of calcite with associated iron oxide (Fig. 2.3a). Early diagenetic changes in subsurface geochemistry have led to the dissolution of early formed ferroan dolomite or siderite cements. Oxidizing waters flowing through the deposits results in the dedolomitization of ferroan carbonates with co-precipitation of non-ferroan calcite and iron oxide (Plate 2.3a and e) (see Section 2.3.4).

It is this fine grained haematite which carries the stable Permian remanence in these deposits. It is an early chemical remanent magnetization C.R.M. and makes it possible to date the dedolomitization event as Permian.

4. Sharp increases in susceptibility (and in many cases intensity) are recorded by some of the Rillo de Gallo samples between 350°C and 55°C (Fig. 2.9). This is probably due to the conversion of pyrite to magnetite which commonly occurs over this temperature range (Turner, 1975). Petrographic studies show that early diagenetic pyrite is present in small amounts within these rocks but much of it has been subsequently oxidised to haematite (Fig. 2.3e). It is difficult to ascertain whether this oxidizing reaction occurred during early or late diagenesis.

X-ray diffraction and petrographic evidence exists for the presence of goethite in these deposits (Fig. 2.5). This is a common alteration mineral, often formed by theweathering of haematite. It is unstable at temperatures above 120°C and thus explains the rapid drop in intensity recorded by most samples between 100°C and 200°C (Fig. 2.9). The steep normal component of magnetization has a blocking temperature of between 100°C and 200°C (e.g. Fig. 2.11b and c), so it is likely that goethite carries this recent component.

CHAPTER THREE

THE AUTUNIAN OF PALMACES

3.1 INTRODUCTION

In addition to Rillo de Gallo, the Lower Permian, Autunian facies was also sampled at Palmaces. The Palmaces section lies approximately 85 km west of the Rillo de Gallo section, close to the town of Palmaces de Jadraque 10° 45' 36"W, 41° 3' 18"N (Fig. 2.2). The section has a total thickness of over 650m with almost 250m of the Autunian facies exposed. Dips are shallow (<20°) and towards the south or southeast.

3.2 STRATIGRAPHY AND SEDIMENTOLOGY

Autunian sediments are exposed along the margins of a large reservoir approximately 2 km northwest of the town of Palmaces de Jadraque (Fig. 3.1, Plate 3.1a). They lie unconformably over a considerable palaeo-relief of Hercynian metamorphic rocks (Sopena, 1979), and are unconformably overlain themselves by the Lower Triassic, Buntsandstein facies. This angular unconformity is well exhibited on the eastern side of the Arroyo del Rizuelo (Rizuelo stream), (Plate 3.1b).

Five lithostratigraphic units have been established for the Permian of this area (Sopena, 1979) (Fig. 3.2). The lowest three, RS1 (Lower Palmaces conglomerates), RS2 (Palmaces volcanics and sediments) and RS3 (Palmaces sandstones) are generally grey, white, green and black in colour. At this locality, their thicknesses are 8m, 50m and 25m respectively. The two upper units RS4 (Palmaces siltstones) and RS5 (Upper Palmaces conglomerates) are much thicker, having average thicknesses of 154m and 350m, respectively. At this locality however, the top part of RS4 and the whole of RS5 are covered by the Palmaces reservoir. These units are red in colour and similar in type to the "red Permian" or "Saxonian" facies. The presence of Estheria tenella (Jordan), however, in the upper part of RS4 suggests that this unit is also of Autunian age (Sopena, 1979).

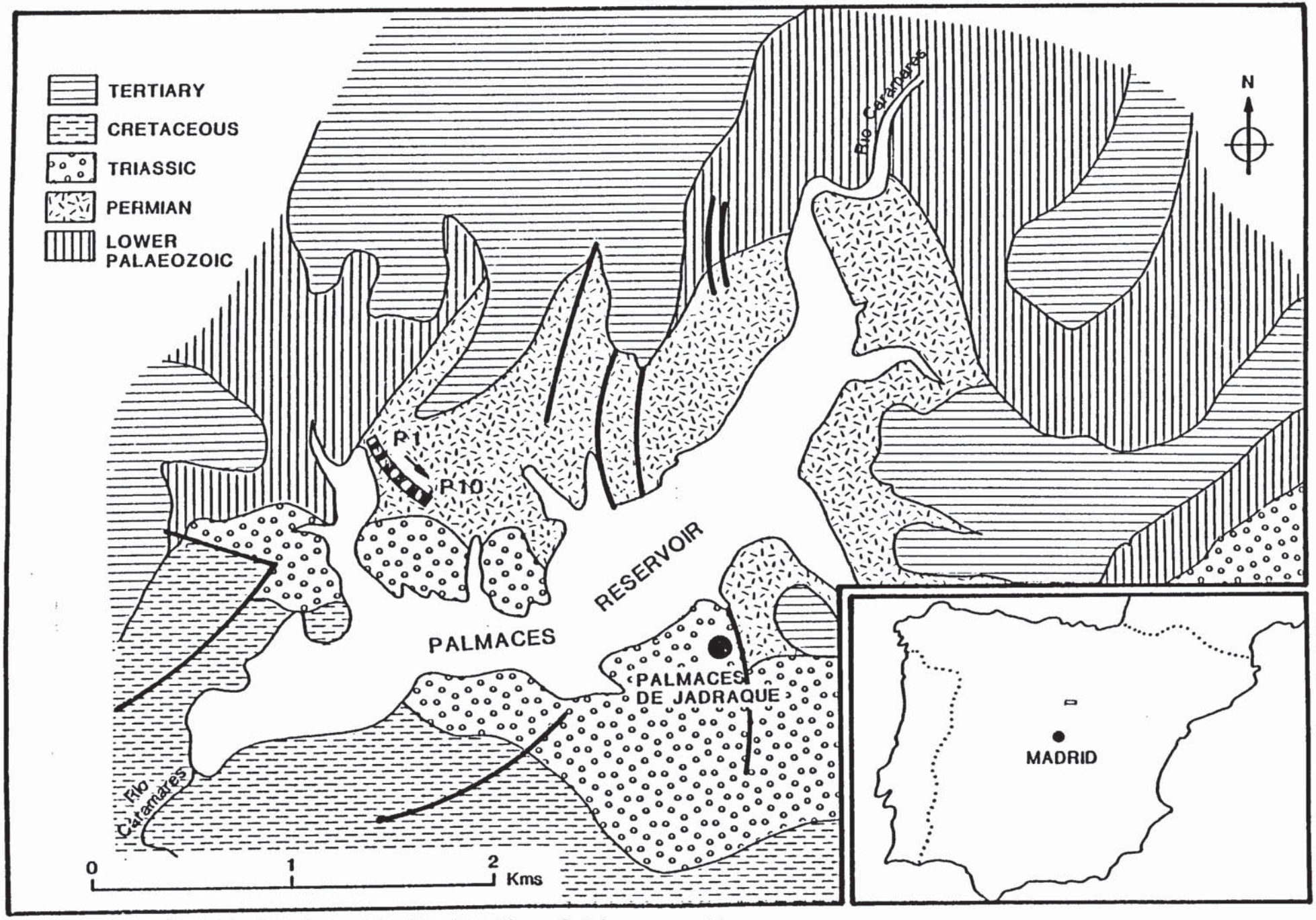

Fig. 3.1 Geological sketch map showing location of Palmaces section.

Fig. 3.2(a) Lithostratigraphic units of the Permian and Triassic of Palmaces (after Sopena, 1979).
(b) Sedimentological column compiled by Sopena (1979) showing horizons from which Palmaces samples were taken.

Ten samples were collected from the Autunian of Palmaces (Fig. 3.2). Samples P1-P4 from unit RS2, P5 from RS3 and P6-P10 from unit RS4.

3.3 DIAGENESIS

3.3.1 Introduction

Compositionally the samples from Palmaces are quite variable. P1 and P4 are rhyodacitic tuffs. The remainder are all sandstones, ranging in composition from lithic arkose (P5) to lithic greywacke (P10) (Fig. 3.3). Grain sizes vary from very fine sand (P10) to medium sand (P5).

The results of point count analyses are shown in Appendix VII. The sandstones have a mineralogy consisting predominantly of quartz (detrital and authigenic, 25%-36%), rock fragments (8%-45%), feldspars (1%-16%), clay minerals (1%-22%), micas (1%-5%), iron oxide cement (1.5%-15%), carbonate cement (6%-30%). Heavy minerals, detrital opaques and zeolites account for a further 1%-12%. Visible porosities of between <1% and 2% make up the remaining fraction of the deposits.

3.3.2 Diagenetic Transformations

The two volcanic samples from Palmaces, P1 and P4, are devitrified rhyodacitic tuffs. They are composed, predominantly, of cryptocrystalline silica. A slight perlitic texture exists in places, evidence for the original glassy nature of the tuff. Small subangular fragments of quartz are present in the matrix and many have strained extinction and/or fractures. Muscovite laths exhibiting a preferred orientation are also common.

Quartz is the most abundant mineral in these deposits. Monocrystalline quartz predominates in the finer grained units of RS2 and RS4, but in the coarser Palmaces sandstones (RS3), polycrystalline quartz is more abundant. Many quartz grains contain inclusions of rutile or zircon. Marginal replacement of quartz by kaolinite is fairly common as is the partial replacement of quartz grains by aggressive carbonate cements (Plate 3.2a). Authigenic quartz, although found in all samples, is not

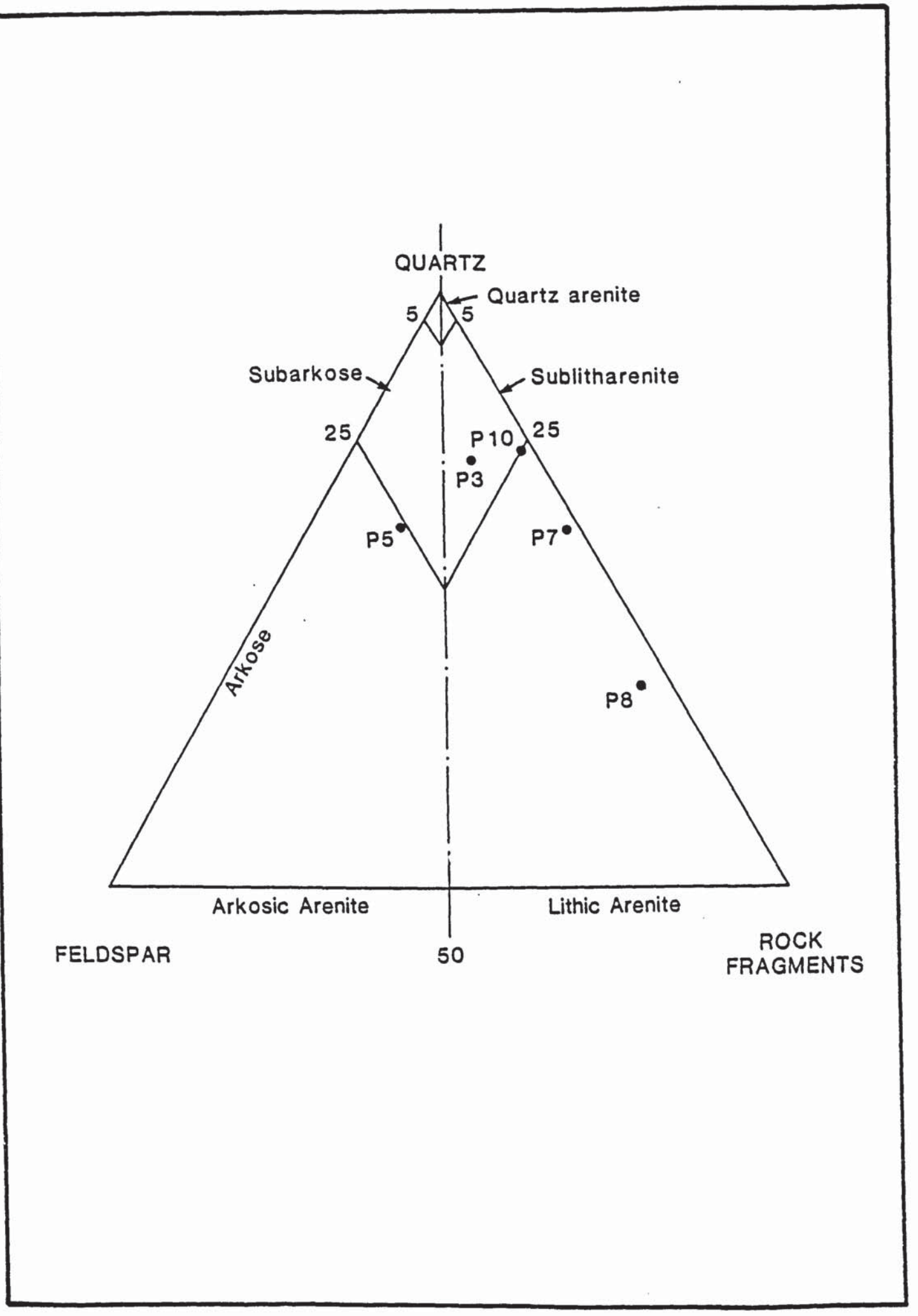

Fig. 3.3 Q.F.R. ternary diagram showing composition of sandstones from the Autunian of Palmaces.

well developed. It occurs as syntaxial overgrowths on detrital grains.

Feldspars consist of both potassium (orthoclase and microcline) and plagioclase varieties, although amounts of the latter are very small (<0.5%). Overgrowths of authigenic potassium feldspar are seen on some detrital feldspars. Dissolution and etching of grains is common and many have been partially replaced by clays (illite, illite/smectite and kaolinite). Illite and illite/smectites tend to replace feldspars along their margins or cleavage traces but kaolinite often replaces the core of the grains (Plate 3.2b).

Rock fragments are abundant in these sediments, comprising up to 45% of the total. Sedimentary, metamorphic and igneous rock fragments are all represented. The igneous rock fragments consist of granitic grains, some showing graphic texture and volcanic grains, mainly composed of cryptocrystalline silica. Many of the rock fragments show considerable diagenetic replacement by clays, and/or iron and iron-titanium oxides (Plate 3.2c). Volcanic and metamorphic rock fragments are especially prone to this type of replacement.

Both biotite and muscovite micas are found in small quantities in these rocks. Muscovite is slightly more abundant, probably because of its greater resistance to weathering. It commonly shows replacement by illite or neomorphic kaolinite. Replacement of biotite by haematite is also seen in these rocks. It first develops in the biotite cleavages but may eventually replace the entire grain.

Clays are abundant in the Autunian of Palmaces. X-ray diffraction studies carried out on Samples P3 and P8 show that, in order of abundance, Montmorillonite, illite, kaolinite and chlorite are present (Table 3.1). Although, the order of abundance of the clays is the same for both samples, P3 has a larger proportion of montmorillonite than P8 but contains relatively less kaolinite.

Table 3.1 Results of semi-quantitative analysis carried out on the <2μm fraction of clays from Autunian of Palmaces

	Illite	Kaolinite	Mont	Chlorite	Total
P3	21	7.5	70	1.5	100
P8	31.5	19.5	45	4	100

Figures 3.4 and 3.5 show diffractograms for P3 and P8 respectively. The strong peak at 12Å for montmorillonite in P3, migrates upon glycolation, to 16Å, due to the expansion of the crystal lattice.

Both allogenic and authigenic clays are present in these sediments. Allogenic clay is best identified using the S.E.M.. It typically occurs as thin grain coatings composed of mixed sized platelets having orientation tangential to the detrital grain boundary (Plate 3.2d).

Allogenic clay accounts for only a minor proportion of the total clay content of these sediments. It is most common in the deposits which overlie relatively impervious horizons, such as mudstones or dolostones, since these acted as barriers to further downward migration of surface water.

Authigenic clays replace feldspars, rock fragments, mica and quartz. As previously mentioned, replacement may occur at the grain margins or within the grain itself (Plate 3.2b). It may also occur along crystallographic planes or in an irregular manner. Some grains have been completely pseudomorphed by clay (Plate 3.2e) and many of these weakened grains have been crushed during compaction of the sediments. These two processes create epimatrix and pseudomatrix respectively, resulting in a reduction in the porosity and permeability of the rocks.

In addition to clays, other authigenic minerals present in these rocks include quartz, dolomite, calcite, siderite, analcime and haematite.

Authigenic quartz, although present in all samples, is not well developed. It is most abundant in sample P3, where it accounts for 4% of the total. It occurs as syntaxial overgrowths on detrital grains (Plate 3.2f) but is sometimes difficult to identify due to the frequent absence of a dust line between host grain and overgrowth.

Dolomite is the most abundant cementing mineral in these sediments. Percentages vary from 6% in P8 to 30% in P3. Staining indicates that it is predominantly non-ferroan dolomite, although patches of ferroan dolomite are also present. It generally occurs as a poikilotopic pore filling cement but in places appears to be replacive, corroding the margins of the framework grains (Plate 3.3a). In more extreme cases relict cleavage traces or replacement clays are all that remain of feldspar grains, now pseudomorphed by dolomite.

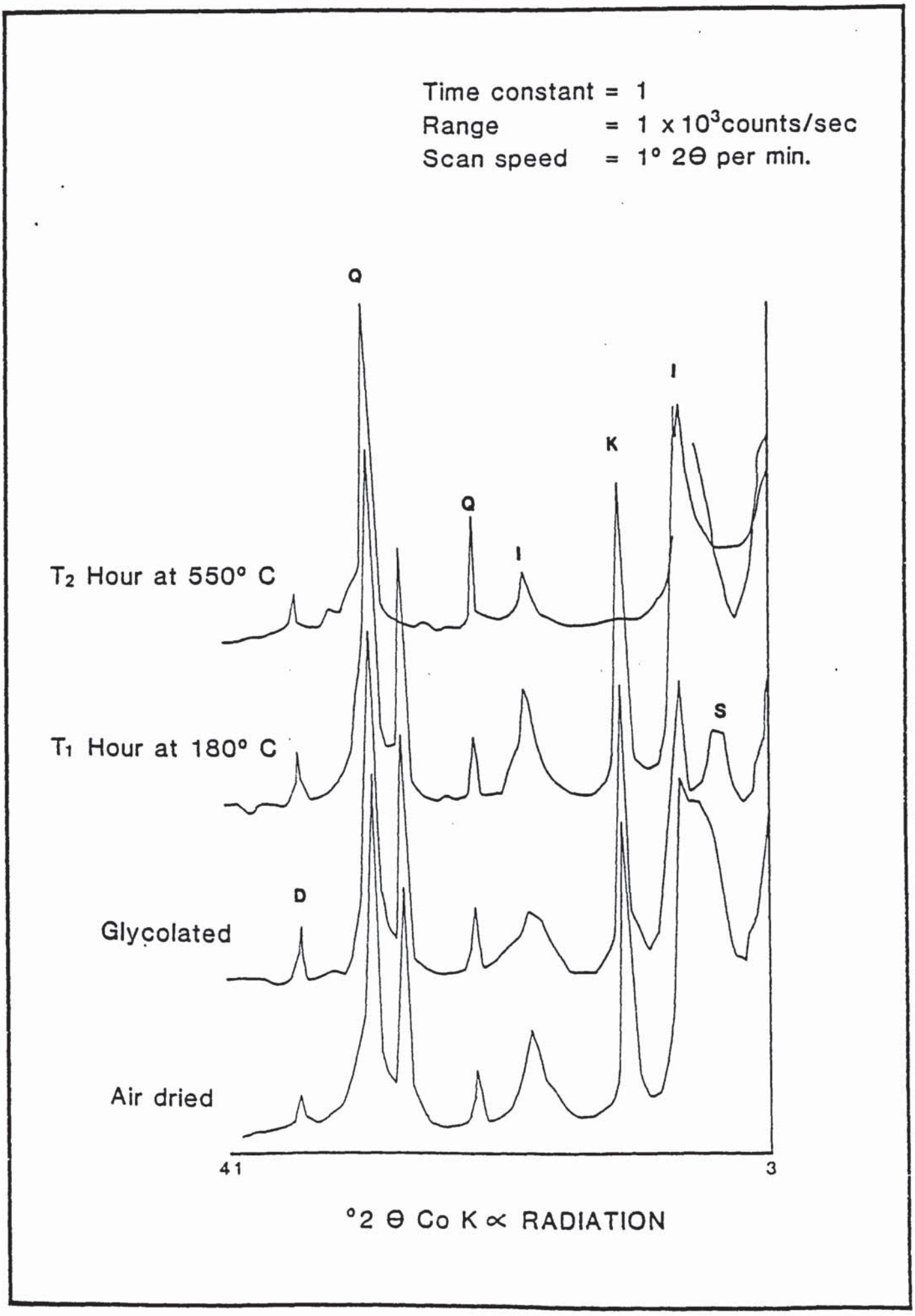

Fig. 3.4 X-ray diffractions for the <2μm clay fraction of Sample P3.

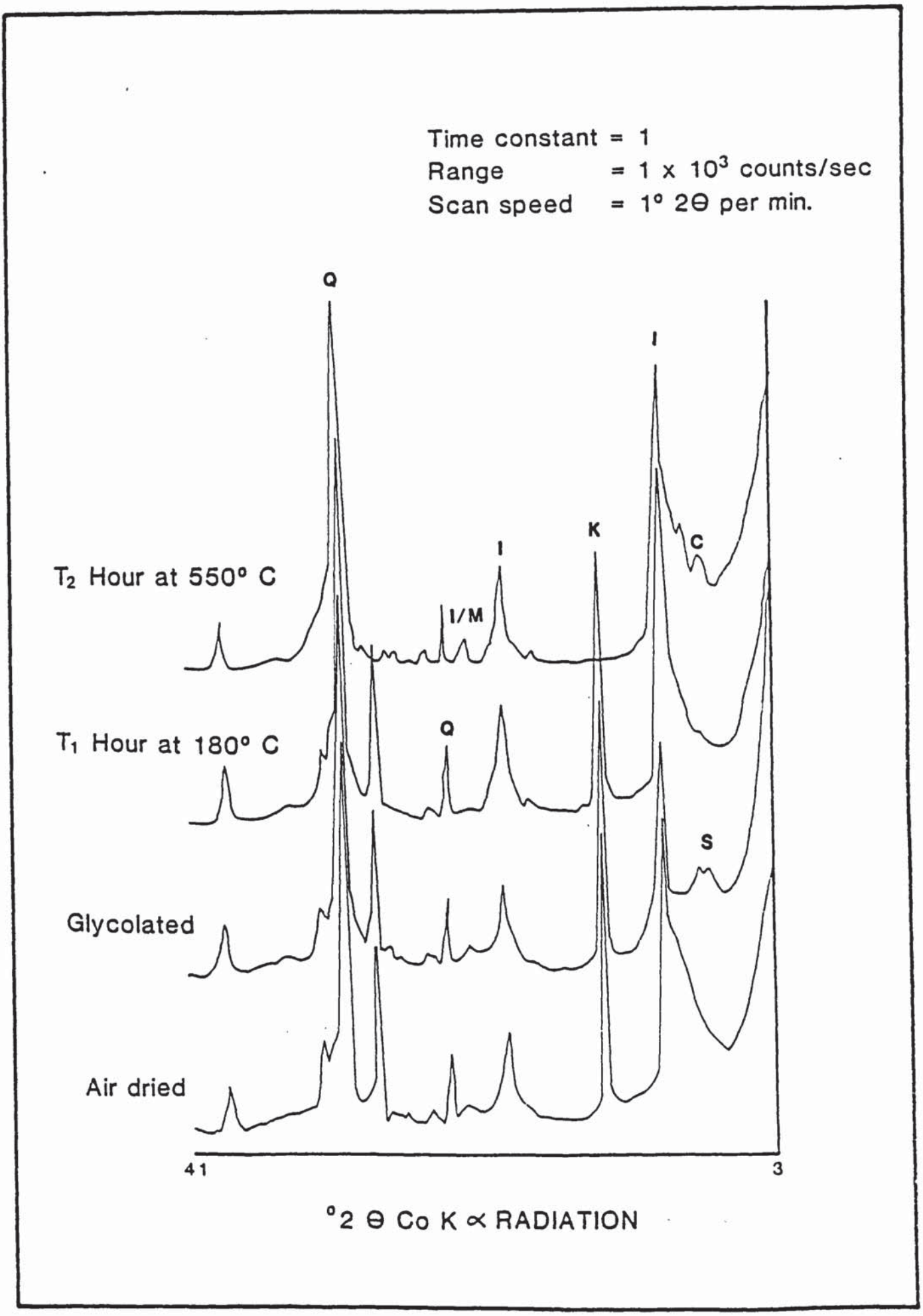

Fig. 3.5 X-ray diffractions for the <2μm clay fraction of Sample P8.

In addition to the poikilotopic cement, lensoid patches and veinlets of ferroan dolomite and, less commonly, non-ferroan calcite, also occur.

The zeolite, analcime ($NaSi_2A10_6\ H_2O$), has also been recorded in these deposits and is closely associated with the dolomite cement. Amounts are small (<1%) but X-ray diffraction confirms its presence (Fig. 3.5). The analcime occurs as authigenic pore filling cement and, more rarely, as subhedral (trapedal) crystals.

Porosity values for these sediments are low (<2%). Any primary porosity originally present in the rocks has been reduced by compaction and the creation of epi-and pseudomatrix. Secondary porosity, due to feldspar dissolution is common. Many grains are etched or show 'hacksaw' terminations. Dolomite crystals also show etching (Plate 3.3b) but widescale dissolution has not taken place.

3.3.3 Magnetic mineralogy

The total detrital opaque content in the Autunian deposits of Palmaces ranges from 1% (P5) to 11% (P10). Coarse, detrital opaques are particularly abundant in samples from the Palmaces siltstone (RS4), comprising 6% (P8) to 11% (P10) of the total. Fine grained iron oxide (authigenic cement and replacement iron oxide) comprises up to 14% (P7)of the total volume of the rock. In the samples from the lower part of the series (RS2 and RS3), however, amounts of opaques are much lower with coarse opaques accounting for up to 2% (P3) of the total and fine grained iron oxide up to 7% (P5).

Transmitted light petrography shows that the opaque oxides present demonstrate a number of textural habits:-

Detrital haematite (Specularite)

Coarse, detrital grains, occurring in the matrix.

Authigenic haematite

a) Small elongate crystals within the cleavages of biotite grains.

b) Fine grained iron oxide which replaces rock fragments (especially volcanic rock fragments), feldspars and accessory minerals such as hornblende and is also found in association with ferroan carbonates (P5).

c) Microcrystalline grains disseminated throughout the matrix and lining pores.

d) Extremely fine grained (pigmentary) iron oxide, found in association with all of the above habits.

Reflected light petrography reveals many more details of the oxide mineralogy of these rocks. All the opaques seen in transmitted light are, with few exceptions, haematite.

The coarse detrital specularite grains range in size between 0.1 mm and 0.5 mm. Many have rounded outlines, indicating some transportation from their source (Plate 3.3c). In samples from the Palmaces siltstones (P7, P8 and P9), many of the specularites contain crystallographically orientated exsolution lamellae of ilmenite (evidence of their high temperature origin). Some grains are also very embayed and altered (Plate 3.3d). Other haematite grains have a more tabular shape (Plate 3.3e). These may represent haematite pseudomorphs after ilmenite and in some examples relict ilmenite is present.

Authigenic haematite is present in all samples in a number of textural forms. Syntaxial overgrowths on detrital grains are occasionally present. These are sometimes euhedral but more commonly occur as irregular projections on the host grain.

Biotite mica shows replacement by haematite. Some biotites appear fresh whilst others have been almost totally pseudomorphed by haematite. Replacement usually begins with the growth of microcrystalline haematite between the cleavages of the mica.

Many rock fragments, especially those with a metamorphic or volcanic origin, show replacement by iron oxide. The micaceous components of schistose rock fragments are very prone to this alteration.

The matrix is stained red in the youngest Palmaces rocks (P6 to P10) owing to the presence of very fine grained pigmentary iron oxide. Microcrystalline haematite is also present, disseminated throughout the matrix. These small crystals may represent fragments of detrital grains or may have grown diagenetically from fine grained pigmentary haematite.

Thick, red stained rims coat many grains, especially rock fragments and feldspars samples from the Palmaces siltstones. Quartz grains with authigenic overgrowths, however, have only a thin clay coat between host and overgrowth, suggesting that iron oxide precipitation post-dates quartz authigenesis.

Fine grained iron oxide occurs in one other textural habit (only found in sample P5). In this example the haematite is closely associated with carbonate cement. Thick rims of iron oxide surround ferroan dolomite crystals and in places the haematite 'appears' to replace the carbonate (Plate 3.3f).

Titanium oxide also occurs in these deposits. Detrital ilmenite is present as tabular grains which occur sporadically throughout the matrix. Many show partial to complete replacement by haematite. Rock fragments sometimes show replacement by amorphous aggregates of titanium oxide (leucoxene). Rutile (TiO_2) is less common. It occurs as inclusions within quartz grains or as isolated needles in the matrix.

Finally, some specularite grains show peripheral alteration to fine grained yellow-brown goethite.

3.3.4 Paragenesis

The earliest diagenetic event to have occurred in the Autunian deposits of Palmaces was the precipitation of authigenic quartz cement. This formed syntaxial overgrowths on detrital grains. Other early diagenetic features include the widespread partial dissolution of feldspars and the replacement of rock fragments and feldspars by clay minerals. Differences in detrital mineralogy and depositional environment led to differences in the early diagenesis of the oldest Palmaces deposits (P1 to P4) and those younger in the sequence (P5 to P10).

The oldest samples have a strong volcanic influence. They contain abundant smectite and zeolites and were deposited in a similar environment

to the Autunian of Rillo de Gallo i.e. a humid climate with abundant organic material in a marginal lacustrine environment. Early porewaters would have been acidic and reducing.

The youngest samples taken from the Autunian of Palmaces show evidence of having a plutonic source. They were deposited in a fluvial environment having a semi-arid climate. Early porewaters would have been both alkaline and oxidising.

The main effect these difference in conditions had on the early diagenesis of the Palmaces deposits was in the stability of iron oxide. Haematite is unstable in reducing conditions and any free iron made available by the dissolution of ferromagnesian silicates would have gone initially into forming iron sulphides (see Chapter 2 section 2.3.4). Below the sulphate reducing zone, iron carbonates would precipitate. Thus the oldest Palmaces sediments are black, white or green in colour and contain very little haematite.

In contrast to the above, oxidizing conditions prevailed during deposition of the younger Palmaces samples (P5 to P10). Haematite was now stable in this environment and precipitated as a grain rimming and pore filling cement imparting a red colouration to the sediments.

At this time, the oxidizing porewaters also reached the oldest Palmaces deposits and haematite replaced many of the iron sulphides and developed in the cleavages of biotite micas.

Petrographic evidence indicates that the precipitation of non-ferroan dolomite and analcime occurred after the early diagenetic reactions described above but before burial of the sequence.

During burial of the sediments, crushing of the physically weak grains, such as schistose and volcanic rock fragments resulted in the development of a pseudomatrix. The large amount of diagenetic matrix present in the rocks considerably reduced the porosity, permeability and textural maturity of the sediments. The term greywackitisation has been used by other workers to describe this process in the Autunian of Central Spain (e.g. Marfil&Pena,1980) Compaction due to burial also resulted in deformation of the micas and in the splayed cleavages of many muscovite grains neomorphic illite developed.

An aggressive ferroan dolomite cement precipitated upon further burial as the porewaters became more alkaline, resulting in further corrosion and replacement of quartz and feldspar grains. The deposits were not buried to a great depth since many samples contain abundant smectite. This is converted to illite with increasing burial.

At some stage another change in porewater chemistry occurred. This time oxidising and acidic conditions (probably associated with uplift) led to the local dissolution of the ferroan dolomite cement. The low porosity and permeability of these sediments restricted the flow of this oxidising water and hence, dolomite was preserved in areas.

As a result of this dedolomitisation non-ferroan calcite precipitated (see Chapter two, Section 2.3.4) and thick rims of authigenic iron oxide formed as Fe ions were released into solution.

The rise in pH associated with dolomite dissolution (Curtis, 1983) also led to the precipitation of kaolinite in the secondary pores.

Finally, recent weathering converted some of the haematite to geothite especially around the margins of the specularite grains.

3.4 PALAEOMAGNETISM

3.4.1 Natural Remanent Magnetization (N.R.M.) Results

The results of palaeomagnetic analyses carried out prior to demagnetization of the samples from Palmaces are summarized in Table 3.2.

The mean intensity of N.R.M. for the Palmaces site was 5.55 mAm^{-1}. Samples from Palmaces had higher intensities than those from Rillo de Gallo, ranging from 0.22 mAm^{-1} (P2) up to 26 mAm^{-1} (P10).

The mean susceptibility value for Palmaces samples was 272 $mAm^{-1}nT^{-1}$. The susceptibilities were also higher than those from Rillo de Gallo, ranging from 180.5 $mAm^{-1}nT^{-1}$ (P1) to 537 $mAm^{-1}nT^{-1}$ (P4).

Mean N.R.M. directions for Palmaces samples lie predominantly in the southeast quadrant when plotted on a stereonet (Fig. 3.6). They are generally more southerly and shallow than those from Rillo de Gallo. They also show a streaking effect from fairly shallow positive (and negative)

TABLE 3.2 N.R.M. RESULTS FOR THE AUTUNIAN OF PALMACES

Sample	Height (m)	F Dec(°)	F Inc(°)	P Dec(°)	P Inc(°)	Pole Long(°)	Pole Lat(°)	N	R	α95(°)	α95(°) Pole	Intensity (mAm^{-1})	Susceptibility ($mAm^{-1}nT^{-1}$)
P1	17	159.2	34.3	155.0	12.7	31.1	-37.1	6	5.91	8.8	7.9	0.55	180.53
P2	18	149.2	63.0	142.6	40.1	34.9	-15.6	7	6.68	14.3	13.6	0.22	231.58
P3	26	153.0	6.6	153.7	-15.5	41.7	-49.5	7	6.90	7.7	6.5	1.27	198.36
P4	33	150.4	26.0	148.6	3.5	41.0	-38.6	5	4.97	7.0	6.3	0.60	537.40
P5	70	12.8	58.2	54.9	62.3	66.2	49.8	7	6.93	6.4	5.9	2.78	436.64
P6	93	169.5	-1.0	170.9	-13.0	15.1	-54.4	7	6.98	3.2	3.0	3.57	186.03
P7	113	170.1	24.3	167.3	6.9	16.8	-43.6	6	5.95	6.8	6.3	5.78	226.98
P8	128	156.0	9.8	155.7	-2.7	34.4	-44.4	6	5.95	6.9	6.4	8.80	244.44
P9	170	157.1	12.5	156.5	-1.3	32.9	-44.2	6	5.96	6.1	5.5	5.23	251.91
P10	186	156.5	4.4	156.7	-8.0	33.5	-46.8	7	6.99	1.6	1.3	26.44	221.77

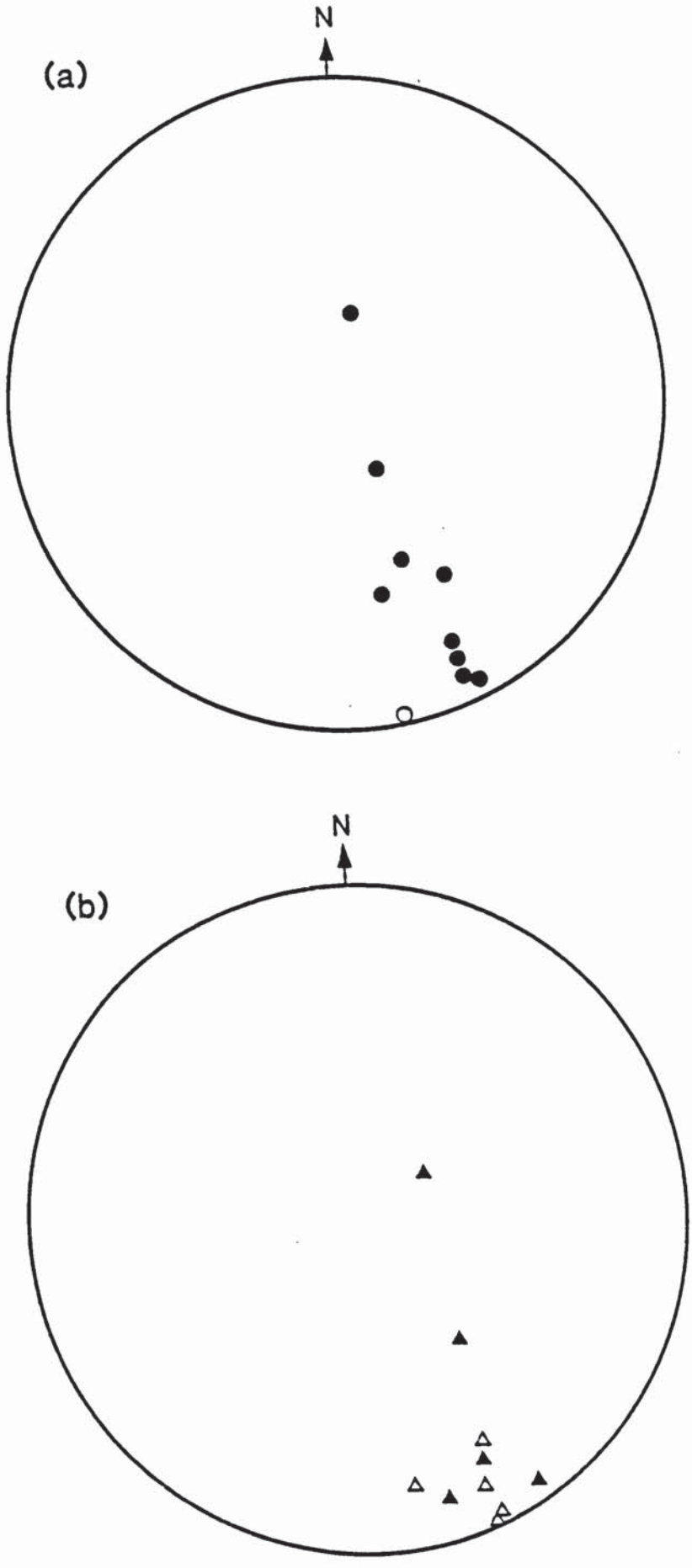

Fig. 3.6 Initial mean N.R.M. directions for the Autunian of Palmaces (a) before and (b) after correction for bedding.

directions in the southeast quadrant towards steeper positive directions in the northeast quadrant. Field corrected directions are generally steeper than those corrected for both field and bedding.

Within sample scatter is quite low, with α_{95} values ranging from 1.6 (P10) to 14(P2). Samples with the highest initial intensities also show the smallest degree of scatter.

3.4.2 Isothermal Remanent Magnetization (I.R.M.) results

I.R.M. curves have been drawn for samples P3 and P9 (Fig. 3.7). P3 showed an initial rapid acquisition of I.R.M. at low fields, followed by a more gradual concave upwards increase. Full saturation however was not reached. The magnitude of the maximum I.R.M. was 160 mT.

The I.R.M. curve for sample P9 was quite different to P3. It showed a more gradual increase in I.R.M. (concave upwards). Full saturation was not reached and the magnitude of the maximum I.R.M. was 1450 mAm^{-1} at 1.4T (almost ten times greater than P3).

The I.R.M. curve shown by sample P9 is typical of one containing a high coercivity mineral such as haematite (i.e. does not saturate even in high fields). P3 also showed evidence of containing a high coercivity mineral but the presence of a low coercivity mineral is also suggested by the rapid acquisition of remanence at low fields. This mineral could be one of a number: poorly crystalline fine grained iron oxide, magnetite or geothite. Petrographic studies, used in conjunction with palaeomagnetism, help to isolate which one is the most likely to be the carrier of this remanence.

3.4.3 Thermal Demagnetization Results

3.4.3.1 Intensity and Susceptibility changes

The normalized intensity and susceptibility decay curves from room temperature to 630°C for specimens from Palmaces are shown in Figure 3.8.

These are generally not as complex as those from Rillo de Gallo. Intensities showed little change between room temperature and 100°C with the exception of P5.2.1. The intensity of this sample dropped to less than 10% of its original value.

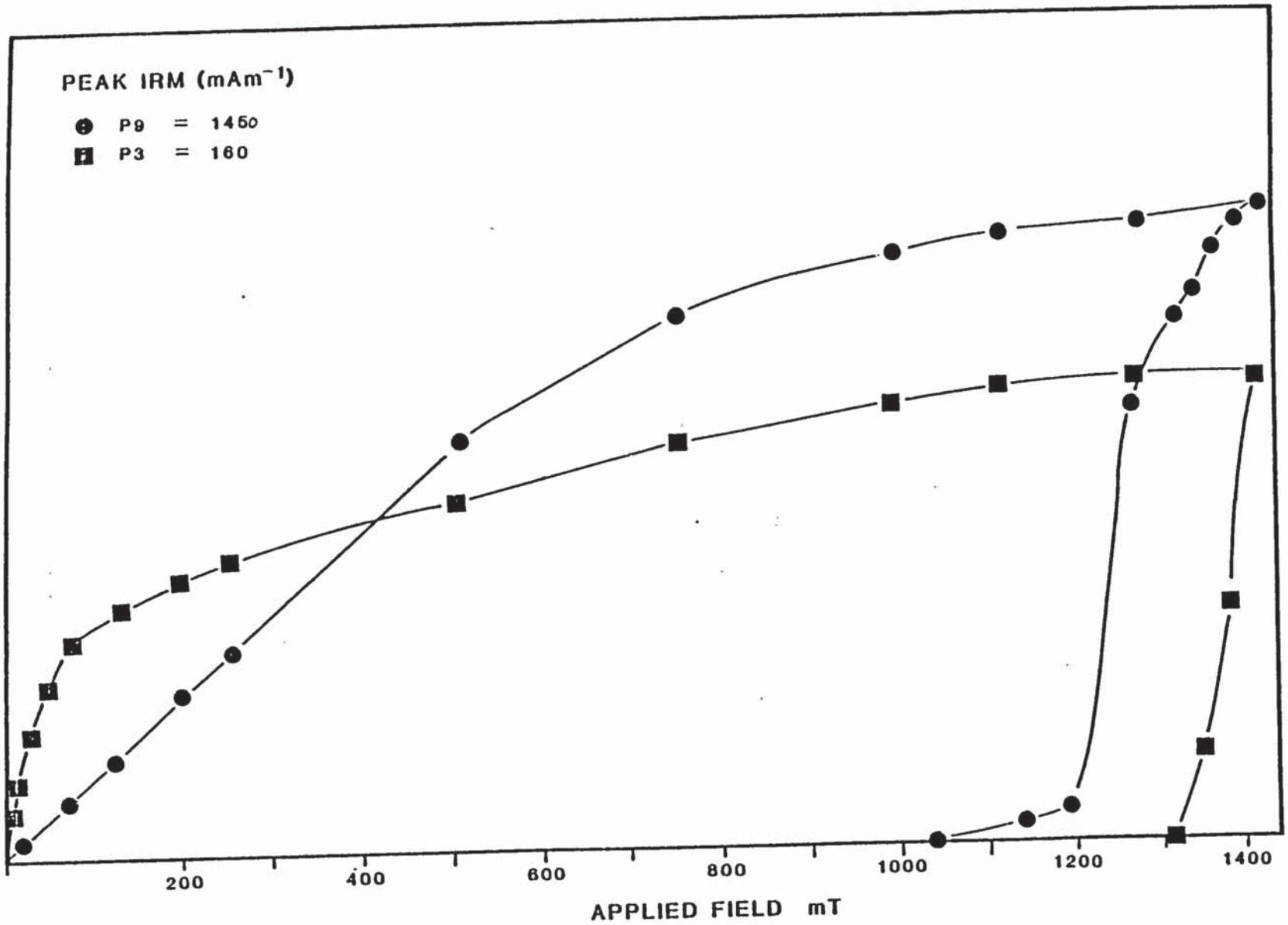

Fig. 3.7 I.R.M. acquisition and reverse field curves for the Autunian of Palmaces.

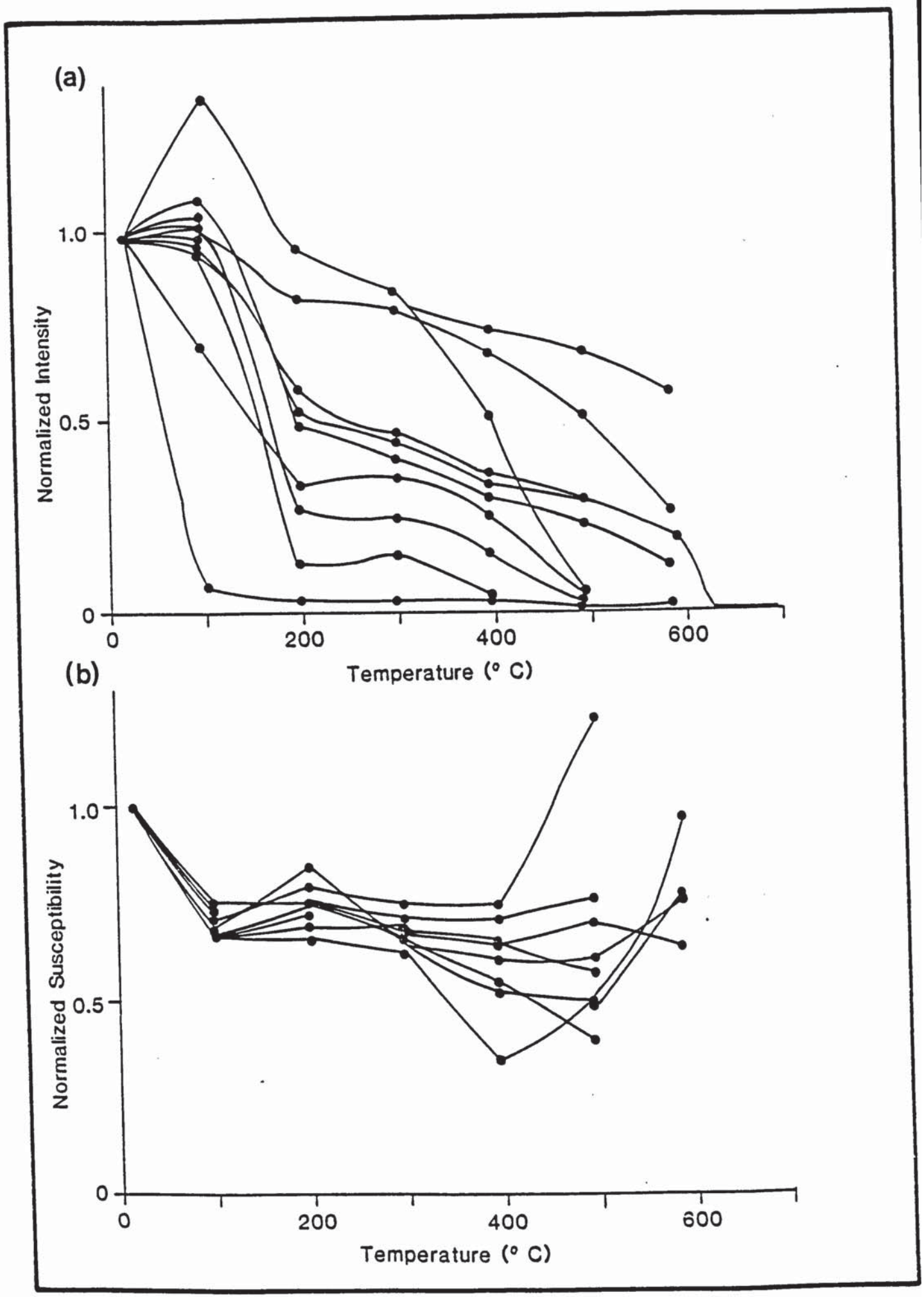

Fig. 3.8 Normalized intensity (a) and susceptibility (b) decay curves for the Autunian of Palmaces.

Between 100°C and 200°C,all specimens showed a sharp drop in intensity, the majority to between 20% and 60% of their original values, reaching a stable plateau between 200°C to 300°C. At temperatures above 300°C, the specimens showed a steady decline in intensity. Specimens P6.3.3 to P10.4.1 were not fully demagnetized even after heating to temperatures above 600°C.

The normalized susceptibilities dropped to 65% to 75% of their original values between room temperature and 100°C. They remained at this value until 400°C. At this temperature specimens P4.1.1 to P6.3.3 showed a sharp increase in susceptibility. The remaining specimens also showed a rise in susceptibility at temperatures above 500°C.

3.4.3.2 Discussion of Intensity and Susceptibility Results

The sharp drop in intensity and susceptibility shown by specimen P5.2.1 between room temperature and 100°C reflects the removal of a low coercivity mineral which is unstable at temperatures above 100°C.

The remaining specimens showed a drop in intensity between 100°C to 200°C. It is likely this represents the removal of a viscous magnetic remanence.

The I.R.M. curve for P3 also suggests the presence of a low coercivity mineral. The fact that specimens P1.2.1 to P5.2.1 were almost completely demagnetized by 500°C indicates that crystalline haematite (which has a Neel point of 625°C) is only present in these samples in very small quantities. The majority of the remanence is probably carried by goethite, magnetite or very poorly crystalline, fine grained iron oxides. Specimens P6.3.3 to P10.4.1 were not demagnetized even after heating to over 600°C suggesting that at least part of their remanence must be carried by haematite. The I.R.M. curve for P9 also supports this view.

The increase in susceptibility shown by specimens P4.1.1, P5.2.1 and P6.3.3 at 400°C may indicate the conversion of small amounts of pyrite to magnetite.

The magnetic mineralogy of the samples from Palmaces seem to indicate that a gradual change to more in oxidising conditions took place with magnetite and pyrite present in the lower part of the series, being superseded by haematite in the youngest parts of the section. Goethite (probably due to recent weathering) is abundant in all samples.

3.4.3.3 Directional Changes

Like the Autunian of Rillo de Gallo, the Palmaces specimens demonstrate three different types of demagnetization behaviour.

Specimen P7.7.1 is a good example of the first type of behaviour (Fig. 3.9). The stereographic projection (Fig. 3.9a) shows that initial directions (corrected for bedding) are shallow, predominantly negative, and lie in the southeast quadrant. This direction remains fairly constant until temperatures in excess of 600°C are reached. At this point the direction moves northwestwards towards a shallow positive direction in the northwest quadrant.

The orthogonal vector plot (Fig. 3.9b) shows the existence of a small viscous remanence between room temperature and 100°C. Between 100°C and 630°C one major component of magnetization exists which is progressively removed upon heating.

The normalised intensity and susceptibility decay plots for this specimen (Fig. 3.9c and d) confirm the presence of one major stable component of magnetization. The intensity decay plot shows that after an initial rapid drop in intensity between 100°C and 200°C, the remanence is only gradually removed. By 630°C it is less than 5% of its original value.

The susceptibility decay plot shows a relatively stable remanence between 100°C and 580°C. Above 580°C the susceptibility increases rapidly and the remanence directions may not be reliable.

The most stable direction of magnetization (S.I. = 2.5) occurs over the range 400°C to 580°C and has a bedding corrected direction of: D = 160°, I = 4°, α_{95} = 9.1, with a pole position of 48.5°N 163.3°W.

The majority of the specimens from Palmaces show the type of demagnetization behaviour described above (i.e. P3.2.3, P4.1.1, P6.3.3, P7.7.1, P8.2.2, P9.4.1, P10.4.1).

A second type of demagnetization behaviour is shown by two of the Palmaces specimens (P1.2.1 and P2.3.2). This behaviour is well demonstrated by specimen P2.3.2 (Fig. 3.10). In this example initial directions are steeper than those in the previous group. Specimen P1.2.1 has an initial

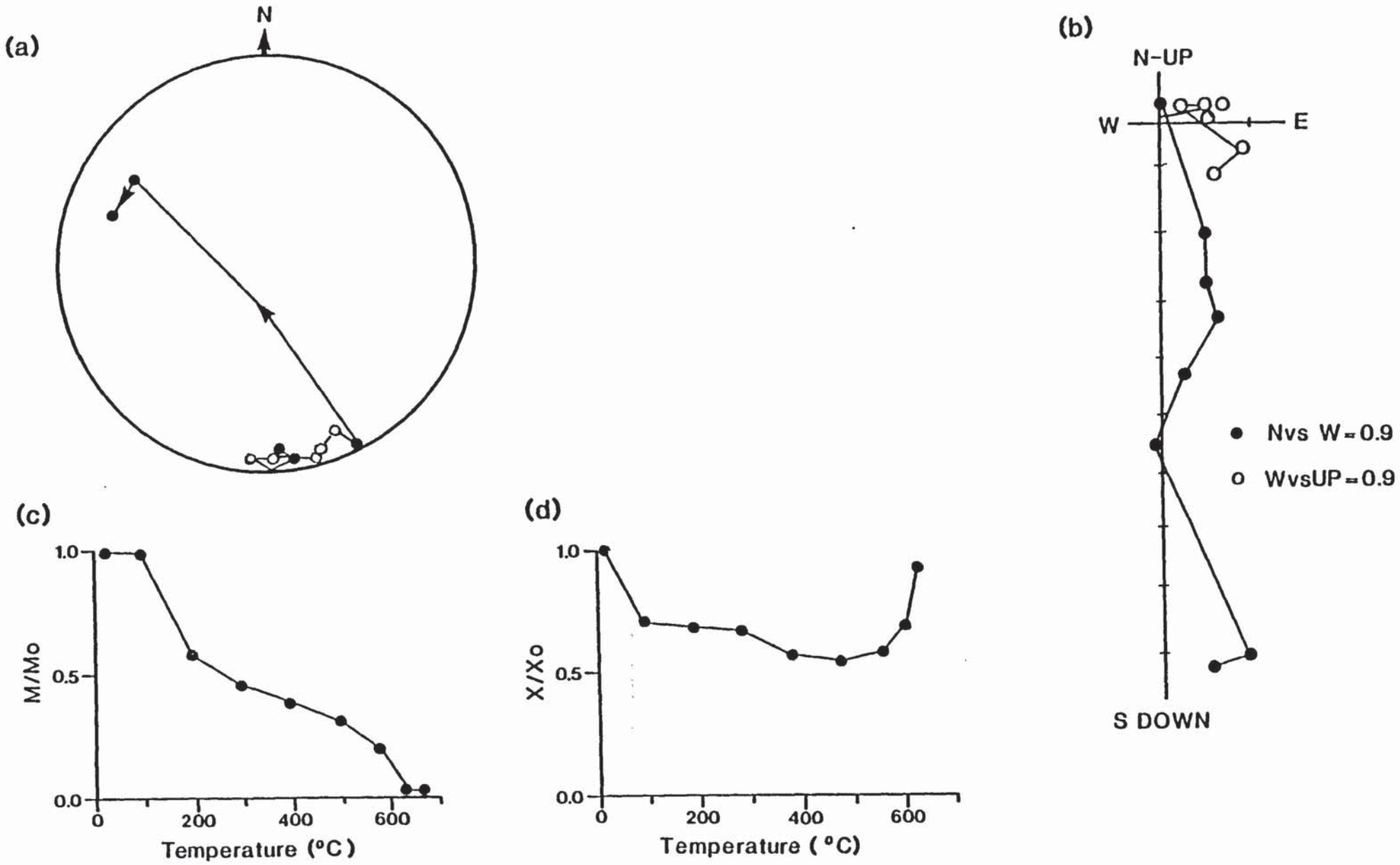

Fig. 3.9 Palaeomagnetic behaviour demonstrated by specimen P7.7.1 during partial thermal demagnetization. (a) Stereographic projection, (b) Orthogonal vector plot, (c) Normalized intensity decay curve, (d) Normalized susceptibility decay curve.

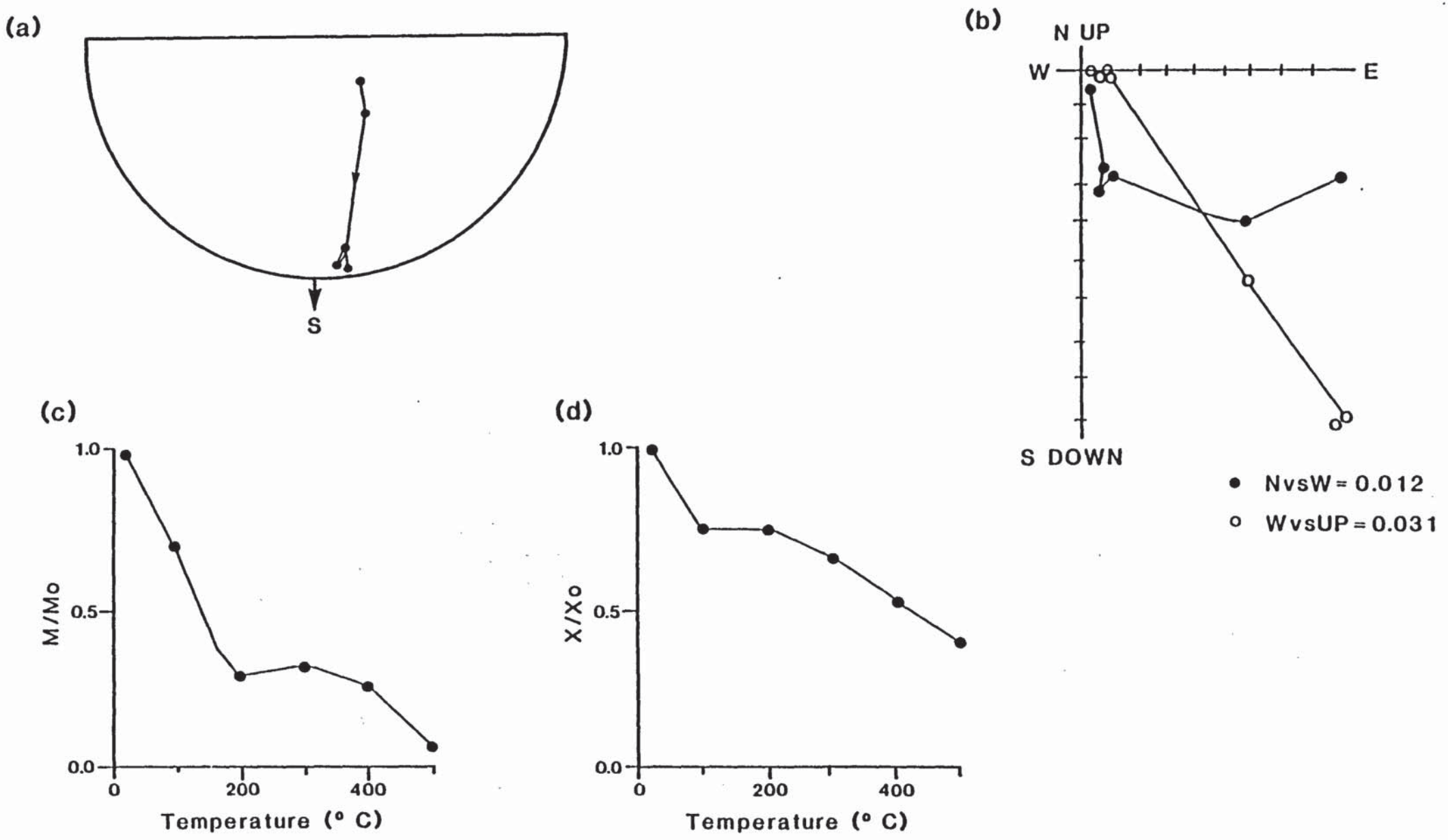

Fig. 3.10 Palaeomagnetic behaviour demonstrated by specimen P2.3.2 during partial thermal demagnetization. (a) Stereographic projection, (b) Orthogonal vector plot, (c) Normalized intensity decay curve, (d) Normalized susceptibility decay curve.

direction almost coincident with that of the present-day field for this area. The stereographic projection for P2.3.2 (Fig. 3.10a) shows a movement southwards to a very shallow direction. This occurs in both samples between room temperature and 200°C. Above 200°C the direction remains constant until the specimen is completely demagnetized.

The orthogonal vector plot (Fig. 3.10b) shows the removal of a major component of remanence between room temperature at 200°C. A secondary component is removed gradually at temperatures above 200°C.

The normalized intensity versus temperature plot (Fig. 3.10c) shows the rapid removal of remanence between room temperature and 200°C. The intensity drops to only 30% of its original value over this temperature range. Between 200°C and 500°C a more gradual drop in intensity is recorded. The remanence is almost completely removed by 500°C.

The normalized susceptibility versus temperature plot (Fig. 3.10d) shows an initial rapid drop between room temperature and 100°C followed by a more gradual drop to about 40% of its original value by 500°C.

The most stable bedding corrected direction for this specimen was over the range 200°C-500°C (S.I. = 6) with D = 173.5° and I = 4°, α_{95} = 3.3. The calculated pole position is 46.5°N, 171°W.

Another type of magnetic behaviour was demonstrated by just one of the specimens (P5.2.1) during thermal demagnetization. Fig. 3.11a shows the directional changes which occurred during demagnetization. The initial direction is steep, positive and lies in the northeast quadrant. This direction remains virtually unchanged with heating. The orthogonal vector plot shows that only one component of remanence is present and it is almost totally removed upon heating to 100°C.

The normalized intensity decay plot (Fig. 3.11c) shows clearly this initial, rapid drop in intensity upon heating to only 100°C. At this temperature the remanence is only 6% of its original value. Between 100°C and 500°C the intensity drops very slowly. The specimen is completely demagnetized at 500°C. The normalized susceptibility (Fig. 3.11d) also shows a sharp rise at this point.

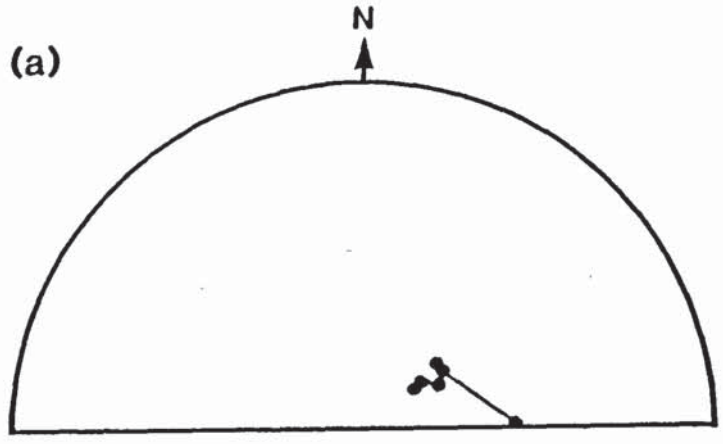

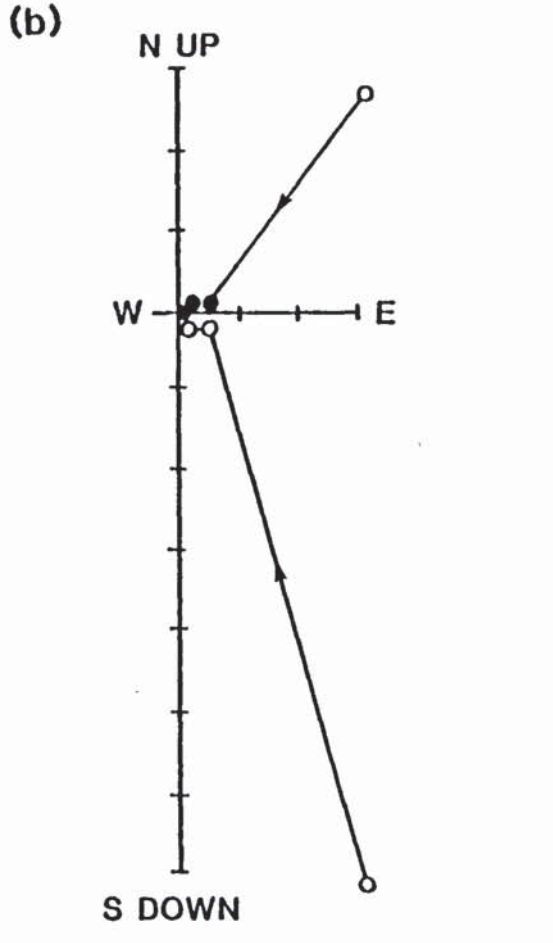

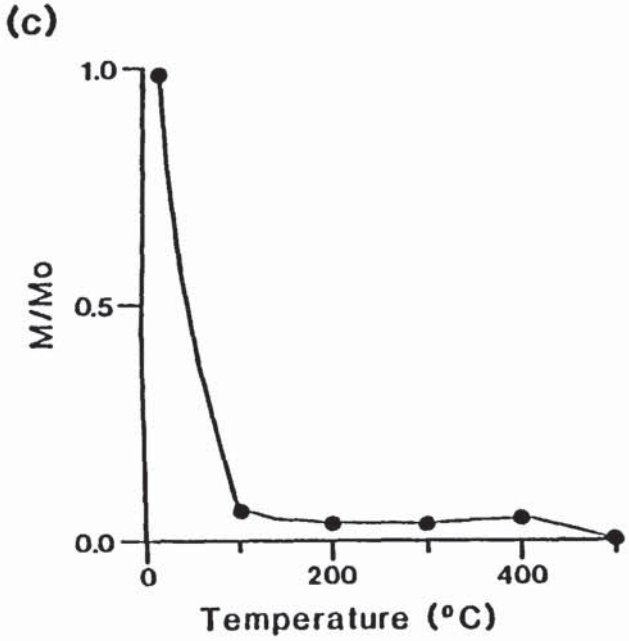

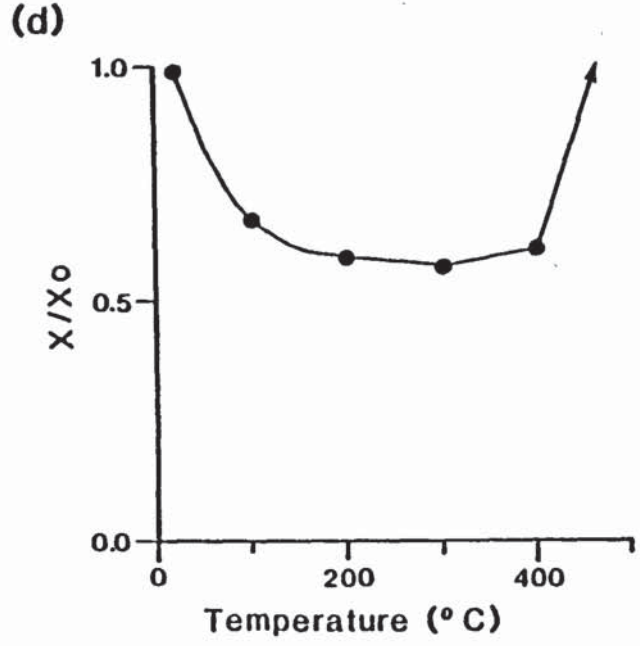

Fig. 3.11 Palaeomagnetic behaviour demonstrated by specimen P5.2.1 during partial thermal demagnetization. (a) Stereographic projection, (b) Orthogonal vector plot, (c) Normalized intensity decay curve, (d) Normalized susceptibility decay curve.

3.4.3.4 Thermal Demagnetization Summary

Table 3.3 shows the results of thermal demagnetization of the Palmaces sediments. The most stable directions isolated during thermal cleaning are shown in Fig. 3.12. The stabilities are generally good to excellent ranging from 2.1 (P4) up to 19.3 (P10). α_{95} values are also good. These range from 8.7° (P4) to 1° (P10). The majority of the specimens show a shallow direction which is predominantly negative and lies in the southeast quadrant. One specimen (P.2.1) shows a direction close to the present day geomagnetic field position (especially in the field position). The mean bedding corrected direction for these Palmaces specimens (excluding P5.2.1) is: D = 164°, I = -6°, α_{95} = 11.5°.

Directions which pass the 10° linearty test (Fig. 3.13) are similar to the most stable directions. These lie in the southeast quadrant and have shallow inclinations. Both positive and negative directions are seen. Three directions (all demonstrated by specimen P5.2.1) are steep and positive and lie close to the present-day geomagnetic field position for this area.

3.4.3.5 Bulk Demagnetization Results

Bulk demagnetization of the Palmaces samples was carried out over the temperature range of 400°C to 630°C (Table 3.4, Fig. 3.14). Two groups of directions can be roughly defined after correction for bedding.

The first is shallow negative and lies in the southeast quadrant. This is similar to the most stable directions identified during stepwise thermal cleaning of the pilot specimens. Samples P3, P6, P7, P8, P9 and P10 lie in this group.

A second, less well defined group, comprises samples P1, P2, P4 and P5. All these samples have positive directions which lie predominantly in the southwest quadrant. They show a streaking effect from shallow inclinations (P1) to steep inclinations (P5). The samples which fall into this group, generally have much lower intensities than those in the previous group.

TABLE 3.3 STEPWISE THERMAL AND CHEMICAL (C) DEMAGNETIZATION RESULTS FOR THE AUTUNIAN OF PALMACES

Specimen	S.I.	Most stable directions Dec(°)	F Inc(°)	P Dec(°)	P Inc(°)	Pole Long(°)	Lat(°)	N	R	α95(°)	Directions passing 10° linearity test Range (°C)	Range(°C)	F Dec(°)	F Inc(°)	P Dec(°)	P Inc(°)
P1.2.1	3.3	180.7	45.1	169.1	27.3	12.0	-33.5	4	2.99	5.9	100	300-0	181.4	45.7	169.4	28.1
												300-500	177.5	41.8	167.8	23.5
P2.3.2	6	177.2	21.7	173.5	4.1	8.7	-46.5	4	3.99	3.3	200-500	400-0	177.1	23.71	72.8	6.1
												20-200	14.0	73.6	89.4	69.2
P3.2.3	3.1	170.9	-10.8	179.5	-29.3	7.1	-64.2	3	2.99	6.9	200-400	400-0	175.3	-15.2	182.8	-31.8
P4.1.1	2.1	154.8	15.4	153.1	-7.7	39.1	-45.2	5	4.95	8.7	20-400	100-500	157.5	13.6	157.0	-7.9
												400-0	2.3	58.9	47.9	67.0
P5.2.1	2.7	11.7	57.5	56.0	62.4	51.4	67.1	3	2.99	8.0	200-400	300-500	0.2	59.1	46.5	68.0
												20-300	12.1	53.7	47.9	59.5
P6.3.3	11.1	168.6	-3.4	170.3	-15.6	17.1	-55.5	6	5.99	1.6	100-500	500-0	167.7	-2.9	169.3	-15.2
P7.7.1	2.5	160.6	14.3	159.9	-4.3	16.7	-48.5	3	2.99	8.1	400-580	400-660	158.3	14.7	157.7	-4.2
												200-400	214.6	1.1	215.0	-3.7
P8.2.2	8.1	163.1	13.1	160	0.7	27.9	-44.9	5	4.99	2.3	100-500	100-0	161.9	11.7	161.2	-0.2
P9.4.1	8.8	158.2	-4.3	160.9	-17.1	34.0	-53.1	3	2.99	2.5	300-500	400-580	146.2	14.6	145.8	0.1
												100-0	160	0.2	160.8	-13.7
P10.4.1	19.3	157.0	21.8	157.4	-10.6	35.1	-48.7	4	3.99	1.0	300-580	500-0	156.4	2.2	156.8	-10.3
												300-500	165.8	-3.8	167.1	-15.2
CHEMICAL DEMAGNETIZATION RESULTS																
P9.1.9(C)	1.6	159.0	11.6	158.5	-2.0	30.8	-45.5	6	5.97	5.6	4-125 hrs	56-150 hrs	152.2	27.1	150.5	12.8

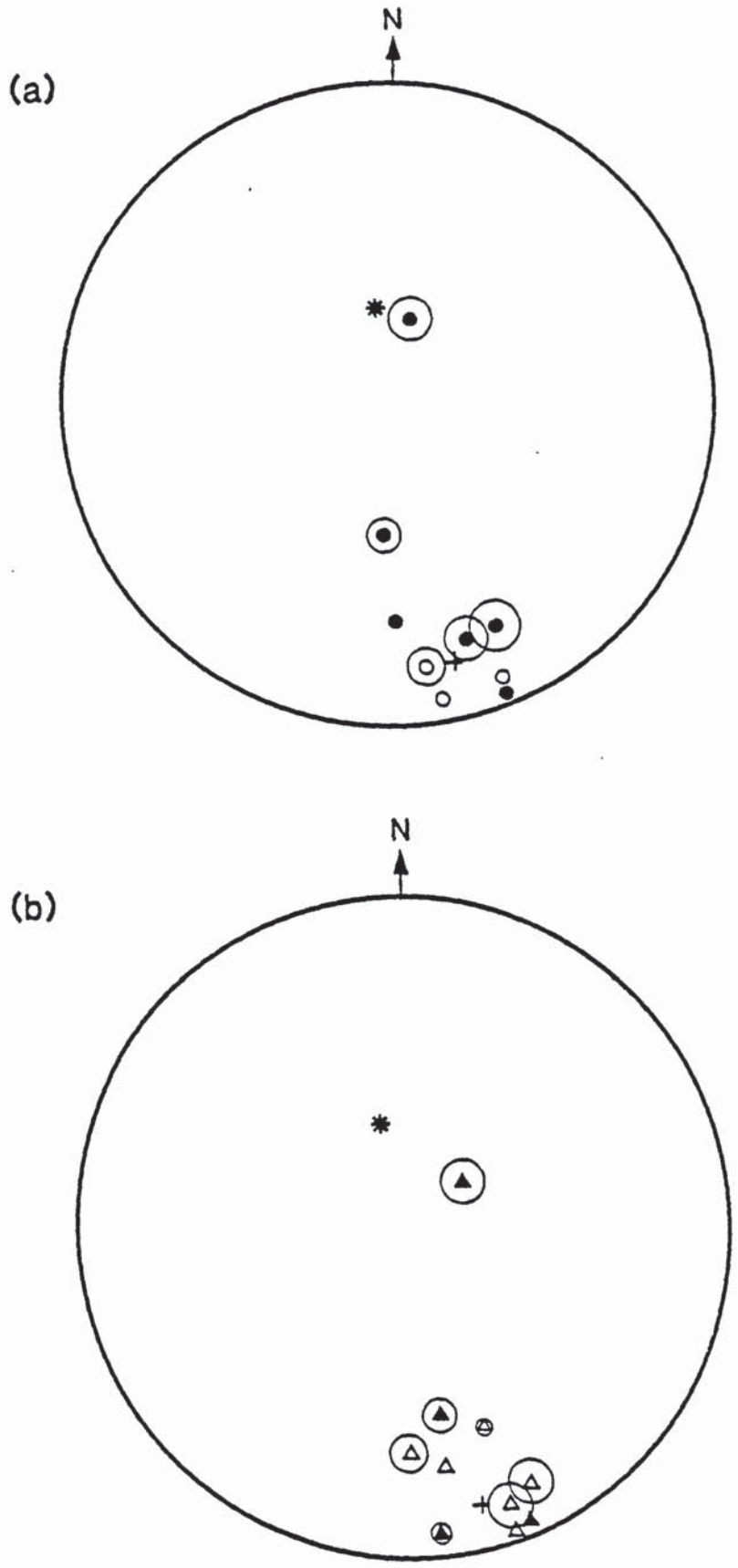

Fig. 3.12 Most stable directions isolated during partial thermal demagnetization for the Autunian of Palmaces (a) before and (b) after correction for bedding. Circles represent α_{95} values and asterisk represents present-day local geomagnetic field position.

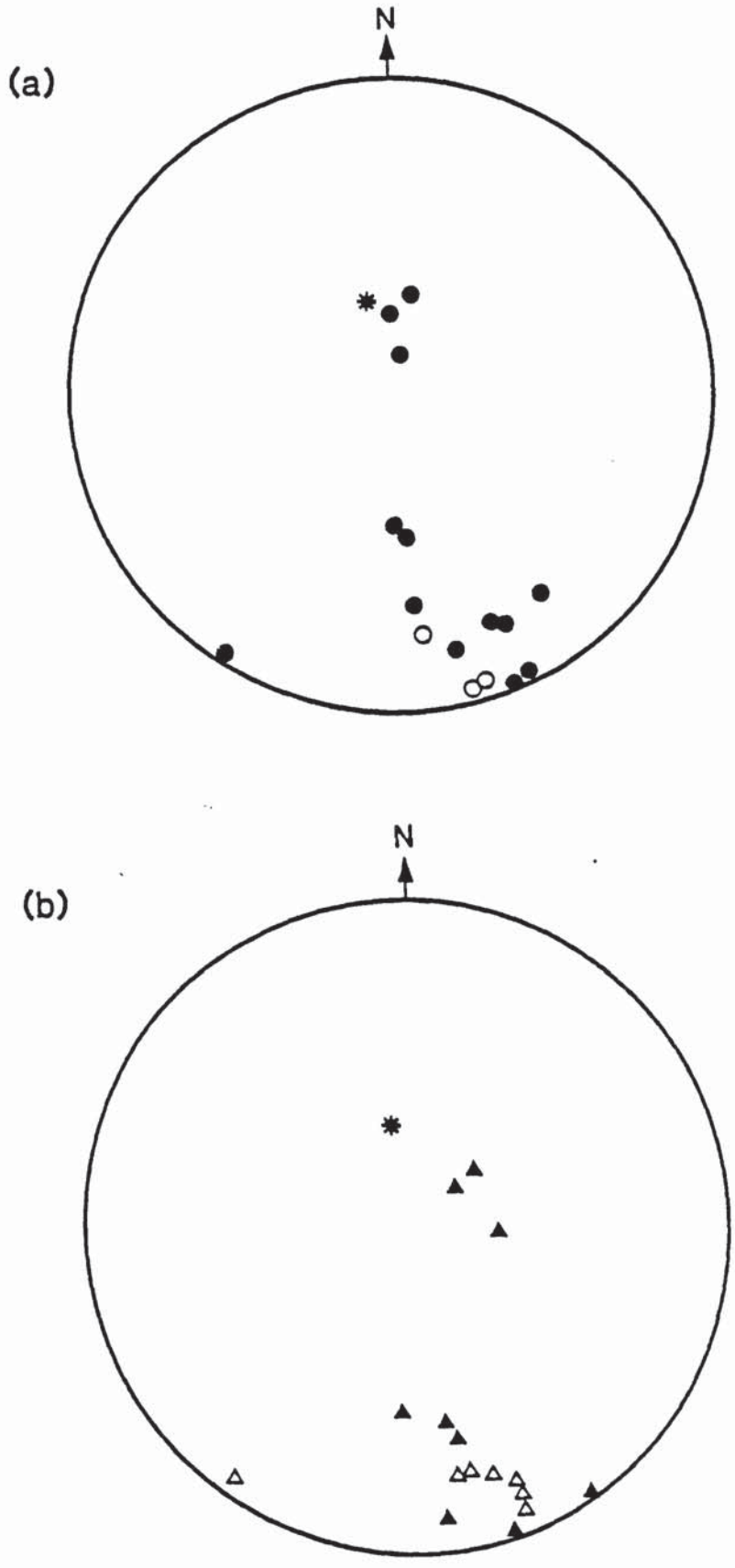

Fig. 3.13 Directions passing 10° linearity test for the Autunian of Palmaces (a) before and (b) after correction for bedding. Asterisk represents present-day local geomagnetic field position.

TABLE 3.4 BULK DEMAGNETIZATION RESULTS FOR THE AUTUNIAN OF PALMACES

Sample	Height (m)	F Dec(°)	F Inc(°)	P Dec(°)	P Inc(°)	Pole Long(°)	Pole Lat(°)	N	R	α95(°)	α95(°) Pole	Intensity (mAm^{-1})	Susceptibility ($mAm^{-1}nT^{-1}$)	Temp (°C)
P1	17	211.0	21.7	203.3	15.1	332.8	-31.6	3	2.98	12.9	11.7	0.07	89.77	500
P2	18	6.7	22.2	17.7	34.4	142.5	62.0	5	4.94	9.4	8.2	0.03	93.40	500
P3	26	171.6	-6.6	176.0	-24.6	4.8	61.2	7	6.89	8.1	6.5	0.25	144.31	400
P4	33	226.9	44.3	204.8	41.2	40.8	54.5	3	2.57	65.5	60.3	0.26	182.77	400
P5	70	351.8	68.2	67.4	75.2	62.2	64.6	5	4.95	8.8	7.1	0.20	272.00	400
P6	93	169.0	-2.0	170.9	-14.1	15.9	-55.1	4	3.91	5.0	4.7	14.45	599.99	580
P7	113	174.6	-2.8	184.1	-43.2	49.0	-56.3	5	4.35	33.2	27.4	0.42	157.14	630
P8	128	160.3	-2.0	161.2	-14.0	31.1	-48.2	6	5.95	6.7	5.9	2.06	148.41	580
P9	170	160.5	-1.4	161.5	-14.7	27.0	-53.9	4	3.95	11.6	10.3	1.36	197.33	580
P10	186	155.1	1.6	155.5	-11.0	37.6	-48.3	7	6.99	1.6	1.3	17.60	208.47	580

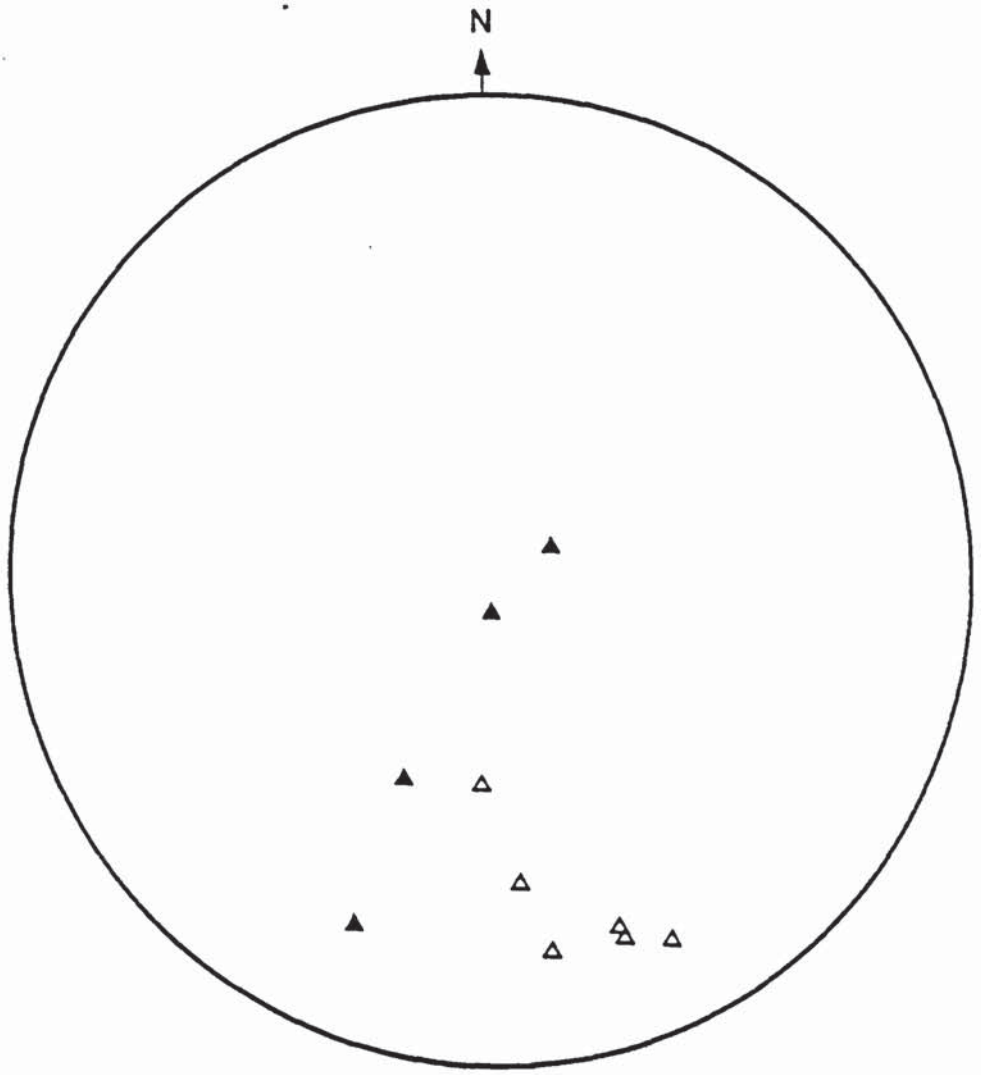

Fig. 3.14 Mean bedding corrected directions isolated during bulk thermal demagnetization of Autunian samples from Palmaces.

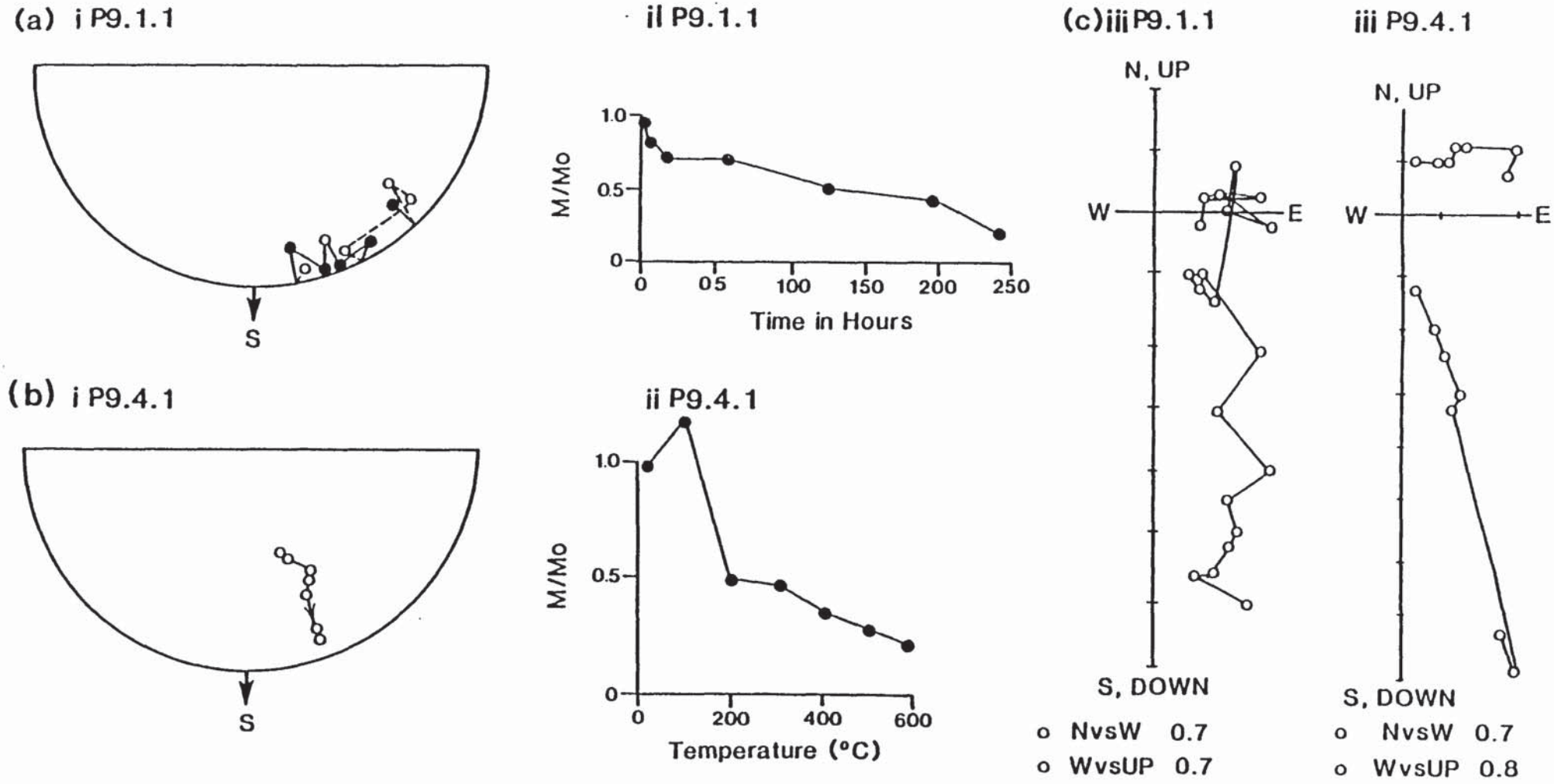

Fig. 3.15 Results of (a) Chemical demagnetization of specimen P9.1.1 compared with those of (b) Thermal demagnetization of specimen P9.4.1. (i) Stereographic projections, (ii) Normalized intensity decay curves and (iii) Orthogonal vector plots.

TABLE 3.5 PREVIOUSLY PUBLISHED PERMIAN DIRECTIONS AND POLES FOR STABLE EUROPE AND IBERIA TOGETHER WITH THOSE FOUND FOR THE AUTUNIAN OF PALMACES

Letter/ No.	Locality (formation)	D(°)	I(°)	N	α95(°)	Lat	Long	Reference
STABLE EUROPE								
A	Exeter, England (Volcanics)	198	-25	23	7°	49.5°N	148.5°E	Zijderveld (1967b)
B_1	Nahe region Germany (Volcanics)	196	-18	34	8°	48°N	168°E	Nijenhuis (1961)
B_2	Nahe region Germany (Volcanics)	201	-9	28	4°	42°N	163°E	Nijenhuis (1961)
C	Nideck region France (Volcanics)	192.5	-12.5	37	5°	47°N	169°E	Roche et al. (1962)
IBERIA								
1	Rio Aragon C.Pyrenees (Andesites)	152	-22.5	14	6°	51°N	133°W	Schwarz (1962)
2	Anayet C.Pyrenees (Andesites and Sandstones)	164	-14	11	10°	52°N	154°W	Van der Lingen (1960)
3	Serra del Cadi E.Pyrenees (Andesites)	169.5	-3	41	4°	48.5°N	163°W	Van Dongen (1967)
4	Borges Catelan Coast (Granodiarites)	168	-4	-	-	-	-	Banda et al. (in press)
5	Atienza C.Spain (Andesites)	165	+6.5	25	2°	-	-	Hernando et al. (1980)
6	Viar Sevilla (Dikes and Sills)	155.5	+10.5	14	4°	41°N	152°W	Van der Voo (1969)
7	Viar Sevilla (Redbeds)	151	+2	8	4.5°	42.5°N	144°W	Van der Voo (1969)
8	Bacaco Coimbra Portugal (Redbeds)	149	+11	17	5°	35.5°N	148.5°W	Van der Voo (1969)
P1	Palmaces (Redbeds)	169.1	+27.3	4	5.9	33.5°N	168°W	This Study
P2	Palmaces (Redbeds)	173.0	+4.0	4	3.3	46.5°N	171°W	This Study
P3	Palmaces (Redbeds)	179.5	-29.3	3	6.9	64.2°N	173°W	This Study
P4	Palmaces (Redbeds)	153.1	-6.7	5	6.9	45.2°N	141°W	This Study
P5	Palmaces (Redbeds)	53.0	62.4	3	8.0	67.1°N	128.6°E	This Study
P6	Palmaces (Redbeds)	170.3	-15.6	6	1.6	55.5°N	162.9°W	This Study
P7	Palmaces (Redbeds)	159.9	-4.3	3	8.1	48.5°N	163.3°W	This Study
P8	Palmaces (Redbeds)	162.5	-0.7	5	2.3	44.9°N	152.1°W	This Study
P9	Palmaces (Redbeds)	157.9	-17.1	3	2.5	53.1°N	146.0°W	This Study
P10	Palmaces (Redbeds)	157.4	-10.6	4	1.0	48.7°N	144.9°W	This Study
Mean (Exluding P5)	Palmaces (Redbeds)	164.2	-5.8	9	5.3	48.9°N	158°W	This Study

3.4.4 Chemical Demagnetization Results

One specimen (P9.1.1) from the Autunian of Palmaces was selected to undergo chemical demagnetization. Results of the chemical cleaning are shown in Fig. 3.15a and compared with results from thermal cleaning of specimen P9.4.1 (Fig. 3.15b).

Both specimens show shallow, negative directions of magnetization which lie in the southeast quadrant and show only minor changes in direction during the demagnetization process.

The normalized intensity decay curves for the two specimens are slightly different. The chemically demagnetized specimen shows a gradual loss of intensity with time immersed in acid. The thermally demagnetized specimen, however, shows an initial gain in intensity, between room temperature and 100°C, followed by a rapid loss in intensity (to 50% of its original value) between 100°C and 200°C. The orthogonal vector plots also show this difference in remanence loss during the early stages of demagnetization.

3.4.5 Discussion of Palaeomagnetic Results

Initial intensities are higher in the Palmaces samples than in those from Rillo de Gallo. This is primarily due to the presence of larger amounts of haematite in the deposits. This is especially true for samples taken from the Palmaces siltstones (P6 to P10), which contain numerous coarse specularite grains of igneous origin.

I.R.M. results from sample P9 also suggest the presence of abundant crystalline haematite. Sample P3 contains haematite, together with a low coercivity mineral, (similar to the Rillo de Gallo samples).

The majority of N.R.M. directions are very shallow and lie in the southeast quadrant close to previously described Permian directions for Spain (Table 3.5). Thermal and chemical cleaning does not have much effect on this direction, indicating that it is a stable magnetic remanence. Two specimens (P1.2.1 and P2.3.2) show initial directions which are steep and normal and lie close to the present day field direction for Spain. This component is removed by heating to 200°C. Above this temperature, a second, stable component is revealed lying in the southeast quadrant and similar to the previously described direction. This

'viscous' overprint is probably due to the presence of small amounts of poorly crystalline iron oxide and/or goethite, formed during weathering of the rocks.

Specimen P5.2.1 is the only notable exception to the above results. It has a steep normal direction which does not move towards the shallow negative direction shown by the other specimens during heating. The remanence is almost completely removed upon heating to temperatures above 100°C. It is unlikely that this remanence is carried by detrital crystalline haematite, which has a Neel point of over 600°C, but rather by fine grained poorly crystalline haematite, precipitated at some later stage during the diagenetic history of the deposits or perhaps an iron hydroxide such as goethite.

Palaeopole positions have been calculated for the Palmaces samples (Table 3.5, mean: D = 164, I = 6). These show close agreement with previously described Permian Pole directions for Iberia and also those of the Rillo de Gallo samples (Fig. 3.16). All of the above are consistently different to pole directions quoted for the Permian rocks of stable Europe.

3.5 RELATIONSHIP BETWEEN DIAGENESIS AND PALAEOMAGNETISM

Differences in detrital mineralogy, depositional environment and early diagenesis have had a significant effect on the palaeomagnetic characteristics of the Autunian deposits of Palmaces:-

1. Initial intensities are low (0.22 mAm^{-1} to 1.27 mAm^{-1}) in the oldest Palmaces samples collected (P1 to P4) but high (2.78 mAm^{-1} to 26.44 mAm^{-1}) in the youngest samples (P5 to P10). This is due to

(a) Differences in detrital mineralogy: The oldest samples contain very little detrital haematite whereas the youngest samples contain abundant, coarse, plutonically derived specularite grains.

(b) Depositional environment: Climatic conditions changed from humid to semi-arid during the Autunian and from a lacustrine to a fluvial environment (see section 3.3.4) thus increasing the stability of haematite with time.

(c) Early diagenesis: As a result of changes in (a) and (b), early diagenetic geochemical conditions also changed with time (section 3.3.4), resulting in differences in iron oxide content in the samples and hence differences in palaeomagnetic characteristics.

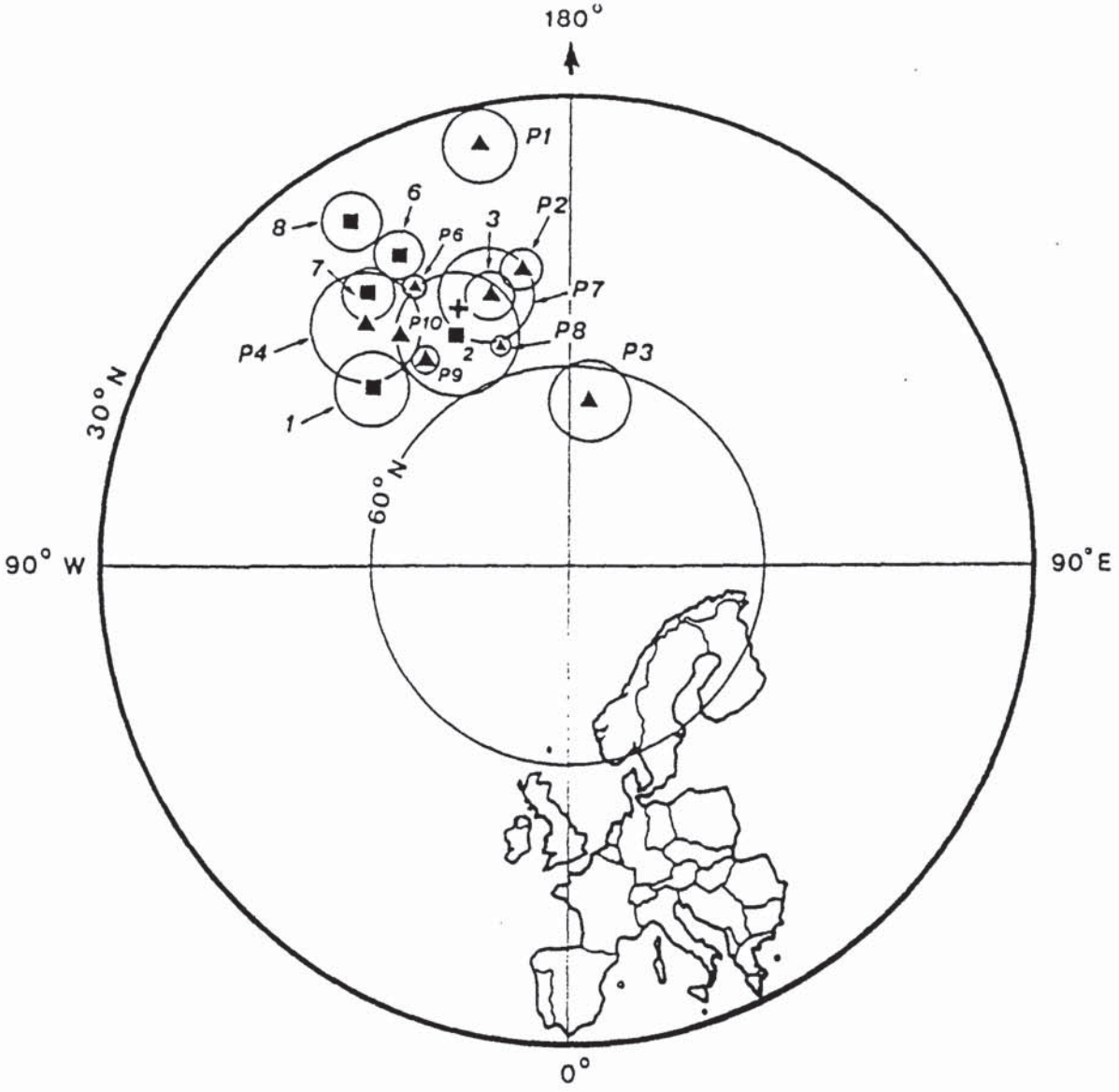

Fig. 3.16 ■ Previously published pole positions from Iberia (Numbers refer to Table 3.5).
▲ Palaeopole positions obtained from the Autunian of Palmaces.
+ Mean pole position for most stable Palmaces directions.
N.B. circles represent α_{95} values.

2. All samples (with the exception of P5) revealed stable Permian directions of magnetization (Tables 3.3 and 3.5). Diagenetic studies indicate that this stable remanence is carried primarily by coarse grained detrital specularite (especially in the Palmaces siltstones (P6 to P10) and also by early diagenetic fine grained haematite which replaced unstable rock fragments, micas and in the oldest deposits, pyrite.

3. The detrital secularity has a blocking temperature of approximately 630°C (Fig. 3.8). The finer grained early diagenetic iron oxide has a lower blocking temperature of between 400°C and 500°C.

4. Sample P5 contains significant amounts of fine grained iron oxide and hydroxide which has formed in association with the dissolution of an iron carbonate cement. Palaeomagnetic results indicate that this iron oxide has a remanence direction almost coincident with that of the present-day geomagnetic field (fig. 3.11). Over 90% of the remanence is removed by heating the sample to 100°C suggesting that either:

a) The iron oxide is very poorly crystalline or fine grained.

b) It contains a significant amount of iron hydroxide which has formed as a result of intense weathering of the rock in recent times.

5. Samples P1 and P2 also show a recent palaeomagnetic overprint which is probably due to weathering. This is removed by heating to over 200°C, revealing a stable Permian direction.

CHAPTER FOUR

THE SAXONIAN FACIES

4.1 INTRODUCTION

The Upper Permian, Saxonian facies was examined at three localities in Central Spain (Fig. 4.1), Barranco de la Hoz (01° 59' 00"W, 40° 41' 50"N) near Molina de Aragon in Guadalajara, Pozo Nuncio (01° 32' 12"W, 40° 23' 25"N), and Torres de Albarracin (01° 32' 12"W, 40° 26' 00"N). The last two localities lie approximately 60-70 km southeast of the first, close to the town of Torres de Albarracin in the Province of Teruel.

Two different lithostratigraphic classifications exist for the Saxonian of these areas. The Saxonian sediments of Barranco de la Hoz are known as the "Capas de Montesoro" (Montesoro Cap) (Sacher, 1966). Further south the equivalent unit is called "Lutites y Areniscas de Tormon" (Tormon mudstones and sandstones). This unit has only recently been defined by Perez-Arlucea, (1985).

The term "Saxonian" has no chronostratigraphic significance and this red continental facies contains very little palaeontological data (Ramos, 1979). The Tormon mudstones and sandstones do, however, contain a palynological association of Upper Permian (Thuringian) age (Perez-Arlucia, 1985).

Samples collected from Barranco de la Hoz are prefixed by the letters MA, those collected from Pozo Nuncio by PN and those from Torres de Albarracin by the letters TA.

4.2 STRATIGRAPHY AND SEDIMENTOLOGY

4.2.1 Barranco de la Hoz

The section of Barranco de la Hoz is situated 9.5 km west of Molina de Aragon, along the road to Torete; 46m of Saxonian deposits are exposed, lying unconformably over Lower Palaeozoic shales and unconformably below conglomerates of the Buntsandstein facies. The sediments strike northeast-southwest and dip gently (<10°) towards the northwest.

Fig. 4.1 Geological sketch map showing location of Saxonian sections.

Five samples (MA112-MA116) were taken from the Capas de Montersoro at this locality (Fig. 4.2). The unit is divided into two subunits M1, and M2. M1 is composed predominantly of breccias with angular clasts (<60 cm). These have a varied lithology which includes quartz, quartzite, shale and volcanic rock fragments. The matrix is sandy and has a composition similar to that of the larger clasts. Interbedded with the breccias are sandstones, siltstones and mudstones. The sandstones are usually discontinuous. They often contain pebbles and are sometimes cross-bedded. Samples MA112-MA115 were collected from these sandstones.

Subunit M2 is formed of red mudstones with intercalated sandstones and quartzite conglomerates (and rare carbonate levels). The mudstones have been gently compacted and are often silicified. The sandstones are red, white and green in colour and often show trough cross-bedding, erosive bases and have a channel-like morphology. Sample MA116 was taken from one such sandstone horizon.

The deposits are interpreted as high viscosity debris flows with channel sands (Ramos, 1979). They formed part of an alluvial fan system and were deposited in an arid to semi-arid type climate.

4.2.2 Pozo Nuncio

The Saxonian sediments of Pozo Nuncio crop out 7km south of the town of Torres de Albarracin. They dip fairly gently (10°-20°) towards the northwest or southwest.

The section has a total thickness of 232m, with 137m of the Saxonian facies exposed. The series lies unconformably over black shales of Lower Palaeozoic age. Overlying the Saxonian deposits (in apparent conformity) are sandstones of the Buntsandstein facies. These may be traced laterally into conglomerates.

Five samples were collected from this section, PN1-PN5 (Fig. 4.3). Pollen of Thuringian age has been discovered in the bed from which sample PN3 was taken.

The Saxonian deposits of this area were named "Lutites y Areniscas de Tormon" (Tormon mudstones and sandstones) by Perez-Gonzales (1985) who divided them into two subunits, T1 and T2. T1 is predominantly

Fig. 4.2 Sedimentological column compiled by Ramos (1979), showing horizons from which Barranco de la Hoz samples were taken.

Fig. 4.3 Sedimentological column compiled by Perez-Arlucea (1985), showing horizons from which Pozo Nuncio samples were taken.

composed of conglomerates with occasional thin lenticular sandstones and mudstones. T2 is comprised of interbedded mudstones, sandstones and conglomerates which exhibit a wide variety of facies. The mudstones are commonly massively bedded with evidence of bioturbation, elsewhere they are laminated. The sandstones, which generally occur as tabular bodies, often have erosive bases and show parallel bedding and planar, trough and epsilon cross-bedding. Some sandstones are massively bedded and have been extensively bioturbated. In others, ripples are present. The conglomerates are composed of quartzite clasts and have horizontal or massive stratification. Some show graded bedding whilst others have trough cross-bedding. All the samples from the Saxonian of Pozo Nuncio were taken from sandstones in subunit T2.

These sediments are interpreted as being continental deposits, laid down in an alluvial fan environment (Sopena, 1979; Perez-Gonzales, 1985), with a proximal conglomerate facies (T1), passing to a distal facies of mudstones with small sandstone channels (lower part of T2). A change back to a more proximal, mid-fan facies occurred (upper part of T2), with coarse grained sands and conglomerates, i.e. braided river deposits. This was probably due to tectonic reactivation (Perez-Arlucea, 1985).

4.2.3 Torres de Albarracin

Samples were collected from two sections close to the town of Torres de Albarracin. The first crops out 1km west of the town (Plate 4.1). The second lies approximately 1.5km further east, along the road between Torres de Albarracin and Calomarde. This section is known as "Barranco de las Fuentes". The sediments of both sections strike northwest-southeast and dip fairly steeply (40°-50°) towards the southwest.

The Saxonian of Torres de Albarracin lies unconformably over white quartzites of Lower Palaeozoic age; the top of the sequence is covered. At Barranco de las Fuentes, the Saxonian is unconformably underlain by Lower Palaeozoic shales and is overlain by a brecciated dolomite.

Eight samples were collected from Torres de Albarracin. TA1-TA6 from the column of Torres de Albarracin and TA7 and TA8 from Barranco de las Fuentes (Fig. 4.4). All samples were taken from subunit T2 of the "Lutites y Arenscas de Tormon".

Fig. 4.4 Sedimentological column compiled by Perez-Arlucea (1985), showing horizons from which Torres de Albarracin and Barranco de la Fuentes samples were taken.

4.3 DIAGENESIS

4.3.1 Introduction

The samples from the three localities are compositionally quite similar (Fig. 4.5). The majority are classified as quartzose sublitharenites. Samples from Barranco de la Hoz (MA112-MA116), are particularly rich in quartz and those from Torres de Albarracin (TA1-TA8) are more feldspathic than those from the other two areas.

The results of a point count analysis are shown in Appendix VII. They show that the mineralogy of the Saxonian deposits consists predominantly of quartz (detrital: 35%-64%, authigenic: 10%-18%), feldspars (1%-8%), rock fragments (2%-17%), micas (<1%-4%), clays (1%-15%), iron oxide (8%-28%) and carbonate cement (<15%). Accessory minerals account for <1% of the total and consist mainly of tourmaline, zircon, rutile and barite. Visible porosities are generally quite low ranging from <1%-7%. The rocks are fine-medium grained sandstones, with average grain sizes ranging from 0.13mm to 0.26mm.

4.3.2 Diagenetic Transformations

4.3.2.1 Barranco de la Hoz

As mentioned in the last section, the sandstones of Barranco de la Hoz are rich in quartz (47%-64%) and when authigenic quartz is added, the total reaches up to 73% (MA112). The vast majority of the detrital grains are monocrystalline. Many contain abundant vaccuoles. Some grains have undulose extinction and a few show stress cracks (evidence of compaction). Between 1% and 6% of the grains are polycrystalline, probably derived from a low rank metamorphic source. Many of the detrital quartz grains and other framework minerals are coated by a very thin layer of iron oxide stained detrital clays.

Feldspars comprise less than 3% of the total and consist almost entirely of potassium rich orthoclase. This low figure may not reflect the total amount of feldspar present in the rocks at the time of deposition since all existing grains show extensive alteration and replacement. Partial dissolution of grains, preferentially along cleavages, is accompanied by replacement by clay minerals.

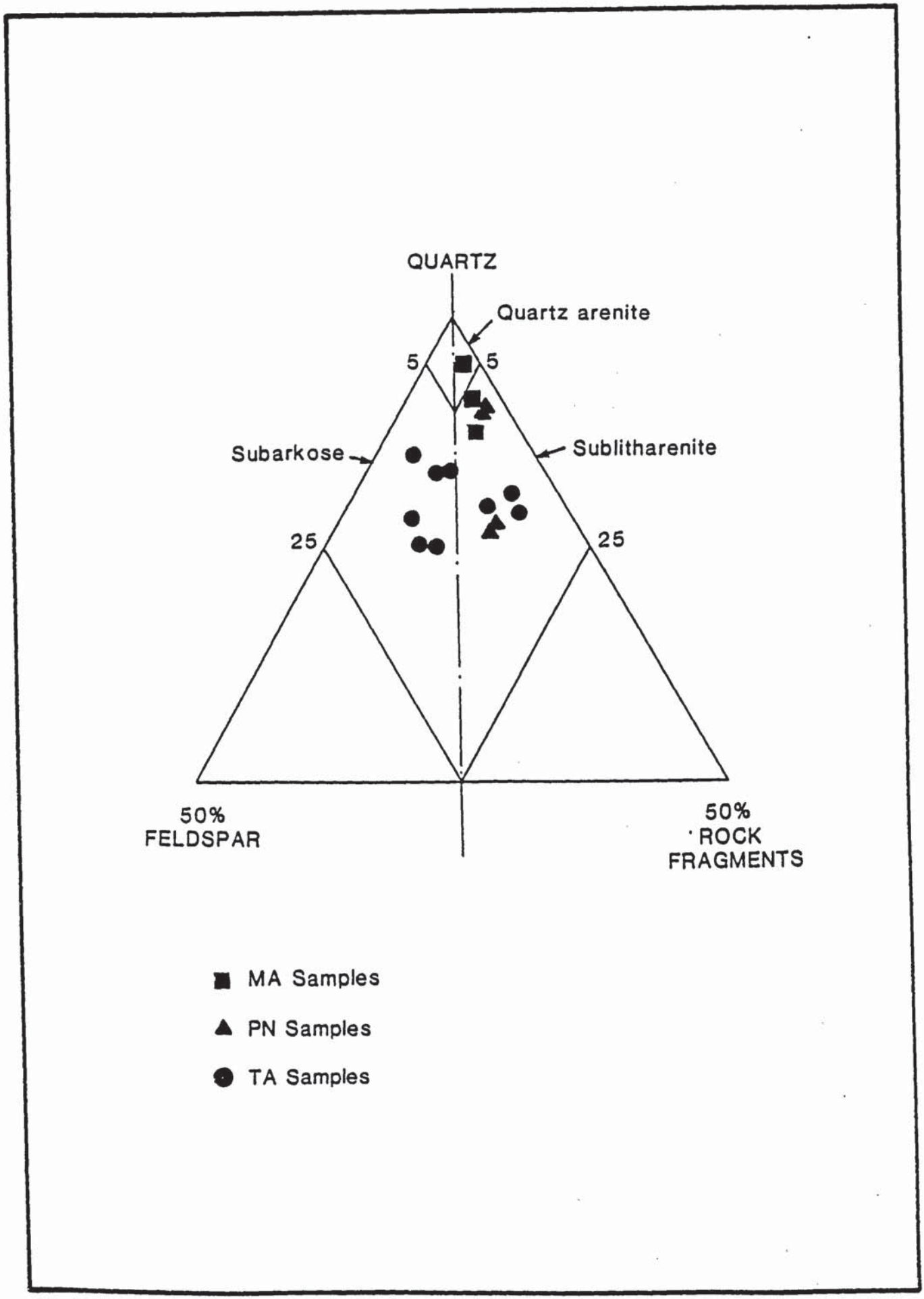

Fig. 4.5 Q.F.R. ternary diagram showing composition of sandstones from the Saxonian.

Rock fragments account for up to 5% of the total. Sedimentary rock fragments are the most abundant, mainly consisting of recycled quartz grains with authigenic overgrowths which have been rounded during transport. Metamorphic and volcanic rock fragments are also present but most have been almost totally replaced by clays and/or iron oxide. Micas too, have been partially replaced by clays in many cases (Plate 4.2a).

Authigenic quartz is by far the most abundant authigenic mineral in these deposits accounting for 9%-18% of the total volume of the rocks. It occurs as syntaxial overgrowths on detrital grains and, in places, as a pore occluding cement. Two phases of authigenic quartz can be identified in places (Plate 4.2b). A thin dust line separates the two phases.

Authigenic clay is abundant in these sediments. It has replaced many of the more labile framework grains including feldspars, rock fragments and micas (Plate 4.2c) hence creating an epimatrix. X-ray diffraction analyses (Fig. 4.6 and Table 4.1) show that illite is the most abundant clay mineral in these deposits ranging from 39% of the total in sample MA112 gradually increasing to 77% in sample MA116. Kaolinite is also very abundant in the lower two samples, comprising 32%-39% of the total clay content. Amounts are much lower in the upper part (6%-11%). Petrographic work shows that the kaolinite is primarily a pore filling clay and rarely replaces other minerals (Plate 4.2c).

TABLE 4.1. Results of semi-quantitative analysis carried out on the <2μm fraction of clays from Saxonian deposits.

	Illite	Kaolinite	Mont.	Chlorite	Total
MA112	39	32	26	3	100%
MA114	48	39	8	5	100%
MA115	63	6	39	2	100%
MA116	77	11	7	5	100%
PN3	70	7	21	2	100%
TA4	96	3	0.5	0.5	100%
TA8	89	6	4	1	100%

Montmorillonite shows an irregular distribution. Samples MA112 and MA115 contain abundant smectite (26% and 39% of the total respectively) but samples MA114 and MA116 contain less than 10%. Amounts of chlorite are low in all samples (5% or less).

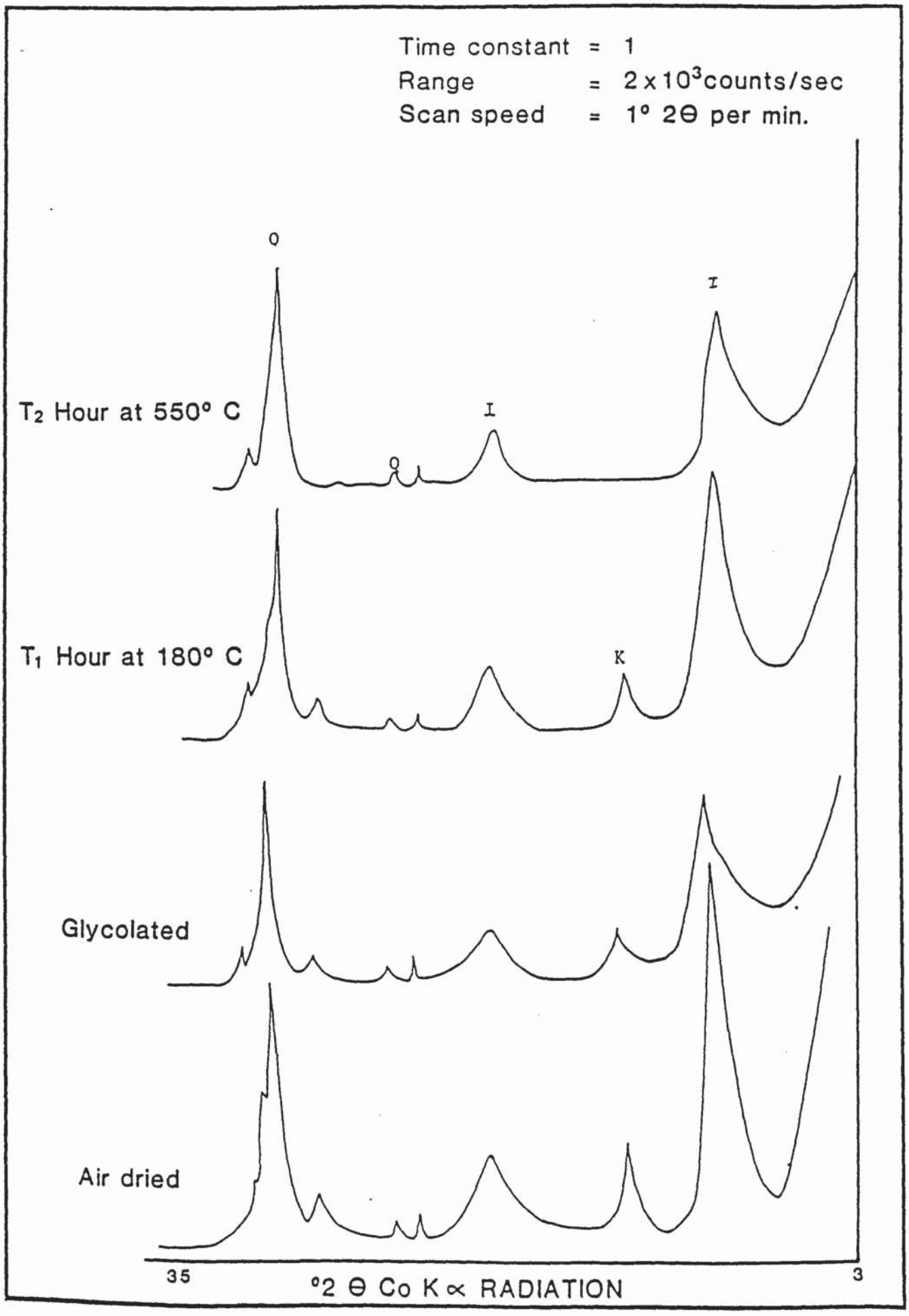

Fig. 4.6 X-ray diffractograms for the <2μmclay fraction sample MA115.

In addition to clay minerals, small X-ray diffraction peaks for analcime, corrensite, anhydrite, gypsum and barite were also detected in the Barranco de la Hoz samples. Of these, only barite was seen commonly in thin section e.g. MA116. It occurs as a late cementing mineral (Plate 4.2d), post dating authigenic quartz but is also patchy in nature.

X-ray diffraction peaks for siderite, calcite and dolomite were confirmed by the presence in thin section of all three carbonates. Non-ferroan dolomite is only rarely present. It occurs as small relict crystals often showing a rhombic outline. Calcite is difficult to identify in thin section. It occurs mainly as relict crystals, often engulfed by pore filling iron oxide. Siderite is more common than the other carbonates. It occurs as a patchy pore filling cement which corrodes all other minerals. Almost total alteration of the siderite to iron oxide and/or iron hydroxide has occurred. Quartz grains often show 'V' shapes indentations (Plate 4.2e) or have been partially replaced by siderite. Sometimes grains are left 'floating' in this thick, pore filling, iron oxide cement (Plate 4.2f).

Porosities in these Saxonian rocks are generally low (1%-7%) but originally were probably much higher. Reduction of the porosity has occurred mainly due to the creation of epimatrix and the growth of authigenic minerals. Evidence of secondary porosity is seen in all samples and is predominantly moldic or grain dissolution porosity. A small proportion of the porosity is also due to fractures.

4.3.2.2 Pozo Nuncio

The samples collected from Pozo Nuncio are red, fine grained silty sandstones. Detrital quartz makes up the majority of the framework grains and of these 60%-70% are monocrystalline, 12%-25% show undulatory extinction and 10%-15% are polycrystalline grains. Some grains contain stress cracks and more rarely, inclusions of numerous rutile needles. In certain areas, many of the grains have corroded and embayed margins.

Feldspars comprise up to 7% of the total composition of the rocks. Both plagioclase and potassium feldspars are present, although the latter are much more abundant. Rock fragments of sedimentary, igneous and metamorphic origin are all present in the deposits. Both the feldspars and the rock fragments show replacement by clays (creating epimxatrix) and iron oxide. Pseudomatrix has also been created in places due to the gentle compaction of the sequence.

Micas show replacement by iron oxide and clays. The growth of neomorphic kaolinite within the splayed cleavages of muscovite laths is fairly common.

Authigenic minerals are similar to those found in samples from the previous locality i.e. quartz, clay minerals, iron oxide, dolomite and barite.

Authigenic quartz often forms euhedral overgrowths on detrital grains with little or no dust line visible. This suggests that quartz authigenesis occurred very early. As in the samples from Barranco de la Hoz, more than one phase of authigenic quartz has been identified.

X-ray diffraction analysis carried out on sample PN3 reveals that illite is the major clay in these deposits (Table 4.1). Semi-quantitative analysis indicates that it comprises 70% of the total. Montmorillonite is the next most abundant with 21%, kaolinite accounts for 7% and chlorite the remaining 2%. Kaolinite occurs either as a pore filling clay (Plate 4.3a) or grows neomorphically in muscovite cleavages. The remaining clays replace all the framework grains except quartz.

Patches of 'aggressive' siderite are seen in sample PN4 (Plate 4.3b). In places where this cement occurs, framework grains are severely etched and embayed and often 'float' in the now oxidised cement. The siderite clearly post dates authigenic quartz since overgrowths of quartz also show etching and 'V' shaped indents.

Dolomite cement is present in only one sample (PN3). It is a poikilotopic non-ferroan dolomite cement which fills pores and has a blocky appearance (Plate 4.3c). The dolomite is an aggressive cement, it replaces all the framework grains including quartz, hence the previously described corroded margins. In thin section the dolomite often shows microporosity and appears, in place, to be partially dissolved. This sample also contains a small amount of non-ferroan calcite cement.

Porosities in the Pozo Nuncio samples are low (<6%), and are entirely secondary in nature. Over sized pores (Plate 4.3d) and microporosity are the major porosity types present. Both are due to the dissolution of dolomite cement. Moldic porosity due to framework grain dissolution is also present.

4.3.2.3 Torres de Albarracin

The Saxonian deposits of Torres de Albarracin contain more feldspar than those in the previously described areas. The rocks are predominantly subarkoses with subordinate sublitharenites (Fig. 4.5). Micas and heavy minerals are also abundant. Rock fragments are mainly of volcanic origin.

The diagenetic transformations which have occurred in these samples are similar to those described for the Saxonian in the other localities. They include the in situ dissolution of chemically weak grains, the replacement of detrital grains by clays and iron oxides, the precipitation of authigenic minerals, compaction features and the creation of secondary porosity.

Feldspars are the most common detrital grains demonstrating in situ grain dissolution. Other labile minerals, e.g. amphibole or pyroxene, may also have been completely removed from these deposits soon after deposition, all evidence of their presence has now gone.

Micas, rock fragments and feldspars all show at least partial replacement by clays and/or iron oxide. Muscovite is commonly altered to kaolinite (Plate 4.e) and biotite frequently shows replacement by iron oxide.

Authigenic quartz, in the form of well developed syntaxial overgrowths and authigenic potassium feldspar, forming non-syntaxial overgrowths, both appear to be early diagenetic features since dust rims are rarely present between detrital grain and overgrowth. Authigenic feldspar may also infill previously etched parts of the detrital grain. Evidence for later corrosion and dissolution of these authigenic phases is seen in many places. Feldspar overgrowths often show 'saw tooth' margins and even quartz overgrowths are commonly embayed. Under S.E.M., 'V' shaped dissolution notches can be seen on the surface of some authigenic overgrowths of quartz (Plate 4.3f).

Clays are common in these deposits, although their abundance is severely restricted in areas where authigenic quartz is well developed. This suggests that most of the clay is authigenic. Illite is the predominant clay. Many of the phyllosilicates, rock fragments and feldspars show replacement by illite. This replacement was probably pre-compaction, since much of the illite has subsequently been squeezed between framework grains to form pore filling matrix. Under S.E.M. the pore filling illite has a matted fibrous appearance.

X-ray diffraction work on sample TA4 and TA8 (Figs. 4.7, Table 4.1) also indictes that illite is the most abundant clay in these deposits. Kaolinite, montmorillonite and chlorite are also present in small amounts. The kaolinite, besides replacing muscovite, is also found as a pore filling clay. Mixed layer illite/montmorillonite is the next most abundant clay after illite and kaolinite. It commonly demonstrates 'honeycomb' texture (Plate 4.4a) when viewed under the S.E.M..

Non-ferroan dolomite is present in all samples. It occurs mainly in association with feldspars. It is not clear whether this carbonate infills previously etched grains or else involves straight forward partial replacement of the detrital grains. The dolomite also infills pores and corrodes detrital and authigenic quartz (Plate 4.4b).

Siderite, in the form of an aggressive patchy cement corrodes and embays all the previously described phases. Rhombic shaped indentations into authigenic quartz are frequently seen (Plate 4.4c). Oxidation of much of this siderite to iron oxides and hydroxides (Plate 4.4d) has occurred, leaving only relict siderite crystals in a thick opaque cement.

Compaction features in these deposits include bent and broken micas, stress cracks in quartz and punctured and crushed grains. The latter giving rise to pseudomatrix.

Porosity varies from 1%-6% in the samples studied and is almost entirely of secondary origin. It is mainly due to the dissolution of dolomite cement. Embayed and corroded grains (often lined with a later iron oxide coat) are evidence of the former presence of carbonate. Over sized and irregular shaped pores, some containing relict dolomite are also seen as well as the previously described dissolution pits on authigenic quartz. Moldic porosity due to dissolution of feldspars accounts for the remaining porosity.

Phases of late pore filling quartz and kaolinite fill secondary pores lined with thick iron oxide, thus, reducing the porosity of the rocks to their present levels. The quartz shows no signs of corrosion and forms secondary overgrowths on previously corroded authigenic quartz.

4.3.3 Iron Oxide Mineralogy

The magnetic mineralogy of the Saxonian sediments from all three localities sampled is similar and will be discussed together.

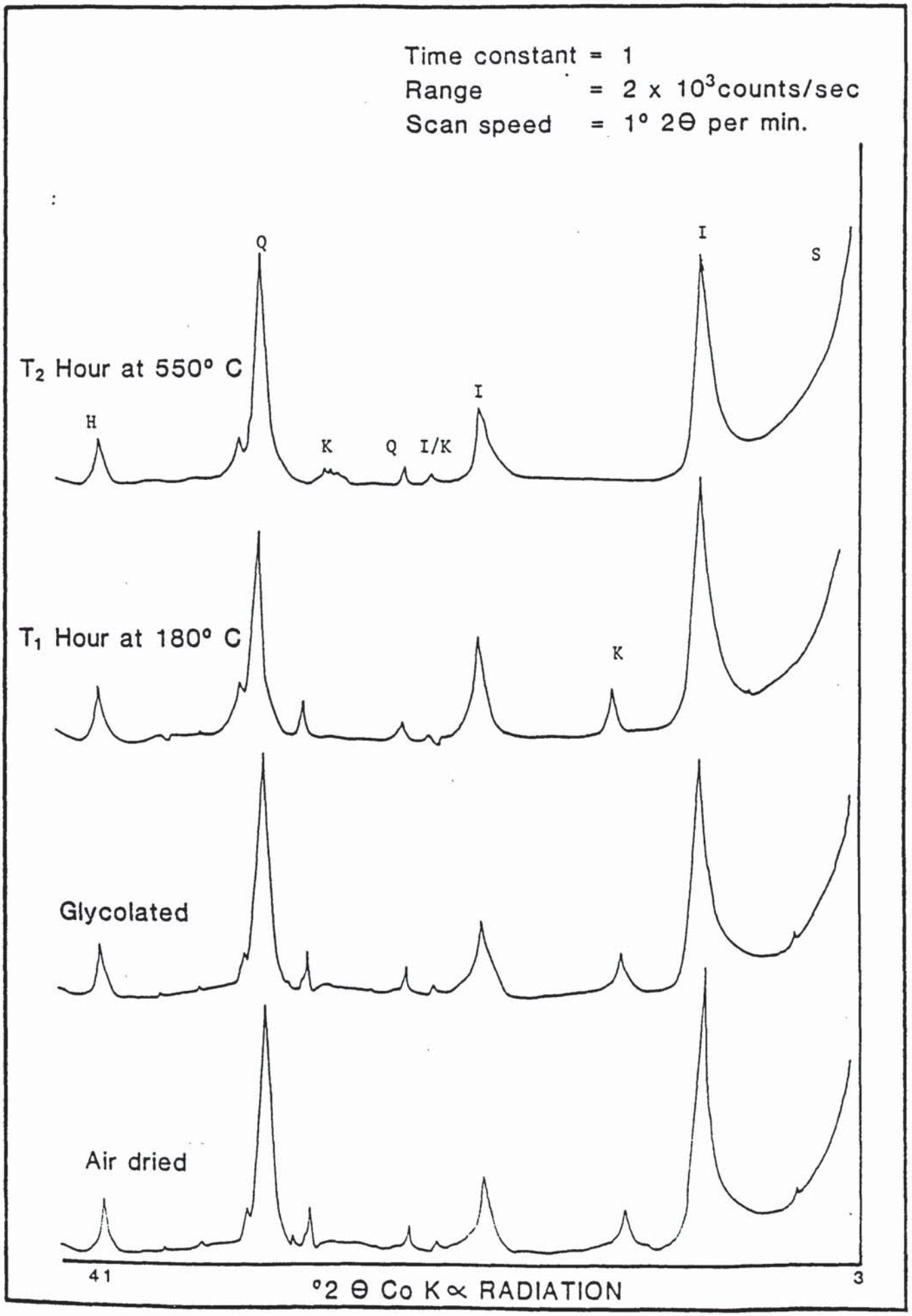

Fig. 4.7 X-ray diffractograms for the <2μm clay fraction sample TA8.

The total iron oxide content of these deposits (as revealed by point count analysis) is high, with an average of 20% in the Barranco de la Hoz deposits, 16% in the Pozo Nuncio samples and 13.4% in the rocks from Torres de Albarracin. Petrographic studies show that most of the iron oxide is diagenetic with only 5%-12% of the total having a detrital origin.

Detrital haematite and ilmenite occur predominantly as monocrystalline grains of between 50μm-200μm. Specularite grains containing ilmenite crystals are also present (Plate 4.4e). The detrital grains frequently have an embayed or skeletal appearance and many also show replacement by fine grained, pigmentory iron oxide or titanium oxide (Plate 4.4f). Martites are not present.

Authigenic haematite is present in a number of different phases. The earliest phase is associated with the fine grained clay which, in places, coats the detrital grains (Plate 4.5a). This grain rimming haematite occurs predominantly as very fine grained, poorly crystalline pigment, but in some instances, microcrystalline haematite has developed (Plate 4.4d).

Rock fragments (especially schistose rock fragments), feldspars and phylosilicates (mainly biotite) also show replacement by haematite (Plate 4.5c). This occurs along cleavage traces and at grain margins initially, but in many cases, complete pseudomorphs are formed.

Authigenic titanium oxide is common in these sediments. It often occurs as euhedral acicular crystals (Plate 4.5d). Authigenic haematite, besides lining detrital grains, also forms syntaxial overgrowths on specularites and occurs within the matrix.

Most of the iron oxide in the Saxonian deposits occurs as pore filling cement (Plate 4.5e). Reflected light petrography shows this phase to be composed of microcrystalline haematite and probably derived from the oxidation of siderite (Plate 4.5f).

4.3.4 Paragenesis

The diagenesis of the Saxonian sediments from Barronco de la Hoz, Pozo Nuncio and Torres de Albarracin appears to be very similar (probably due to the similarities in original composition and depositional environment of the sediments).

The earliest diagenetic transformations to occur in these deposits resulted from the attempted equilibrium of depositional pore waters and the detrital sediments. Aerobic bacterial bicarbonate production would have lowered pH values, and in dilute fresh water promoted dissolution of amorphous and relatively unstable detrital aluminosilicates (cf. Curtis, 1978).

These transformations include the in situ dissolution of labile grains, including feldspar. During wetter periods the porous sediments enabled a supply of fresh water to circulate in the rocks maintaining aerobic, oxidizing conditions with low ionic strength. This suppressed ferrous iron formation and with a supply of alumina and silica from mineral dissolution, quartz overgrowths and kaolinite precipitated (Garrels and Christ, 1965; Curtis and Spears, 1971).

As bacterial ferric iron reduction commenced pH rose and bicarbonate concentrations rose. Illite and potassium feldspar overgrowths precipitated locally and in places a non-ferroan dolomite cement formed when oxigenated fresh water was periodically introduced.

Siderite was the next major authigenic mineral to form, replacing and enclosing all the minerals described above. Kantorowicz (1985), has described similar siderite precipitation in the non-marine clastic sediments from the Middle Jurassic Ravenscar Group of Yorkshire. Isotopic evidence from these deposits suggested that siderite precipitation was from a fresh water source but in anoxic conditions and hence, probably occurred during dryer periods when there was little or no water recharge.

As burial of the sequence took place pore waters became more reducing and ferroan carbonate precipitated. A second change of pore water composition to a lower pH, perhaps due to uplift, resulted in the widespread dissolution of carbonate cements (especially siderite) creating secondary porosity. Iron oxide and iron hydroxide (goethite) precipitated when Fe ions were released into solution, forming thick pore rims or pore filling cement. A second phase of kaolinite and quartz also precipitated in the secondary pores. Finally, weathering of the rocks resulted in clay alteration and the further conversion of siderite and haematite to iron hydroxides.

4.4 PALAEOMAGNETISM

4.4.1 Natural Remanent Magnetization (N.R.M.) Results

Table 4.2. shows the results of initial palaeomagnetic analyses carried out on Saxonian specimens from Barranco de la Hoz, Pozo Nuncio and Torres de Albarracin.

The mean intensity of N.R.M. for each of these sites was 6.81 mAm^{-1}, 2.63 mAm^{-1} and 1.75 mAm^{-1} respectively. The mean initial susceptibility value for the Pozo Numcio specimens was 98 $mAm^{-1}nT^{-1}$ and 134.6 $mAm^{-1}nT^{-1}$ for those from Torres de Albarracin. Susceptibility readings for specimens from Barranco de la Hoz were not taken, since palaeomagnetic measurements were carried out at Aston University, which does not possess a susceptibility bridge.

The majority of the Saxonian samples have initial directions which are steep and positive (Fig. 4.8) and lie close to the present day geomagnetic field direction for this area (especially in the field position). Some scatter is seen, however, with directions extending from the northeast towards the southwest quadrant. This is best demonstrated by the bedding corrected directions of the TA samples.

4.4.2 Isothermal Remanent Magnetization (I.R.M.) Results

I.R.M. curves for four Saxonian samples (MA115, PN3, TA1 and TA6) are shown in Fig. 4.9.

All four samples show a fairly slow rate of remanence acquisition with MA115 and PN3 showing the most rapid acquisition and TA1 the slowest acquisition of remanence (this curve is initially concave downwards).

None of the samples reaches full saturation although MA115 comes the closest. Reverse field demagnetization curves are also shown. These also demonstrate a fairly gradual decrease in remanence with increasing field strength. Samples MA115 and PN3 fall to zero intensity by 0.3T. Sample TA6 by 0.4T and TA1 by 0.55T. The peak intensity of magnetic remanence reached by MA115 was 238 mAm^{-1}. The other three samples reached intensities of over 3000 mAm^{-1} with TA1 exceeding 5000 mAm^{-1}.

The above results suggest that the magnetic remanence of all these samples is carried primarily by haematite.

TABLE 4.2 N.R.M. RESULTS FOR THE SAXONIAN

Sample	Height (m)	F Dec(°)	F Inc(°)	P Dec(°)	P Inc(°)	Pole Long(°)	Pole Lat(°)	N	R	α95(°)	α95(°) Pole	Intensity (mAm^{-1})	Susceptibility ($mAm^{-1}nT^{-1}$)
MA112	6	83.5	58.4	57.7	62.2	48.2	63.3	5	4.90	8.9	12.0	3.41	-
MA114	9	45.7	17.8	41.8	12.6	118.6	39.9	3	2.42	80.5	42.3	8.18	-
MA115	18	354.9	54.1	347.6	43.1	211.8	69.6	5	4.94	6.7	7.6	8.49	-
MA116	24	11.3	70.7	350.1	62.6	316.5	82.6	5	4.14	39.9	61.0	7.14	-
PN1	92	138.3	64.3	148.7	78.9	11.3	26.0	5	3.81	49.3	82.5	1.06	79.20
PN2	118	337.8	49.8	332.8	40.0	240.0	61.1	5	4.85	15.2	17.6	1.67	99.18
PN3	125	223.9	57.9	243.4	55.3	312.2	7.5	3	2.94	22.6	25.5	2.04	85.27
PN3I	125	11.4	57.6	357.5	49.5	197.3	80.3	4	3.92	15.5	18.3	1.81	-
PN4	35	356.4	46.5	344.7	57.2	265.1	77.8	6	5.93	7.9	9.2	3.93	109.09
PN5	29	351.1	42.1	338.7	35.6	226.4	62.7	6	5.91	9.3	9.5	4.45	117.21
TA1	12	348.6	64.2	238.2	55.8	315.9	4.4	5	4.90	12.1	17.6	6.22	252.46
TA2	24	26.4	-9.7	25.0	32.3	122.9	57.9	4	3.54	39.0	37.0	0.60	58.41
TA2I	24	222.1	76.1	216.8	33.7	319.7	-19.8	4	3.56	38.2	38.1	0.97	58.41
TA3	37	202.3	75.2	211.2	33.0	325.5	-24.5	6	5.85	11.7	12.1	2.12	61.35
TA4	52	33.8	78.1	215.4	50.9	328.3	-10.6	5	4.78	18.5	23.8	0.96	27.05
TA5	58	334.0	74.9	259.6	61.6	309.0	20.1	5	4.88	13.5	19.3	1.62	534.41
TA6	66	300.7	61.4	258.3	54.9	302.8	15.0	5	4.53	27.8	38.3	1.19	57.89
TA6I	66	357.0	26.9	346.2	49.4	247.0	75	3	2.76	45.3	39.5	0.91	57.89
TA7	51	211.7	80.2	197.5	32.6	338.6	-29.2	6	5.79	14.2	14.5	0.75	50.38
TA8	41	349.5	48.7	308.0	61.8	293.3	52.6	4	3.86	20.1	27.1	0.57	36.36

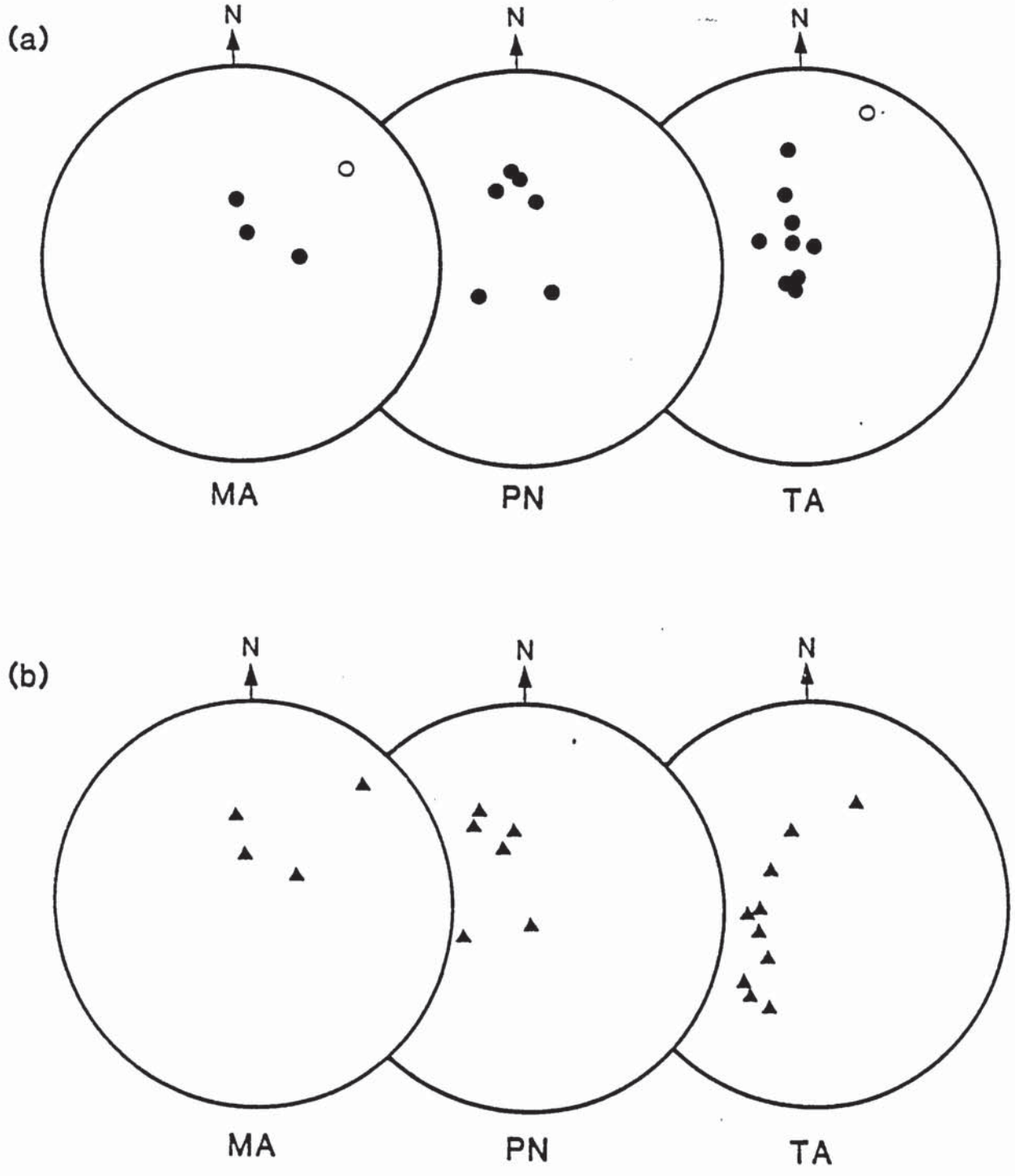

Fig. 4.8 Initial mean N.R.M. directions for the Saxonian (a) before and (b) after correction for bedding.

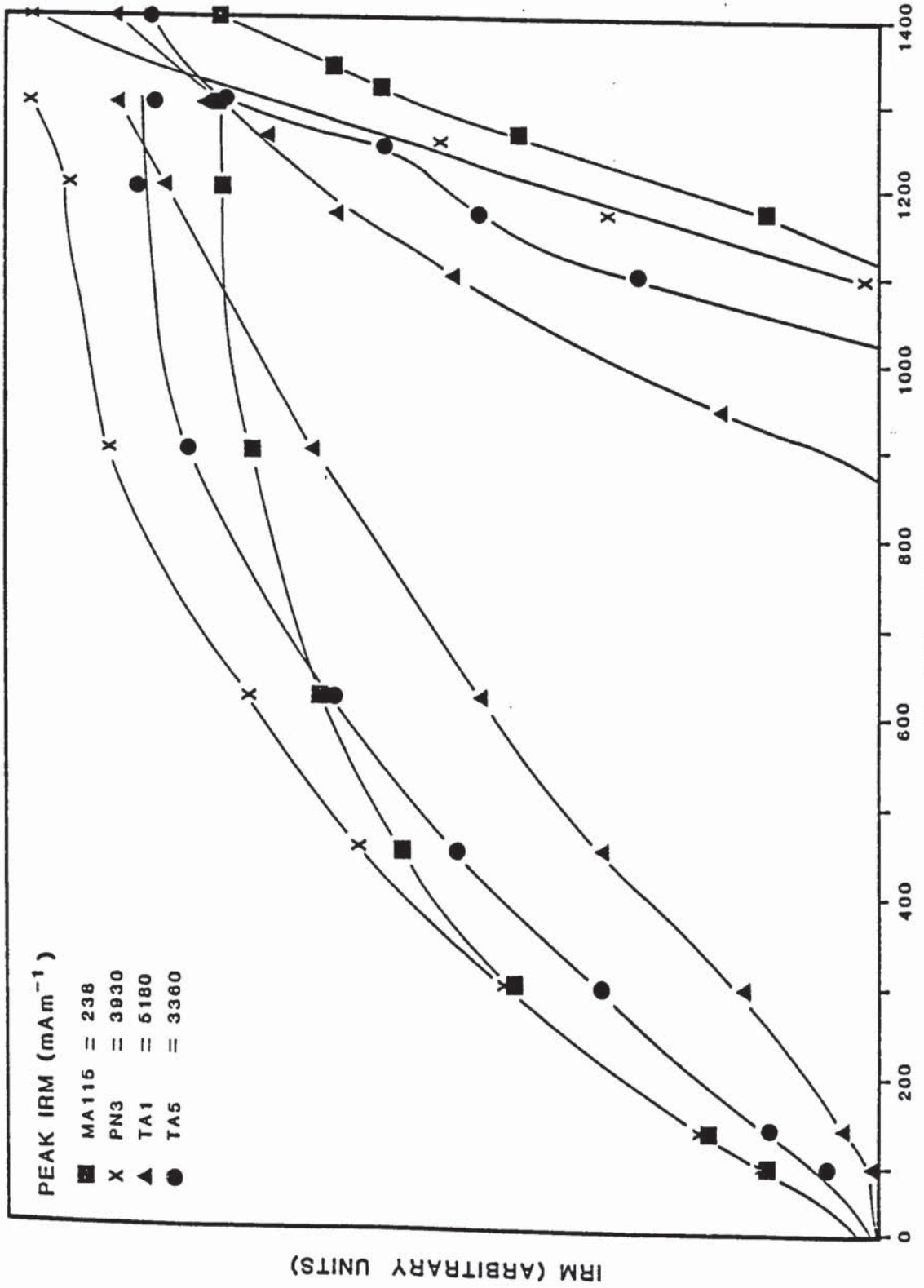

Fig. 4 9 I.R.M. acquisition and reverse field curves for the Saxonian.

Sample MA115 also shows evidence for the presence of a second, low coercivity mineral, since the I.R.M. acquisition curve shows a fairly rapid acquisition of remanence at low field strengths and almost reaches full saturation by 1.4T.

4.4.3 Thermal Demagnetization Results

4.4.3.1 Intensity and Susceptibility Changes

Normalized intensity and susceptibility versus temperature curves are shown for the Saxonian specimens in Fig. 4.10. (susceptibilities were not measured for the MA samples).

Two types of behaviour can be identified from these results:

a) The majority of specimens show no loss in intensity between room temperature and 100°C but do show a drop in susceptibility to approximately 60% of their original value. Between 100°C and 200°C, a slight drop in intensity is recorded by most specimens, to between 70% and 80% of their original values. Stabilities remain fairly constant over this temperature range. Intensities are again fairly constant between 200°C and 400°C. Above this temperature, a gradual loss in intensity occurs, with a maximum blocking temperature of approximately 650°C. Stability curves remain fairly constant up to this point and then show a steep rise.

b) Four specimens (MA112.2.1, MA115.4.1, TA1.1.2, TA5.1.1) show a different type of intensity decay (the susceptibility curves are similar to the previous group). These four specimens show an initial rapid drop in intensity between room temperature and 200°C to between 6% (TA1.1.2) and 50% (MA112.2.1) of their original values. A more gentle drop in intensity is shown by the samples between 200°C and 500°C. Above 500°C, MA112.2.1, and TA5.1.1 show a large gain in intensity. TA5.1.1 also shows a gain in susceptibility, specimen TA1.1.2 continues to lose intensity until 660°C, at which point the specimen is totally demagnetized.

c) One specimen (TA2.3.1) shows an initial rise in intensity between room temperature and 300°C, to 115% of its original value. Above this point a fairly rapid drop in intensity to zero at 660°C is seen.

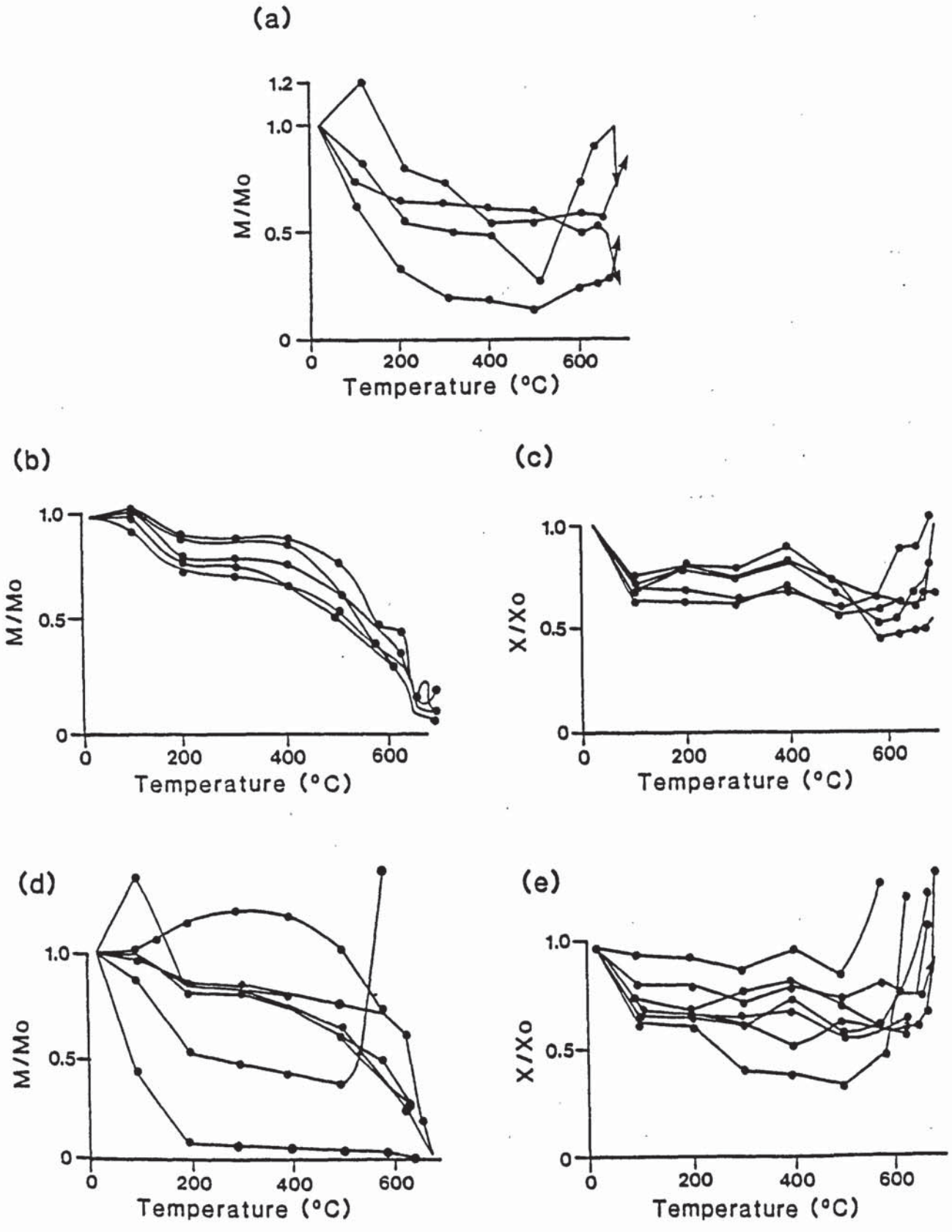

Fig. 4.10 Normalized intensity and susceptibility decay curves for the Saxonian specimens (a) Intensity curve, Barranco de la Hoz, (b) Intensity and (c) Susceptibility curves for Pozo Nuncio, (d) Intensity and (e) Susceptibility curves for Torres de Albarracin.

4.4.3.2 Discussion of Intensity and Susceptibility Results

The majority of the specimens show normalized intensity decay curves consistent with the removal of one predominant magnetic component. This component has a maximum blocking temperature in excess of 600°C and must, therefore, be carried by haematite.

The small drop in intensity and susceptibility shown by the specimens between room temperature and 200°C probably represents the removal of an unstable 'viscous' component of magnetization. Probably carried by poorly crystalline iron oxide or iron hydroxide. Loss of initial susceptibilities during heating may also be due to changes in the relatively soft defect or structure sensitive moment (Dunlop, 1971; Bucur, 1978). Specimens showing the initial rapid drop in intensity probably contain a greater proportion of poorly crystalline iron oxide or iron hydroxide. The reason for the large increase in intensity and susceptibility shown by MA112.2.1 and TA5.1.1 at 500°C is unknown. No common magnetochemical reactions, likely to have caused such sudden increases, have been reported at this temperature.

4.4.3.3 Directional Changes

A variety of directional changes are shown by the Saxonian specimens during thermal demagnetization. Figure 4.11 shows a typical example from Barranco de la Hoz (MA115.4.1).

The initial direction is steep and positive and lies in the northwest quadrant. Above 300°C the direction gradually moves southwards to a shallow direction in the southeast quadrant. Above 630°C, the direction moves northwards to a shallow negative direction in the northwest quadrant.

The normalized intensity decay curve (Fig. 4.11b) shows an initial rapid drop in intensity between room temperature and 300°C. Between 300°C and 500°C the intensity remains fairly constant at about 20% of the original value. Above 500°C the intensity rises slightly. It does not fall to zero. The orthogonal vector plot shows a similar demagnetization sequence.

The three other specimens from Barranco de la Hoz show similar behaviour i.e. an initial steep positive direction is gradually removed to reveal a second shallow direction in either the northeast (MA114.2.1) or southeast (MA112.2.1, MA116.2.1) quadrant.

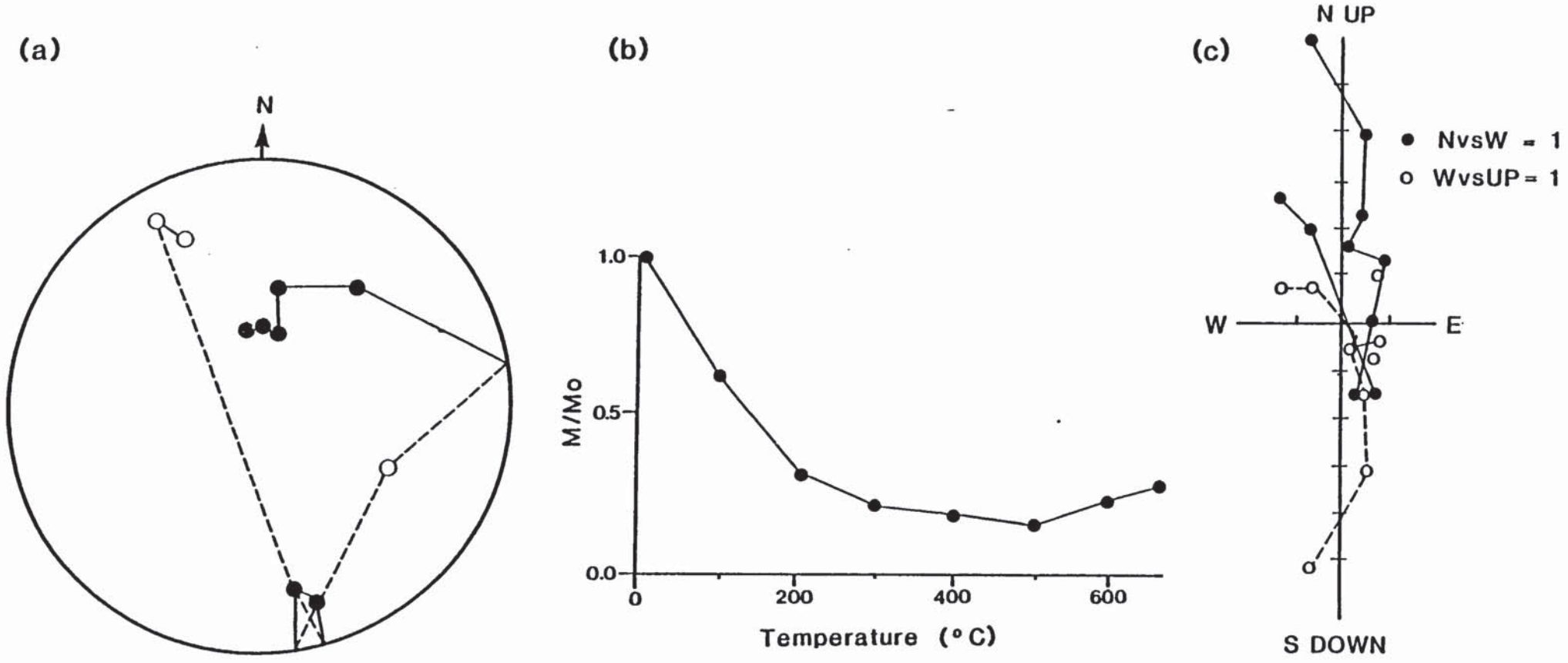

Fig. 4.11 Palaeomagnetic behaviour demonstrated by MA115.4.1 during partial thermal demagnetization (a) Stereographic projection, (b) Normalized intensity decay, (c) Orthogonal vector plot.

The specimens from from Pozo Nuncio show two characteristic types of behaviour.

TYPE A: The first type is well demonstrated by specimen PN2.7.1 (Fig. 4.12a-c). Initially, the direction is normal and lies in the northwest quadrant. Above 580°C, the direction moves first northeastward and then to a shallow negative direction in the northwest quadrant. The intensity decay curve shows a gradual drop in intensity to 630°C followed by a rapid drop to zero by 690°C. The orthogonal vector plot also shows the gradual removal of one main component of magnetization.

TYPE B: A second type of demagnetization behaviour is shown by specimen PN1.4.1 (Fig. 4.12d-f). (This specimen also demonstrates one major component of magnetization, the most stable bedding corrected direction is D = 54.4°, I = 45.2°, S.I. = 5, over the temperature range 200°C to 580°C). This is fairly steep positive and lies in the northeast quadrant. It is gradually removed (as seen on the intensity decay and orthogonal vector plots) but does not move direction until temperatures of over 580°C are reached. The final direction is shallow, negative and in the northern part of the stereogram.

Specimens from Torres de Albarracin show more variation than those from the previously described localities. Three basic types of behaviour can be identified.

TYPE A: The majority of specimens (TA1.1.2, TA3.2.1, TA4.2.1, TA5.1.1 and TA7.1.1) fall into the first type of behaviour which is well demonstrated by specimen TA4.2.1 (Fig. 4.13a-c). The initial direction is positive and lies in the southwest quadrant with an inclination of approximately 40° from the horizontal (The most stable direction is D = 220°, I = 42°, S.I. = 11.1 over the range 20°C to 500°C). During thermal demagnetization this direction remains stable until temperatures in excess of 650° are reached. Above this point the direction moves northwards to an end point in the northwest quadrant with a shallow, negative inclination.

The normalized intensity decay plot (Fig. 4.13b) shows an unusual gain in intensity between room temperature and 300°C followed by a more rapid drop to zero intensity at 690°C. The specimen has a very low intensity at this temperature and the direction may not be reliable. The orthogonal vector plot (Fig. 4.13c) shows the gradual removal of one stable magnetic component.

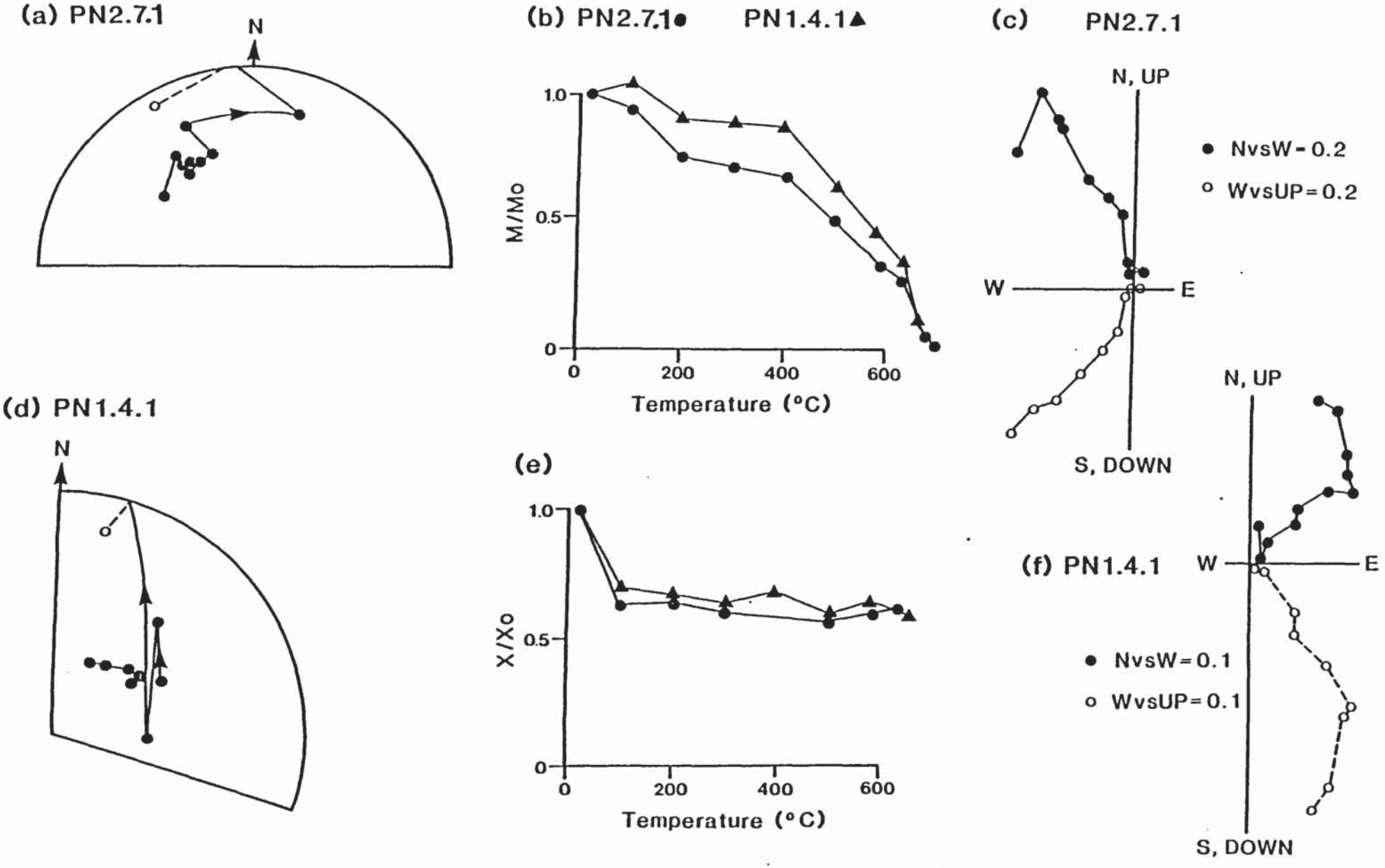

Fig. 4.12 Palaeomagnetic behaviour demonstrated by specimens PN2.7.1 and PN1.4.1 during partial thermal demagnetization; (a) and (d) Stereographic projections, (b) Normalized intensity decay curves, (c) and (f) Orthogonal vector plots, (e) Normalized susceptibility decay curves.

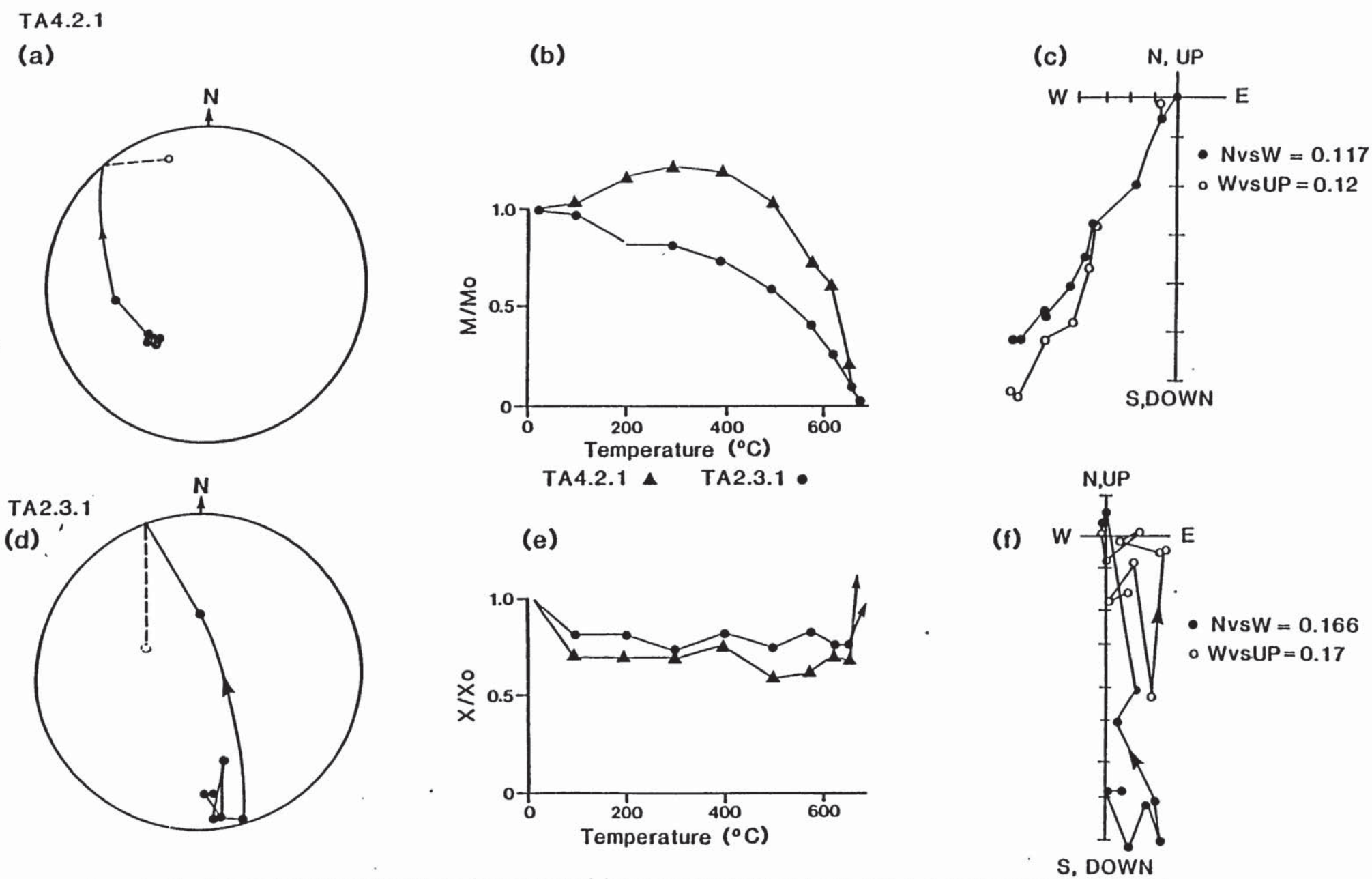

Fig. 4.13 Palaeomagnetic behaviour demonstrated by specimens TA4.2.1 and TA2.3.1 during partial thermal demagnetization; (a) and (d) Stereographic projections, (b) Normalized intensity decay curves, (c) and (f) Orthogonal vector plots, (e) Normalized susceptibility decay curves

The other specimens in this group show the same stable component of magnetization in the southwest quadrant. At high temperatures, however, the directions vary considerably although a general movement norheastwards is noted.

TYPE B: Two specimens (TA6.5.2 and TA8.3.1) show steep, normal initial directions of magnetization lying in the northwest quadrant. At temperatures above 500°C the direction moves slightly northwards.

TYPE C: The final type of behaviour deomonstrated by the Torres de Albarracin sediments is shown by specimen TA2.3.1 (Fig. 4.13b, d-f). Initial directions for this specimen are shallow, positive and lie in the south when plotted on a sterographic projection (Fig. 4.13d) (the most stable bedding corrected direction occurs between 400°C to 630°C and is D = 168°, I = 3°, S.I. = 3). The direction remains stable until 630°C at which point it moves northwards into the northwest quadrant. The normalized intensity and susceptibility decay plots appear to show the presence of just one component of remanence which is gradually removed. The orthogonal vector plot however, (Fig. 4.13f) shows that at least two components are present.

4.4.3.4 Thermal Demagnetization Summary

The results of partial thermal demagnetization of the Saxonian deposits are shown in Table 4.3.

The specimens from Barranco de la Hoz show most stable directions (after correction for both field and bedding) grouped around the present-day local geomagnetic field position for the area (Fig. 4.14a). Stability values range from S.I. = 1.9 (MA115.4.1) up to S.I = 5.6 (MA112.2.1). Directions which pass the 10° linearity test also show a steep positive component of magnetization which lies close to the present day local field position. Directions also extend into the southeast quadrant. These include two shallow components (Fig. 4.14b) which are both stable above 600°C.

The most stable directions and directions passing the 10° linearity test are shown in Fig. 4.15 for specimens from Pozo Nuncio. These, both show directions which are predominantly fairly steep, positive and lie in the northwest or northeast quadrants. Stability values for these specimens are generally fairly high (S.I. = 5.0-5.6) except for PN5.2.2 (S.I. = 0.8).

TABLE 4.3 STEPWISE THERMAL AND CHEMICAL (C) DEMAGNETIZATION RESULTS FOR THE SAXONIAN

Specimen	S.I.	Most stable directions Dec(°)	F Inc(°)	F Dec(°)	P Inc(°)	Pole Long(°)	Pole Lat(°)	N	R	α95(°)	Range (°C)	Directions passing 10° linearity test Range(°C)	F Dec(°)	F Inc(°)	P Dec(°)	P Inc(°)
MA112.4.1	5.6	28.6	66.3	6.4	57.3	116.9	84.3	3	2.99	3.7	20-210	115-320	7.9	59.2	356.3	49.0
												20-210	28.5	73.0	0.6	63.8
MA114.2.1	2.3	307.6	39.4	311.4	25.7	249.6	39.7	3	2.99	9.4	200-400	100-300	177.4	61.7	190.8	75.3
MA115.4.1	1.9	13.2	51.3	3.2	40.2	168.7	71.8	3	2.98	11.0	20-200	640-675	155.6	4.2	156.1	19.1
												600-660	100.2	10.0	161.7	24.3
												100-300	17.7	54.7	5.7	43.8
												20-200	348.2	56.9	343.5	42.5
MA116.2.1	2.7	345.8	72.1	337.0	57.8	267.7	72.2	4	3.98	7.0	115-400	115-400	353.8	53.4	348.2	41.8
												500-675	346.5	79.6	342.3	81.1
PN1.4.1	5.0	67.3	39.9	54.4	45.2	88.2	43.5	5	4.99	3.7	200-580	400-580	76.9	33.1	67.2	41.1
												200-400	351.1	37.3	345.4	25.4
PN2.7.1	15.6	332.7	39.2	329.8	29.1	234.1	53.9	3	3.00	1.4	200-400	400-630	321.3	40.2	319.6	29.4
PN4.3.1	6.1	359.0	38.2	351.0	49.5	217.6	77.6	6	5.99	3.0	20-500	100-690	358.5	38.6	350.3	49.8
PN5.2.2	0.8	16.2	40.1	1.6	40.6	40.6	1.6	4	3.87	19.4	500-600	100-690	4.2	44.1	348.7	40.9
TA1.1.2	3.4	220.8	34.8	218.8	-14.3	301.5	-42.1	3	2.98	6.4	300-500	580-660	234.0	31.8	230.6	-14.2
												20-300	346.8	41.0	282.5	59.0
TA2.3.1	3.0	157.6	30.5	168.2	3.4	15.7	-46.5	4	3.98	5.8	400-630	400-660	159.7	26.1	167.4	-1.3
TA3.2.1	5.0	204.7	59.9	209.6	17.8	322.7	-33.4	4	3.99	3.9	200-500	580-660	218.4	78.2	215.8	35.7
												400-580	192.4	36.8	197.1	-3.3
												200-400	294.8	51.3	260.3	30.1
												20-200	56.3	85.2	212.1	52.0
TA4.2.1	11.1	344.9	85.2	219.9	42.0	321.1	-15.4	6	5.99	1.6	20-500	400-690	348.5	86.7	218.2	41.2
												100-300	3.7	73.5	229.0	52.4
												20-200	351.8	75.3	230.2	48.8
TA5.1.1	4.0	5.8	65.7	285.6	70.9	312.3	40.5	3	2.98	5.0	20-200	20-580	311.9	51.7	282.6	40.9
TA6.5.2	0.5	229.1	65.3	216.9	40.7	323.1	-30.8	6	4.64	40.7	100-580	580-660	337.2	19.7	326.3	36.3
												400-580	201.9	57.2	202.2	31.2
TA7.1.1	4.3	224.7	73.9	203.2	27.7	332.1	-30.8	3	2.98	5.1	200-400	630-675	270.9	68.0	220.1	33.9
												500-630	170.7	55.9	181.0	9.8
TA8.3.1	8.9	26.3	49.3	5.9	78.1	3.6	63.0	4	3.99	2.2	200-500	630-675	64.5	56.5	125.1	74.3
												100-630	16.9	55.1	323.6	79.1
CHEMICAL DEMAGNETIZATION RESULTS																
PN4.1.1C	2.1	348.5	52.6	334.5	61.5	284.3	68.6	3	2.99	6.9	33-125 hrs	56-150 hrs	3.4	52.5	350.7	63.9
												33-150 hrs	359.7	52.5	345.5	63.6
TA6.1.1C	0.4	31.8	80.7	197.6	73.2	349.3	10.3	14	10.81	22.6	0-296 hrs	150-240 hrs	355.7	43.13	33.4	64.0
												1.0-16 hrs	130.7	48.9	152.0	36.0

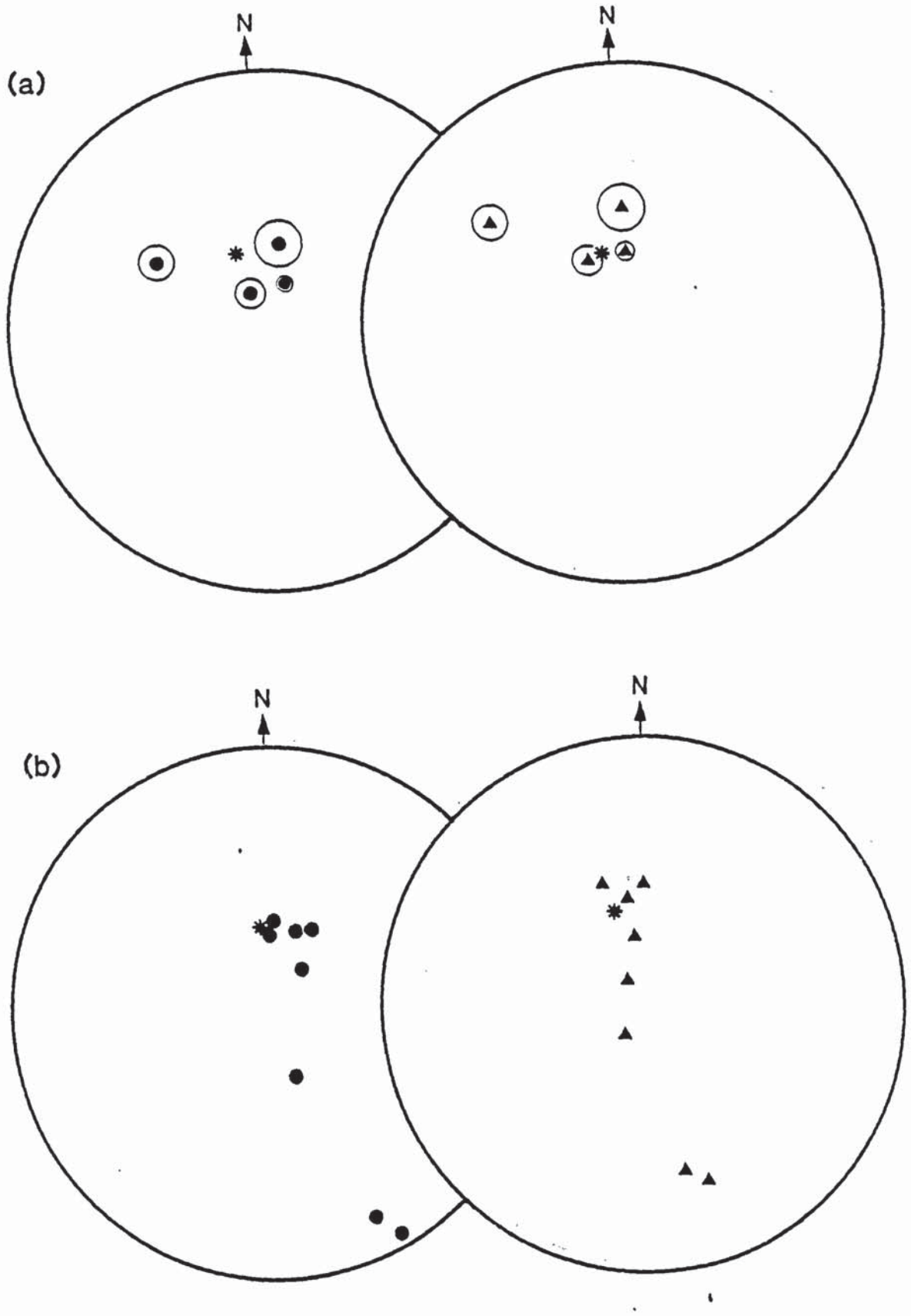

Fig. 4.14 Most stable directions (a) and directions passing 10° linearity test (b) isolated for samples from Barranco de la Hoz.
● field corrected directions.
▲ field and bedding corrected directions
Circles represent α_{95} values.
Asterisk represents present-day geomagnetic field position.

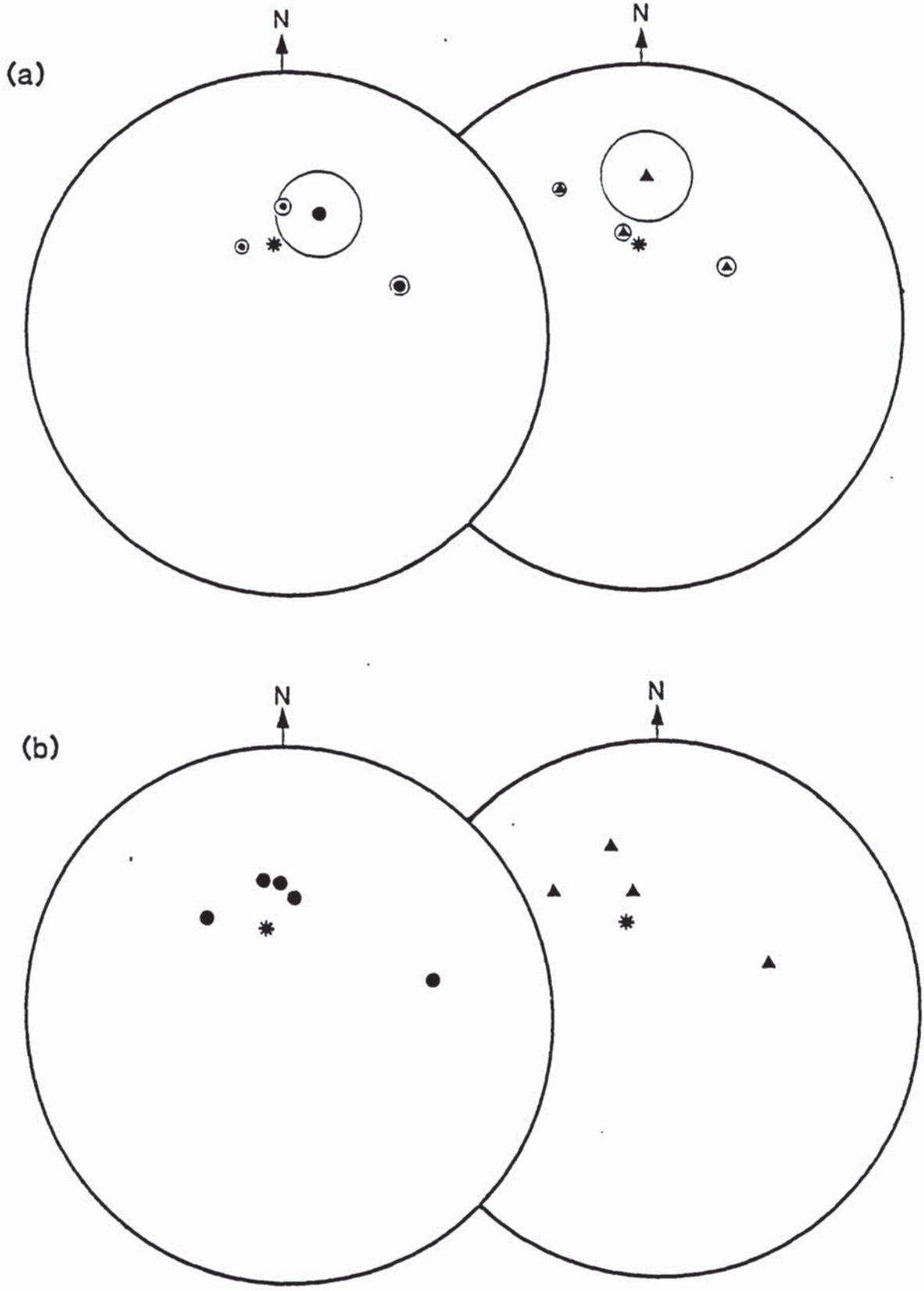

Fig. 4.15 Most stable directions (a) and directions passing 10° linearity test (b) isolated for samples from Pozo Nuncio.
● field corrected directions.
▲ field and bedding corrected directions.
Circles represent α_{95} values.
Asterisk represents present-day geomagnetic field position.

Specimens from Torres de Albarracin have the most stable directions which extend from the northeast quadrant (steep inclinations) towards the southwest quadrant with more shallow directions (Fig. 4.16a). Stability values range from S.I. = 0.5 (TA6.5.2) up to 11.1 (TA4.2.1). One specimen (TA2.3.1) shows a very shallow direction in the southeast quadrant (D = 168°, I = 3°).

Directions which pass the 10° linearity test are numerous (Fig. 4.16b). After correction for bedding three basic groupings can be identified:

(i) Positive and in the northwest quadrant. These are most commonly stable at lower temperatures (20°C-300°C).
(ii) Positive with inclinations of approximately 35° - 50° from the horizontal in the southwest quadrant (directions in this group are common at higher temperatures (>580°C)).
(iii) These have directions which are very shallow (positive and negative) and lie in the southeast quadrant. Directions lying in this group are generally revealed upon heating the specimen to temperatures in excess of 400°C.

4.4.3.5 Bulk Demagnetization Results

Bulk demagnetization of the Saxonian samples was carried out over the temperature range 400°C to 675°C (see Table 4.4). The majority of samples, however, were demagnetized over the range 630°C to 660°C.

All samples from Barranco de la Hoz were thermally demagnetized at temperatures of 630°C or 650°C (except for MA112 which was heated to the 510°C) and results plotted on a stereogram (Fig. 4.17a). Directions (after correction for bedding) are similar to those passing the 10° linearity test, isolated during demagnetization. One group of directions lies close to the present day geomagnetic field direction for Spain. Two samples (MA114 and MA115) show shallow directions in the southeast quadrant.

Figure 4.17b shows the mean bulk demagnetized directions for each sample from Pozo Nuncio (two PN2 directions are plotted). Sample PN1 was heated to 400°C. The remaining PN samples were heated to to 660°C.

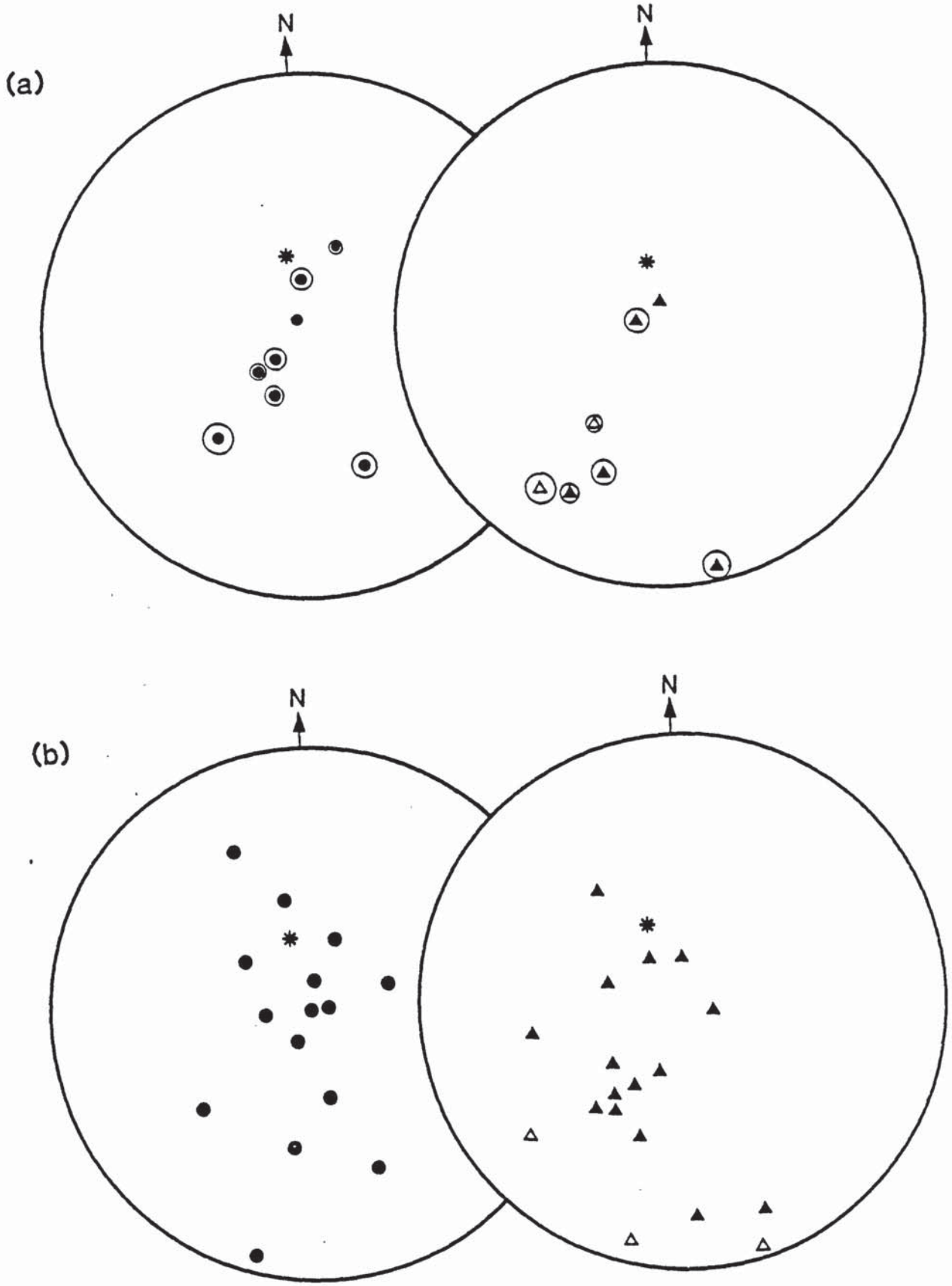

Fig. 4.16 Most stable directions (a) and directions passing 10° linearity test (b) isolated for samples from Torres de Albarracin.
● field corrected directions.
▲ field and bedding corrected directions.
Circles represent α_{95} values.
Asterisk represents present-day geomagnetic field position.

TABLE 4.4 BULK DEMAGNETIZATION RESULTS FOR THE SAXONIAN

Sample	Height (m)	F Dec(°)	F Inc(°)	P Dec(°)	P Inc(°)	Pole Long(°)	Pole Lat(°)	N	R	α95(°)	α95(°) Pole	Intensity (mAm^{-1})	Susceptibility ($mAm^{-1}nT^{-1}$)	Temp (°C)
MA112	6	56.7	75.0	11.0	68.9	-	-	8	6.49	28.8	-	1.25	-	510
MA114	9	171.7	-7.8	171.6	5.6	-	-	1	-	-	-	2.56	-	630
MA114I	9	36.0	53.8	19.9	46.6	-	-	1	-	-	-	1.41	-	650
MA115	18	126.3	-11.0	128.9	2.5	-	-	4	-	25.0	-	2.24	-	630
MA115I	18	60.4	63.5	31.9	60.8	-	-	2	-	39.0	-	2.17	-	650
MA116	24	10.5	53.8	358.5	47.2	-	-	4	-	22.5	-	3.86	-	650
PN1	92	49.6	16.7	44.9	18.6	113.0	39.9	4	3.84	21.7	15.6	0.09	50.0	400
PN2	118	11.0	29.5	6.1	24.1	162.0	62.4	4	3.62	34.9	33.5	0.17	60.0	660
PN2I	118	355.1	-25.6	359.2	-32.8	182.4	29.8	3	2.49	72.7	77.2	0.19	60.0	660
PN3	125	73.7	42.9	61.6	48.5	76.6	39.9	5	4.57	26.6	29.0	0.08	-	660
PN4	35	268.4	73.9	242.9	63.6	326.5	20.9	4	2.57	87.2	90.0	0.22	97.0	660
PN5	29	33.3	55.1	7.2	59.2	71.1	76.7	4	2.65	83.0	90.0	0.50	79.0	660
TA1	12	18.2	30.6	185.0	-15.4	349.6	-58.6	5	4.27	36.1	31.5	0.26	124.0	580
TA2	24	8.9	-12.7	6.7	25.6	164.8	63.6	5	4.50	28.8	25.4	0.10	38.0	660
TA3	37	345.5	62.9	257.1	58.9	307.3	19.1	5	3.70	52.5	72.3	0.10	39.0	630
TA4	52	143.0	75.5	198.4	33.3	338.8	-28.5	4	3.69	31.1	31.5	0.29	21.0	630
TA5	58	121.4	71.3	189.0	60.8	349.2	-1.0	3	2.73	48.5	68.2	0.70	463.0	500
TA6	66	286.5	20.5	278.0	15.7	269.4	11.9	4	3.81	23.9	20.2	0.31	36.0	630
TA7	51	306.5	48.7	308.0	61.8	293.3	52.6	4	3.86	20.1	27.1	0.57	33.0	630
TA8	41	131.9	43.9	155.5	33.9	27.4	23.2	3	2.54	67.8	66.3	0.08	22.0	630

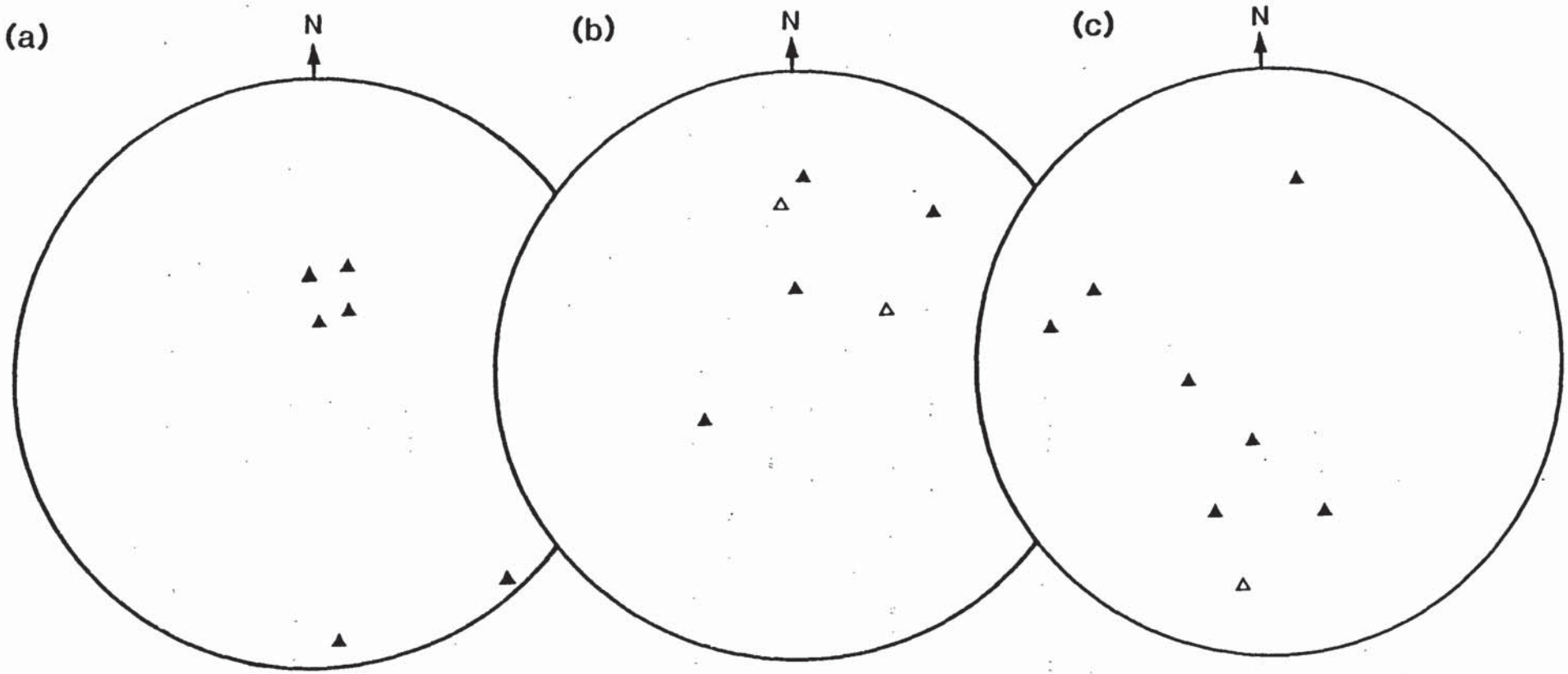

Fig. 4.17 Mean bedding corrected directions for Saxonian samples from (a) Barranco de la Hoz, (b) Pozo Nuncio and (c) Torres de Albarracin, after bulk demagnetization at temperatures of 400-675°C.

Directions show a fair amount of scatter but lie predominantly in the northwest quadrant. Inclinations are both positive and negative and quite variable. Intensities have a mean value of 0.2 mAm^{-1} after bulk demagnetization.

Torres de Albarracin samples were bulk demagnetized at temperatures of between 500°C (TA5) and 660°C (TA2). No strong grouping of directions is apparent, although most lie in the southern and western portion of the stereogram (Fig. 4.17c). Intensities ranged between 0.08 mAm^{-1} (TA8) up to 0.70 mAm^{-1} (TA5), with a mean value of 0.3 mAm^{-1}.

4.4.4 Chemical Demagnetization Results

One specimen from the section of Pozo Nuncio (PN4.1.1) and one from Torres de Albarracin (TA6.1.1) were selected for chemical demagnetization by immersion in a bath of dilute HCl acid.

Results of this chemical cleaning are shown in Figs. 4.18 (PN4.1.1) and 4.19 (TA6.1.1) together with results of thermal demagnetization of another specimen taken from the same sample. Specimen PN4.1.1 shows little change in direction from its original position (i.e. steep, positive and in the northwest quadrant) even after immersion in acid for over 250 hours (Fig. 4.18a(i)). These are similar to the results shown by PN4.3.1 during stepwise thermal cleaning (Fig. 4.18b(i)). One main component of magnetization exists, which is stable up to a temperature of 630°C. Above this temperature, the intensity of remanence is very low and the directions of magnetization are probably unreliable.

The normalized intensity decay plot for PN4.1.1 (Fig. 4.18a (ii)) shows an initial gain in intensity after a short amount of time in the acid. This is followed by a rapid drop to 50% of its initial intensity value after approximately 35 hours. A more gradual drop in intensity is recorded up to 250 hours immersion time in the acid. Specimen PN4.3.1 shows a fairly gradual decrease in intensity between room temperature and 690°C, at which point the intensity is zero (Fig. 4.18b (ii)).

The two orthogonal vector plots (Figs. 4.18a and b (iii)) show similar results i.e. the removal of one major component of magnetization.

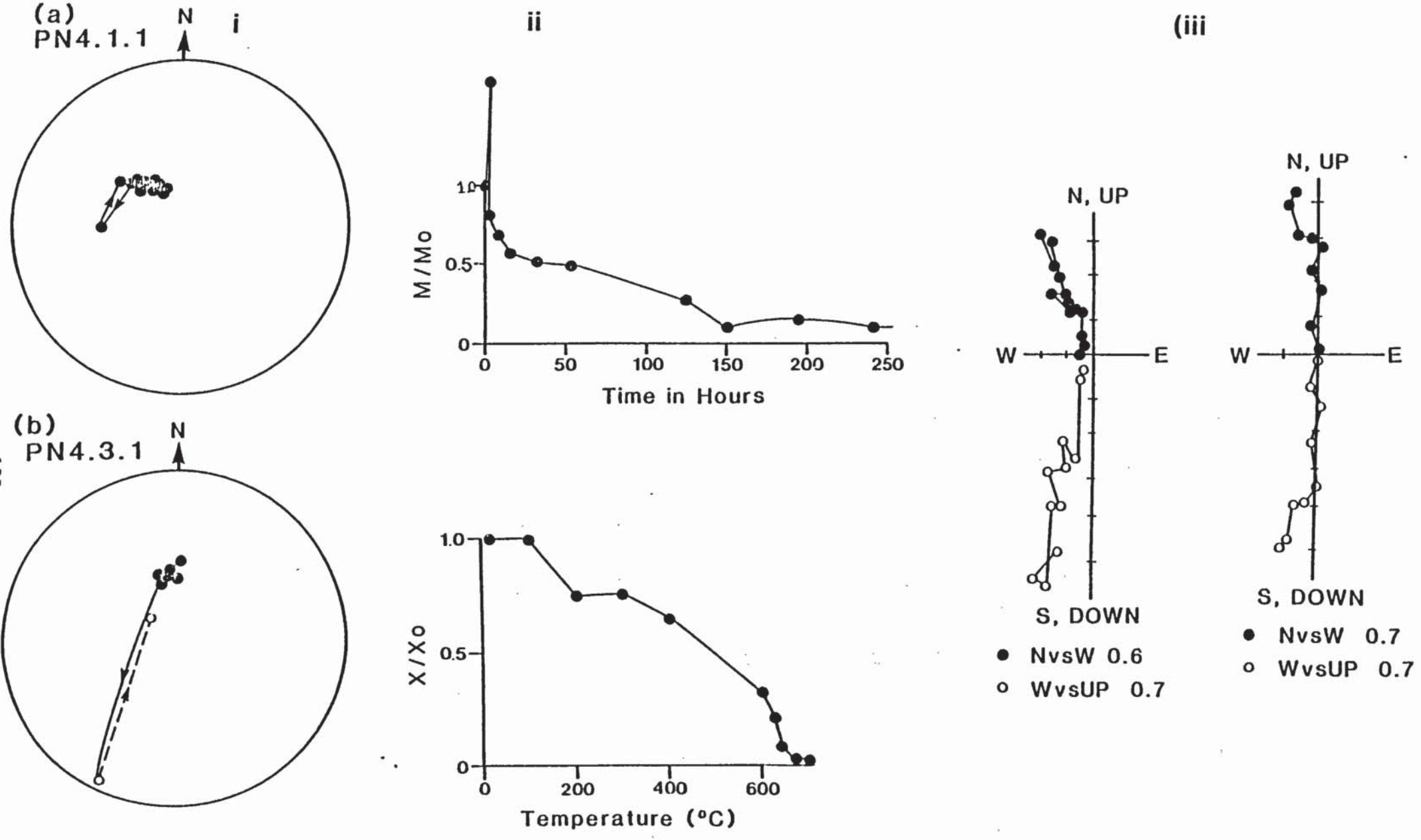

Fig. 4.18 Results of (a) Chemical demagnetization of specimen PN4.1.1 compared with those of (b) Thermal demagnetization of specimen PN4.3.1. (i) Stereographic projections, (ii) Normalized intensity decay curves, (iii) Orthogonal vector plots.

Results of chemical demagnetization of specimen TA6.1.1 also reveal the gradual removal of one main component of magnetization. This is fairly steep and positive and lies in the southern part of the sterogram (Fig. 4.19a (i)).

This direction remains fairly constant for up to 35 hours of immersion in acid. Longer periods of leaching give rise to a gradual movement northwards into the northwest quadrant. After 250 hours the direction moves to the northeast quadrant but intensities are very low (Fig. 4.19a (ii)). The thermally cleaned specimen TA6.5.2 shows an initial stable component of magnetization which is also steep and normal but lies further west than the previous specimen (Fig. 4.19b(i)). This direction is maintained until temperatures exceed 580°C. At this point, the direction first moves south and then northwards to a shallow position in the northeast quadrant. The normalized intensity decay plot (Fig. 4.91b(ii)) shows only a gradual removal of intensity up to 630°C (at this temperature 60% of the original remanence still remains) followed by a very rapid drop in intensity to almost zero by 690°C.

The two orthogonal vector plots (Figs. 4.19 a and b (iii)) show quite different initial directions of remanence. The chemically leached specimen also shows a fairly rapid loss of remanence over the first few demagnetization steps, where as, the thermally demagnetized sample shows only a gradual loss. After longer periods of leaching (TA6.1.1) and exposure to higher temperatures (TA6.5.2) both specimens reveal a second component of magnetization.

4.4.5 Discussion of Palaeomagnetic Results

Mean initial intensities for Saxonian samples are higher than those for the Autunian deposits. This is mainly due to increased amounts of haematite within the sediments.

I.R.M. results indicate that haematite is the principal remanence carrier in these deposits. Sample MA112, however, also contains a second, low coercivity mineral (probably goethite or poorly crystalline iron oxide).

Thermal demagnetization of the Saxonian samples shows that one predominant magnetic component is present in the majority of specimens.

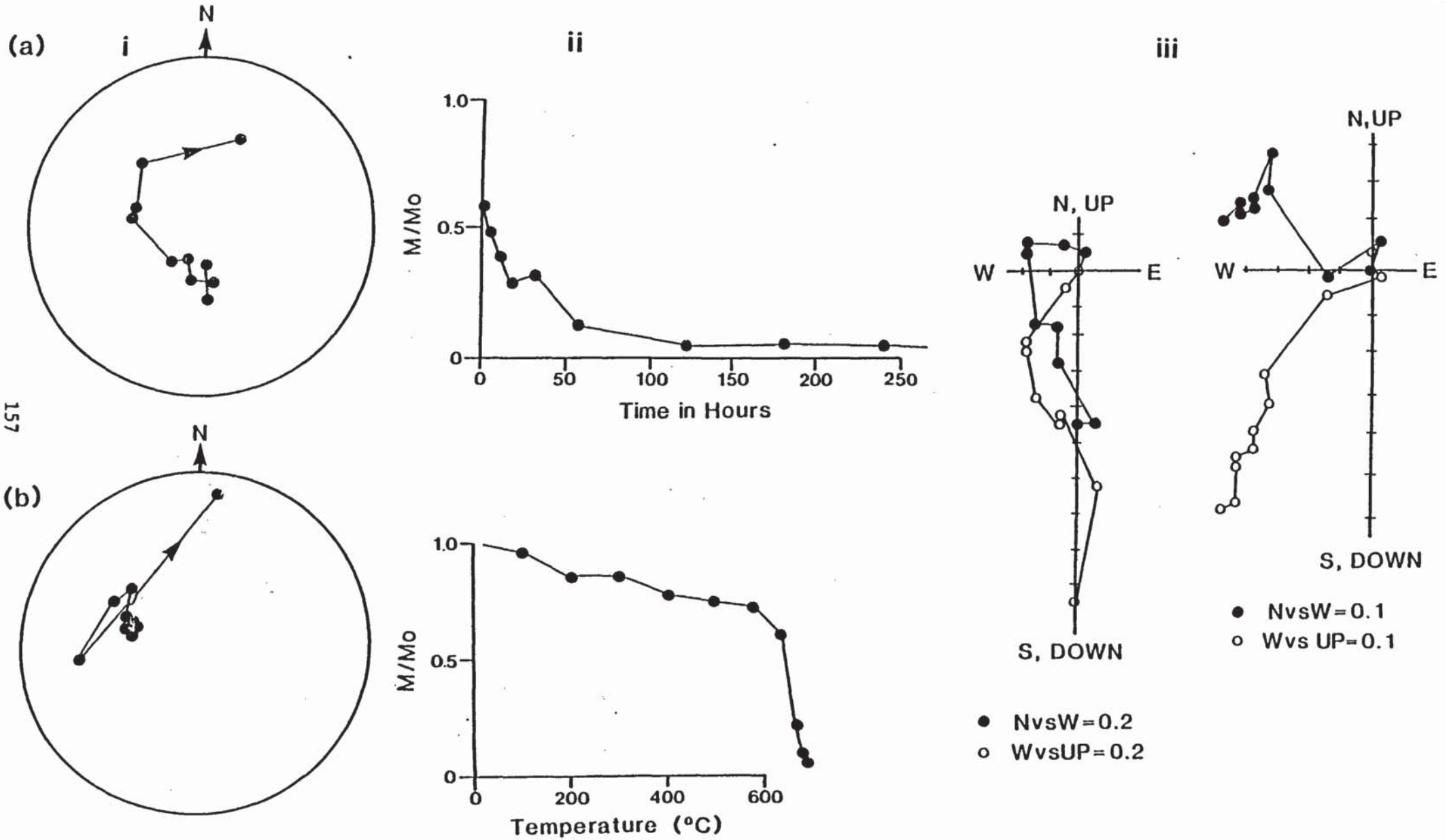

Fig. 4.19 Results of (a) Chemical demagnetization of specimen TA6.1.1 compared with those of (b) thermal demagnetization of specimen TA6.5.2. (i) Stereographic projections, (ii) Normalized intensity decay curves, (iii) Orthogonal vector plots.

The most stable directions shown by specimens from Barranco de la Hoz and Pozo Nuncio are steep, positive and lie in the northwest quadrant close to the present day geomagnetic field position. Specimens from Torres de Abarracin have most stable directions which are fairly steep, positive and lie in the southwest quadrant.

These stable components of remanence are usually only removed upon heating to temperatures in excess of 600°C (indicating once again that haematite is the principal remanence carrier). Above this temperature, many specimens show a change in the remanence direction towards a more shallow direction in the southeast quadrant e.g. MA115.4.1, MA112.2.1, (TA2.3.1 exhibits this direction from room temperature). This direction lies close to previously documented Permian directions for this area (Van der Voo, 1967, 1969) and it is likely that this is a depositional (D.R.M.) or early post depositional (P.D.R.M.) remanent magnetization acquired during deposition or early diagenesis.

Specimen MA112.2.1 also shows a shallow negative direction in the northwest quadrant after heating to temperatures in excess of 650°C. This may be a spurious result but it is interesting to note that this direction is almost antiparallel to the shallow positive direction in the southeast quadrant present between 580°C and 630°C. Specimens TA4.2.1 and TA2.3.1 (Fig. 4.13) also show movement towards shallow negative directions in the northwest quadrant after heating to temperatures above 650°C.

Normal events, however, have been documented for the Spanish Triassic (Van der Voo, 1969) but have not been reported for the Permian. The Triassic "normal" direction is shallow, positive and lies in the northwest quadrant. This high temperature component of magnetization, shown by some of the specimens, may be:

(i) A spurious result caused by instrument error when intensities are very low.

(ii) A true palaeomagnetic component of Late Permian or Triassic age (a chemical remanent magnetization) acquired during diagenesis.

Most specimens from Torres de Albarracin exhibit stable directions of magnetization quite different to those shown by the other Saxonian specimens i.e. positive, in the southwest quadrant with inclinations of between 35° and 50°. A streaking of directions towards the northeast quadrant is also noted.

No previously documented directions of magnetization have been recorded in these positions for Iberian rocks of Permian age. It is likely, therefore, that these results represent either:

(i) Intermediate directions, comprising more than one component of magnetization. These components would have to have very similar blocking temperatures since heating does not separate them.

(ii) A secondary magnetization which totally overprints any Permian remanence component. The only likely age of this component is Tertiary. Previously reported Eocene directions from Spain (normal and reversed) lie in the northeast and southwest quadrants respectively (Van der Voo, 1969, Banda et al in press). However, the reversed Eocene direction (in the southwest quadrant) has a negative inclination unlike the specimens from Torres de Albarracin, which show positive inclinations.

Palaeopole positions calculated for the Saxonian samples are shown in Fig. 4.20. None of the samples shows agreement with previously calculated Permian pole positions for Iberia. This implies that none of the most stable directions isolated for the Saxonian samples is an original remanence, but has instead been acquired subsequent to deposition (during diagenesis) of the sediments.

4.5 RELATIONSHIP BETWEEN DIAGENESIS AND PALAEOMAGNETISM

Similarities in the nature of the original sediments, environment of deposition and diagenetic history of the Saxonian deposits studied, has led to similarities in their Palaeomagnetic results.

Samples having the highest iron oxide contents (as revealed using point count analysis), in general, have the highest intensities of initial remanence. Samples from Barranco de la Hoz have a mean total iron oxide content of 20% and a mean initial intensity of 6.8 mAm^{-1}. Samples from Pozo Nuncio contain 16% iron oxide and have a mean initial intensity of 2.63 mAm^{-1} and those from Torres de Albarracin have an iron oxide content of 13.4% and a mean initial intensity of 1.75 mAm^{-1}.

TABLE 4.5 PREVIOUSLY PUBLISHED UPPER PERMIAN DIRECTIONS AND POLES FOR IBERIA AND THOSE FOUND IN THIS STUDY FOR THE SAXONIAN OF CENTRAL SPAIN

Letter/ No.	Locality (formation)	D(°)	I(°)	N	α95(°)	Lat	Long	Reference
1	Rio Aragon C. Pyrenees (Andesites)	152	-22.5	14	6°	51°N	133°W	Schwarz (1962)
2	Anayet C. Pyrenees (Andesites & Sandstones)	164	-14	11	10°	52°N	154°W	Van der Lingen (1960)
3	Serra del Cadi E. Pyrenees (Andesites)	169.5	-3	41	4°	48.5°N	163°W	Van Dongen (1967)
4	Spain	-	-	30	6°	53°N	138°W	Van den Berg (1979)
5	Spain	-	-	12	9.5°	56°N	134°W	Van den Berg (1979)
6	Spain	-	-	8	25.5°	49°N	130°W	Van den Berg (1979)
MA112	Barranco de la Hoz Redbeds	6.4	57.3	3	3.7°	84.3°S	116.9°E	This Study
MA114	Barranco de la Hoz Redbeds	311.4	25.7	3	9.4°	39.7°S	110.3°W	This Study
MA115	Barranco de la Hoz Redbeds	3.2	40.2	3	11.0°	71.8°S	168.7°E	This Study
MA116	Barranco de la Hoz Redbeds	337.0	57.8	4	7.0°	72.2°S	92.7°W	This Study
PN1	Pozo Nuncio Redbeds	54.4	45.2	5	3.7°	43.5°S	88°E	This Study
PN2	Pozo Nuncio Redbeds	329.8	29.1	3	1.4°	53.9°S	125.9°W	This Study
PN4	Pozo Nuncio Redbeds	351.0	49.5	6	3.0°	77.6°S	142.4°W	This Study
PN5	Pozo Nuncio Redbeds	1.6	40.6	4	19.4°	1.6°S	40.6°W	This Study
TA1	Torres de Albarracin	218.8	-14.3	3	6.4°	42.1°N	58.5°W	This Study
TA2	Torres de Albarracin	168.2	3.4	4	5.8°	46.5°N	15.7°E	This Study
TA3	Torres de Albarracin	209.6	17.8	4	3.9°	33.4°N	37.3°W	This Study
TA4	Torres de Albarracin	219.9	42.0	6	1.6°	15.4°N	38.9°W	This Study
TA5	Torres de Albarracin	285.6	70.9	3	5.0°	40.5°S	47.7°W	This Study
TA6	Torres de Albarracin	216.9	40.7	6	40.7°	30.8°N	36.9°W	This Study
TA7	Torres de Albarracin	203.2	27.7	3	5.1°	30.8°N	27.9°W	This Study
TA8	Torres de Albarracin	5.9	78.1	4	2.2°	63.0°S	3.6°E	This Study
Mean	Barranco de la Hoz	344.5	45.3	4	22.3°	67.0°S	159.6°W	This Study
Mean	Pozo Nuncio	4.2	41.1	54	15.5°	44.2°S	145.2°W	This Study
Mean	Torres de Albarracin (TA1,3,4,6,7)	213.6	22.9	5	10.0°	30.5°N	39.9°W	This Study

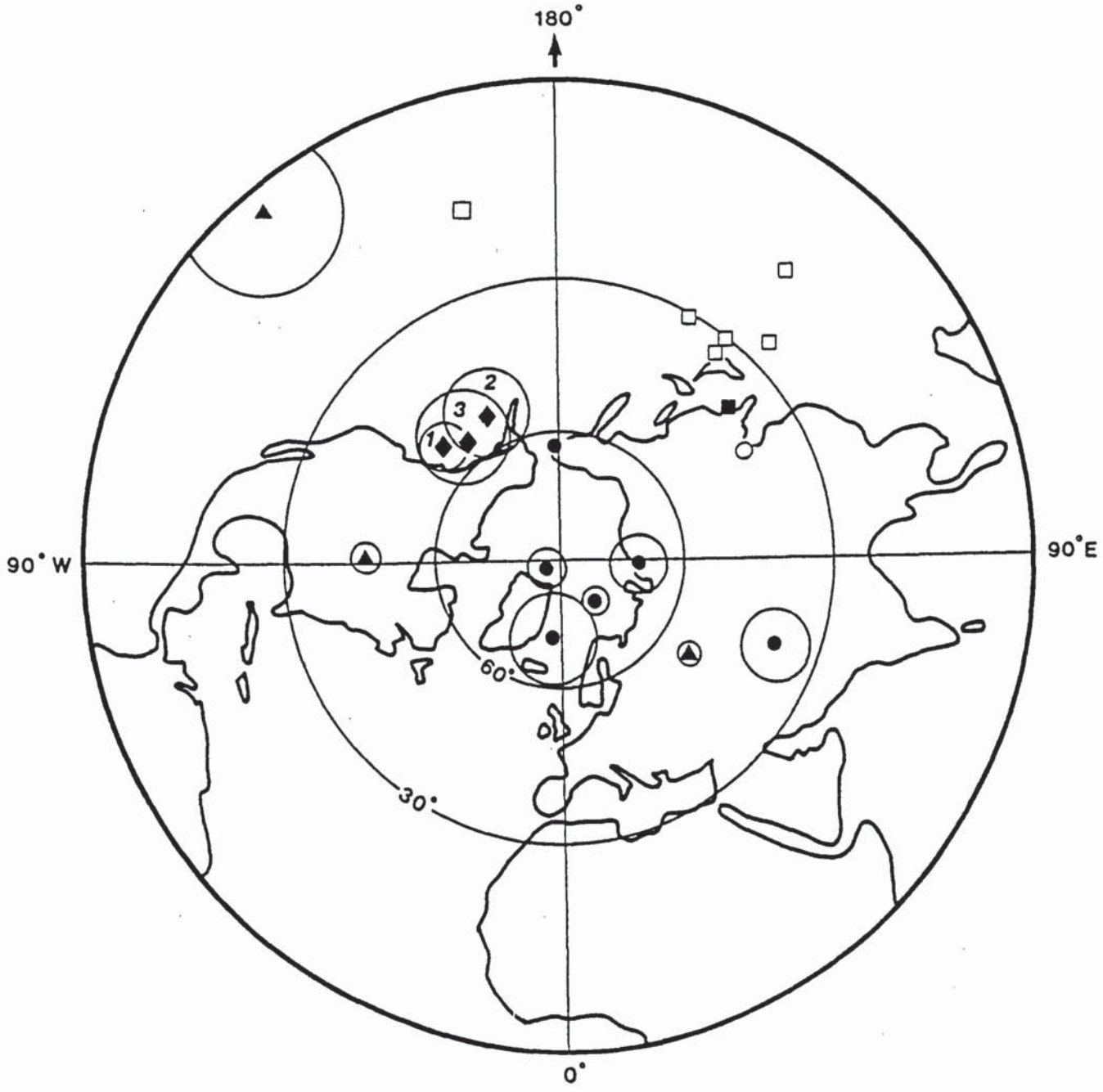

Fig. 4.20 Palaeopole positions for the Saxonian of Iberia.
- ♦ Previously described Permian pole positions from Iberia (Numbers refer to Table 4.5).
- ● Palaeopole positions isolated for specimens from Barranco de la Hoz.
- ▲ Palaeopole positions isolated for specimens from Pozo Nuncio.
- □ Palaeopole positions isolated for specimens from Torres de Albarracin.

Detrital haematite (specularite) and early diagenetic haematite (principally formed by the replacement of micas and rock fragments and the aging of iron rich clay grain coats (Plates 4.4e, 4.5a and e)) account for only 5% to 12% of the total iron oxide content of the deposits. The shallow directions of remanence in the southeast and northwest quadrants revealed, only after heating to high temperatures, are probably carried by this detrital and early diagenetic haematite.

The majority of the samples contain abundant pore filling iron oxide cement (Plate 4.2f, 4.3b, 4.5b) This precipitated during late diagenesis (Telogenesis) due to the influx of slightly acidic, oxidizing meteoric waters. These waters dissolved much of the carbonate cement, including the siderite (Fe_2CO_3) which resulted in the release of Fe ions into solution. These combined with free oxygen to form iron oxide or a precursor hydroxide which soon converted to haematite. It is this haematite which is responsible for the remagnetizing of the Saxonian sediments.

One main magnetic component is now present in most samples, which is almost coincident with the present-day geomagnetic field position for the area. It seems likely, that this component was acquired very recently, probably during the Brunhes epoch (the present normal event) which began approximately 700,000 years ago.

A few specimens (MA112.2.1, MA115.4.1, TA1.1.2 and TA5.1.1) show a rapid loss of intensity to between 5% (TA1.1.2) and 50% (MA112.2.1) of their original values, upon heating to only 200°C. Goethite has a Neel temperature of about 110°C and petrographic studies show this mineral to be present in the samples. The type of palaeomagnetic behaviour shown by these samples is due, therefore, to the presence in the sediments of abundant goethite. This probably formed as a result of intense weathering.

CHAPTER FIVE

THE LOWER BUNTSANDSTEIN OF MOLINA DE ARAGON

5.1 INTRODUCTION

The Buntsandstein facies was sampled at three sections close to the town of Molina de Aragon in northern Guadalajara (Fig. 5.1), Rio Arandilla, Hoz del Gallo and Rillo de Gallo. A total of seventy eight samples were taken from six Buntsandstein units. The Lower Buntsandstein will be described in this chapter and the Upper Buntsandstein in Chapter Six.

The Lower Buntsandstein samples were collected from the Hoz del Gallo section (MA1-MA13 and MA41-MA54), (Plate 5.1a). This lies 7 km west of Molina de Aragon in a road cutting (01° 59' 24"W, 40° 49' 48"N). In total over 600m of Buntsandstein sediments are exposed. A small number of samples were also collected from the section at Rillo de Gallo (MA55-MA59) (Plate 5.1b). This section is exposed along the banks of the Viejo stream in a road cutting between Rillo de Gallo and Pardos (01° 55' 48"W, 40° 52' 48"N). Approximately 490m of Buntsandstein sediments are present here.

The sediments dip towards the southwest at both localities, with inclinations of up to 20°.

5.2 STRATIGRAPHY AND SEDIMENTOLOGY

In this area the Buntsandstein has been divided into six clastic units (Ramos, 1979), which range from Thuringian to Ladinian in age (Fig. 5.2). The lowest three units, "Conglomerates de la Hoz del Gallo" (Hoz del Gallo conglomerates), "Areniscas de Rillo de Gallo" (Rillo de Gallo sandstones) and "Nivel de Prados" (Prados beds) are described in this chapter.

The lowermost unit, the "Conglomerates de la Hoz del Gallo" consists of quartzitic conglomerates with very little sandy matrix and some thin sandstone beds. In the section at Hoz del Gallo this unit is 157m thick. Samples MA1-MA13 were taken from this unit. The overlying unit, "Areniscas de Rillo de Gallo", is composed of medium grained red sandstones with some conglomerate beds. Samples MA41-MA54 were taken from this unit which is approximately 110m thick. The "Nivel de Prados" consist of


Aston University
Illustration removed for copyright restrictions

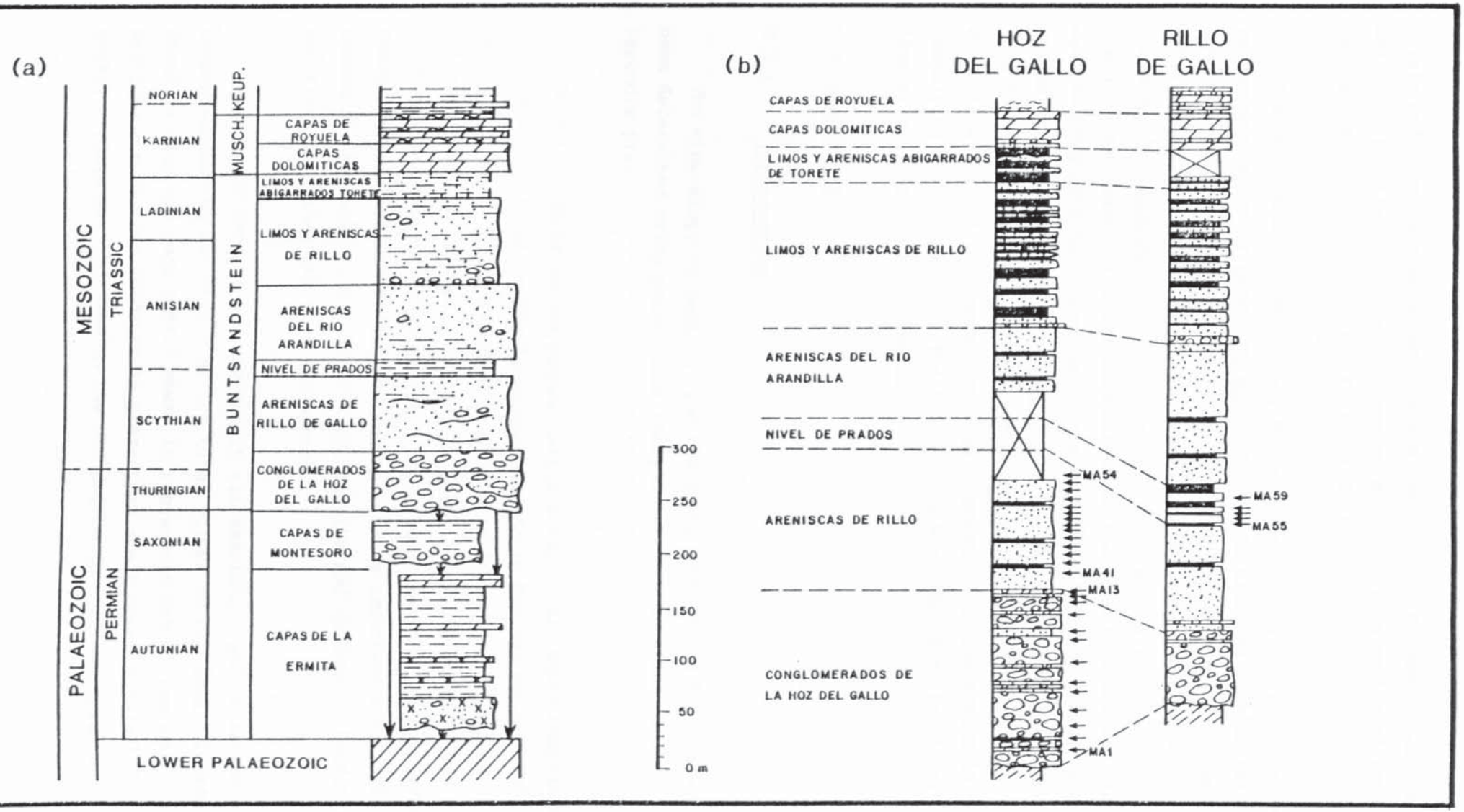

Fig. 5.2 (a) General lithostratigraphic column for the Permian and Triassic of the Molina de Aragon area, Central Spain (after Ramos, 1979).
(b) Sedimentological columns for the sections of the Hoz del Gallo and Rillo de Gallo, compiled by Ramos (1979), showing the horizons from which samples MA1-MA59 were taken.

thinly bedded micaceous sandstones and mudstones. Pedogenic carbonates and trace fossils are common. Samples MA55-MA59 were collected from this unit which is 31m thick in the Rillo de Gallo section.

The deposition of these Lower Buntsandstein units is closely related to tectonic activity (Ramos et al., 1986). An alluvial complex related to late Hercynian faults developed with the "Conglomerates de la Hoz del Gallo" representing the result of fan-lobe progradation produced by low-sinuosity channels (Ramos and Sopena, 1983) with a north-northeastern trend. The overlying units accumulated as the result of braided fluvial systems producing transverse or linguoid bars that change upward into channel fill deposits (Ramos et al., 1986). Palaeocurrent directions are from the north-northwest (nearly perpendicular to the conglomerate directions) indicating deposition from a separate fluvial system to the underlying conglomerates. The Prados beds were deposited by higher sinuosity, lower energy streams.

5.3 DIAGENESIS

5.3.1 Introduction

The mineralogy of samples from the lower part of the Buntsandstein has been determined using point count analysis of thin sections (see Appendix IV).

Detrital quartz is the predominant mineral in all units comprising 42%-48% of the total in the "Conglomerates de la Hoz del Gallo", 42%-63% in the "Areniscas de Rillo de Gallo" and 31%-44% in the "Nivel de Prados". Feldspar accounts for up to 13% of the total in all three units and rock fragments make up a further 2%-14%. Micas represent <5% of the rocks. Heavy minerals are common but not volumetrically important <2%. The most common are tourmaline, zircon, rutile, apatite and epidote. Detrital iron and titanium oxides are also widespread.

Authigenic cements are present in all samples. Quartz is the most common accounting for 6%-19% of the total volume of the rock. Dolomite is found in only one sample MA57 where it represents 36% of the total. Authigenic potassium feldspar is present in small amounts in all 3 units (<2%). Clays are abundant in the Hoz del Gallo conglomerates, accounting

for between 5% and 20% of the total. Amounts are lower in the overlying units (4%-14%). Porosities are generally quite low 2%-8% in the Hoz del Gallo conglomerates, 4%-8% in the Rillo de Gallo sandstones and 1.5%-7% in the Prados beds. Locally, exceptions to these low values are found, e.g. MA7 which has a visible porosity of 17%.

When plotted on a Q.R.F. Terniary diagram (Fig. 5.3) the sandstones lie predominantly in the subarkose field. Sandstones from the conglomerate unit, however, lie in the sublitharenite field.

The average grain size of sandstones from the Hoz del Gallo conglomerate unit is 0.358mm. The Rillo de Gallo sandstones have an average of 0.351mm and the average for the Prados beds is 0.347mm. All lie in the medium sandstone range.

5.3.2 Diagenetic Transformations

Detrital quartz, the most common mineral in these deposits, occurs predominantly as subrounded-subangular monocrystalline grains. These frequently contain numerous vaccuoles or inclusions of heavy minerals. In the upper part of the Hoz del Gallo conglomerates and lower part of the Rillo de Gallo sandstones there is an increase in the proportion of polycrystalline quartz (probably representing removal of material from a metamorphic source area). Some quartz grains show strained extinction, and concavo-convex grain boundaries, indicating that at least moderate compaction has occurred.

Orthoclase accounts for virtually all the feldspar present in these rocks although some microcline is also present. Small amounts of plagioclase have been detected using X.R.D. but not by optical methods. Feldspar grains commonly show replacement by clays and iron oxide especially along cleavage traces. Many grains are severely etched and show hacksaw terminations (Plate 5.2a). Sometimes dissolution is so extreme, that almost total removal of the grain has occurred leaving secondary moldic porosity. Clay replacement and/or dissolution has weakened some grains to such an extent that they have split or broken.

Sedimentary, metamorphic and igneous (both volcanic and plutonic) rock fragments are all represented in the deposits.

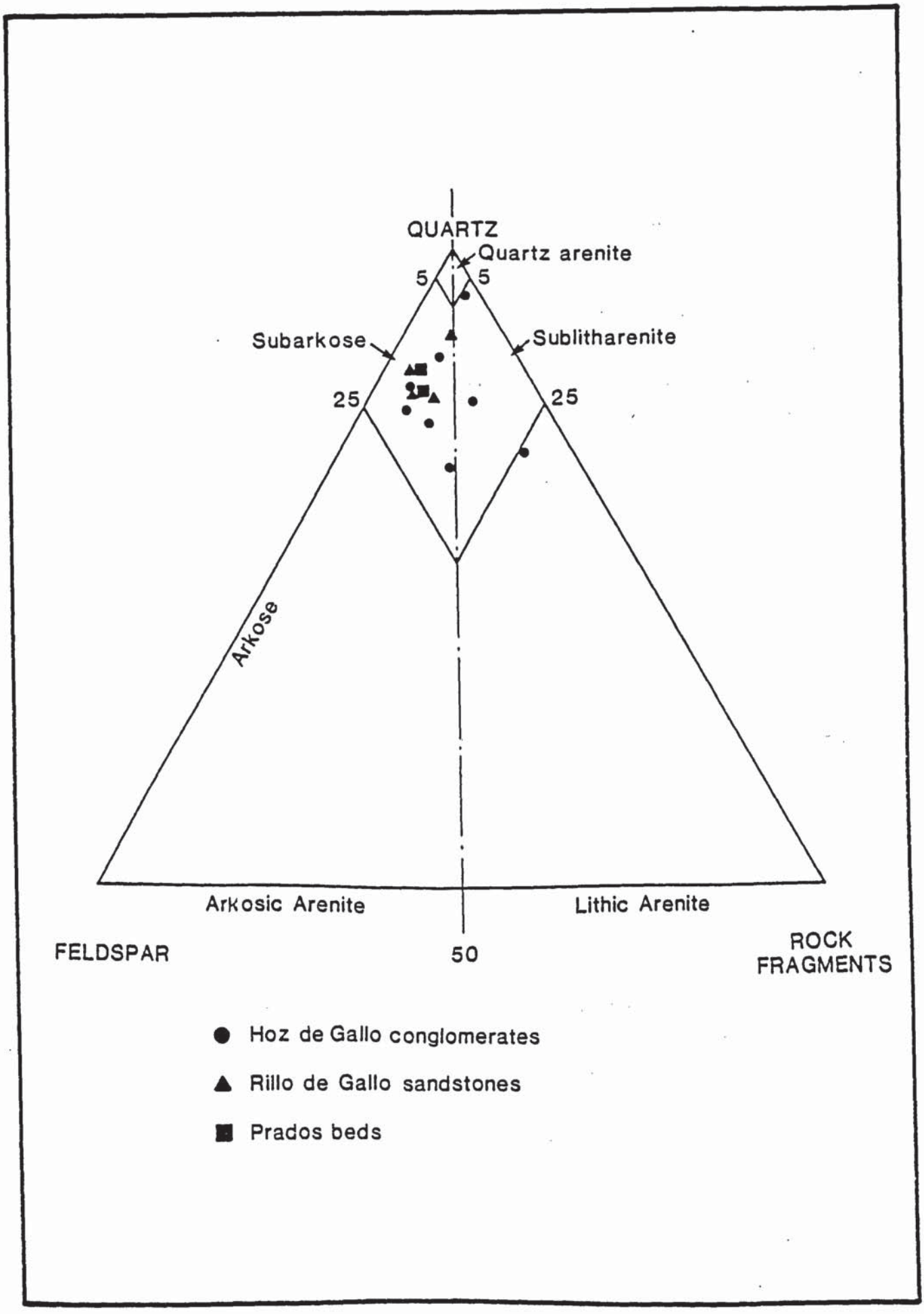

Fig. 5.3 Q.F.R. ternary diagram showing the composition of point counted sandstone samples from the Lower Buntsandstein.

Sedimentary rock fragments consist of either lithic fragments as in the case of mud flakes which are (particularly common in the Prados beds) or else consist of quartz grains with rounded authigenic overgrowths. Polygranular quartz grains are also present (Plate 5.2b). These sedimentary rock fragments were almost certainly derived from the underlying Permian sediments.

Metamorphic rock fragments are mostly schistose, consisting of polycrystalline quartz grains with muscovite micas and illite.

Igneous rock fragments derived from both volcanic and plutonic sources are present in these deposits. Plate 5.2c shows an igneous rock fragment demonstrating graphic texture (high temperature intergrowth between quartz and alkali feldspar) which is characteristic of plutonically derived rocks.

The majority of the rock fragments present in the Buntsandstein show replacement by clays and/or iron oxide.

Both muscovite and biotite micas are present in these rocks, they often show splayed cleavages due to compaction. Biotite grains, have, in nearly all cases been partially replaced by haematite. Muscovite shows replacement by illite and kaolinite.

Detrital clays are present in these deposits in small amounts . They are most common at the base of the Hoz del Gallo conglomerates and consist predominantly of illite which coats detrital grains.

Authigenic quartz is abundant in all samples, accounting for 10%-20% of the total in most samples. Its distribution is restricted only locally by the presence of detrital clays. Dust lines are often absent between detrital grain and syntaxial authigenic overgrowth, indicating it is a very early diagenetic phase. The original grain boundary, in such cases can be identified by the absence of vaccuoles in the overgrowth. Triple junctions, formed by the joining of authigenic quartz overgrowths of adjacent grains, are common and locally quartz cement completely fills all intergranular pore spaces (Plate 5.2d). More than one stage of quartz authigenesis is witnessed in these rocks and many of the quartz grains also show evidence of later dissolution.

Authigenic potassium feldspar is volumetrically much less important than authigenic quartz, accounting for <2% of the total. It is, however, present in all three Lower Buntsandstein units and occurs as non- syntaxial overgrowths on the host grains (Plate 5.2e). S.E.M. studies show that a slight difference in composition between detrital grain and authigenic overgrowth (the overgrowth contains a greater proportion of potassium than the host grain) is responsible for the optical discontinuity between the two phases.

Authigenic feldspar pre-dates authigenic quartz (Plate 5.2e) (suggesting it is a very early diagenetic phase) and in places clearly restricts its growth. The authigenic feldspar generally shows less alteration than the detrital grains, but locally, also shows evidence of partial dissolution. Clay minerals are abundant in these deposits, accounting for up to 20% of the total (MA1). Amounts decrease towards the top of the Lower Buntsandstein. The Hoz del Gallo conglomerates have an average clay content of 12.5%. The Rillo de Gallo sandstones contain 8% clay and the Prados beds 6% clay.

Results of semi-quantitative X-ray diffraction analysis are presented in Table 5.1.

TABLE 5.1 Results of semi-quantative analysis on <2μm clay fraction of samples from the Lower Buntsandstein.

	Illite	Kaolinite	Mont.	Chlorite	Total
MA6	43	52	2	3	100%
MA7	98	1	-	1	100%
MA10	98	1	-	1	100%
MA12	98	1	-	1	100%
MA13	98	1.5	-	0.5	100%
MA51	97	2	-	1	100%
MA52	73	1.5	25	0.5	100%
MA56	60	0.5	39	0.5	100%

The above results show that illite is the dominant clay in these Lower Buntsandstein deposits. In many samples it accounts for nearly 100% of their total clay content. In one sample (MA6) a large amount of kaolinite was recorded (52%), this is clearly seen on the X-ray diffractogram traces

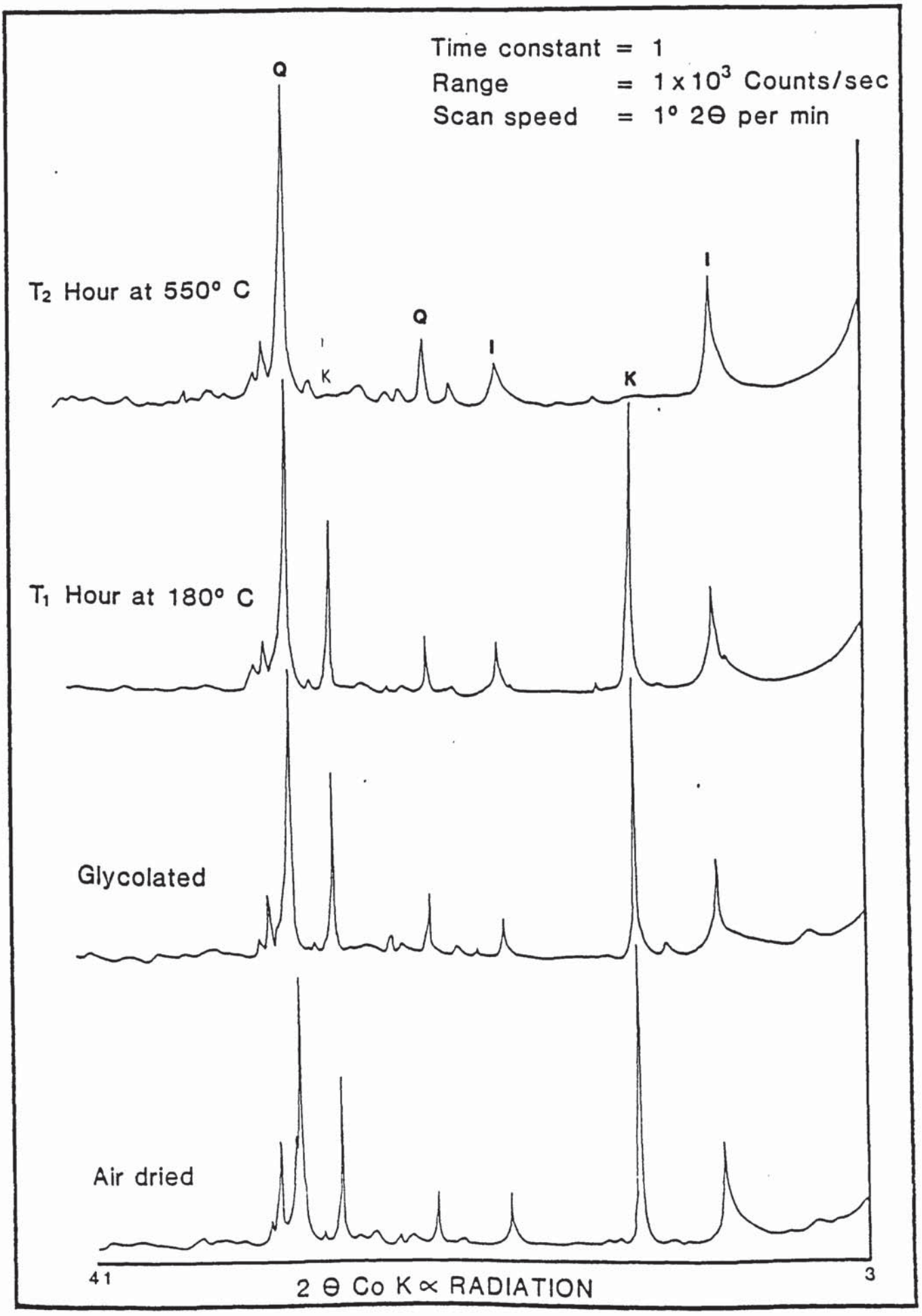

Fig. 5.4 X-ray diffractograms for the <2um clay fraction of sample MA6.

(Fig. 5.4), but in other samples, only accounts for <2% of the total. Montmorillonite is virtually absent from the two lowest Buntsandstein units but is very abundant in the Prados beds where percentages of between 25% and 39% are reached. Figure 5.5 shows the X-ray diffractogram traces for sample MA52. They clearly show the relative abundance of illite and smectite and the virtual absence of any kaolinite and chlorite in the deposits.

The low percentage of kaolinite, found using X.R.D. methods, in samples from the Hoz del Gallo Conglomerates (relative to their illite contents), contradicts petrographic observations which indicate that kaolinite is abundant in all Hoz del Gallo samples examined. The reason for the very low amounts of kaolinite detected by X.R.D. methods could be because the kaolinite is in the form of coarse, vermiform booklets, which often exceed 50μm in length and 20μm in width (Plate 5.3a). Since the X.R.D. diffractograms represent the <2μm clay fraction much of this kaolinite will not be detected. This will distort the true proportions of clay minerals in the deposits. Sample MA6 may be anomalous because a coarser than <2μm sample was run (experimental error) or the kaolinite present in the sample is much finer grained than in the other Hoz del Gallo samples.

The majority of the clays present in the sediments are of authigenic origin, occurring both as a grain replacement phase and filling secondary pores (Plate 5.2f).

Illite occurs as a grain rimming detrital clay and also replaces muscovite mica, rock fragments (especially schistose rock fragments) and feldspars. It is also present within the matrix.

Kaolinite often occurs in association with muscovite, forming neomorphic booklets in the splayed ends of deformed grains. Coarse crystal aggregates of vermiform kaolinite also exist. (Plate 5.2f, 5.3a). Frequently, the authigenic kaolinite booklets are found in close association with pore filling, authigenic iron oxide cement.

A small amount of chlorite (0.5%-3%) is also present in these sediments. It occurs mainly as a replacement of biotite grains.

Authigenic opaque minerals (predominatly iron oxides and iron-titanium oxides) replace micas and rock fragments and occur as pore lining or pore filling aggregates.

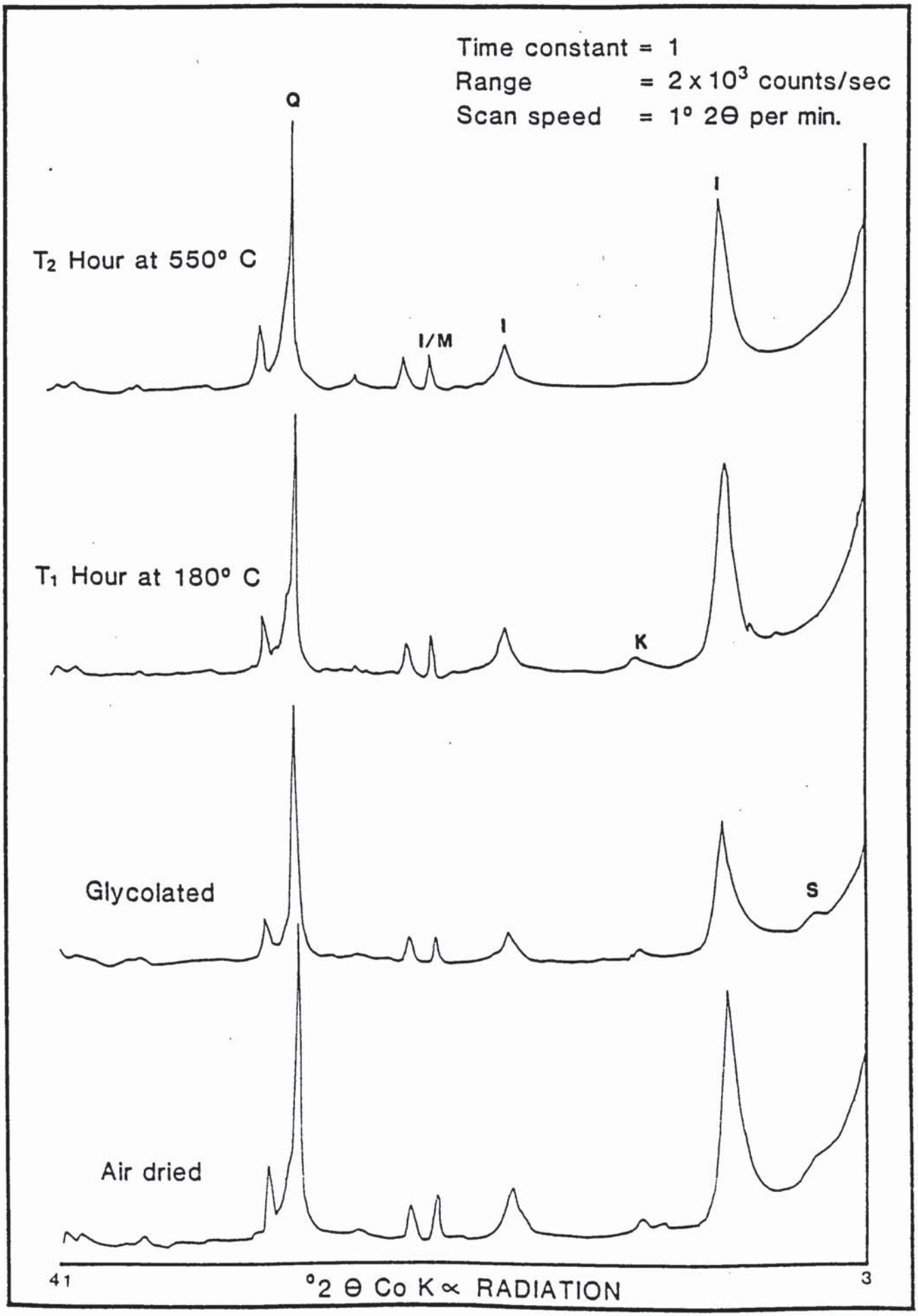

Fig. 5.5 X-ray diffractograms for the <2μm clay fraction of sample MA52.

Authigenic carbonates are only found in the upper part of the Lower Buntsandstein, although evidence for the former existence of a widespread carbonate cement is found in many samples from lower in the series.

In the Prados beds the carbonate occurs as a poikilotopic non-ferroan dolomite cement (a small amount of siderite is also present locally). In sample MA57, dolomite accounts for 36% of the total. This high percentage is partly due to replacement of many of the silicate grains by authigenic carbonate (in addition to pore filling cement) (Plate 5.3b). 'Floating' grains, with highly embayed margins, are seen within carbonate cement which has a dirty appearance. The presence of undeformed muscovite mica laths in this sample implies that cementation took place before any significant compaction had occurred.

Evidence for the former existence of an aggressive carbonate phase is found in many of the other Lower Buntsandstein samples. Small 'V' shaped notches etched into authigenic and detrital quartz and feldspars are seen in MA41 (Plate 5.3c) and rhombic shaped secondary pores occur in MA44 (Plate 5.3d).

Porosities range from a minimum of 2% (MA57) in the Prados beds, to 17% (MA7) in the Hoz del Gallo conglomerates. Average porosities are, however, similar for each unit ranging from 4.5%-6%. A general rise in porosity with increasing grainsize was also noted.

Both primary and secondary porosity are present in these deposits but the latter is much more abundant.

Primary porosity has been vastly reduced due to the growth of authigenic minerals and by the creation of an epimatrix and pseudomatrix. The range of pore sizes and shapes and porosity distribution is more variable than would be expected for primary porosity. Clear evidence for the secondary nature of the porosity is found in many samples. Dissolution of framework grains, especially feldspars is widespread (Plate 5.2a). In extreme cases only molds of the original grains remain.

Porosity formed due to the dissolution of vein filling minerals is also found in these deposits. The most common type of porosity, however, is oversized and irregular shaped intergranular pores (Plate 5.3c). These are clearly secondary in origin since they embay and indent detrital and authigenic quartz and feldspars.

The sample with lowest porosity also contains the highest proportion of carbonate cement (MA57) and porosities are highest where there is evidence for the former presence of an aggressive cement (e.g. MA7, MA44).

Finally, the porosity of the deposits would be much higher in many cases but for the presence of kaolinite. This has precipitated in the oversized pores substantially reducing porosity. It does however contain micropores which add to the overall porosity of the rock.

Grain contacts are often long and/or concavoconvex, suggesting that some degree of compaction has occurred in these rocks. Evidence for pressure solution is also seen in some samples. Stress cracks in quartz grains are occassionally present but the deformation of micas and crushing of mechanically weak grains are the most commonly occurring compaction features present in the rocks.

5.3.3 Magnetic Mineralogy

The total iron oxide content of these deposits is variable ranging from 1% (MA7 and MA53) up to 13% (MA10). A number of textural habits have been identified for haematite using transmitted and reflected light petrography and the S.E.M.

1. Specular haematite: Detrital haematite grains are found in all three Lower Buntsandstein units although they are not as abundant as in the Saxonian facies. Martites are once again absent. Typically, the grains are rounded in shape and commonly have a very embayed and corroded appearance (Plate 5.3e). Rare polycrystalline specularites are also seen. Detrital titianium oxides are present in all samples studied (Plate 5.3f) and grains containing both haematite and ilmenite are fairly common (Plate 5.4a).

2. Grain rimming haematite (Plates 5.3c and 5.4b). This type of haematite is associated with clay coatings. It is generally microcrystalline, although it appears to have a cement like morphology in places (Plate 5.4b).

3. Replacement haematite: This is more common than the previous two types of haematite. Rock fragments, feldspars and micas all show widespread replacement by fine grained iron oxide together with clay minerals. The presence of rows of parallel haematite crystals in the cleavages of biotite micas is particularly common in these deposits. No

fresh biotites are found in any of the samples and in many cases the mica has been totally pseudomorphed by haematite e.g. MA41. Detrital haematite grains also show replacement by fine grained pigmentory haematite at their margins.

4. Pore filling haematite: This is also a common habit of haematite. Many pores (mostly over sized, secondary pores) are filled with a mixture of fine grained iron oxide and clay (almost always kaolinite) (Plate 5.4c). This type of pore fill is particularly common in samples from the Hoz del Gallo conglomerates (MA1-MA13). Viewed in reflected light (Plate 5.4d) the pore filling haematite is microcrystalline and completely interdigitated with the authigenic Kaolinite.

5. Haematite associated with siderite: Samples from the Prados beds and parts of the Rillo mudstones and sandstones contain an early siderite cement which has been partially dissolved in places. Fine grained iron oxide and goethite have precipitated in the secondary pores associated with carbonate dissolution.

6. Goethite: Yellow/brown coloured goethite is present in small amounts in all samples. In MA2, however, it is particularly abundant, occurring as a pore filling cement (Plate 5.4e). Under the S.E.M. the goethite has a 'nobbly' appearance with unusual elongate projections (Plate 5.4f).

5.3.4 Paragenesis

The earliest diagenetic event to have occurred in the Lower Buntsandstein deposits was the mechanical infiltration of clays. These formed a tangential 'skin' coating the detrital grains. Rapid dissolution and replacement of unstable silicates such as plagioclase, alkali feldspar, pyroxenes, amphiboles and micas also occurred during early diagenesis. This process released a variety of ions into solution, chiefly K (Na,Ca), Fe, Mg, Al and Si. Precipitation of authigenic minerals occurred in response to the alkaline, oxidising geochemical conditions of the early pore waters found in association with arid climatic conditions. These minerals consisted of illite (illite/smectite?) rich clay, non-ferroan dolomite authigenic feldspar and quartz. Authigenic haematite which replaces many of the framework grains, especially biotite also formed at this time.

The fact that the proximal sandstones of the two lowest Buntsandstein units are dominated by illitic clays in contrast to the more distal Prados

sandstones which contain significant amounts of smectite, may be due to differences in the original detrital mineralogy of the deposits. Highly feldspathic proximal sandstones would contribute large quantities of potassium to the intersitial pore waters through feldspar dissolution and hence illite would be the likely authigenic clay mineral. Quartz dominated distal sandstones would contribute much less potassium to the pore waters and smectite rich clay would result as ions were supplied from the dissolution of ferromagnesian grains.

Burial of the sequence resulted in mechanical compaction of the rocks, with brittle fracturing, crushing of the weaker grains, creation of long grain contacts and even pressure dissolution occuring in places. This reduced the primary porosity of the sediments considerably. Where extensive framework supporting cement existed (e.g. quartz or carbonates) the effects of mechanical compaction and grain-to-grain contact pressure dissolution were much less pronounced.

The maximum depth to which the deposits were buried could not have been very deep (2-2.5 km?) since abundant smectite is still present in some samples. If depths greater than 2.5 km had been reached most of the mixed-layer illite/smectite clay would have been converted to illite (Burst, 1969).

Uplift of the sequence at some later stage brought aggressive, acidic and oxidizing, meteoric pore waters into the sediments. Dissolution of carbonate cements and further dissolution of detrital feldspars, creating secondary porosity, was accompanied by the precipitation of kaolinite and iron oxide which infilled the secondary pores. Some carbonate cement was preserved, however, in the finer grained, less permeable sediments of the Prados beds.

Intense weathering of the sediments led to the conversion of haematite and siderite to goethite.

5.4. PALAEOMAGNETISM

5.4.1 Natural Remanent Magnetization (N.R.M.) Results

The results of palaeomagnetic analyses carried out prior to demagnetization of the Lower Buntsandstein samples are presented in Table 5.2.

TABLE 5.2 N.R.M. RESULTS FOR THE LOWER BUNTSANDSTEIN

Sample	Height (m)	F Dec(°)	F Inc(°)	P Dec(°)	P Inc(°)	Pole Long(°)	Pole Lat(°)	N	R	α95(°)	α95(°) Pole	Intensity (mAm^{-1})	Susceptibility ($mAm^{-1}nT^{-1}$)
MA2	18	354.1	58.1	343.4	70.0	326.3	71.5	6	5.93	7.9	13.4	0.54	-
MA4	50	9.6	61.5	349.8	76.4	348.6	63.6	6	5.84	12.0	19.0	0.23	1.78
MA5	64	351.0	49.7	11.5	53.0	122.4	78.8	7	6.72	13.2	17.0	0.67	8.87
MA6	74	346.5	53.2	327.9	63.0	290.1	66.5	4	3.96	11.1	14.6	1.32	-
MA7	102	352.6	42.8	342.5	53.7	249.9	74.7	7	6.91	7.3	8.5	0.21	13.36
MA8	110	52.9	71.7	98.9	81.7	16.2	31.9	6	4.12	51.3	82.2	1.22	-
MA9	122	343.1	54.2	324.6	62.7	290.3	62.7	5	4.80	17.6	25.7	2.12	-
MA10	138	352.1	70.0	310.0	78.4	330.0	52.2	5	4.97	6.2	11.6	2.43	-
MA11	152	352.3	56.0	334.7	66.3	300.5	70.5	6	6.00	2.1	3.3	7.83	-
MA12	156	349.8	54.3	332.8	64.2	292.1	69.7	5	5.00	2.1	2.7	4.84	-
MA13	157	3.5	61.6	345.1	73.5	336.4	69.2	6	5.99	2.1	3.6	9.57	-
MA41	182	34.4	71.1	33.0	80.1	15.2	54.2	6	5.80	13.7	24.3	0.69	-
MA42	192	348.8	68.2	326.9	73.0	320.9	62.5	7	6.93	6.5	10.6	0.70	-
MA43	195	42.5	10.4	42.8	19.3	114.6	41.2	5	4.60	25.6	24.9	0.10	18.03
MA46	221	38.1	52.6	38.7	61.6	61.8	60.4	7	5.04	30.2	41.6	0.12	4.30
MA48	234	355.8	51.7	346.8	58.1	264.2	80.0	7	6.94	6.0	7.9	2.79	10.31
MA49	241	349.8	62.8	333.7	68.2	307.5	68.6	7	6.90	7.8	12.5	1.42	1.67
MA50	246	350.3	59.1	329.0	68.8	306.9	66.1	7	6.99	2.0	3.1	1.68	1.82
MA51	252	340.1	59.9	315.6	67.3	300.2	58.1	6	5.99	2.8	4.0	6.73	-
MA52	256	359.0	62.4	337.0	73.5	328.0	66.6	6	6.00	1.3	2.2	20.82	-
MA53	260	355.2	65.6	326.0	75.6	327.8	61.0	6	5.88	10.5	17.9	3.76	1.73
MA54	262	349.3	53.0	333.1	62.9	287.1	70.0	7	6.99	2.3	3.5	9.41	8.65
MA55	171	358.2	55.6	336	60.6	279.8	80.4	7	6.80	6.3	15.0	0.93	10.73
MA58	180	352.3	51.1	342.9	54.8	255.2	75.9	5	4.90	12.6	15.3	0.53	92.44
MA59	185	342.7	36.3	336.9	39.1	232.0	63.8	5	4.87	15.2	14.1	0.23	76.24

The mean intensity of N.R.M. for samples from the Hoz del Gallo conglomerates was 2.8 mAm^{-1} and from the Rillo de Gallo sandstones, 2.2 mAm^{-1} (excluding MA52 which had an unusually high intensity of 20.8 mAm^{-1}). The mean initial intensity of N.R.M. for the Prados beds was 0.6 mAm^{-1}.

Mean initial susceptibility values for the three units were 13 $mAm^{-1}nT^{-1}$ (Hoz del Gallo conglomerates), 5.8 $mAm^{-1}nT^{-1}$ (Rillo de Gallo sandstones) and 59.8 $mAm^{-1}nT^{-1}$ (Prados beds).

N.R.M. directions for the Lower Buntsandstein are closely grouped having a steep, positive, north-northwesterly direction both before and after correction for bedding (Fig. 5.6). Two samples from the Rillo de Gallo sandstones (MA43 and MA46) show shallower mean directions, lying in the northeast quadrant. Mean directions for the Lower Buntsandstein samples (excluding MA43 and MA46) were D = 352.2° I = 57.6° α_{95} = 8° N = 26, in the field position and D = 336.0°, I = 65.3°, α_{95} = 13°, N = 26 in the palaeo position.

5.4.2 Isothermal Remanent Magnetization (I.R.M.) Results

I.R.M. curves for three Lower Buntsandstein samples (MA7, MA50 and MA54) are shown in Fig. 5.7

MA7 shows a fairly rapid acquisition of remanence at low fields, reaching 70% of its maximum intensity by 0.3T. At higher fields the intensity rises less rapidly and by 1.3T the sample is almost fully saturated. The I.R.M. for MA7 has a peak intensity of 603 mAm^{-1}.

Samples MA50 and MA54 show similar behaviour. Both demonstrate a steady rise in intensity reaching approximately 45% and 30% of their peak values by 0.3T respectively. The curves remain fairly steep until applied fields of >0.8T are reached. At higher field strengths, both curves level off but neither of the two samples reaches full saturation. Peak I.R.M. intensities are 710 mAm^{-1} (MA50) and 906 mAm^{-1} (MA54).

Reverse field demagnetization curves for the three samples are all fairly steep. MA7 falls to zero intensity by 0.2T, MA50 and MA54 reaches zero intensity by 0.35T and 0.45T respectively.

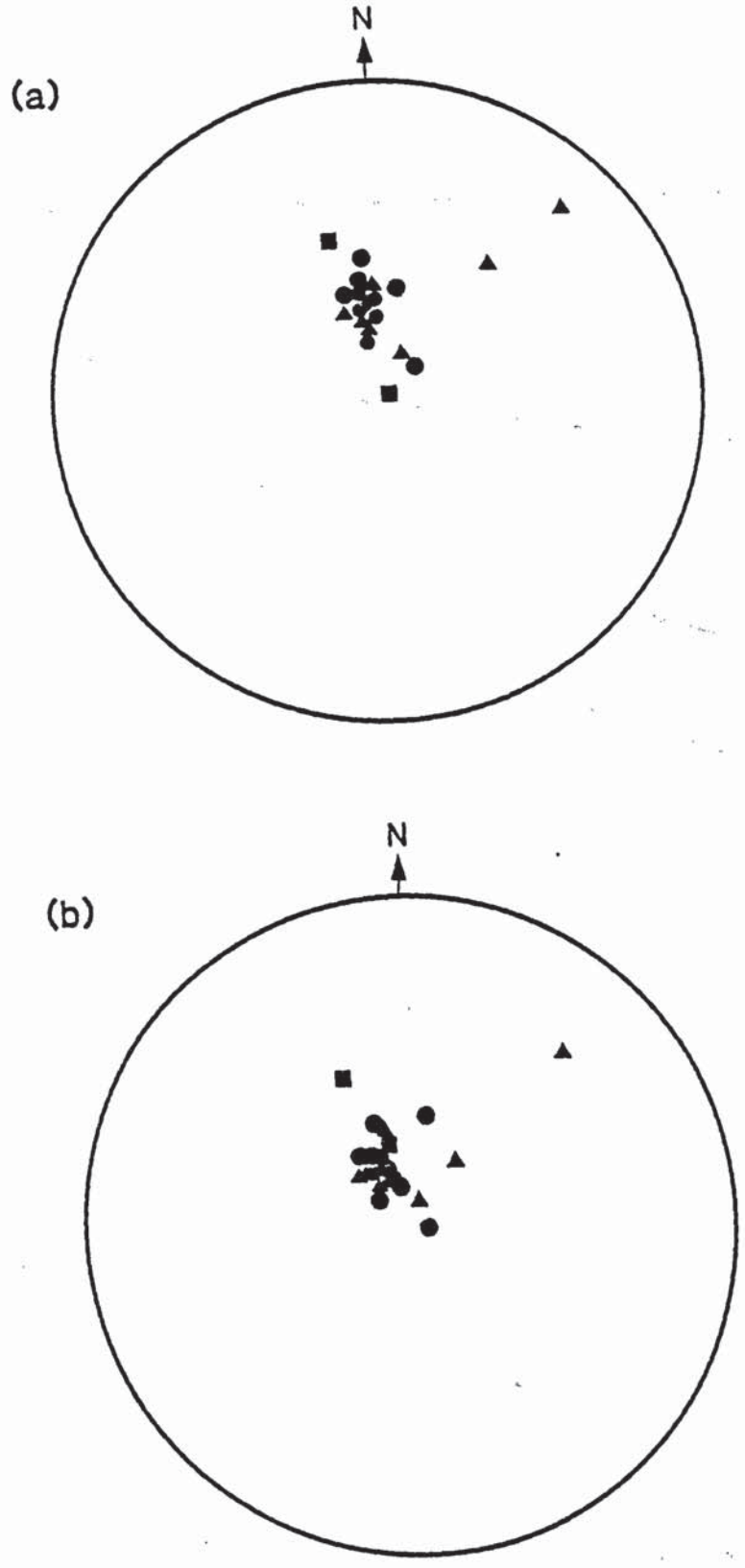

Fig. 5.6 Initial mean N.R.M. directions for the Lower Buntsandstein samples (a) before and (b) after correction for bedding. ● Hoz del Gallo conglomerates, ▲ Rillo de Gallo sandstones, ■ Prados beds.

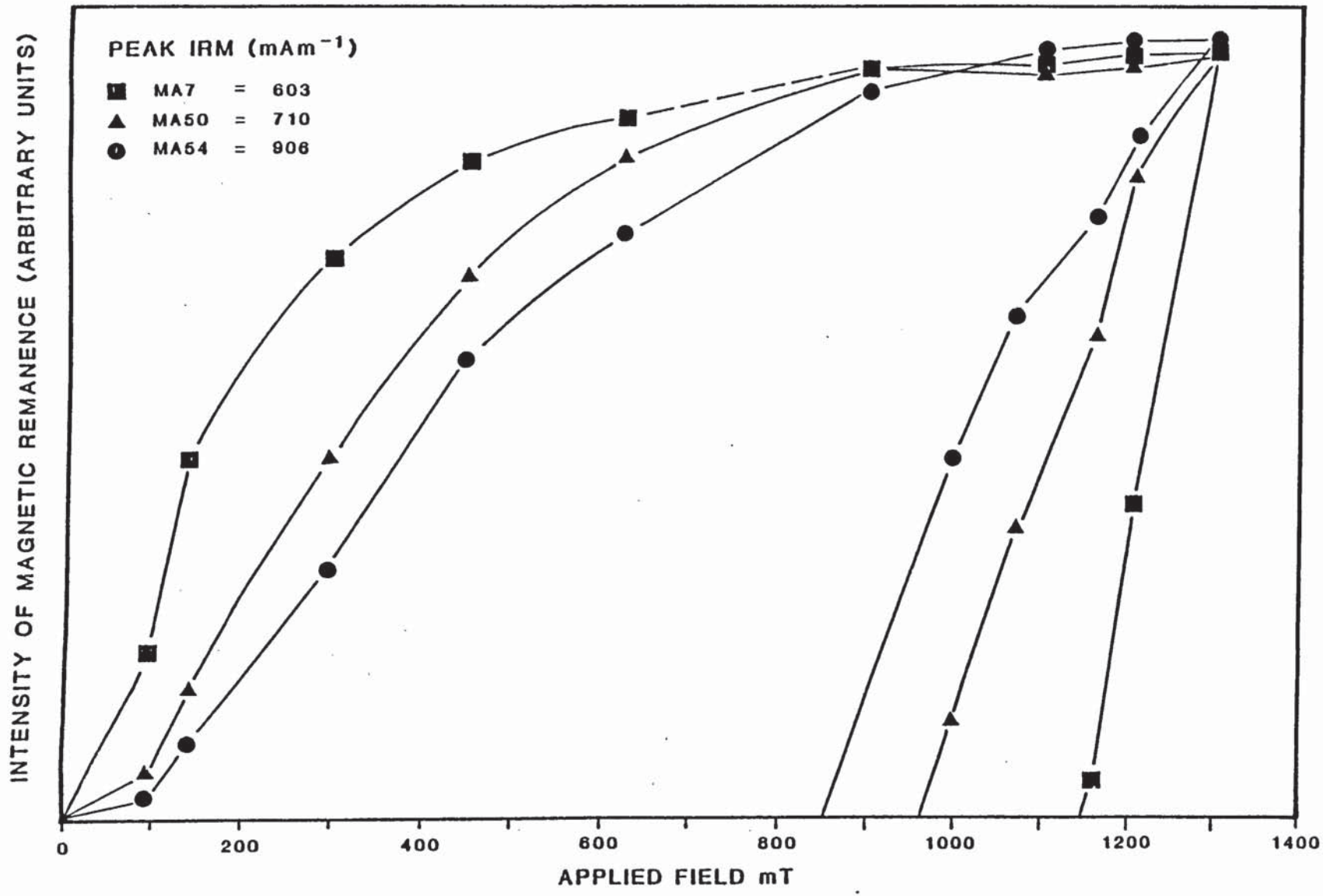

Fig. 5.7 I.R.M. acquisition and reverse field curves for three Lower Buntsandstein samples (MA7, MA50 and MA54).

The results indicate that the majority of the remanence in these Lower Buntsandstein samples is carried by haematite. A second, low coercivity mineral may also be present in MA7 as this sample showed rapid acquisition of remanence at low field strengths.

5.4.3 Thermal Demagnetization Results

5.4.3.1 Intensity and Susceptibility Changes

Normalized intensity and susceptibility versus temperature curves are shown for the three Lower Buntsandstein units in Fig. 5.8. (Specimens demagnetized at Aston University do not have susceptibility curves).

The majority of specimens from all three units show similar intensity decay curves. Susceptibility curves, however, show more variation. Most demonstrate an initial drop between room temperature and 100°C. Between 100°C and 200°C susceptibilities are more stable. Above 200°C a variety of behaviour is seen although the majority of specimens show another drop in susceptibility.

The specimens show a gradual removal of remanence between room temperature and 630°C at which point intensity values are very low. No sudden drops or rises in intensity are noted and a broad blocking temperature spectrum is envisaged.

In contrast to the above behaviour, four specimens (MA43.1.1, MA44.2.1, MA45.2.1 and MA46.5.1) from the Rillo de Gallo sandstones show a rapid drop in intensity between 200°C and 300°C to between 10% and 30% of their original values. Three of these specimens also show a rise in intensity between 400°C and 500°C followed by another drop between 500°C and 630°C. These intensity changes are accompanied by changes in normalized susceptibility. Between 200°C and 300°C the specimens show a rapid rise in susceptibility.

One specimen (MA2.1.1) shows a rapid drop in intensity and susceptibility to less than a quarter of its original value after heating to only 100°C. Both intensity and susceptibility values fall to almost zero by 300°C.

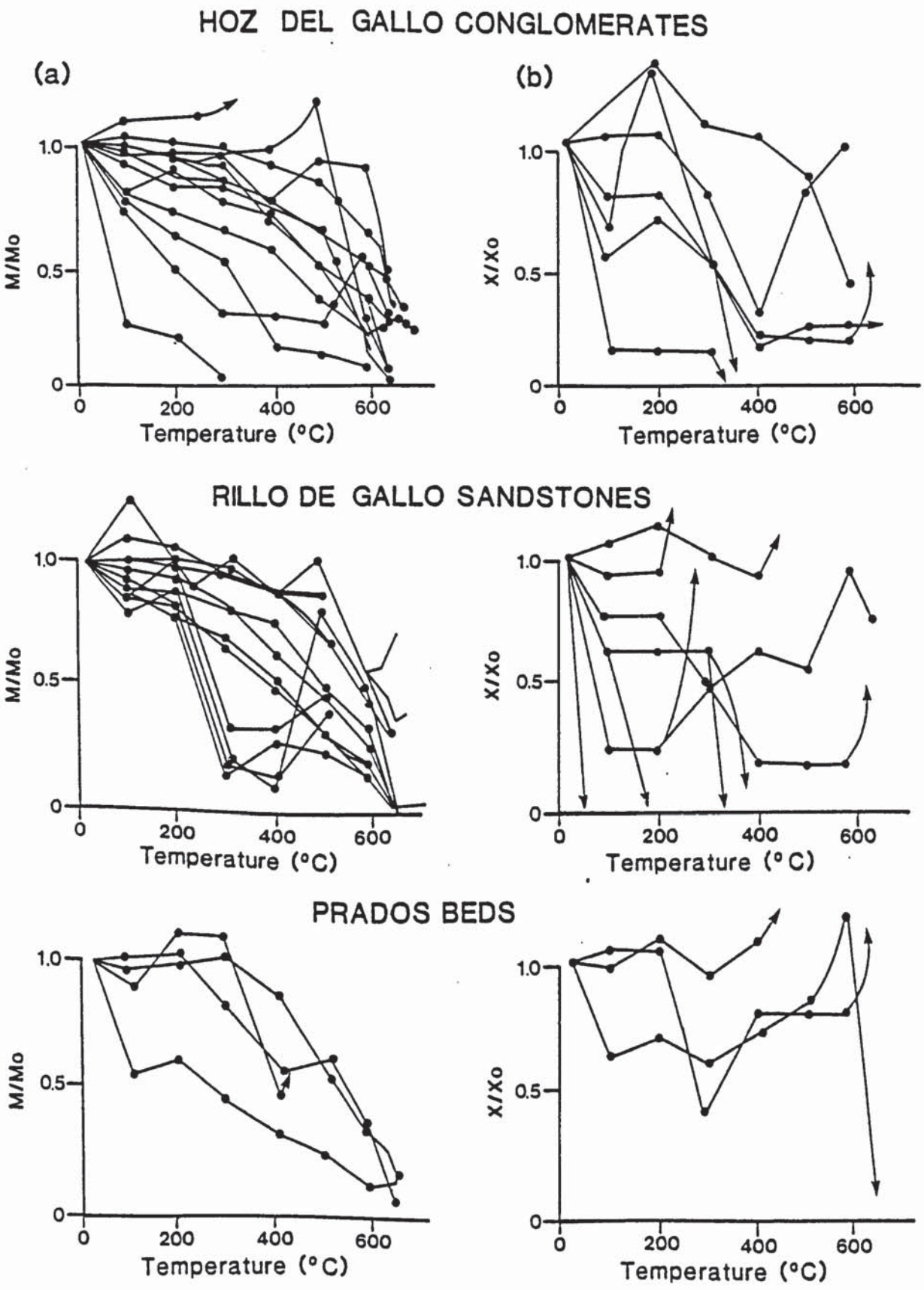

Fig. 5.8 Normalized intensity (a) and susceptibility (b) decay curves for Lower Buntsandstein specimens.

5.4.3.2 Discussion of Intensity and Susceptibility Results

Lower Buntsandstein intensity and susceptibility decay curves show more variation than those seen in the underlying Saxonian facies. Despite this, the majority of these blocking temperature curves show an absence of low blocking temperatures, about 50% of the N.R.M. removed by 500°C and an important maximum blocking temperature at 630°C. Susceptibility curves show more variation than the intensity curves. A drop in susceptibility, however, is recorded by most specimens between room temperature and 100°C.

These results (together with those from I.R.M. analyses) indicate that the majority of specimens contain one major component of magnetization which is gradually removed and has a maximum blocking temperature of 630°C. This suggests that haematite is the primary remanence carrier in these deposits as it is the only magnetic mineral with a Neel point above 600°C.

Specimens which showed a significant drop in intensity between 200°C and 300°C accompanied by a sharp rise in susceptibility probably contain siderite cements. Siderite converts to magnetite over this temperature range and this conversion is accompanied by a rise in susceptibility. Above 500°C, intensities and susceptibilities decrease as the magnetite is demagnetized.

Specimen MA2.1.1 shows a rapid drop in both intensity and susceptibility between room temperature and 100°C and is demagnetized at 300°C. This suggests that goethite is the main remanence carrier in this specimen as it has a Neel temperature of about 110°C.

5.4.3.3 Directional Changes

Specimens from the Lower Buntsandstein show three types of directional behaviour upon partial thermal demagnetization:

A. Steep positive initial directions which lie close to the local geomagnetic field direction and which are superimposed on a higher temperature component with north-northwest or south-southeast declinations and shallow inclinations.

B. Magnetization comprising a stable component near the local geomagnetic field direction superimposed on a weak, shallow component which cannot be precisely defined.

C. Fairly shallow positive directions in the northeast quadrant which move towards more shallow directions above 500°C.

Type A: 23% of the Lower Buntsandstein specimens have magnetizations of this type. Specimens MA9.4.1 and MA41.3.1 are good examples showing Type A behaviour. The stereographic projection for specimen MA9.4.1 (Fig. 5.9a) shows an initial, steeply dipping, positive direction close to the local geomagnetic field for the present day. At temperatures above 400%, the direction moves gradually southwards until it reaches a shallow negative direction in the southeast quadrant. The normalized intensity decay plot (Fig. 5.9b) shows that remanence is lost quite slowly at first (over 50% still remains at 500°C) but then a rapid drop between 500°C and 580°C to only 15% of its original value occurs. Above 580°C the intensity rises rapidly again.

Specimen MA41.3.1 has an initial direction which is, once again, steep and positive and lies close to the present-day local geomagnetic field direction. Above 400°C the direction moves northwards. Between 580°C and 630°C it moves to a position in the southeast quadrant and then, above 630°C, moves once again northwards to a very shallow negative direction in the northwest quadrant.

The normalized intensity decay is similar to that of the previous specimen with only slight loss of remanence intensity up to 500°C, followed by a rapid drop in intensity between 500°C and 580°C.

Type B: The majority (57%) of the Lower Buntsandstein specimens have magnetizations of this type. They consist almost entirely of a single component of magnetization near to the present earth field direction for the area, and is very stable during partial thermal demagnetization.

A typical example is shown in Fig. 5.10 (MA50.4.2). The initial field direction of D=347.3°I=56.2° is virtually unchanged up to 600°C. There is only a slight loss of N.R.M. up to 300°C (fig. 5.10b) with no associated direction change. More rapid loss above this temperature is not associated with directional change until 580°C. Above this

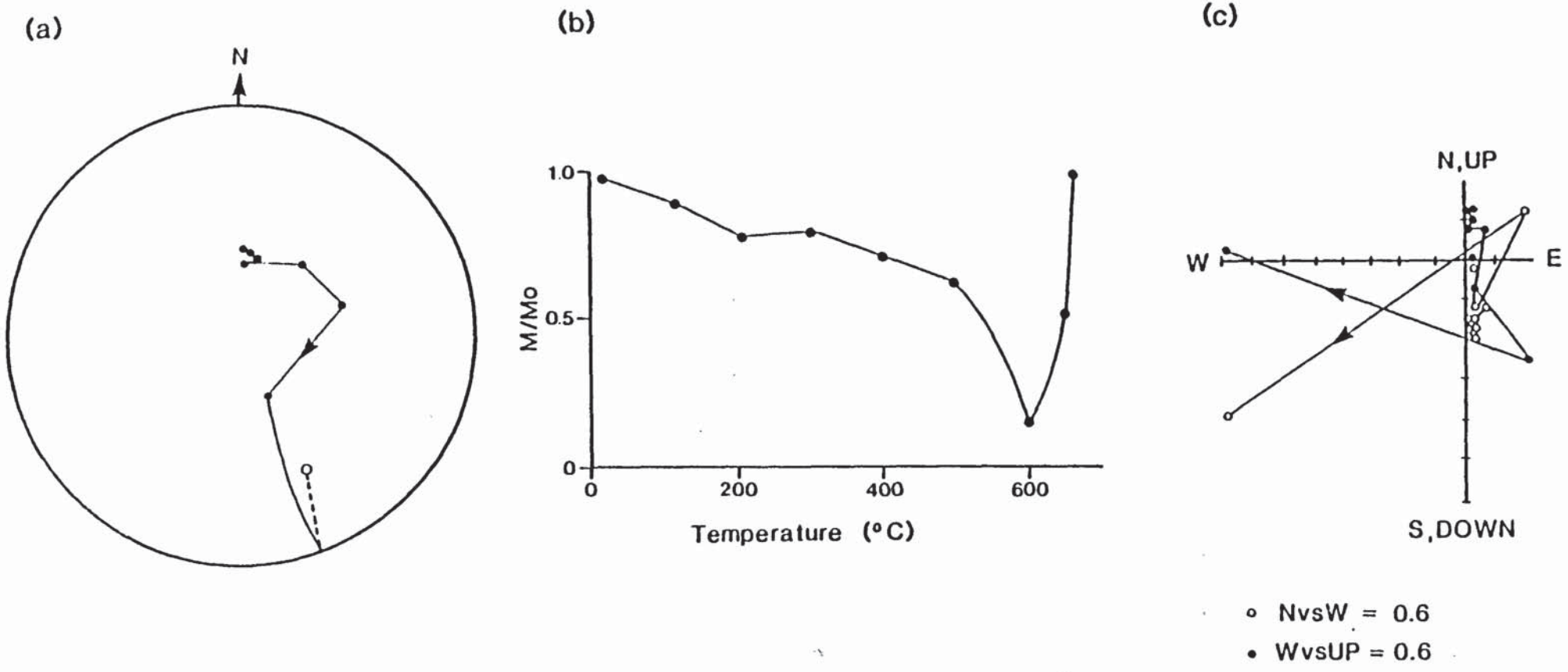

Fig. 5.9 Palaeomagnetic behaviour demonstrated by MA9.4.1 during partial thermal demagnetization. (a) Stereographic projection, (b) Normalized intensity decay curve, (c) Orthogonal vector plot.

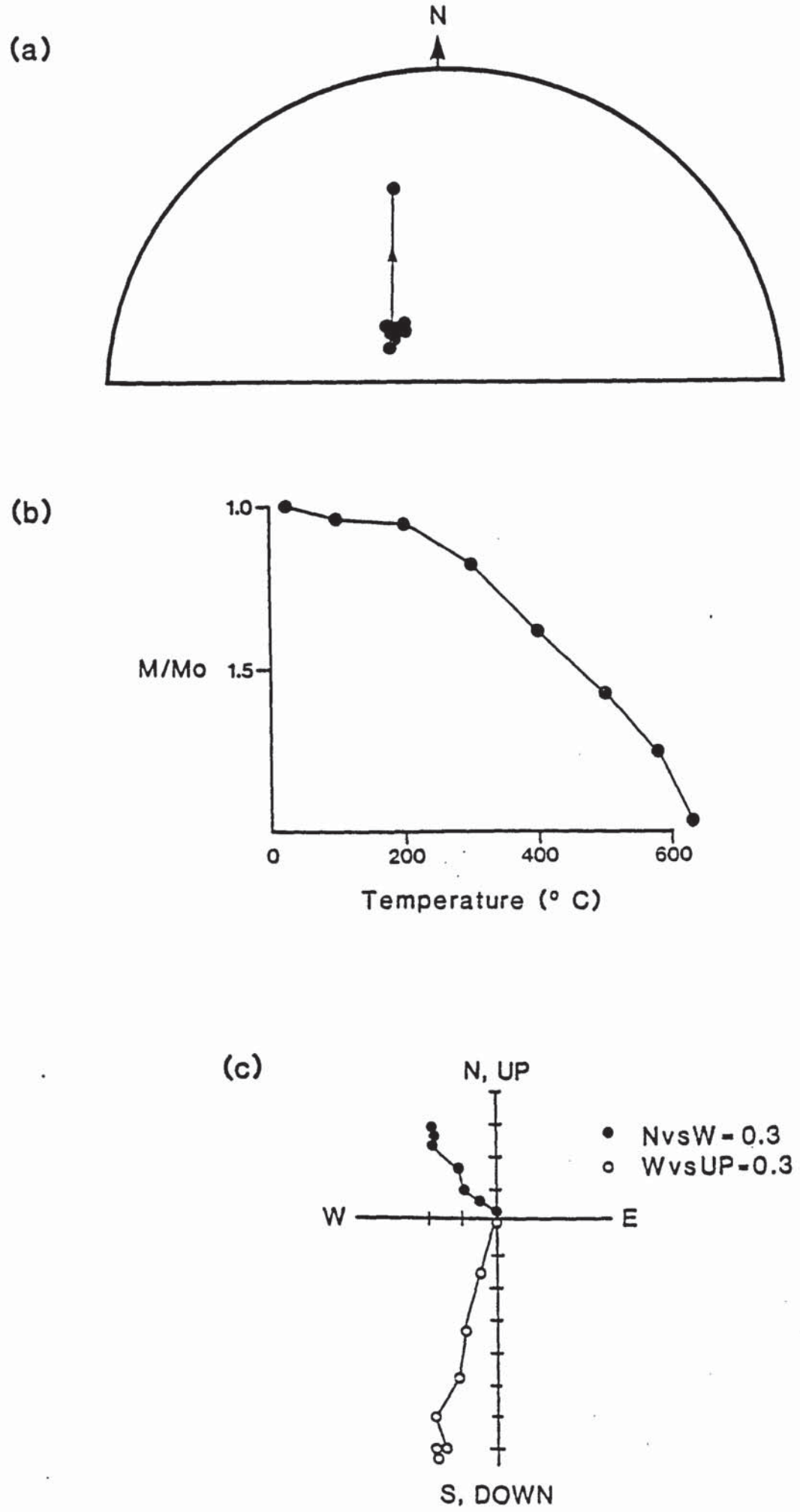

Fig. 5.10 Palaeomagnetic behaviour demonstrated by MA50.4.2 during partial thermal demagnetization (a) Stereographic projection, (b) Normalized intensity decay curve, (c) Orthogonal vector plot.

temperature the direction moves towards a shallower inclination in the northwest quadrant. At 630°C only 4% of the original remanence (0.09 mAm^{-1}) remains and reliable directions cannot be measured above this temperature. In other examples (e.g. MA49.4.1) the normalized intensity decay curve is almost identical to that of specimen MA50.4.2, as is the initial direction, but at higher temperatures, the directional movement is towards the southeast.

Type C: The final type of magnetization shown by these deposits is demonstrated by 20% of the specimens. MA59.1.3 is a good example showing this type of behaviour (Fig. 5.11). The initial direction lies in the northeast quadrant and is fairly shallow. This direction remains fairly constant up to 500°C and has a maximum stability over the range 20°C-300°C (S.I. 2.6, D=342.7°, I=25.2° and α_{95}=7.3°). Above 500°C the direction moves westwards to reach a final position which is in the northwest quadrant but has a negative inclination.

The normalized intensity decay curve (Fig. 5.11c) shows a two stage loss of N.R.M. The intensity remains unchanged up to 200°C. Between 200°C and 400°C a drop in intensity to about 60% of the original value is recorded. Between 400°C and 500°C the intensity remains stable. Above 500°C, another rapid drop is demonstrated. The normalized susceptibility curve (Fig. 5.11d) shows an initial drop in susceptibility followed by a fairly stable plateau between 100°C and 500°C. The susceptibility rises between 500°C and 580°C to a value greater than the initial susceptibility. Above 580°C it falls steeply to less than 20% of the original value.

5.4.3.4 Thermal Demagnetization Summary

The results of stepwise partial, thermal demagnetization of the lower Buntsandstein deposits are shown in Table 5.3. The majority of specimens have "most stable" directions isolated over the ranges 20°C-200°C or 20°C-300°C. Stabilities are high in the Hoz de Gallo conglomerates (mean S.I.=11.7) and Rillo de Gallo sandstones (mean S.I.=10.1) but moderate to poor in the Prados beds (mean S.I.=1.5). Most stable directions are very similar, for the majority of specimens, lying very close to the present-day geomagnetic field position for the area. The mean field corrected direction for the Hoz de Gallo conglomerates is D=357°, I=54°, α_{95}=6° (excluding MA8.6.1). For the Rillo de Gallo sandstones the mean field direction is D=351°, I=59°, α_{95}=11° (excluding MA43.1.1, MA45.2.1 and MA52.2.1) and D=350°, I=48°, α_{95}=30° for the Prados beds (excluding MA57.4.1).

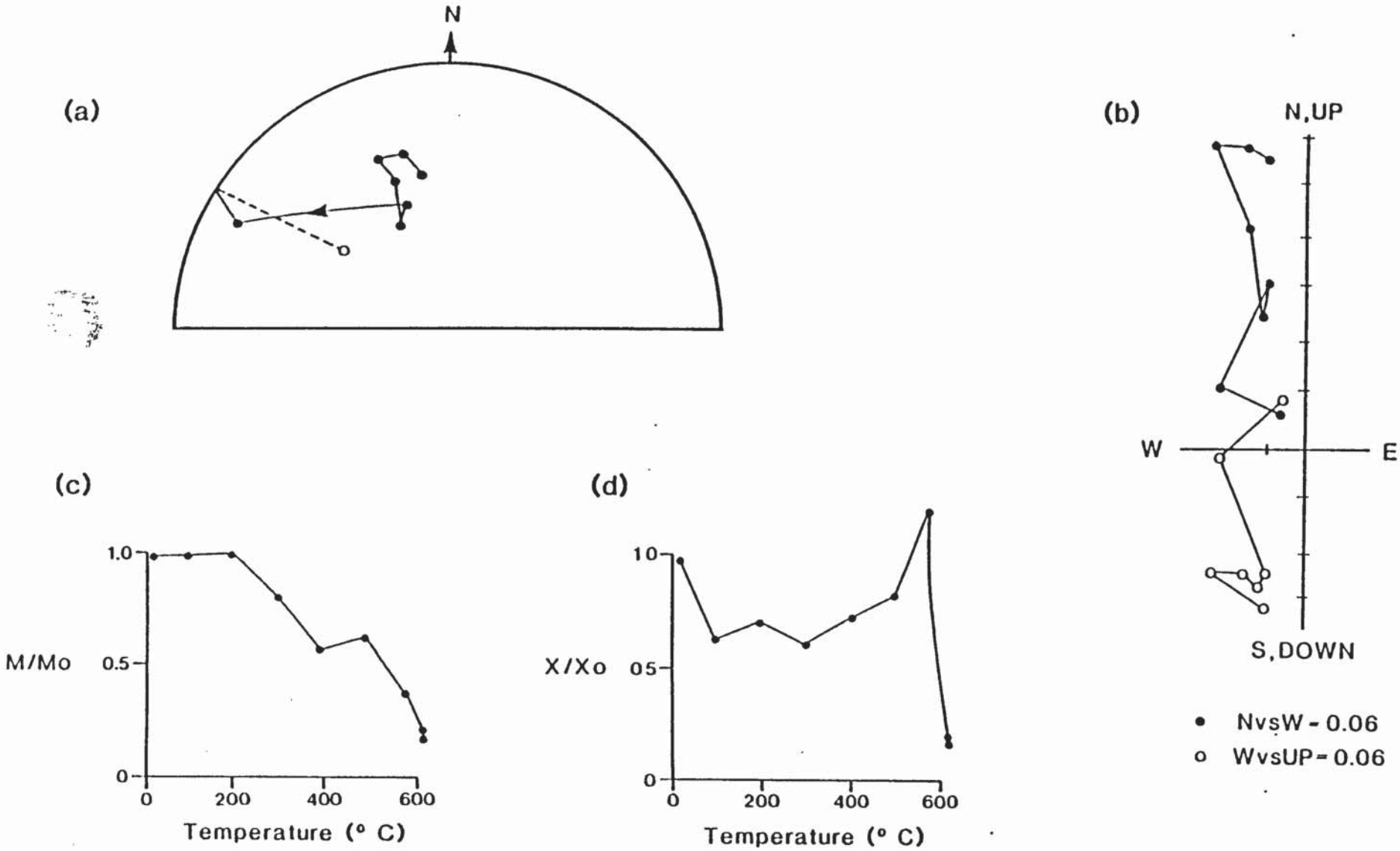

Fig. 5.11 Palaeomagnetic behaviour demonstrated by MA59.1.3 during partial thermal demagnetization. (a) Stereographic projection, (b) Orthogonal vector plot, (c) Normalized intensity decay curve, (d) Normalized susceptibility decay curve.

TABLE 5.3 STEPWISE THERMAL AND CHEMICAL (C) DEMAGNETIZATION RESULTS FOR THE LOWER BUNTSANDSTEIN

		Most stable directions				Pole					Range	Directions passing 10° linearity test				
			F		P								F		P	
Specimen	S.I.	Dec(°)	Inc(°)	Dec(°)	Inc(°)	Long(°)	Lat(°)	N	R	α95(°)	(°C)	Range(°C)	Dec(°)	Inc(°)	Dec(°)	Inc(°)
MA1.2.1	1.3	353.7	38.1	344.6	49.8	233.7	73.9	5	4.87	14.0	20-400	400-580	81.0	50.5	99.4	57.6
MA2.1.1	2.0	347.1	51.4	336.8	63.3	288.9	72.6	3	2.98	11.4	20-245	115-320	78.2	46.1	92.7	49.7
MA4.4.1	5.5	2.8	60.8	338.8	74.5	332.3	66.1	3	2.99	3.7	20-200	100-400	358.8	60.0	333.7	72.9
												20-200	9.8	65.2	342.4	79.8
MA5.1.1	9.1	345.7	57.4	13.3	61.3	74.9	79.9	4	3.99	2.2	100-400	200-630	344.9	57.9	13.1	61.9
MA7.1.1	32.8	352.9	46.3	341.4	57.1	261.9	75.3	4	4.00	0.6	20-300	100-630	351.7	45.3	340.5	56.0
MA8.6.1	2.3	122.5	48.5	137.1	45.3	36.3	-11.5	6	5.93	7.8	20-500	500-630	120.9	45.4	134.3	42.8
												20-245	314.4	58.2	291.0	59.7
MA9.4.1	8.3	12.0	38.7	7.8	52.1	138.1	79.7	3	2.99	2.5	20-210	None				
MA10.1.1	10.4	16.7	69.7	8.1	81.5	2.3	57.2	3	2.99	2.5	20-300	200-400	35.6	49.4	40.1	61.0
MA11.2.1	19.4	353.0	58.3	344.7	67.3	314.3	75.9	4	3.99	1.0	100-400	200-500	334.7	67.1	313.1	73.0
MA12.5.1	20.8	351.3	55.3	333.9	65.5	296.9	70.2	3	2.99	1.0	20-210	None				
MA13.1.1	16.5	357.0	62.0	334.6	72.8	323.7	66.3	3	2.99	1.2	320-500	320-500	14.2	60.8	3.6	74.2
MA41.3.1	3.0	350.1	80.2	289.4	82.6	338.8	44.1	4	3.98	6.5	20-325	None				
MA42.1.1	9.8	359.3	71.8	334.0	77.8	337.3	60.5	3	3.0	2.1	20-200	20-400	354.7	76.2	315.1	80.8
MA43.1.1	2.0	23.7	2.6	23.4	11.4	140.8	49.1	3	2.99	10.1	20-200	100-300	19.6	-0.8	19.5	7.8
MA45.2.1	2.3	134.9	71.5	158.1	68.3	11.5	4.3	3	2.99	8.8	20-200	200-400	124.1	62.5	141.0	61.4
												100-300	137.6	61.4	152.3	58.4
MA46.5.1	2.3	338.0	36.8	331.6	41.1	240.8	60.7	3	2.99	9.1	20-200	100-300	207.3	9.0	207.4	0.1
												300-500	82.2	24.3	85.7	30.3
MA48.4.1	16.3	353.2	50.4	344.3	56.5	255.9	77.2	3	2.99	1.3	100-300	20-660	345.1	50.7	345.1	56.9
MA48.4.1	12.5	345.1	60.7	329.9	65.5	295.7	67.5	4	3.99	1.6	200-500	300-630	346.6	61.0	331.4	65.9
MA50.4.2	15.6	346.9	56.6	327.2	65.7	296.2	65.7	3	2.99	1.3	20-200	300-630	340.8	58.2	318.3	65.9
MA51.6.1	10.0	338.7	62.4	310.8	69.1	304.7	55.0	6	5.99	1.8	20-500	420-590	3.7	48.6	354.4	61.0
												220-420	316.3	55.6	295.0	57.8
MA52.2.1	8.1	355.2	11.2	352.8	23.0	192.3	60.5	5	4.98	2.3	20-400	630-675	2.8	4.4	1.6	17.1
MA53.2.1	17.3	3.9	58.3	349.0	70.5	333.8	74.3	3	2.99	1.2	300-500	200-690	5.7	59.0	351.1	71.4
MA54.3.2	16.4	337.7	55.0	317.7	62.3	287.4	58.9	3	2.99	1.3	100-300	500-630	341.1	52.6	323.6	60.9
MA55.2.2	16.1	13.7	54.2	5.7	60.3	81.7	85.7	3	2.99	1.3	200-400	300-630	12.2	55.6	3.3	61.6
MA57.4.1	0.5	256.0	56.5	251.7	49.2	302.2	7.1	4	3.35	48.3	20-323	320-500	269.8	42.3	290.7	38.7
MA58.1.3	2.0	354.9	74.5	324.5	77.3	331.2	58.2	4	3.97	9.4	20-300	20-200	9.8	50.1	2.4	55.9
MA59.1.3	2.6	345.9	21.9	342.7	25.2	211.7	58.8	4	3.98	7.3	20-300	200-400	339.2	-5.0	339.7	-2.3
CHEMICAL DEMAGNETIZATION RESULTS																
MA1.1.1C	0.5	8.5	56.5	355.2	70.1	346.0	76.3	6	5.41	24.4	33-240 hrs	0.5-2.0 hrs	174.5	-23.5	169.4	-35.6
MA53.1.1C	1.2	180.3	58.2	187.4	45.3	350.9	-22.1	4	3.96	10.9	56-240 hrs	150-240 hrs	228.4	33.5	225.9	20.3
												1.0-8.0 hrs	6.9	57.5	354.0	70.1

The excluded specimens have most stable directions after correction for bedding which are either shallower than the majority of specimens but still in the north, e.g. MA43.1.1, D=23.4°, I=11.4°; MA52.2.1, D=352.8°, I=23.0°, or else fairly steep but in the southeast or southwest quadrants, e.g. MA8.6.1, D=137.1°, I=45.3°; MA45.2.1, D=158.1°, I=68.3°; MA5.1.3, D=251.7°, I=49.2°.

Fig. 5.12a shows the most stable directions plotted on a stereographic projection in the field and palaeo positions. The tight grouping of directions around the present-day geomagnetic field position is clearly seen. The directions also show a streaking effect towards shallower directions in the northwest and southeast quadrants. The α_{95} values (shown as circles around the points) are small in most cases.

Fig. 5.12b demonstrates the directions which pass the 10° linearity test. Three groups of directions can be identified.

A) The majority of specimens show directions close to the local geomagnetic field direction.

B) Three specimens show shallow directions in the north (MA43.1.1, MA52.2.1 and MA59.1.3). These were isolated over the range 100°C-300°C, 630°C-675°C and 200°C-400°C respectively.

C) Five specimens show bedding corrected directions in the southeast quadrant, these are MA1.2.1, MA2.1.1, MA8.6.1, MA45.2.1, MA46.5.1. These directions were isolated over a broad temperature range (100°C-630°C). They all have stability index values of less than 3, indicating that these directions are not very stable.

5.4.3.5 Bulk Demagnetization Results

Bulk demagnetization of the Lower Buntsandstein samples was carried out over the temperature range 580°C to 675°C. Five samples were bulk demagnetized at temperatures of 300°C or 400°C. One sample (MA2) was demagnetized using an alternating field of 60 mT. The results of these analyses are shown in Table 5.4.

Intensity values are generally less than 1.0 mAm^{-1} with over 40% of the samples showing intensity values of less than 0.1 mAm^{-1}. Bedding

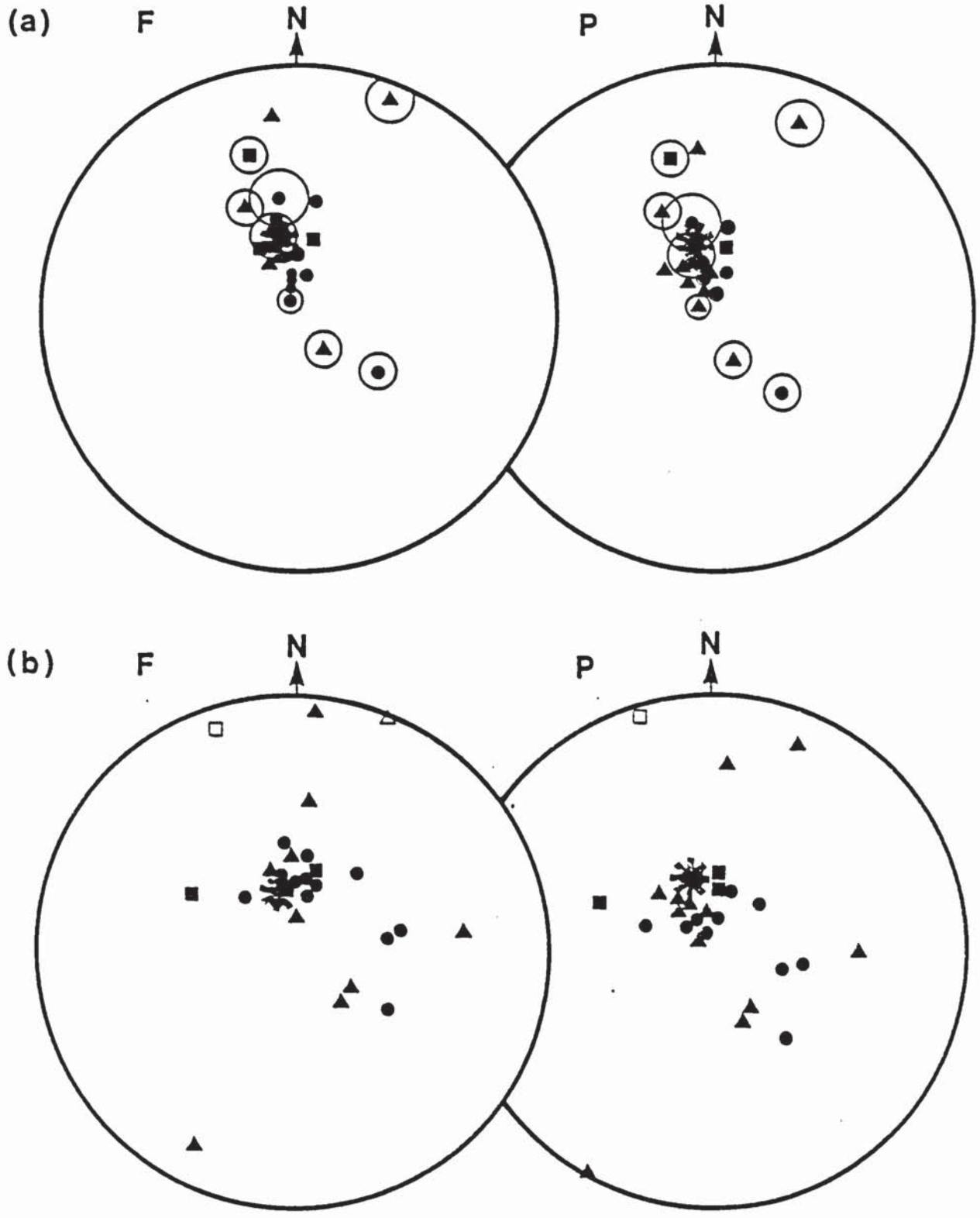

Fig. 5.12 Most stable directions (a) and directions passing 10° linearity test (b) isolated for Lower Buntsandstein samples. F = field corrected and P = field and bedding corrected directions. Circles represent α_{95} values, asterisk represents present-day local geomagnetic field direction.
For key to symbols see Fig. 5.6.

TABLE 5.4 BULK DEMAGNETIZATION RESULTS FOR THE LOWER BUNTSANDSTEIN

Sample	Height (m)	F Dec(°)	F Inc(°)	P Dec(°)	P Inc(°)	Pole Long(°)	Pole Lat(°)	N	R	α95(°)	α95(°) Pole	Intensity (mAm^{-1})	Susceptibility ($mAm^{-1}nT^{-1}$)	Temp (°C)
MA1	12	313.2	8.8	310.5	12.4	244.0	34.0	5	4.84	15.2	13.5	0.07	4.40	400
MA2	18	6.3	57.3	3.4	70.2	6.7	76.3	3	2.99	7.3	12.4	0.04	-	60 mT
MA3	30	173.3	19.9	179.5	12.9	358.7	-42.6	1	1.00	-	-	0.09	14.36	600
MA4	50	329.3	39.2	315.4	46.3	266.4	55.6	6	5.39	24.8	22.9	0.17	-4.46	400
MA5	64	296.6	28.4	287.6	28.3	268.6	22.9	3	2.96	16.6	16.4	0.06	-	600
MA6	74	166.0	57.0	170.0	60.0	-	-	3	-	5.4	-	0.47	-	600
MA7	102	253.9	1.9	254.4	-7.6	275.2	-14.2	3	2.86	33.2	30.6	0.09	3.40	675
MA8	110	106.3	30.4	114.8	32.0	57.1	-5.5	4	3.67	32.1	25.6	0.47	-	630
MA9	122	330.5	49.1	314.1	55.2	289.2	60.1	3	2.39	84	87.8	0.24	-	630
MA11	152	341.0	68.0	346.0	66.0	-	-	7	-	5.2	-	3.41	-	640
MA12	156	304.0	69.0	301.0	70.0	-	-	6	-	2.5	-	4.70	-	650
MA13	157	349.0	72.0	351.0	77.0	-	-	6	-	10.8	-	6.11	-	640
MA41	182	117.8	75.4	151.0	74.1	14.4	17.3	4	3.81	23.5	36.6	0.30	-	580
MA42	192	218.9	33.4	218.6	24.4	315.6	-25.5	2	1.99	-	-	0.09	-	660
MA43	195	300.2	31.2	294.9	29.9	265.1	31.2	4	3.61	35.3	31.2	0.07	98.11	580
MA44	-	99.9	28.0	104.7	30.3	67.0	1.4	3	2.63	59.4	61.9	0.05	-1.60	580
MA45	-	151.9	13.6	151.9	13.6	33.1	-35.7	1	1.00	-	-	0.03	1.11	300
MA46	221	157.0	70.0	162.0	68.0	194.0	15.0	4	3.69	39.3	51.1	0.06	58.04	300
MA48	234	357.0	47.0	349.0	54.0	254.0	78.0	6	5.90	11.9	10.1	0.81	14.80	630
MA49	241	366.5	59.0	298.0	64.0	313.0	59.0	6	5.35	21.0	30.9	0.29	1.60	630
MA50	246	347.2	47.9	333.7	57.7	290.3	69.8	6	5.32	26.6	31.0	0.26	3.47	630
MA51	252	-	-	316.0	70.0	-	-	4	-	17.3	-	3.54	-	640
MA52	256	-	-	333.0	68.0	-	-	6	-	4.1	-	12.18	-	600
MA53	260	71.6	32.5	79.6	41.8	72.3	23.7	4	2.83	73.1	77.6	0.08	-	675
MA54	262	271.4	33.2	264.4	26.3	282.4	4.8	2	1.98	-	-	0.06	-6.60	675
MA55	171	259.2	40.9	256.4	33.6	291.4	4.7	3	2.79	42.8	33.3	0.16	11.95	675
MA57	-	133.5	53.9	144.6	54.1	23.2	-7.3	4	2.91	19.1	84.7	0.53	-	400

corrected, bulk demagnetization directions show considerable scatter (Fig. 5.13) but about half of the samples show a grouping of directions near to the present-day local geomagnetic field direction, especially those from the Hoz del Gallo conglomerates. The other directions lie predominantly in the southern and western parts of the stereogram.

5.4.4 Chemical Demagnetization Results

Two specimens from the Lower Buntsandstein were selected for chemical demagnetization (MA1.1.1 and MA53.1.1) (Table 5.3).

MA1.1.1 shows a most stable palaeo direction over the range 33-240 hours immersion in acid, with a direction of D=355.2°, I=70.1°, α_{95}=24.4° (S.I.=0.5). It also shows a direction passing the 10° linearity test of D=169.4°, I=-35.1°, which is stable over the 0.5-2 hours immersion time range.

Fig. 5.14 shows the results of chemical cleaning of specimen MA53.1.1, together with results of thermal cleaning of specimen MA53.3.1. The chemically cleaned specimen shows a very steep initial direction close to the vertical. With increasing immersion time in the acid the direction moves towards the south-southeast portion of the stereogram, although the movement is not simple. The intensity first increases slightly between 0 and 0.5 hours and then drops very rapidly to less than 20% of its original value after 16 hours of immersion in the acid (Fig. 5.14a (ii)). The orthogonal vector plot (Fig. 5.14a(iii)) shows the removal of this steep component of magnetization after only a relatively short time in the acid.

The most stable direction was isolated between 56 and 240 hours and has a bedding corrected declination of 187.4° and inclination of 45.3°, α95=10.9, S.I.=1.2. Two directions pass the 10° linearity test. The first was isolated over the range 1-8 hours, D=354.0°, I=70.1° and the second between 150 and 240 hours D=228.4°, I=33.5°.

The thermally demagnetized specimen (MA53.3.1) shows slightly different demagnetization behaviour. This has an initial direction which lies close to the present-day geomagnetic field (Fig. 5.14b(i)), D=349.9°, I=72.9 after correction for bedding. This direction remains unchanged up to 580°C. Above this temperature the direction moves first east then west and finally at 690°C, reaches a shallow direction in the northeast quadrant D=334.1°, I=0.8°. The intensity at this temperature is only 0.02 mAm^{-1}, and thus may not be a reliable direction.

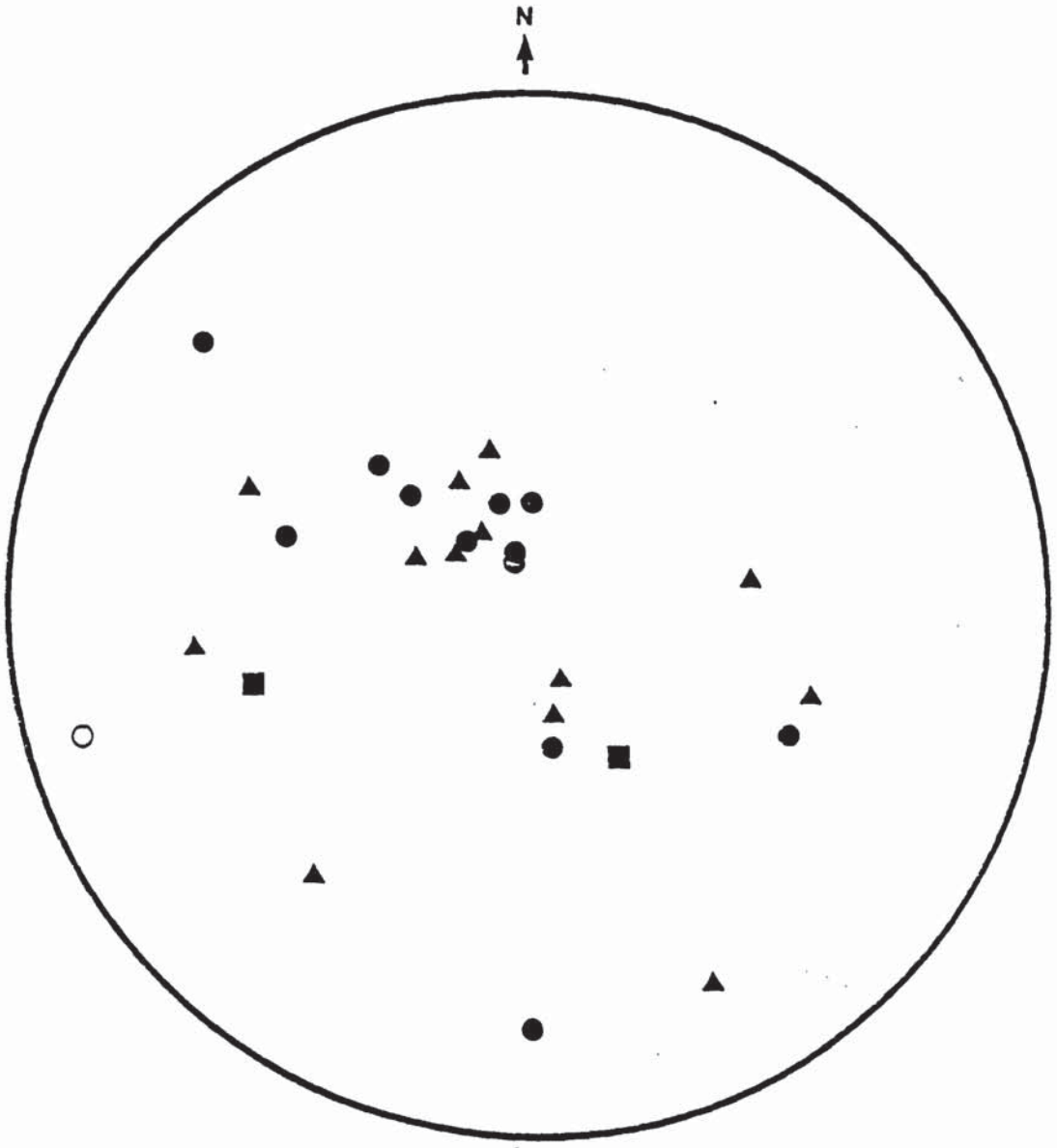

Fig. 5.13 Mean bedding corrected directions isolated during bulk demagnetization of Buntsandstein samples.
for key to symbols see Fig. 5.6.

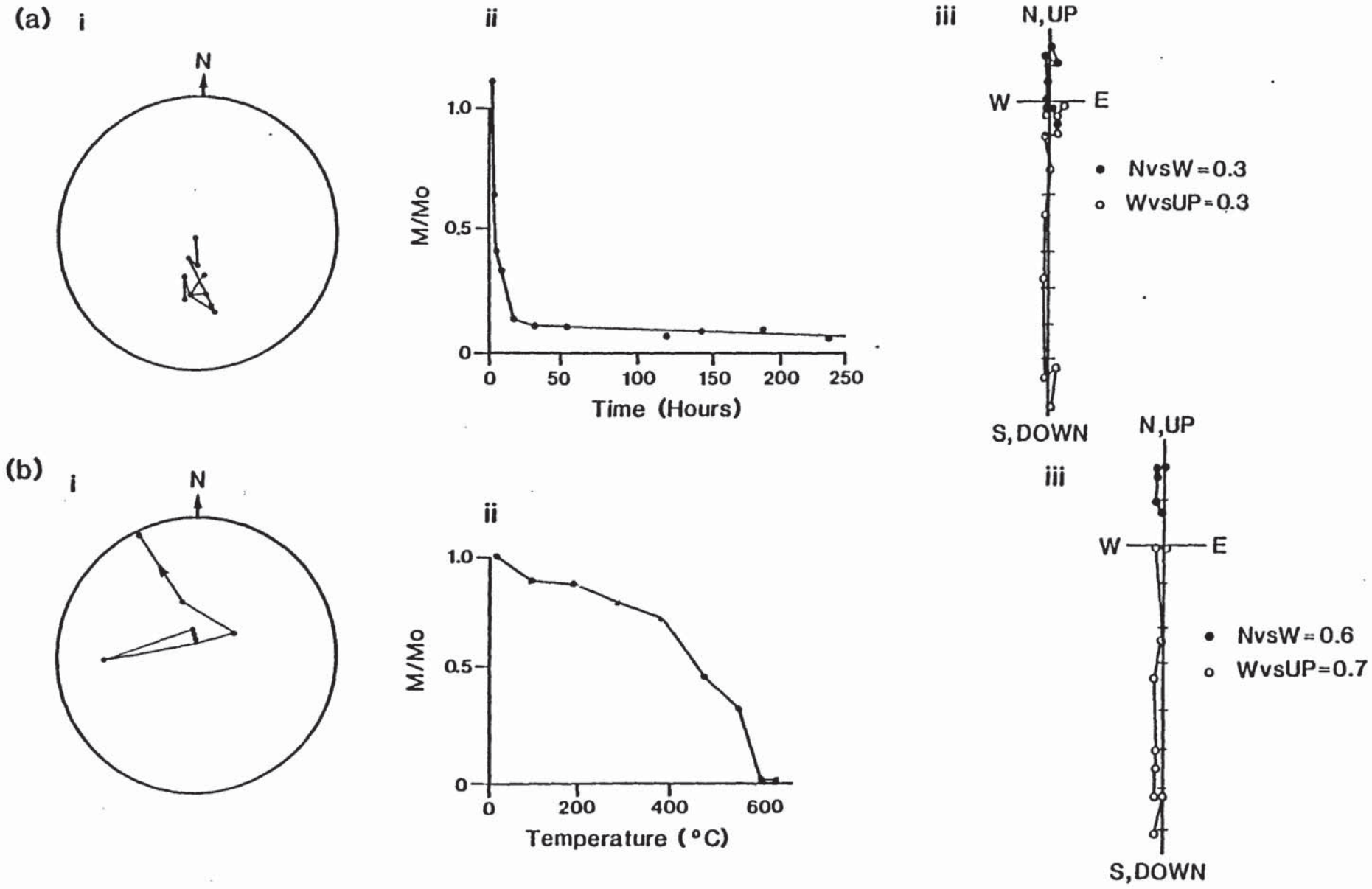

Fig. 5.14 Results of (a) Chemical demagnetization of specimen MA53.1.1 compared with those of (b) Thermal demagnetization of specimen MA53.3.1. (i) Stereographic projections, (ii) Normalized intensity decay curves and (iii) Orthogonal vector plots.

The intensity decay curve shows only a small loss of intensity up to 400°C followed by a more rapid drop between 400°C and 630°C. At this point, the intensity is less than 5% of its original value.

The orthogonal vector plot is very similar to that of the chemically demagnetized specimen (Fig. 5.14b(iii)). One direction passed the 10° linearity test. This was over the range 200°C to 690°C and had a direction D=351.1°, I=71.4°, the most stable direction was D=349°, I=70.5°, α_{95}=1.2, S.I.=17.3 on the range 300°C to 500°C.

5.4.5 Discussion of Palaeomagnetic Results

Mean initial intensities are quite variable in the Lower Buntsandstein deposits ranging from 0.1 mAm^{-1} (MA43) up to 20.8 mAm^{-1} (MA52) although most samples have initial intensities between 0.2 mAm^{-1} and 3.0 mAm^{-1}. Samples with higher initial intensities are found in the upper part of the Hoz del Gallo conglomerates (MA11-MA13) and upper part of the Rillo de Gallo sandstones (MA51-MA54).

Mean initial susceptibilities when measured are generally low (<20 $mAm^{-1}nT^{-1}$) except in the Prados beds where susceptibilities of 76.2 $mAm^{-1}nT^{-1}$ and 92.4 $mAm^{-1}nT^{-1}$ were recorded.

Most samples show initial directions which are closely grouped near the local geomagnetic field and are exclusively of the same polarity. This strongly suggests that remagnetization occurred in Holocene times during the Brunhes epoch and thus, the directions effectively represent the present-day Earth's field.

I.R.M. analysis indicates that this magnetic remanence is carried almost exclusively by haematite. Some samples e.g. MA7 also show evidence for the presence of a small amount of a low coercivity mineral such as magnetite, goethite or perhaps poorly crystalline iron oxide.

Partial thermal demagnetization of the Lower Buntsandstein deposits indicate that the majority of specimens contain one stable component near the present-day local geomagnetic field. This is superimposed on a weak, higher temperature component with north-northwest or south-southeast declinations and shallow inclinations (see section 5.4.3.3).

The stable component shows a broad blocking temperature spectrum (usually between 300°C and 630°C). The second, weaker component is only revealed after thermal cleaning at temperatures above 630°C. The weaker secondary component has a direction either in the northwest (e.g. MA41.3.1) or southeast (e.g. MA9.1.1, Fig. 5.9) quadrants and nearly antiparallel. These high temperature magnetizations are interpreted as a Triassic normal and Triassic reversed component respectively, since they lie close to previously published Triassic directions for Spain (see Table 5.5).

Four specimens from the lower part of the Rillo de Gallo mudstones and sandstones (MA43.1.1, MA44.2.1 and MA46.5.1) show intensity and susceptibility behaviour which suggests that during partial thermal demagnetization, siderite ($FeCO_3$), which occurs as a cementing mineral in these deposits, is converted to magnetite.

One specimen (MA2.1.1) shows evidence of containing large amounts of goethite since both the intensity and susceptibility drop rapidly by heating to only 100°C. Fig. 5.15 shows the palaeopole positions calculated for the Lower Buntsandstein samples. Previously published Triassic pole positions for Stable Europe (A-E) and Iberia (1-4) are also shown. Virtually all the specimens have pole positions which are steep and positive, lying close to the present-day pole position. They do not show agreement with previously published Triassic directions for Spain. In fact, they have directions which are nearer to the Triassic poles for Stable Europe. This suggests that none of the stable palaeo directions, nor calculated pole positions, represents an original remanence, but has instead been acquired at some later stage during the burial history of the sediments. Results suggest the acquisition of this remanence occurred during the Brunhes epoch (i.e. up to 700,000 years ago).

5.5 RELATIONSHIP BETWEEN DIAGENESIS AND PALAEOMAGNETISM

Initial intensities from the Lower Buntsandstein show positive correlation with amounts of coarse (detrital) opaques as revealed by point count analysis (see Appendix VII). Samples with the highest initial intensities, in general, contain the most coarse opaques. Reflected light studies show that the majority of these opaques are in fact detrital haematite grains.

TABLE 5.5 PREVIOUSLY PUBLISHED LOWER TRIASSIC DIRECTIONS AND POLES FOR STABLE EUROPE AND IBERIA, TOGETHER WITH THOSE FOUND IN THIS STUDY FOR THE LOWER BUNTSANDSTEIN OF MOLINA DE ARAGON

Letter/ No.	Locality (formation)	D(°)	I(°)	N	α_{95} (°)	Pole Position Lat	Pole Position Long	Reference
STABLE EUROPE								
A	Triassic sediments, USSR	-	-	-	-	51°N	159°E	Irving (1964)
B	Arran sandstone, Scotland	-	-	-	-	54°N	118°E	Irving (1964)
C	Buntsandstein, Germany	-	-	-	13	55°N	169°E	Irving (1964)
D	Vosge sandstone, France	-	-	-	-	28°N	143°E	Irving (1964)
E	Vosge sandstone, France	-	-	-	-	62°N	167°E	Irving (1964)
IBERIA								
1	Rio Aragon C. Pyrenees (undesites)	152.0	-22.5	14	6	51°N	133°W	Schwarz (1962)
2	Anayet C.Pyrenees (andesites and sandstones)	164.0	-14.0	11	10	52°N	154°W	Van der Lingen (1960)
3	Serra del Cadi E.Pyrenees (redbeds)	169.5	-3.0	41	4	48.5°N	163°W	Van Dongen (1967)
4	Alcazar de San Juan, Central Spain (redbeds)	359.5	23.0	36	6	63°N	177.5°E	Van der Voo (1967)
LOWER BUNTSANDSTEIN OF MOLINA DE ARAGON MEANS								
H	Hoz de Gallo conglomerates	348.0	64.5	10	7.5	72°N	113°E	This Study
R	Rillo de Gallo sandstone	330.0	65.0	10	10	65°N	110°E	This Study
P	Prados beds	306.0	50.5	3	3	38°N	102°E	This Study

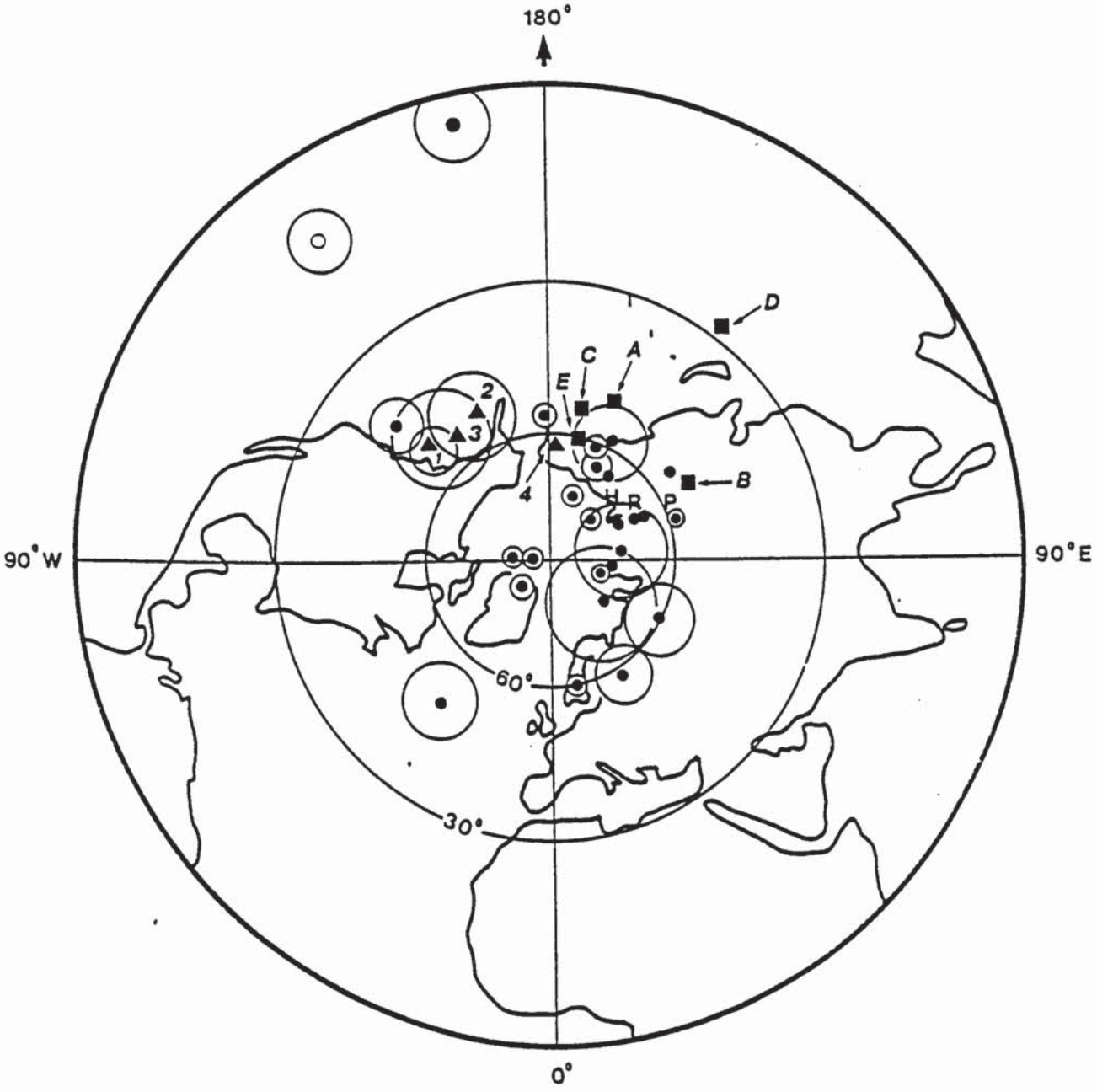

Fig. 5.15 Palaeopole directions for the Lowar Buntsandstein. ■ Letters A-E represent previously published palaeopoles for Stable Europe (see Table 5.5). ▲ Numbers 1-5 represent previously published palaeopoles for Iberia (see Fig. 5.16a and Table 5.5). ● Letters H, R and B correspond to mean palaeopole positions isolated for the Hoz del Gallo conglomerates, Rillo de Gallo sandstones and Prados beds respectively. Circles represent α_{95} values.

Total amounts of opaques (fine and coarse grained) do not show such good correlation with initial intensity. This could be because much of the fine grained iron oxide has not reached sufficient grain size to carry a magnetic remanence (i.e. it has not passed the superparamagnetic threshold). Another possibility is that the fine grained iron oxide, which is in many places intimately associated with the clays, gives them a red pigmentation.

Distinguishing what is clay and what is iron oxide using point count analysis is made very difficult and red stained clays may have been counted as fine grained opaques.

A number of different phases of iron oxide are present in these deposits, each of which carries a component of magnetic remanence. Diagenetic studies have helped to define when this remanence was acquired.

Only a small amount of coarse detrital haematite is present in these deposits and much of it has been severely altered (Fig. 5.3e). This specularite probably carries the second, high temperature component shown by many of the Lower Buntsandstein specimens.

Another common textural phase of haematite in these deposits is microcrystalline haematite which has replaced framework grains. It is especially common in biotite micas, where rows of haematite crystals occur in the cleavages of the mica. Mica's are much more abundant in the Lower Buntsandstein than in the underlying Saxonian facies, hence this associated magnetic component is more important in the younger deposits.

It is likely that this microcrystalline haematite is an early diagenetic phase which grew between the cleavages of the biotites in the early oxidising pore waters. This phase of haematite carries a remanence of Triassic age, which has either a normal or reversed polarity. Grain rimming microcrystalline haematite also carries a Triassic remanence. This maybe due to the 'ageing' of early iron oxide rich detrital clay coats on framework grains.

The most abundant phase of haematite in the Lower Buntsandstein deposits is fine grained pore filling or pore lining iron oxide cement (Plate 5.4b and d). This is a later phase which precipitated in secondary

pores, often in close association with kaolinite (plate 5.4c). Kaolinite is known to precipitate due to a rise in pH which accompanies carbonate dissolution (Curtis, 1983), and evidence for the wide-scale dissolution of such a carbonate cement is common in these deposits (Plate 5.3c, section 5.3.2). If this cement contained iron it its lattice e.g. Ferroan dolomite, ankerite, siderite etc. then during dissolution the iron would quickly combine with any free oxygen and precipitate as iron oxide or iron hydroxide in the secondary pores.

In the finer grained deposits of the Prados beds carbonate cement has been preserved and amounts of pore filling iron oxide are reduced (as are the initial intensities).

Siderite is present in MA57 and although not identified in samples MA43-46 using petrographic analysis, palaeomagnetic results strongly suggest its presence in these samples (section 5.4.3.2). It may also have formed an early cement which was subsequently removed creating secondary porosity. Amounts of fine grained iron oxide are very low in these samples and in hand specimen the rocks have a much paler appearance than the other samples. Directions isolated during thermal demagnetization are not consistent with the majority of specimens (i.e. they do not show a recent overprint). The reasons for the very low iron oxide content and unusual palaeomagnetic behaviour remain unclear but differences in pore water chemistry or diagenetic environment are the most likely causes.

Goethite is abundant in sample MA2 (Plates 5.4e & f). Where it occurs as a pore filling mineral. Specimen MA2.1.1 carries an N.R.M. with a field corrected direction of D=354.1°, I=58.1°, α_{95}=7.9° which is very close to the present-day geomagnetic field position. The reduction in intensity of remanence to only 5% of its original value after heating to 100°C confirms that geothite is the major remanence carrier in this specimen. It is likely that this was not a fresh sample but affected by intense weathering which resulted in the replacement of haematite and siderite by goethite.

CHAPTER SIX

THE UPPER BUNTSANDSTEIN OF MOLINA DE ARAGON

6.1 INTRODUCTION

Samples from the upper three Buntsandstein units were taken from sections at Rio Arandilla, Hoz del Gallo and Rillo de Gallo (Fig. 5.1 and 6.1). The Rio Arandilla section lies approximately 10 km west of Molina de Aragon, near the village of Cobeta (02° 07' 12"W, 40° 52' 12"N). 685m of Buntsandstein sediments are exposed alongside the Arandilla river. The location of the sections of Hoz del Gallo and Rillo de Gallo have been previously described (Section 5.1).

6.2 STRATIGRAPHY AND SEDIMENTOLOGY

The three upper Buntsandstein units in this area are: The "Areniscas del Rio Arandilla" (Rio Arandilla sandstones), "Limos y Areniscas de Rillo" (Rillo mudstones and sandstones) and the "Limos y Areniscas abigarrados de Torete" (Torete mudstones and sandstones).

The Areniscas del Rio Arandilla is comprised of red sandstones with some thinly bedded mudstones. Sedimentary features include tabular (Plate 6.1a) and epsilon (Plate 6.1b) cross-bedding. Samples MA60-MA70 (Rillo de Gallo) and RA1-RA4 (Rio Arandilla section) were taken from this unit.

The Rillo mudstones and sandstones comprise trough cross-bedded channel sandstones with well preserved fine-grained overbank deposits. Samples MA71-MA92 and RA5-MA10 were collected from this unit which is 103m thick in the Rillo de Gallo section and 178m thick in the Rio Arandilla section.

The youngest Buntsandstein unit recognised in this area is the Torete mudstones and sandstones which is comprised of interbedded mudstones and arkosic sandstones. Salt pseudomorphs are common and thin carbonate horizons containing algal laminations are also present. Samples MA93-MA95 were taken from this unit which is 34m thick in the Rillo de Gallo section.

The Rio Arandilla sandstone is similar to the underlying units of the Lower Buntsandstein units in that it also accumulated as a result of

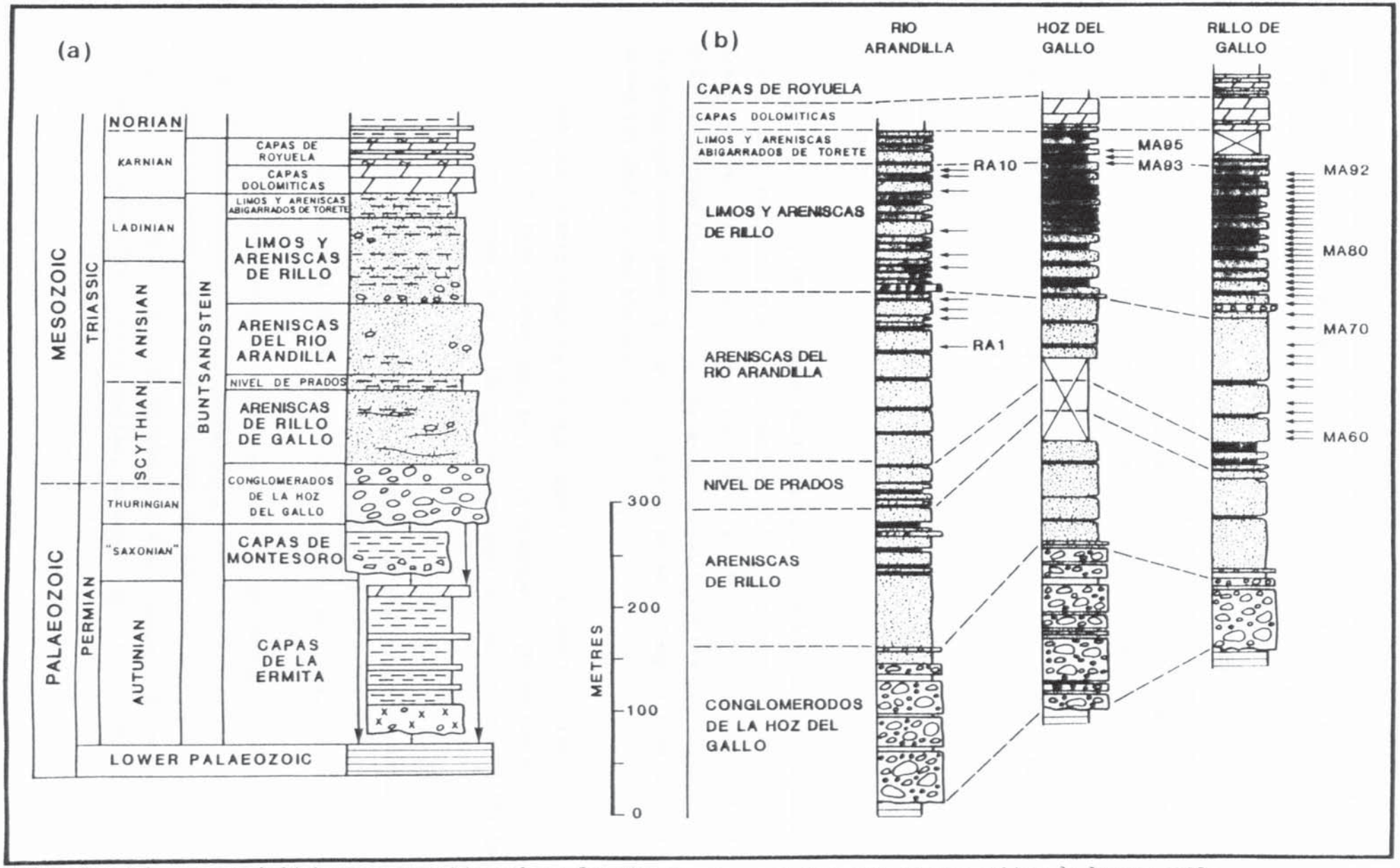

Fig. 5.1 (a) General lithostratigraphic column for the Permian and Triassic of the Molina de Aragon area, Central Spain (after Ramos, 1979).
(b) Sedimentological columns for the sections of Rio Arandilla, Hoz del Gallo and Rillo de Gallo,

braided fluvial systems. It was deposited by lower sinuosity streams than those of the underlying Prados beds, reflecting, a new reactivation episode caused by tectonic movements. The sediments of the lower part of the Rillo mudstones and sandstones are similar to those of the previous unit. A gradual change to higher sinuosity deposits is seen in the middle part of the unit evolving from a distal fluvial environment to one of tidal influence. This probably took place during the late Anisian as a palynological assemblage of this age is located in the upper part of the unit (Ramos, 1979). This marine influence marks the beginning of the Tethys transgression over this part of Western Europe. The Torete mudstones and sandstones contain several palynological assemblages of Ladinian age which show clear evidence of deposition in a supra-tidal environment in a semi-arid climate.

6.3 DIAGENESIS

6.3.1 Introduction

The mineralogy of the Upper Buntsandstein units has been determined using point count analysis (see Appendix VII). The samples fall in the Arkose and Subarkose fields when plotted on a Q.F.R. ternary diagram (Fig. 6.2). Towards the top of the series a general trend towards higher feldspar and lower rock fragment content is noted. Samples from the Rio Arandilla section are the most feldspathic.

Detrital quartz accounts for 30% (MA89) to 66% (MA61) of the total composition of these sandstones, having an average of 47% in the Rio Arandilla sandstones, 42% in the Rillo mudstones and sandstones and 38% in the Torete mudstones and sandstones.

Detrital feldspars, which consist mainly of the potassium variety account for between 12% and 23% of the total in the Rio Arandilla sandstones and between 4% and 16% in the other two sections.

Micas (predominantly muscovite) account for an average of 3% of the total, although 8% is found in sample RA5. Clays (detrital and authigenic) account for between 0.5% and 10% and heavy/accessory minerals represent up to 1% of the total volume of the sediments. These mainly consist of tourmaline, zircon, rutile, amphibole apatite and epidote.

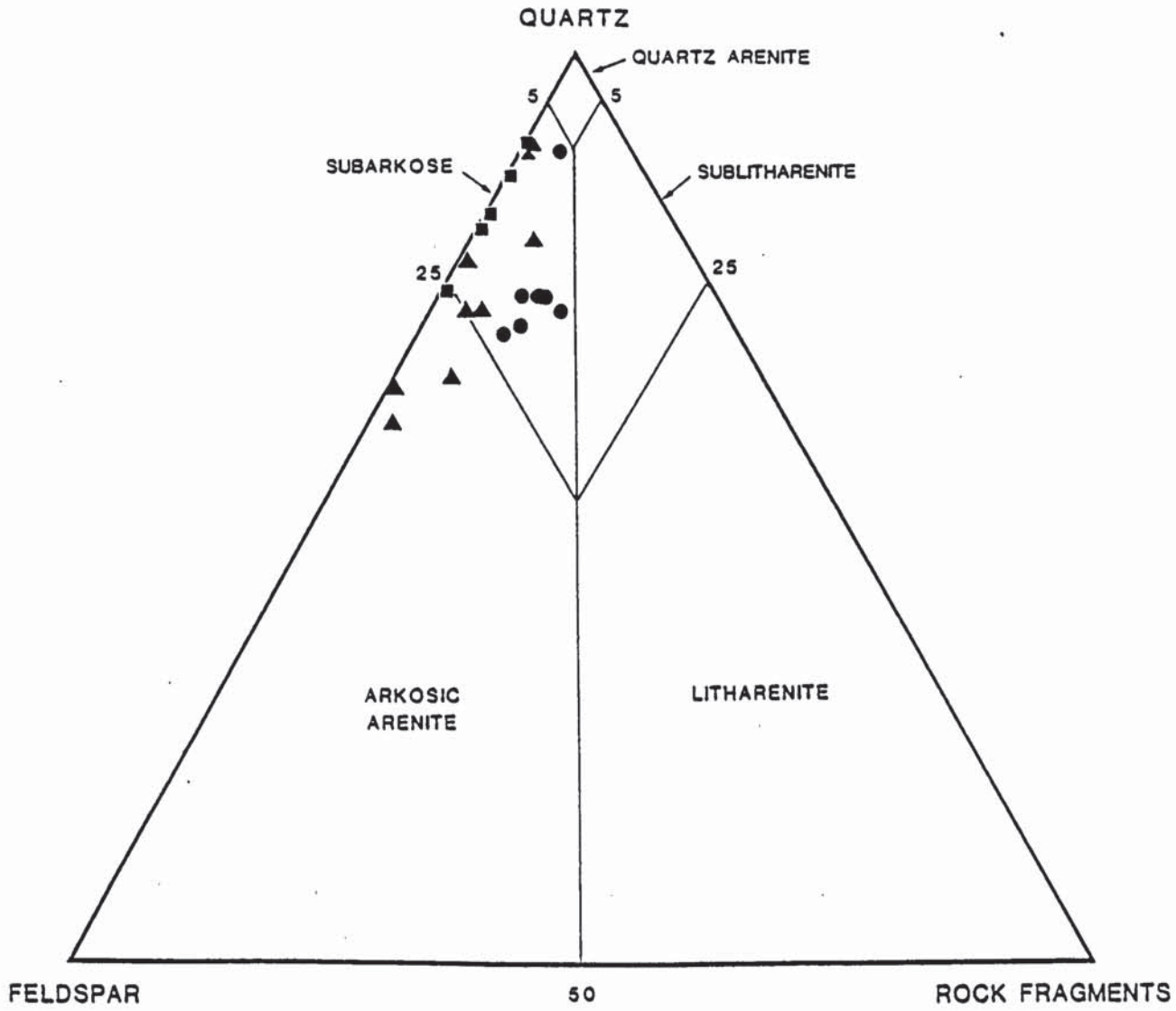

Fig. 6.2 Q.F.R. ternary diagram showing the composition of point counted sandstone samples from the Upper Buntsandstein.
- ● Rio Arandilla sandstones
- ▲ Rillo mudstones and sandstones
- ■ Torette mudstones and sandstones

Authigenic quartz is present in all samples studied. Amounts range from 1.5% (MA93) to 16% (MA63) with an average of approximately 8%. Authigenic potassium feldspar is also present in many samples. Amounts are generally small, usually less than 2%, but exceed 5% in some samples e.g. MA92, RA10.

Carbonate cements are found in many of the samples, especially in the higher parts of the series. Non-ferroan dolomite predominates and amounts reach 23% in some samples, e.g. MA69, MA93.

Iron oxide is also abundant in these deposits. Amounts range from 1.6% in sample MA61 up to 50% in sample MA89.

Visible porosities vary greatly from 2% in RA1 and MA91 to greater than 25% in MA80. The mean value for the Upper Buntsandstein units is 11%.

6.3.2 Diagenetic Transformations

Both mono and polycrystalline varieties of detrital quartz are found in the Upper Buntsandstein deposits, although amounts of the former are much larger. Some grains contain inclusions of heavy minerals, suggesting derivation from a plutonic source.

Orthoclase is the predominant feldspar in these deposits although microcline and plagioclase are also present in small amounts. The majority of the grains have a cloudy appearance due to partial replacement by clays and/or iron oxide.

Authigenic quartz is found in all samples studied. It occurs as syntaxial overgrowths on detrital grains (Plate 6.2a). 'V' shaped dissolution notches are seen in many of these overgrowths.

Authigenic potassium feldspar is also present in many of the samples (especially those from the upper part of the Rillo mudstones and sandstones in the Rillo de Gallo section. It occurs as non-syntaxial overgrowths on detrital grains. These overgrowths often have a euhedral shape and have been etched (Plate 6.2b).

Dust rims between detrital grain (for both quartz and feldspar) and authigenic overgrowth are not well developed and commonly absent altogether, suggesting very early precipitation of these phases.

Clays are present in all samples from the Upper Buntsandstein, although they are most abundant in the Rio Arandilla sandstones (Plate 6.2c). Detrital clays account for only a minor proportion of the total clay content. The majority of the clays have an authigenic origin. Most occur as a replacement of detrital grains such as feldspars, rock fragments and Micas.

Table 6.1 shows the results of semi-quantitative analysis carried out on a number of samples from these Upper Buntsandstein sediments.

Table 6.1 Semi-quantitative analyses carried out on the <2μm fraction of clays from the Upper Buntsandstein.

Sample	Illite	Kaolinite	Mont.	Chlorite	Total
MA63	58	17.5	23	1.5	100
MA71	65	1.0	32.5	1.5	100
MA72	66	0.5	33	0.5	100
MA77	56	1.0	42	1.0	100
MA78	65.0	1.5	32.5	1.0	100
MA80	55.5	1	42.5	1	100
MA83	90	1	8	1	100
MA90	83	2	14	1	100
MA93	27	6	63	4	100
MA94	28	8	55	9	100
MA95	85	7	5	3	100
RA6	60	0.5	39	0.5	100
RA9	71	0.5	28	0.5	100

The results show that illite is the most common clay mineral present in the sediments (accounting for between 27% and 90% of the total clay content). Montmorillonite is the second most abundant clay. This accounts for between 8% (MA83) and 55% (MA94) of the total. Amounts of Smectite are highest in the lower part of the Rillo mudstones and sandstones and the Torete mudstones and sandstones.

Kaolinite is only abundant in one sample MA63 (17.5%). Petrographic studies show this to be a common replacement of muscovite (Plate 6.2d).

The Prados beds also contain amounts of kaolinite between 6% and 8% of the total clay content. The remaining samples contain <2%. Amounts of chlorite are small <2% except in the Prados beds where amounts reach 9% of the total clay content (MA94).

X-ray diffractograms for samples MA71 (Fig. 6.3) and MA95 (Fig. 6.4) show the relative abundance of smectite in the former and chlorite in the latter sample.

Carbonate cement is present in many samples (especially those in the upper parts of the Rillo mudstones and sandstones from the Rillo de Gallo section and the Torete mudstones and sandstones. Samples from Rio Arandilla also show carbonate cement throughout. Non-ferroan dolomite is the most common cement. It's habit is varied, ranging from numerous small 'spot' like patches within the rock to an aggressive poikalotopic cement (Plate 6.2 e & f). Ferroan dolomite and non-ferroan calcite are also present in small amounts. The latter mainly occurs as a late stage fracture filling mineral but it also occurs as a pore filling cement e.g. MA89. Fine grained iron oxide cement is widespread in the Upper Buntsandstein rocks. In some examples framework grains appear to 'float' in a matrix of iron oxide and clays (Plate 6.3a). In places where carbonate cement exists no iron oxide is present - suggesting that the carbonate predates iron oxide precipitation.

Some samples contain large dolomite nodules, these have a subhedral (lensoid) shape and may represent replaced evaporites. Plate 6.3a shows one such nodule, it is approximately 1.5 cm in length and is composed of ferroan calcite crystals, enclosed by non-ferroan dolomite.

Porosities vary greatly from less than 2%, up to 25%. Secondary porosity dominates over primary porosity in terms of volume. The main types seen are moldic porosity, mainly due to framework grain dissolution especially feldspars, and oversized and elongate pores (Plate. 6.3b), almost certainly due to the removal of a pore filling cement.

Many of the secondary pores are lined with thick coats of iron oxide (Plate 6.3c) which post-dates all previous authigenic minerals.

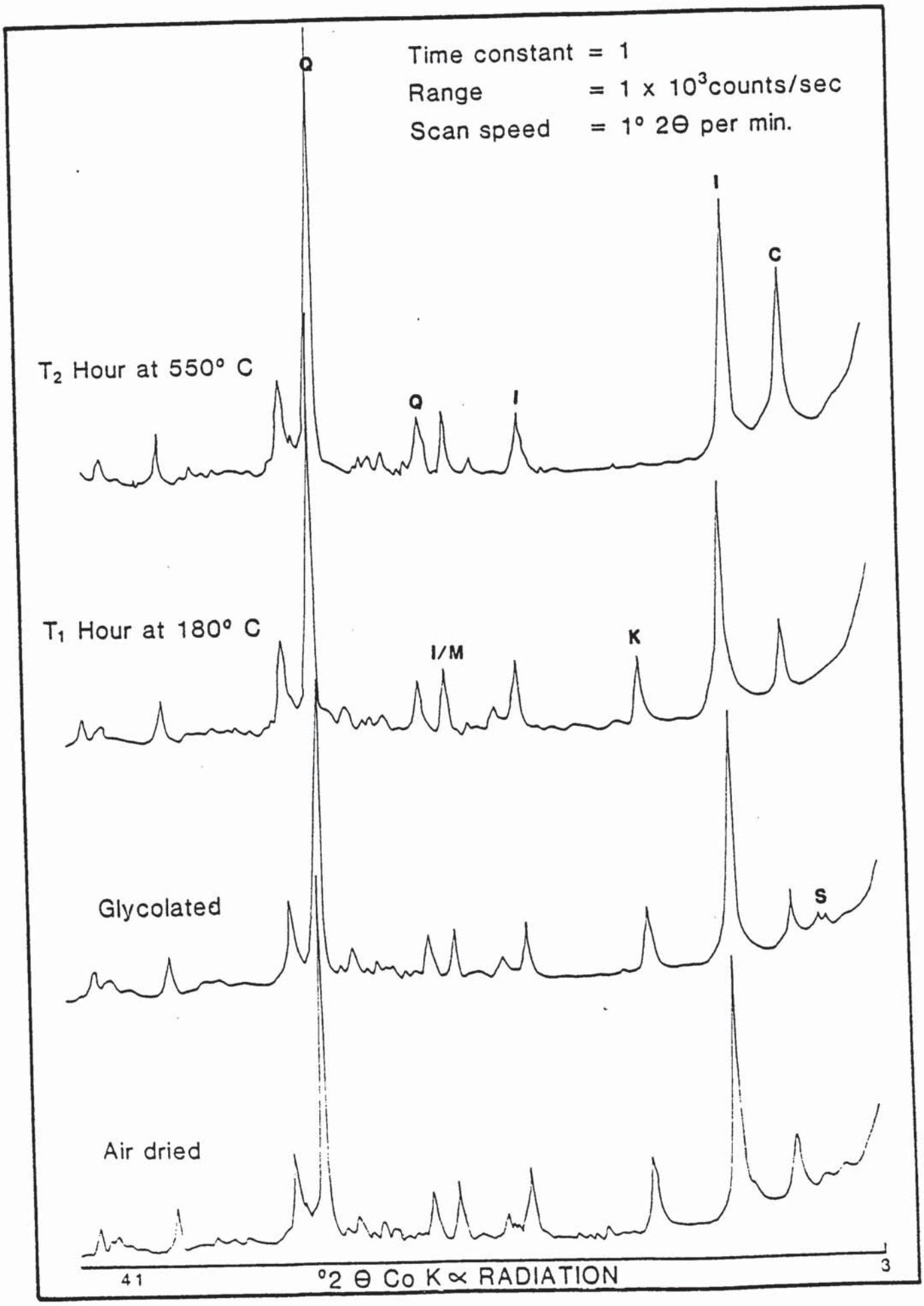

Fig. 5.4 X-ray diffractograms for the <2μm clay fraction of sample MA95.

6.3.3 Magnetic Mineralogy

The total opaque content of the upper Buntsandstein deposits as determined by point count analysis is higher than all previously described facies. Amounts vary from 2% in the lowest part of the sequence (MA61, MA62 and MA63) up to almost 50% in the upper part of the Rillo mudstones and sandstones (MA89). Reflected light petrography shows that the coarse opaques consist primarily of haematite with some ilmenite, magnetite is not present. Fine grained opaques also consist almost exclusively of haematite with some goethite.

Specularite:

Coarse detrital haematite is more abundant in these Upper Buntsandstein deposits than in the Lower Buntsandstein (Place 6.3d). Amounts reach up to 8% (MA83) in some parts of the sequence although the average is 1.6%. The grains range in size from 0.02 mm up to 0.3 mm and are usually subrounded. They commonly have a much embayed and skeletal appearance when viewed under reflected light (Plate 6.3e). Detrital titanium oxide (predominantly ilmenite) is also present in the deposits. It frequently shows replacement by haematite (Plate 6.3f) and leucoxene (amorphous titanium oxide). Like haematite it often has an altered skeletal appearance (Plates 6.4a and b).

Authigenic haematite:

(a) The replacement of framework grains by haematite is a common feature in these deposits. Rock fragments, biotite micas and potassium feldspars all show replacement by microcrystalline haematite (Plate 6.4c). It develops first along cleavage traces, but may eventually pseudomorph the whole grain.

(b) Fine grained haematite also lines and infills secondary pores (Plate 6.3c) and many samples are seen to post-date the authigenic quartz (e.g. MA63).

The fine grained iron oxide is also found in association with pore filling clays (Plate 6.4d) imparting or red pigmentation to them. Many samples show fine grained iron oxide cement in which the framework grains appear to 'float', Plates 6.3a(MA54) and 6.4e(RA9).

Framework grains often have embayed margins suggesting the former presence of an aggressive cement under reflected light. The fine grained pore filling cement is seen to be composed of microcrystalline and pigmentory haematite and titanium oxide (Plate 6.4f).

Goethite is present in small amounts in some samples e.g. RA5 and MA67. It is yellow/brown in colour and occurs as fine grained aggregates within the pores.

6.3.4 Paragenesis

The paragenetic history of the Upper Buntsandstein sediments is similar to that of the underlying Lower Buntsandstein (section 5.3.4).

The earliest diagenetic modifications were the mechanical infiltration of clays and the dissolution and replacement of the less stable grains by clay minerals.

Other eogenetic reactions included the precipitation of authigenic quartz and potassium feldspar and the formation in certain horizons of evaporite nodules.

A change in pore water chemistry led to the precipitation of a non-ferroan dolomite cement. This was an aggressive phase which etched and embayed many of the framework grains and their authigenic overgrowths.

Burial of the sequence followed, but the presence of large amounts of smectite in the deposits indicates that the maximum depth of burial was not more than 2.5 km.

Inversion of the sediments at a later date, brought meteoric porewaters in contact with the deposits. This resulted in dissolution of the carbonate cement and hence the creation of secondary porosity. Precipitation of pore filling iron oxide and authigenic kaolinite (see Curtis. 1983) followed, reducing the porosity in places.

Weathering of the sequence led to the conversion of some of the iron oxide to goethite.

6.4 PALAEOMAGNETISM

6.4.1 Natural Remanent Magnetization (N.R.M.) Results

N.R.M. results for the Upper Buntsandstein of the Molina de Aragon area are shown in Table 6.2.

Mean initial intensities for the Rillo de Gallo samples were 1.4 mAm^{-1} for the Rio Arandilla sandstones, and 6.77 mAm^{-1} for the Rillo mudstones and sandstones. The Rio Arandilla samples had mean initial intensities of 0.99 mAm^{-1} and 5.25 mAm^{-1} for these units. The Torete mudstones and sandstones of the Hoz del Gallo section had a mean initial intensity of 13.74 mAm^{-1}.

Mean initial susceptibility values were 11.7 $mAm^{-1}nT^{-1}$ for the Rio Arandilla sandstones of Rillo de Gallo and 65.4 $mAm^{-1}nT^{-1}$ for those of the Rio Arandilla section. The Rillo mudstones and sandstones had a mean initial susceptibility value of 64.9 $mAm^{-1}nT^{-1}$ and 125.5 $mAm^{-1}nT^{-1}$ from these two sections respectively. Initial susceptibilities for the uppermost unit were not measured.

Mean initial directions for each of the Upper Buntsandstein samples are shown in Fig. 6.5. Like the Lower Buntsandstein samples there is a grouping of directions both, before and after correction for bedding, close to the present-day geomagnetic field position. There is also a diffuse streaking of directions towards the north and southeast portions of the stereograms. All Upper Buntsandstein directions are positive.

Within sample scatter is variable $\alpha 95$ values are high in Rio Arandilla sandstones (mean $\alpha_{95}=31.3°$). Lower in the Rillo mudstones and sandstones (mean $\alpha_{95} = 12.1°$) and the lowest in the Torete mudstones and sandstones (mean $\alpha_{95} = 4.8°$).

6.4.2 Isothermal Remanent Magnetization (I.R.M.) Results

I.R.M. curves have been drawn for five of the Upper Buntsandstein samples (Fig. 6.6).

TABLE 6.2 N.R.M. RESULTS FOR THE UPPER BUNTSANDSTEIN

Sample	Height (m)	F Dec(°)	F Inc(°)	P Dec(°)	P Inc(°)	Pole Long(°)	Pole Lat(°)	N	R	α95(°)	α95(°) Pole	Intensity (mAm^{-1})	Susceptibility ($mAm^{-1}nT^{-1}$)
MA60	224	82.6	39.3	86.8	45.9	65.8	18.6	3	2.79	42.1	48.4	0.12	1.72
MA60I	230	357.4	20.5	354.7	25.2	182.5	65.5	3	2.55	67.4	56.7	0.09	1.72
MA61	230	267.7	82.7	248.1	75.6	328.0	34.4	5	4.26	36.2	59.3	0.30	1.96
MA62	235	350.3	56.7	338.4	60.0	275.4	73.7	7	6.99	1.7	2.3	11.60	9.09
MA63	236	188.8	38.4	192.4	32.2	345.3	-29.8	3	2.72	50.5	50.4	0.10	-
MA64	244	27.6	25.3	25.8	32.7	126.5	58.1	3	2.94	22.3	24.4	0.09	1.12
MA65	266	6.4	47.7	359.3	53.2	187.7	83.3	5	4.87	14.2	18.6	0.28	6.68
MA66	269	354.7	41.0	348.3	45.2	219.3	73.5	5	4.76	19.4	21.7	1.68	-
MA67	284	117.4	43.3	124.9	45.9	44.3	-4.5	2	1.59	-	-	1.20	-
MA68	290	89.8	45.4	96.0	51.3	58.0	18.4	4	3.41	45.2	56.9	1.12	1.11
MA69	299	9.9	51.5	2.2	57.3	158.2	88.1	6	5.81	13.3	17.3	1.53	80.96
MA70	310	338.1	36.7	332.1	38.8	237.3	63.3	5	4.02	43.2	46.5	0.09	1.11
MA71	319	1.1	53.6	351.6	58.4	255.2	83.3	6	5.99	1.8	2.3	39.44	-
MA73	326	346.3	59.2	333.9	61.9	283.7	69.9	6	5.99	3.0	4.4	0.48	6.60
MA74	337	349.4	46.1	341.4	49.6	239.0	71.8	7	6.97	4.6	5.5	3.56	1.77
MA75	345	350.5	42.6	336.4	49.4	247.1	68.3	6	5.95	6.0	6.5	3.00	10.65
MA76	354	262.2	66.7	254.6	59.7	309.5	17.5	3	2.63	41.1	59.4	0.04	-
MA77	368	353.7	17.1	348.8	25.5	200.7	60.9	6	5.97	5.1	4.7	3.43	-
MA78	372	356.8	43.2	343.0	51.5	241.8	74.0	3	2.99	10.1	10.0	1.00	-
MA79	392	51.4	63.7	56.8	78.6	22.7	47.8	6	5.67	17.7	29.9	0.11	19.30
MA80	397	348.2	38.8	336.2	49.0	246.1	67.8	5	4.99	2.8	3.4	16.22	-
MA81	403	138.6	57.5	158.7	50.4	16.9	-15.3	4	3.99	3.1	3.6	8.48	118.46
MA82	406	154.2	72.7	181.2	61.1	356.1	-1.4	5	4.61	25.2	30.1	14.96	109.05
MA83	411	14.7	71.1	320.2	83.0	344.4	50.5	6	5.98	4.3	8.1	13.73	-
MA84	418	1.2	53.3	328.4	64.5	292.4	66.6	6	4.99	3.2	4.8	15.64	62.10
MA85	425	353.2	57.9	327.4	67.2	301.2	65.8	6	5.99	3.6	5.7	2.50	44.18
MA86	432	347.0	51.1	327.0	59.5	278.1	65.2	7	6.98	3.8	5.1	9.09	151.72
MA87	437	354.1	13.8	350.2	25.4	198.2	61.2	7	6.96	4.7	3.7	5.81	169.90
MA90	452	181.1	45.3	190.0	40.8	249.1	-23.5	6	5.53	21.6	20.8	0.31	-
MA91	461	2.1	40.8	351.6	53.6	245.4	84.9	5	4.22	37.3	43.1	0.26	-
MA92	474	263.9	77.0	237.9	63.6	326.5	13.3	4	3.59	36.4	41.9	0.12	-
MA93	548	342.6	49.9	323.1	57.2	274.3	61.9	4	3.97	8.5	11.4	6.93	-
MA94	549	354.9	43.7	346.9	54.8	244.2	78.3	5	4.99	3.5	4.8	10.16	-
MA95	553	359.9	49.4	347.7	60.6	277.0	80.7	6	5.99	2.5	3.4	23.00	-
RA1	467	348.9	20.6	346.9	13.6	190.9	6.6	5	4.90	12.4	13.6	1.38	101.54
RA2	502	0.7	7.3	0.1	1.4	177.8	49.9	6	5.99	3.3	4.0	1.59	79.84
RA3	513	172.5	83.6	266.3	82.7	339.0	34.0	6	4.75	38.3	45.3	0.66	12.60
RA4	517	86.5	50.3	76.9	57.3	62.4	33.5	6	5.81	13.3	12.8	0.31	67.54
RA5	559	118.1	6.1	117.7	15.9	59.9	-8.2	7	6.59	16.4	17.1	1.51	75.40
RA6	575	159.9	19.8	162.6	28.2	14.9	-14.9	4	3.96	10.5	9.9	2.50	65.48
RA7	593	351.9	40.8	346.7	33.5	208.7	64.7	8	7.97	3.2	2.6	9.30	140.66
RA8	635	12.7	5.1	13.1	2.9	158.8	46.0	8	7.91	6.3	7.1	2.80	104.35
RA9	643	315.9	73.6	302.7	69.5	312.0	47.2	5	4.33	34.0	36.5	1.78	245.38
RA10	644	349.0	53.5	341.1	52.8	247.3	73.3	8	7.98	2.9	2.8	13.61	120.31

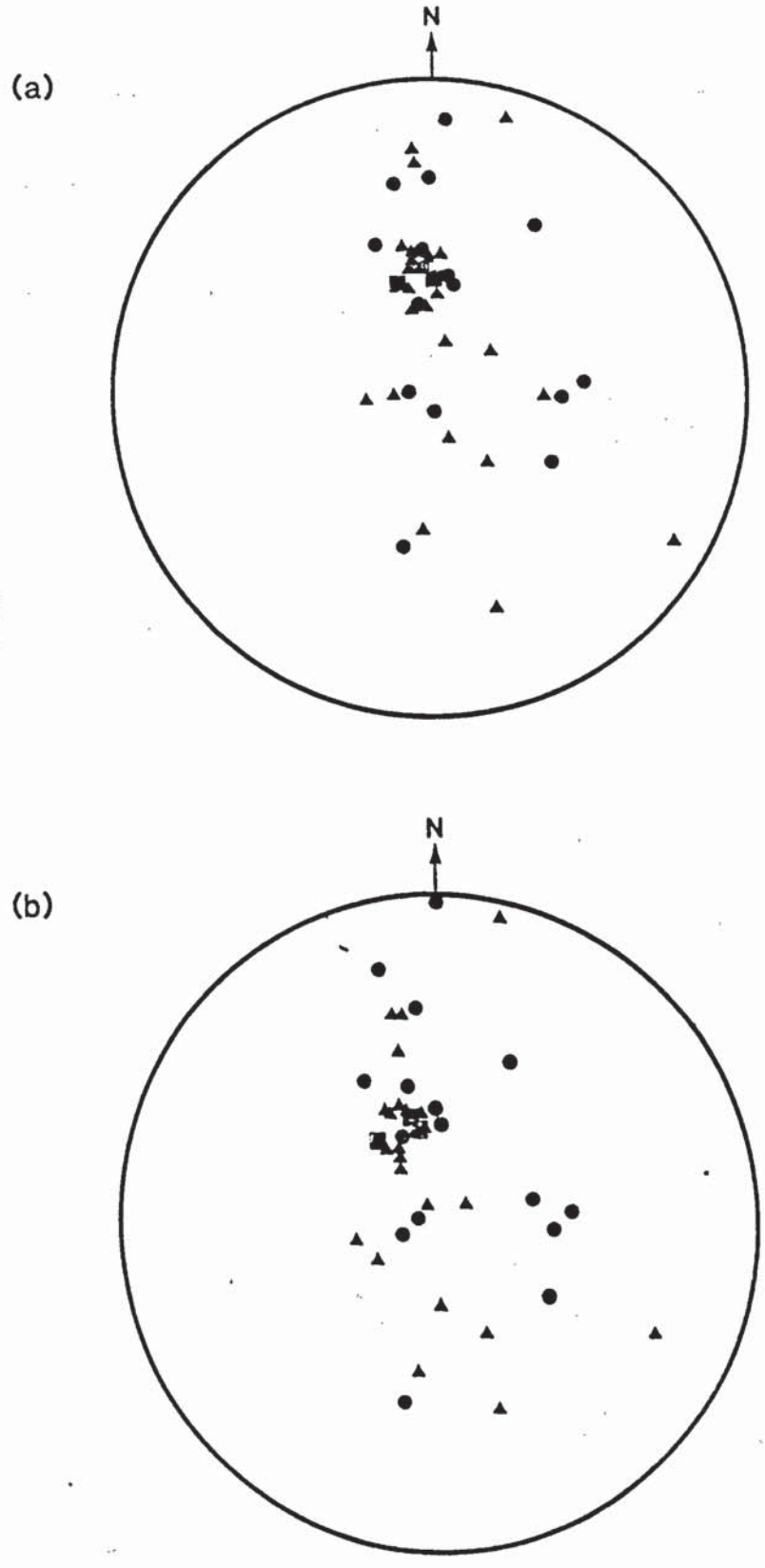

Fig. 6.5 Initial mean N.R.M. directions for samples from the Upper Buntsandstein (a) before and (b) after correction for bedding. For key to symbols see Fig. 6.2.

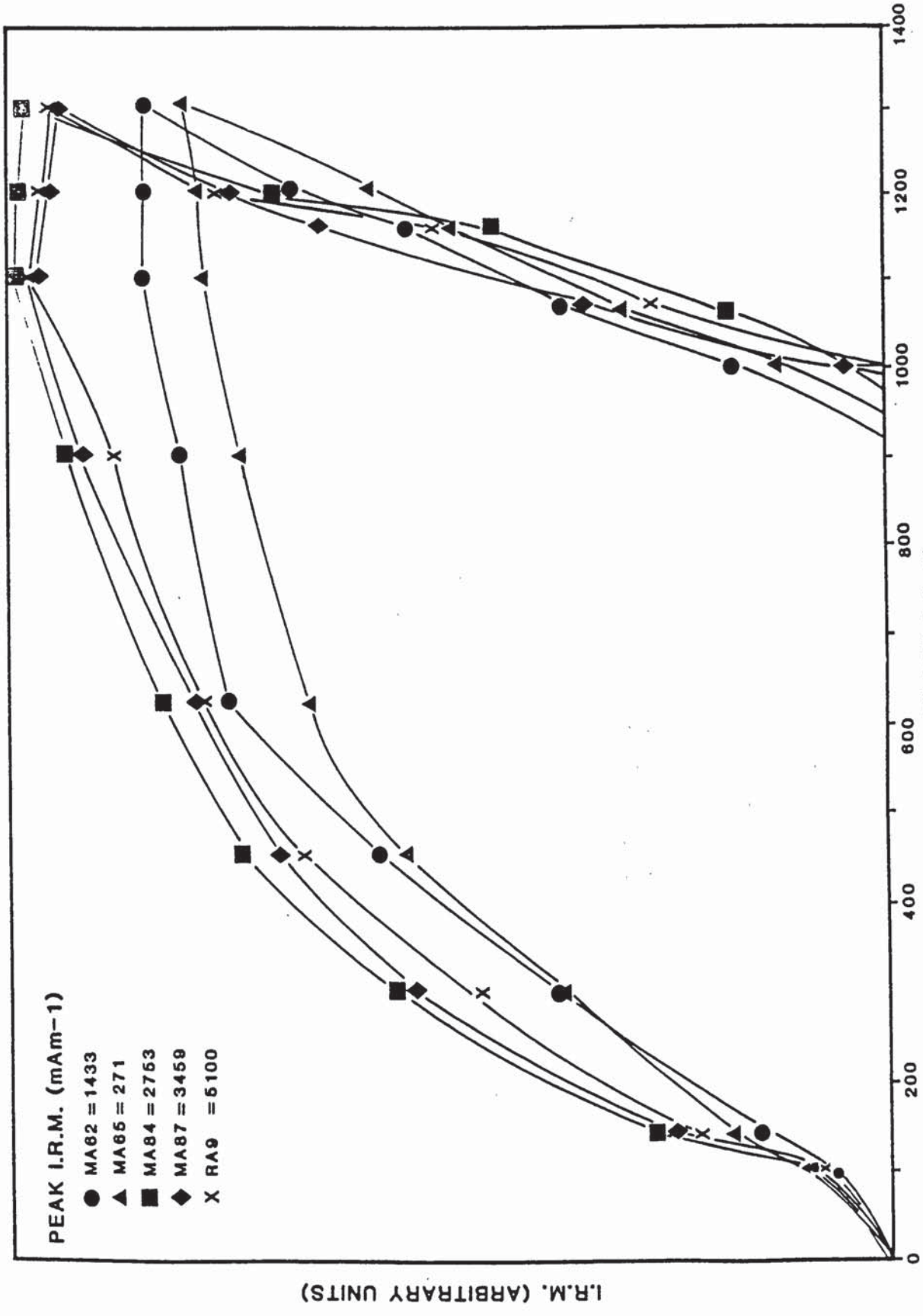

Fig. 6.6 I.R.M. acquisition and reverse field curves for samples from the Upper Buntsandstein.

Results are generally similar for all the samples, except for their Peak I.R.M. intensities. The two samples from the Rio Arandilla sandstones (MA62 and MA65) have maximum intensities considerably lower than those from the overlying unit.

The samples show a fairly rapid acquisition of remanence between 100°C and 300°C. The two samples from the Rio Arandilla sandstones show a more gradual rise in intensity. By 600 mT, all the samples show intensities which exceed 80% of their maximum value. Between applied field values of 600 mT up to 1300mT the curves have a much flatter appearance and the Rillo mudstones and sandstone samples seem to have reached full saturation. Rio Arandilla sandstone samples, however, do not show full saturation. Reverse field demagnetization curves are, in all cases, steep. The intensity falls to zero after back fields of 300mT - 400mT are applied.

The above results suggest the presence of a high coercivity mineral in the Rio Arandilla sandstones, this is probably haematite since it does not saturate even at high field strengths. The flattening of the curves does suggest that full saturation is being approached and thus, a second, low coercivity mineral, such as iron hydroxide, magnetite or poorly crystalline haematite, is also present in these samples.

The more rapid acquisition of magnetic remanence at low field strengths together with the suggestion of full saturation at applied fields of greater than 1100 mT suggests that a low coercivity mineral is the predominant remanence carrier in the Rillo mudstones and sandstones. Petrographic studies discounts the presence of magnetite in the deposits so it is likely that this remanence rests with poorly crystalline haematite or an iron hydroxide such as goethite.

6.4.3 Thermal Demagnetization Results

6.4.3.1 Intensity and Susceptibility Changes

The normalized intensity and susceptibility versus temperature plots are shown for the Upper Buntsandstein specimens in Fig. 6.7.

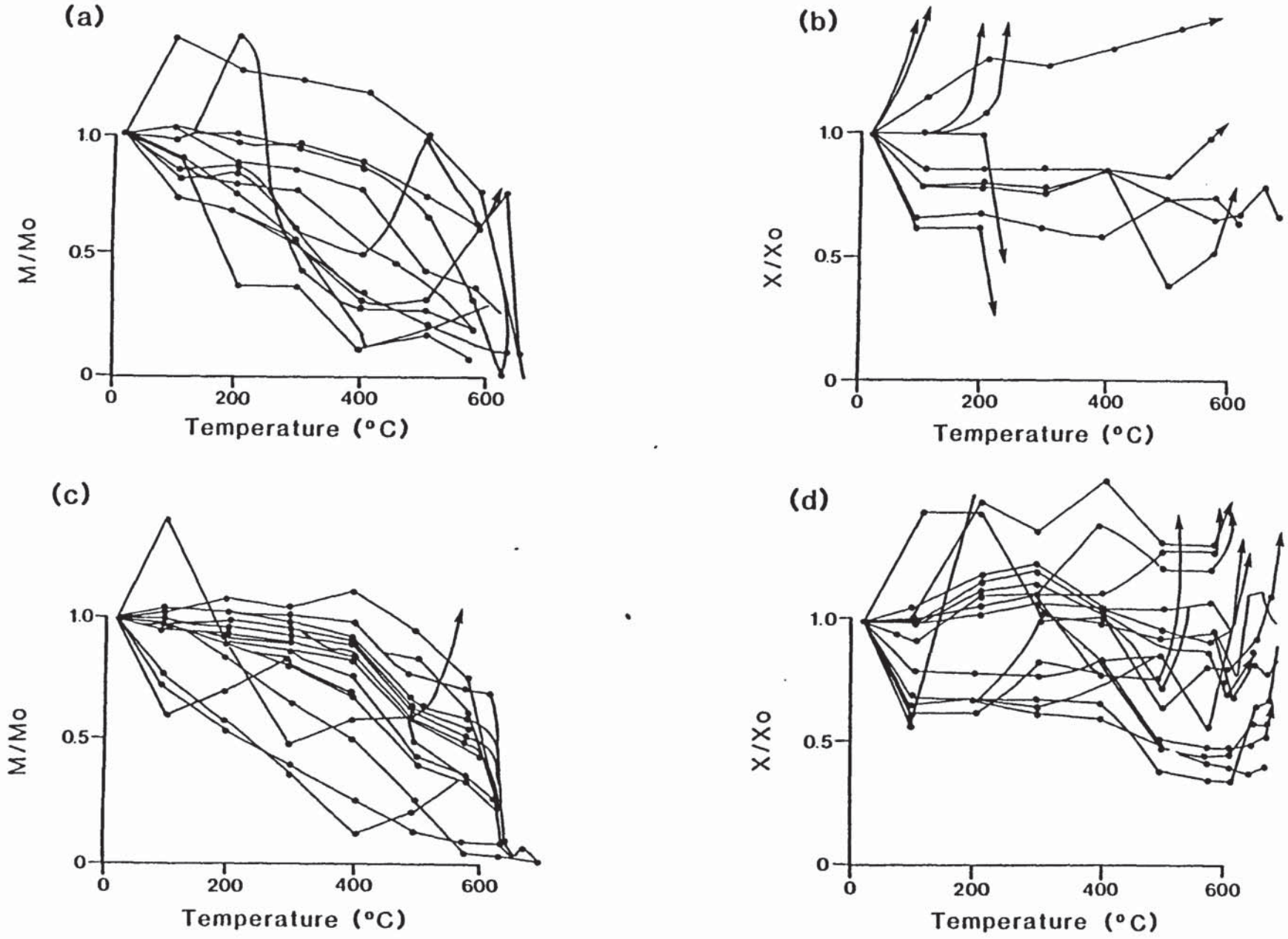

Fig. 6.7 Normalized intensity (a) and susceptibility (b) curves for specimens from the Rio Arandilla sandstones and normalized intensity (c) and susceptibility (d) curves for specimens from the Rillo mudstones and sandstones and Torette mudstones and sandstones.

The intensity decay curves for the majority of specimens from the Rio Arandilla sandstones (Fig. 6.7a) show a gradual removal of magnetic remanence, reaching zero intensity at temperature of between 600°C and 630°C. Although there are exceptions, the curves fall into two main groups. The first group contains decay curves which show an almost linear drop in intensity with increasing temperature e.g. MA61.1.1 and MA65.2.1. The second group of curves have a more convex appearance, with a relatively small intensity loss at lower temperatures, followed by a rapid remanence loss at temperatures above 600°C e.g. MA62.1.2 and RA1.3.1. Normalized susceptibility curves for the Rio Arandilla sandstones (Fig. 6.7b) demonstrate a variety of behaviour. The four specimens from the Rio Arandilla section show an initial drop in susceptibility to between 60% and 80% of the original value after heating to 100°C. Between temperature of 100°C and 400°C very little change in susceptibility is recorded. Between 400°C and 600°C susceptibility values for three of the specimens remain virtually unchanged. Only RA3.1.1 shows a drop in intensity between 400°C and 500°C followed by a sharp rise at temperatures above this value.

The remaining specimens show either a sharp increase in susceptibility upon heating to temperatures of 100°C or 200°C e.g. MA62.1.2, MA65.2.1 or a drop to negative susceptibility values after heating to 300°C (MA60.1.1, MA70.3.2).

The normalized intensity curves for the two upper units (Fig. 6.7c) show close accord. The majority of specimens demonstrate only minor loss in intensity upon 400°C (70%-90% of the original remanence still remains). A small drop in intensity is shown by the specimens between 400°C and 500°C but 50%-60% of their intensity of remanence still remains at 580°C. A very sharp drop in intensity to almost zero occurs upon heating the samples to 630°C or 660°C reflects a blocking temperature probably within range 620°C to 650°C.

Susceptibility decay curves are also fairly consistent for the Rillo and Torete mudstones and sandstones unit (Fig. 6.7d).

Specimens from the Rio Arandilla section all show an initial drop in susceptibility to about 70%-80% of their original values. This is not

demonstrated by the specimens from the Rillo de Gallo and Hoz del Gallo sections. The majority of specimens show fairly stable susceptibility values up to 580°C but at temperatures above 580°C a sharp increase in susceptibility is demonstrated.

6.4.3.2 Discussion of Intensity and Susceptibility Results

Upper Buntsandstein intensity and susceptibility decay curves fall into two main groups. The first is similar to that shown by the majority of Lower Buntsandstein (section 5.4.3.1) specimens. These have curves which show an absence of low blocking temperatures and have a maximum blocking temperature at about 630°C. Susceptibility curves which accompany these intensity changes show little change up to 580°C, but above this temperature a sharp rise in susceptibility is shown by most specimens. Specimens from the Rio Arandilla section, however, show an initial drop in susceptibility upon heating to 100°C but those from the other two sections do not.

These results suggest that specimens in this group contain one major component of magnetization which has a blocking temperature in excess of 600°C and thus must be carried by haematite.

The second group comprises specimens which show a steady loss in intensity between room temperature and about 630°C. These have a broad blocking temperature spectrum which suggests that the remanence lies with more than one magnetic mineral or with one mineral which exists in a variety of textural habits and grain sizes.

6.4.3.3 Directional Changes

The Upper Buntsandstein specimens show directional behaviour similar to that shown by the Lower Buntsandstein.

Four characteristic types of demagnetization behaviour have been identified for these specimens.

(A) A lower blocking temperature component lying near the local geomagnetic field direction which is superimposed on a higher blocking temperature with north-northwest or south-southeast declinations and shallow inclinations determining components of magnetization which have gone unrecorded using the more common thermal demagnetization technique.

(B) Magnetizations comprising a stable component (0-630°C) in the local geomagnetic direction superimposed on a weak, shallow component which cannot be precisely defined.

(C) Magnetizations having a stable component in the local geomagnetic direction superimposed on a weaker, higher temperature component with northeast or southwest declinations and fairly shallow inclinations.

(D) Magnetizations comprising only a steep component near the local geomagnetic direction and in which no remanent of original magnetization can be identified.

Types A and B are the same as those in the lower parts of the Buntsandstein. Types C and D are limited to specimens from the Upper Buntsandstein.

Type A: 20% Upper Buntsandstein specimens have magnetizations of this type. Examples of 'Type A' magnetization are common in the upper part of the Rillo mudstones and sandstones e.g. MA88.3.1. Fig. 6.8 shows the behaviour of this specimen during partial thermal demagnetization. The initial direction (Fig. 6.8a) is steep (near vertical) and has a northnorth-west declination deduced only from the orthogonal vector plot, Fig. 6.8b. The removal of this low temperature component is associated with a blocking temperature at 100°C (Fig. 6.8c). This is followed by a slight but steady rise in the normalized intensity decay. At 400°C (the peak on the normalized intensity curve) the directional movement ceases and there is little or no change up to 660°C. This stable component has D=136.5, I=-4. Other specimens have high temperature components in the northwest quadrant e.g. MA77.1.1 which are almost antiparallel to the component isolated in MA88.3.1.

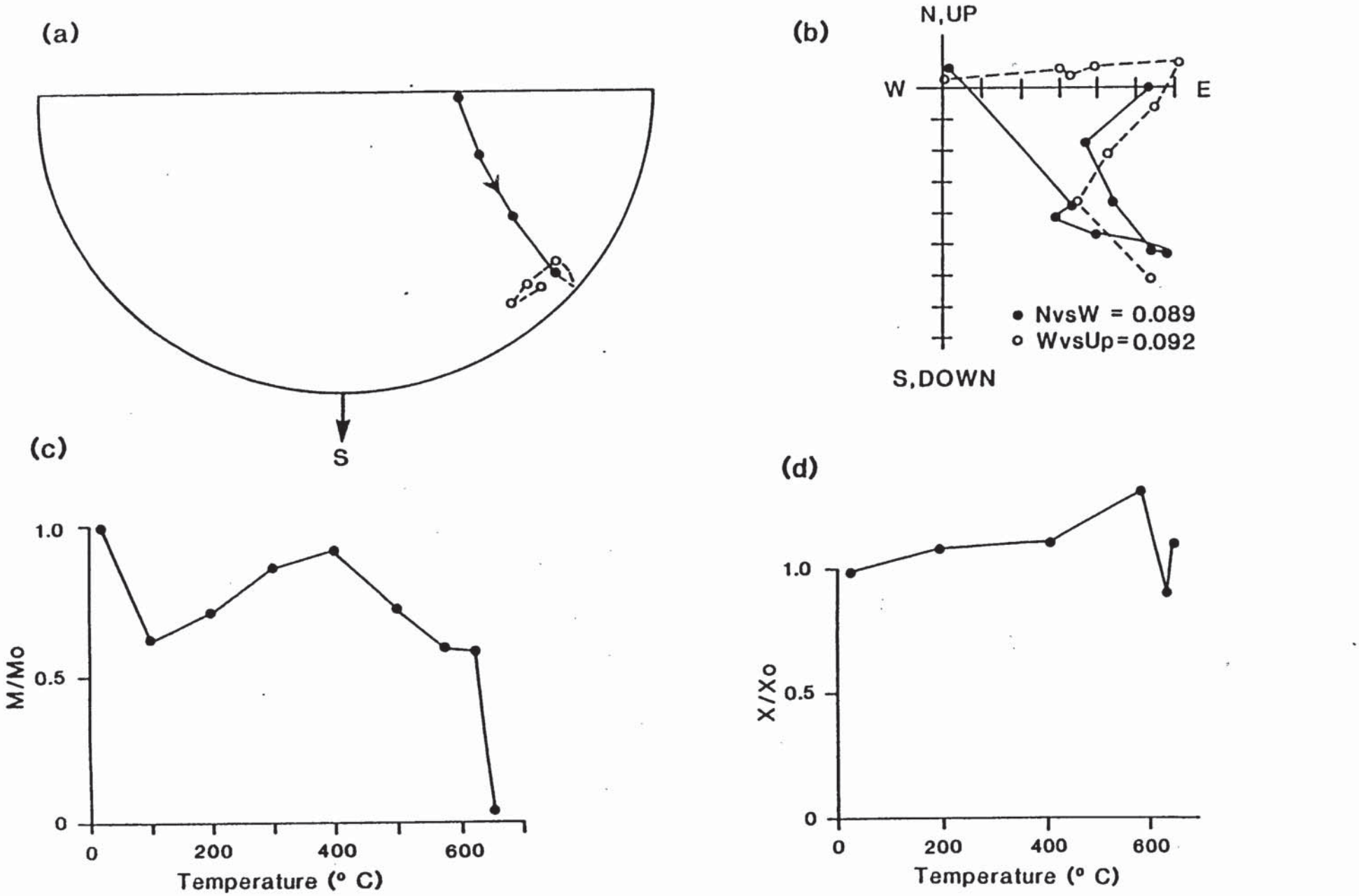

Fig. 6.8 Palaeomagnetic behaviour demonstrated by MA88.3.1 during partial thermal demagnetization. (a) Stereographic projection, (b) Orthogonal vector plot, (c) Normalized intensity decay curve, (d) Normalized susceptibility decay curve

Type B: As in the Lower Buntsandstein, Type B magnetizations consist of one predominant component of magnetization, lying near to the present-day field direction for the area, superimposed on a weaker shallow direction in the northwest or southeast quadrants. The majority of Upper Buntsandstein specimens have magnetizations of this type. Specimen MA61.1.1 is a good example showing this type of behaviour. The initial direction is steep and positive (Fig. 6.9a) and remains unchanged up to 400°C with D=347.8°, I=64.1°, α_{95}=4.5° after correction for bedding. At 400°C about 35% of the original intensity remains. On heating to higher temperatures the direction moves to a shallow position in the northwestern part of the stereonet. Other specimens show movement at high temperatures towards the southeast quadrant.

Type C: The third type of directional behaviour shown by the Upper Buntsandstein specimens is well demonstrated by MA85.5.1 and MA86.2.2. (Fig. 6.10). This type of demagnetization behaviour is very similar to Type B except that the weak high temperature component lies in the northeast or southwest quadrants. Both MA85.5.1 and MA86.2.2 have an initial steep positive direction lying close to the present-day local geomagnetic field direction (Fig. 6.10). This direction remains virtually unchanged up to 500°C in MA85.5.1 and 580°C in MA86.2.2, at which point 50% of the remanence still remains. At higher temperatures, specimen MA85.5.1 shows a change in direction towards a shallower inclination in the southwest quadrant. The both specimens show maximum blocking temperatures excess of 600°C indicating this this high temperature component is carried by haematite.

Type D: The final type of behaviour demonstrated by the specimens is similar to Types B and C but differs in that directional movement is very slight and there is no positive evidence of any original remanence. An example of this type of behaviour is shown in Fig. 6.11 (RA10.1.1). Again the initial direction is near to the local geomagnetic field direction (Fig. 6.10a) but this time there is no change in direction during the thermal demagnetization procedure. The most stable direction occurs over the temperature range 500°C-675°C and has a D=350.9°, I=55.2° in the field position and D=342.3°, I=54.6° in the palaeoposition (SI=18.6 and α_{95}=0.9. The intensity decay plot (Fig. 6.11b) shows only a small drop in intensity

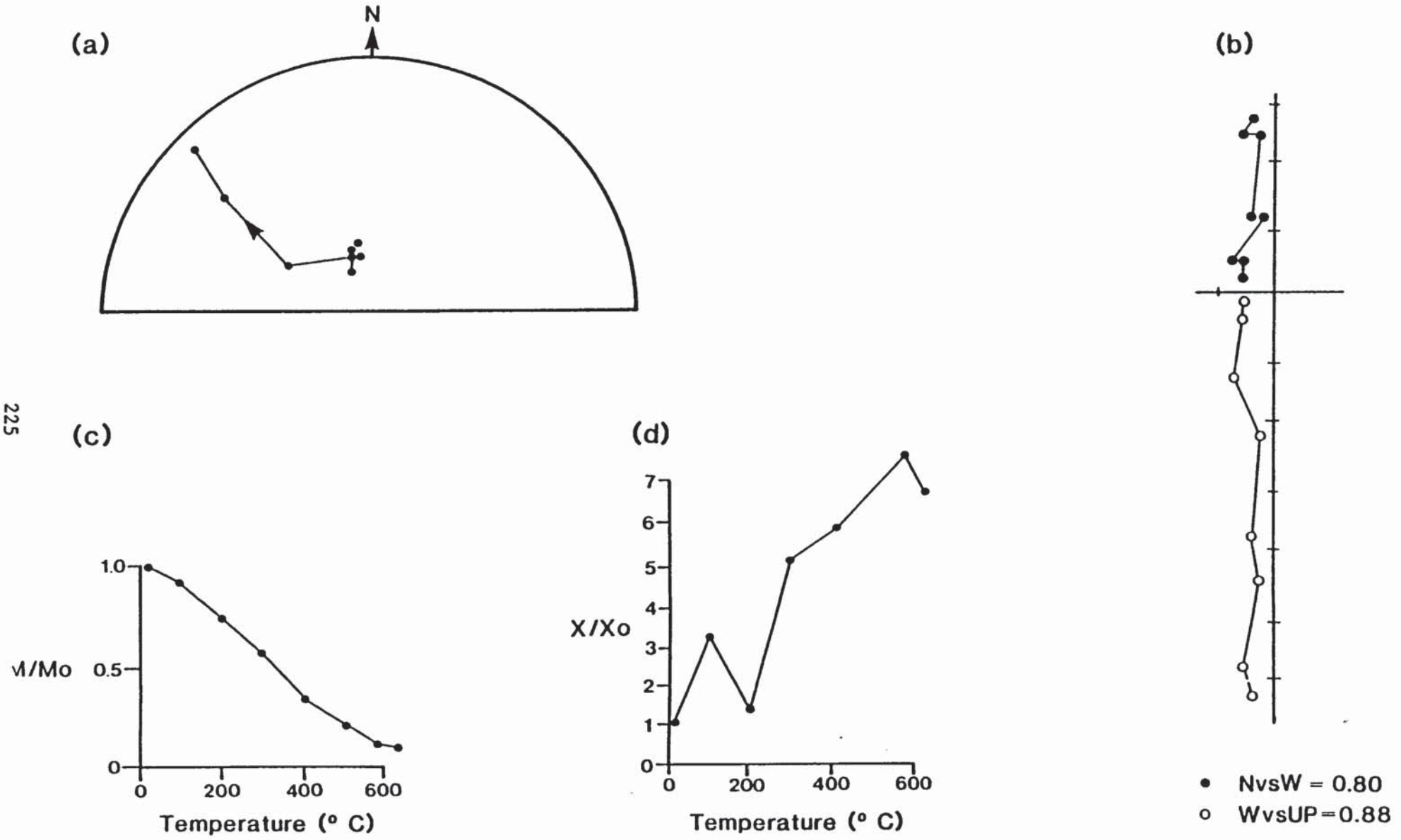

Fig. 6.9 Palaeomagnetic behaviour demonstrated by MA61.1.1 during partial thermal demagnetization. (a) Stereographic projection, (b) Orthogonal vector plot, (c) Normalized intensity decay curve, (d) Normalized susceptibility decay curve.

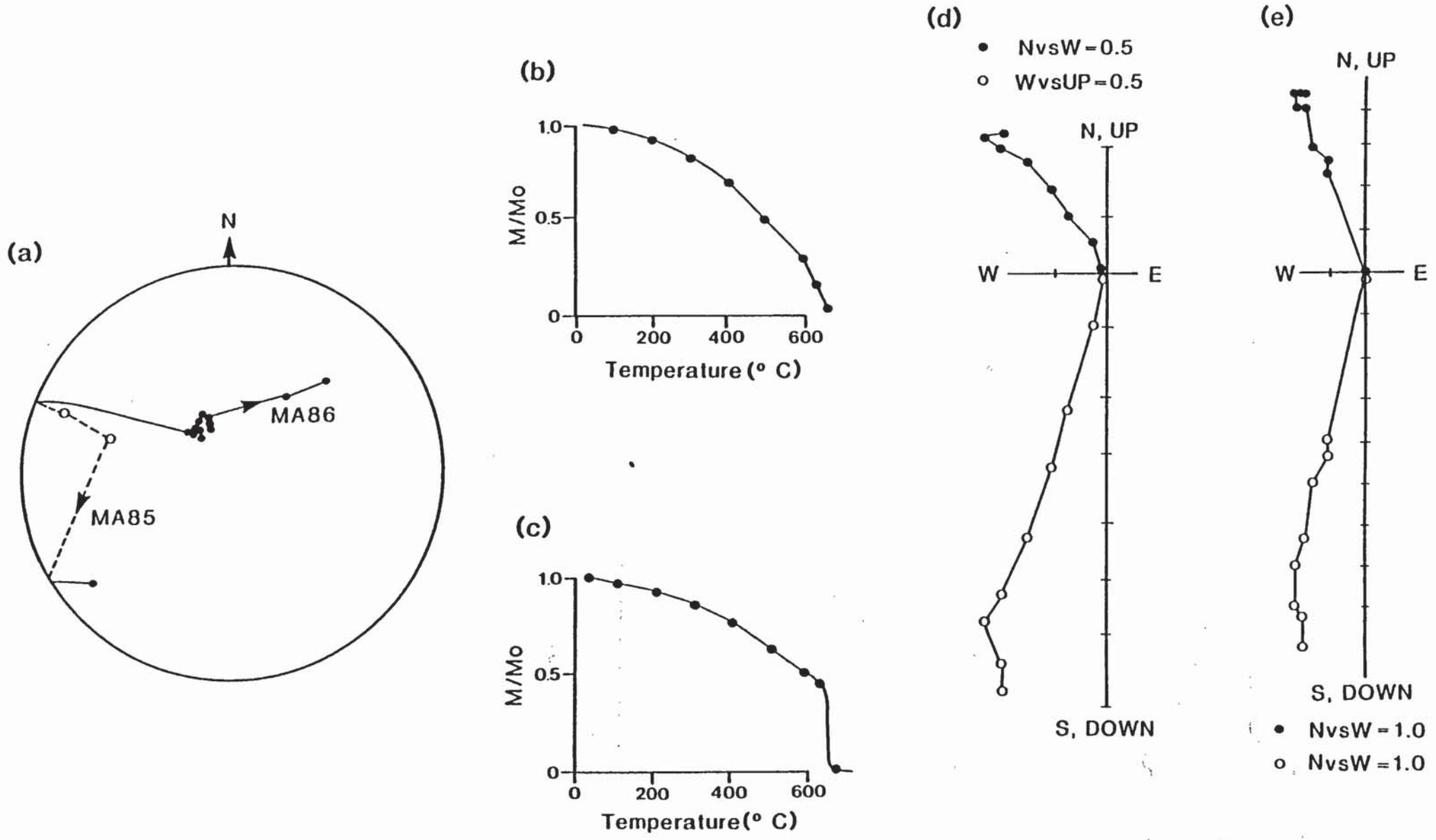

Fig. 6.10 Palaeomagnetic behaviour demonstrated by MA85.5.1 (a), (b) and (d) and 86.2.2 (a), (c) and (e) during partial thermal demagnetization. (a) Stereographic projection, (b) and (c) Normalized intensity decay curves and (d) and (e) Orthogonal vector plots.

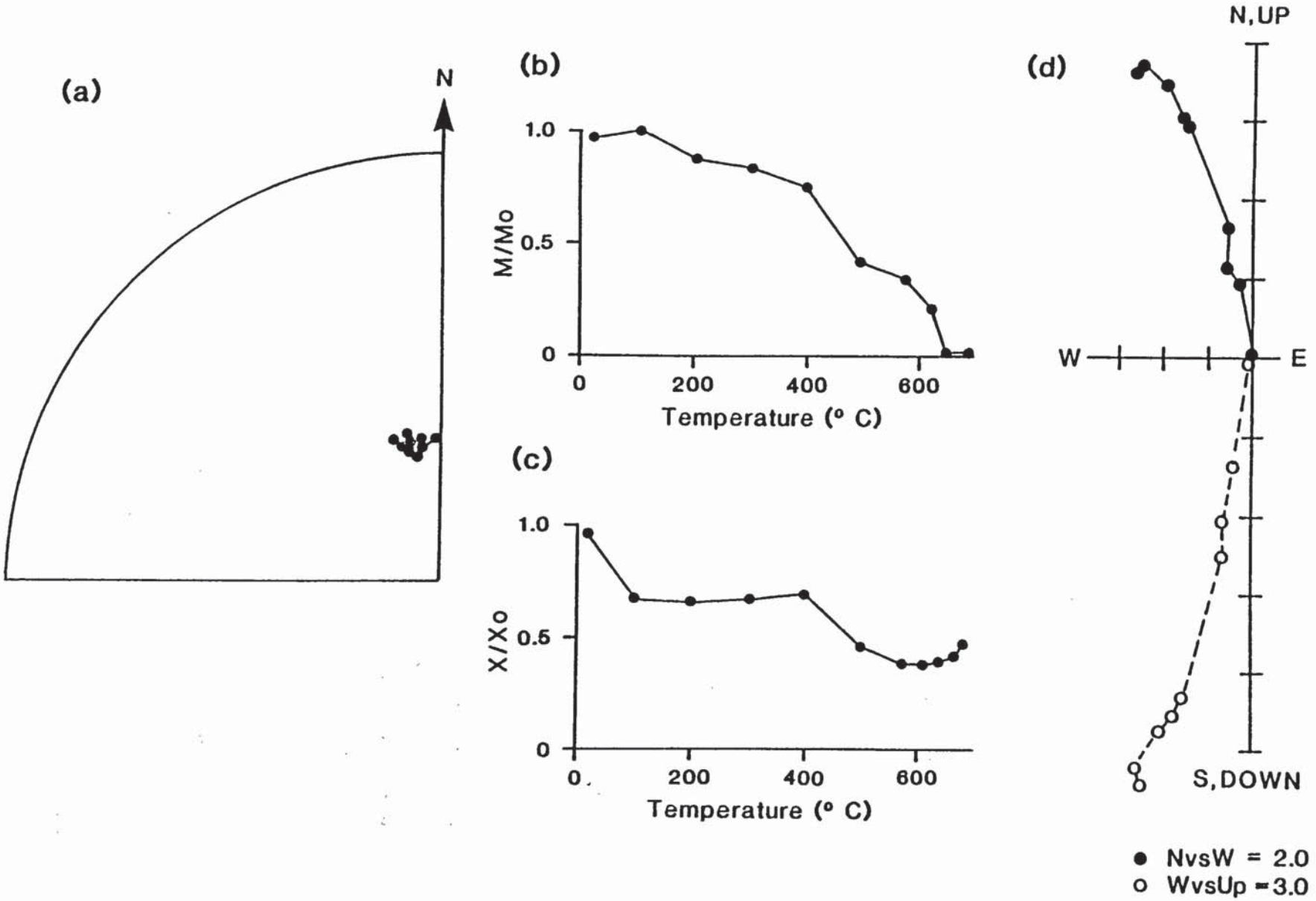

Fig. 6.11 Palaeomagnetic behaviour demonstrated by RA10.1.1 during partial thermal demagnetization. (a) Stereographic projection, (b) Normalized intensity decay curve, (c) Normalized susceptibility decay curve, (d) Orthogonal vector plot.

at lower temperatures and a maximum blocking temperature between 630°C and 660°C.

6.4.3.4 Thermal Demagnetization Summary

The four main types of behaviour shown by the Upper Buntsandstein specimens are interpreted below.

Type A: The low temperature component has a direction close to that of the present-day local geomagnetic field and is probably carried by a low coercivity mineral having a low blocking temperature. This component was acquired during the present normal event i.e. the Brunhes epoch, which began approximately 700,000 years ago.

Superimposed on this recent component is a shallow component which has a declination lying in the northwest or southeast quadrants interpreted as a Triassic normal and Triassic reversed component respectively. This Triassic component has a distinct blocking temperature at 630°C which suggests that this is carried by crystalline haematite.

Type B: The interpretation of this type of magnetic behaviour is similar to that of the previous type except that the recent steep component is stable to higher temperatures and only a fragment of the original remanence is retained. Whilst magnetizations of this type are unsuitable for precise palaeomagnetic determinations, they may be used to establish the magnetic polarity of the Triassic sequence.

Type C: The steep, positive component close to the present-day earths field is thought to be of similar origin to that seen in Types A and B. The higher temperature, weaker component which lies either in the northeast or southwest quadrant is more difficult to explain. It may represent a Triassic direction of intermediate or mixed polarity, acquired during a polar reversal.

Type D: The single directional component shown by specimens with magnetizations of this type is interpreted as being the result of complete remagnetization. The fact that the directions are closely grouped near the local geomagnetic field and exclusively of the same polarity strongly suggests that the remagnetization occurred in Holocene times during the Brunhes epoch.

The results of stepwise, thermal demagnetization of the Upper Buntsandstein specimens are shown in Table 6.3. The most stable directions isolated during the demagnetization procedure are also shown in Fig. 6.12. The directions show a strong grouping close to the present day local geomagnetic field direction, both by one and after correction for bedding. The majority of these directions were isolated over the temperature range of 20°C-200°C or 20°-300°C. It is notable that stabilities are very high and α95 values very small for most of these specimens.

A streaking of directions towards the north-northwest and southeast parts of the stereogram is also seen. These directions are less stable than the previously described group and have large α_{95} values. They were also isolated at higher temperatures. These directions represent components of magnetization acquired during the Triassic.

Fig. 6.13 shows the directions of magnetization which pass the 10° linearity test. They show a greater amount of scatter than the most stable directions but show essentially similar results.

6.4.3.5 Bulk Demagnetization Results

The results of bulk demagnetization of the Upper Buntsandstein samples are shown in Table 6.4. Bulk demagnetization directions are also shown in

Fig. 6.14. Samples from the Rio Arandilla sandstones were demagnetized at temperatures ranging from 300°C up to 675°C. Those from the Rillo mudstones and sandstones and Torete mudstones and sandstones were demagnetized at temperatures of between 400°C and 675°C (the majority at 630°C). Mean intensities for the three units after demagnetization were 0.53 mAm^{-1} for the Rio Arandilla sandstones, 0.47 mAm^{-1} for the Rillo mudstones and sandstones and 3.45 mAm^{-1} for the Torete mudstones and sandstones (although in the last unit only one sample (MA94) was measured).

Directions show a great deal of scatter, except for a small grouping of directions close to the local present-day geomagnetic field direction. These directions also have the lowest α_{95} values. The remaining directions tend to have fairly shallow inclinations but declination which lie in all four quadrants of the stereogram. The majority of these directions have α_{95} values which are greater than 20°.

TABLE 6.3 STEPWISE THERMAL AND CHEMICAL (C) DEMAGNETIZATION RESULTS FOR THE UPPER BUNTSANDSTEIN

		Most stable directions				Pole						Directions passing 10° linearity test				
		F		P									F		P	
Specimen	S.I.	Dec(°)	Inc(°)	Dec(°)	Inc(°)	Long(°)	Lat(°)	N	R	α95(°)	Range (°C)	Range(°C)	Dec(°)	Inc(°)	Dec(°)	Inc(°)
MA60.1.1	11.2	125.5	59.4	139.2	60.4	0.2	27.4	3	2.96	17.6	20-200	100-300	125.1	30.2	129.8	31.9
MA61.1.1	4.1	0.2	59.6	347.8	64.1	301.6	79.8	5	4.98	4.5	20-400	500-630	326.6	74.1	299.3	73.1
MA62.1.2	24.1	346.2	58.1	333.2	60.0	277.0	69.8	4	3.99	0.8	20-300	200-630	345.6	57.5	330.0	60.1
MA63.1.1	1.0	187.0	31.7	189.9	25.7	346.3	-34.8	3	2.93	24.3	20-245	245-415	183.2	22.5	185.3	16.9
												20-245	32.8	-37.7	34.3	-30.0
MA64.6.1	1.0	14.1	19.9	12.1	26.3	153.3	61.0	3	2.94	20.6	20-200	None				
MA65.2.1	4.1	339.1	562.3	27.1	58.0	273.9	64.7	3	2.99	5.0	20-200	580-660	257.0	51.9	253.2	44.6
MA66.1.1	7.5	345.3	58.5	332.2	61.1	280.9	69.2	4	3.99	2.5	20-300	None				
MA67.2.1	1.7	120.0	16.4	122.4	18.9	58.4	-16.8	3	2.98	13.0	115-323	590-660	116.0	20.0	119.0	23.1
												20-245	301.3	8.0	308.5	5.4
MA68.1.1	2.6	59.0	61.0	62.1	68.9	50.8	47.2	3	2.99	7.8	20-200	200-400	25.8	70.6	11.0	77.5
MA69.3.1	18.9	19.9	51.9	13.5	58.6	92.1	79.6	5	4.99	1.0	100-500	500-630	18.3	51.8	11.7	58.3
												400-630	19.1	50.4	13.0	57.0
												100-300	17.4	49.2	11.3	55.7
MA70.3.2	3.1	17.4	78.7	334.0	83.8	349.4	51.7	3	2.99	7.0	100-300	200-400	90.5	79.3	138.3	83.1
MA71.2.1	13.9	2.4	49.7	345.3	54.7	218.2	82.8	7	6.99	1.1	245-660	675-690	2.0	53.1	352.6	58.0
												500-675	2.5	40.6	356.7	45.8
												115-323	237.4	61.9	235.9	54.
MA73.1.1	11.2	349.4	54.3	338.5	57.5	265.7	73.3	7	6.99	1.5	100-630	400-660	348.8	53.9	338.1	57.1
MA74.4.1	19.7	353.7	49.0	345.1	53.0	241.1	76.1	8	7.99	0.9	20-630	630-660	353.9	48.3	345.5	52.5
												400-660	352.2	49.0	343.4	52.8
MA75.3.2	1.0	338.8	34.2	333.4	36.4	233.7	59.4	4	3.93	14.5	500-600	None				
MA76.5.1	0.5	347.6	28.7	339.1	35.4	224.3	62.2	4	3.39	46.4	20-300	None				
MA77.1.1	22.0	353.7	60.7	325.6	67.6	301.9	64.4	3	2.99	1.0	400-600	400-660	353.4	60.8	325.1	67.6
MA78.1.1	15.0	348.0	46.7	331.6	52.6	258.3	66.2	3	2.99	1.4	120-300	400-600	316.8	77.0	268.7	70.2
MA79.4.1	2.8	3.6	38.9	352.6	48.8	208.6	77.4	3	2.99	7.8	100-300	200-400	12.3	29.3	5.8	41.6
												100-300	12.3	52.0	356.1	63.2
MA81.2.1	4.3	138.8	54.7	157.1	47.9	18.9	-17.0	3	3.0	5.0	100-300	660-690	235.2	18.9	234.0	4.1
												630-675	137.3	27.7	144.7	22.6
												400-630	138.8	74.3	175.2	64.8
												200-400	293.9	67.2	263.7	60.7
MA82.2.1	8.4	176.6	69.6	191.6	55.4	348.5	-12.4	4	3.99	2.3	200-500	630-690	173.8	59.9	185.6	46.5
MA83.2.1	24.2	1.3	50.2	332.6	62.0	284.3	69.7	3	2.99	0.8	20-200	400-690	2.1	49.6	334.3	61.7
												100-300	10.7	14.9	4.6	32.3
MA84.2.1	19.0	4.0	66.0	326.3	76.7	330.4	59.4	4	3.99	1.0	20-300	500-650	1.7	87.4	222.0	76.0
MA85.5.1	15.9	341.3	54.0	318.2	60.6	283.5	58.9	4	3.99	1.1	400-630	200.690	337.9	54.1	314.6	59.7
MA86.2.2	22.5	348.4	46.5	331.9	55.6	265.0	67.6	4	3.99	0.8	400-630	300-690	347.4	47.3	330.2	56.1
MA87.1.1	9.1	355.5	-1.6	354.7	10.6	187.2	54.1	3	2.99	1.9	500-630	630-690	356.8	-2.6	356.2	9.8
												500-660	355.6	-2.0	354.9	10.1
												100-300	153.8	62.7	174.0	52.7
												20-200	168.4	81.5	199.5	67.4
MA88.3.1	2.9	140.9	-2.0	139.8	-6.0	52.6	-37.7	3	2.99	6.1	500-630	500-690	140.9	-2.2	139.7	-6.1
												200-400	335.0	46.7	317.2	52.3
												100-300	340.9	30.1	331.5	38.2

CONTINUED

TABLE 6.3 STEPWISE THERMAL AND CHEMICAL (C) DEMAGNETIZATION RESULTS FOR THE UPPER BUNTSANDSTEIN (CONTINUED)

		Most stable directions				Pole						Directions passing 10° linearity test				
			F		P						Range		F		P	
Specimen	S.I.	Dec(°)	Inc(°)	Dec(°)	Inc(°)	Long(°)	Lat(°)	N	R	α95(°)	(°C)	Range(°C)	Dec(°)	Inc(°)	Dec(°)	Inc(°)
MA89.2.2	1.8	353.5	69.9	302.4	76.5	323.5	49.9	3	2.98	12.3	100-300	630-675	153.5	41.9	163.9	33.2
MA90.1.1	0.8	172.4	-2.0	171.9	-4.3	11.0	-50.6	6	5.46	19.9	120-600	None				
MA91.2.1	0.4	349.3	23.3	342.8	34.1	216.7	63.4	10	3.46	66.7	20-690	None				
MA92.2.1	0.6	299.5	64.0	271.9	58.3	298.6	25.5	5	4.40	32.0	20-400	300-500	139.7	45.1	153.4	39.4
MA93.1.1	-	242.0	66.0	232.0	51.0	-	-	-	-	-	-	-	-	-	-	-
MA94.5.1	-	355.0	48.0	345.0	59.0	-	-	-	-	-	-	-	-	-	-	-
MA95.5.1	-	2.0	51.0	350.0	63.0	-	-	-	-	-	-	-	-	-	-	-
RA1.3.1	4.7	340.3	10.1	339.8	1.8	208.8	46.0	5	4.99	3.9	200-580	300-660	342.3	7.4	34.2	-0.7
RA2.3.2	10.3	356.3	3.4	356.2	-3.0	183.5	47.5	3	2.99	2.1	300-500	400-580	355.4	2.0	355.6	-4.5
RA3.1.1	5.7	201.9	68.8	228.0	69.0	330.2	12.1	3	2.99	3.8	100-300	500-630	145.1	39.9	148.7	49.2
												200-580	275.3	50.9	280.3	42.1
RA4.1.2	3.1	76.1	49.6	65.4	55.4	71.1	39.7	5	4.97	6.1	100-500	500-630	96.5	72.2	68.6	79.7
												200-500	70.9	41.8	62.4	46.9
RA5.2.1	11.0	118.6	-12.1	118.8	-2.2	68.9	-22.1	3	2.99	1.9	400-580	400-660	121.8	-11.3	121.9	-1.3
RA6.4.1	7.5	166.7	15.0	168.9	22.5	11.4	-36.5	5	4.99	2.5	20-400	660-690	42.9	-18.0	45.9	-16.5
												580-660	180.0	13.2	182.4	18.9
												500-630	166.3	5.2	167.3	12.7
RA7.1.1	18.8	351.8	44.6	345.8	37.3	214.7	67.0	6	5.99	1.0	20-500	400-675	351.7	44.4	345.9	37.
												100-300	26.5	37.7	19.2	35.4
RA8.2.1	6.3	5.2	49.1	358.2	50.1	186.6	79.9	3	2.99	3.3	20-200	500-675	0.2	46.0	353.9	46.5
RA9.3.1	8.8	343.3	55.2	335.0	53.9	257.7	69.3	3	2.99	2.4	100-300	200-630	342.8	52.7	335.3	51.4
												100-300	347.4	49.4	340.6	48.6
RA10.1.1	18.6	350.9	55.2	342.3	54.6	251.2	75.0	3	2.99	0.9	500-630	200-675	343.3	54.4	335.5	53.1
CHEMICAL DEMAGNATIZATION RESULTS																
MA74.2.1	6.5	355.6	48.2	346.8	52.5	243.1	69.9	8	7.99	1.8	2-150 hrs	1-150 hrs	355.9	47.8	347.3	53.1
RA7.1.1	3.6	358.3	47.3	351.1	40.6	203.7	70.8	8	7.98	2.3	2-150 hrs	2-150 hrs	358.7	49.3	350.9	42.7

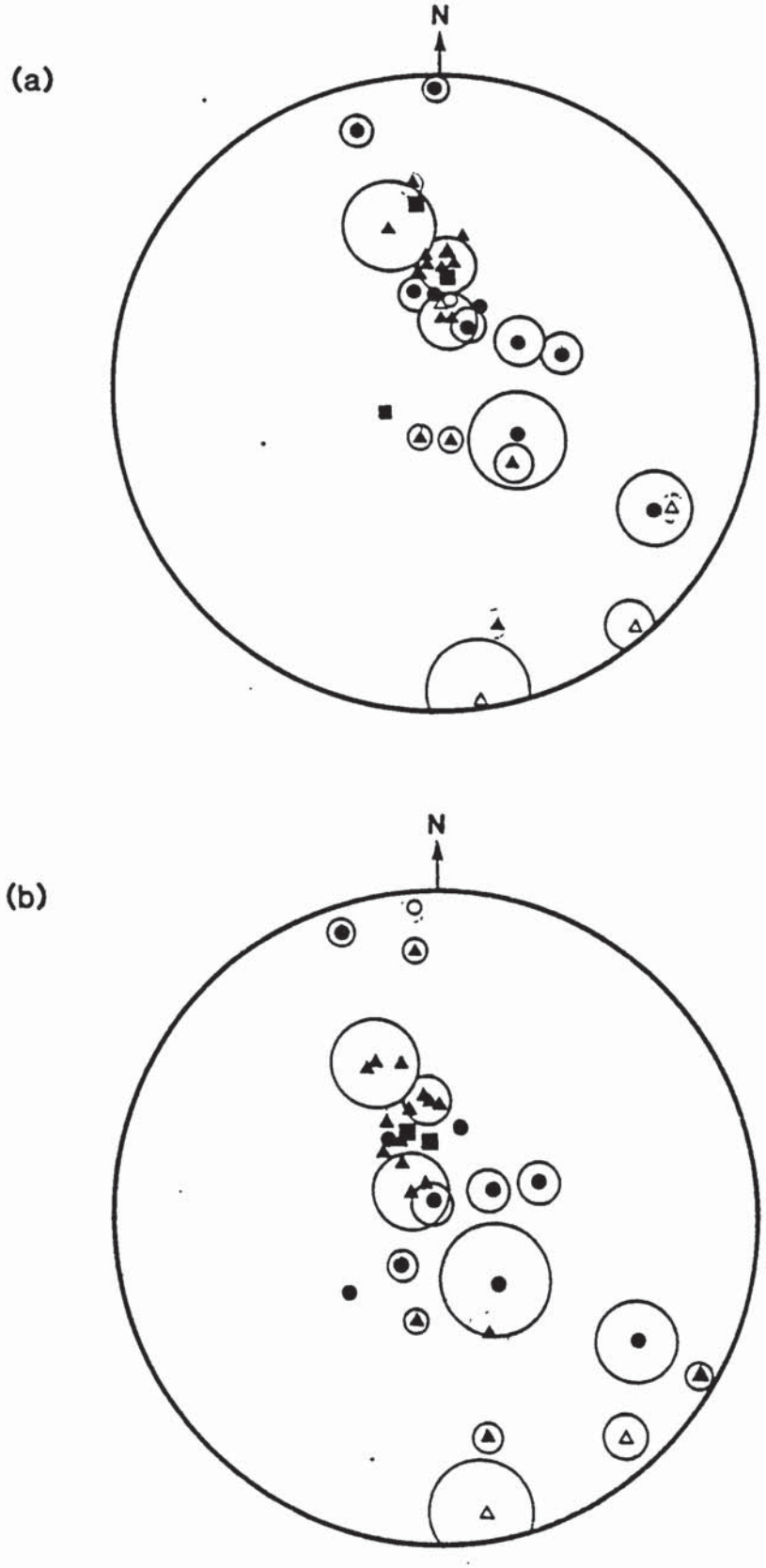

Fig. 6.12 Most stable directions isolated for Upper Buntsandstein samples (a) before and (b) after correction for bedding. For key to symbols see Fig. 6.2.

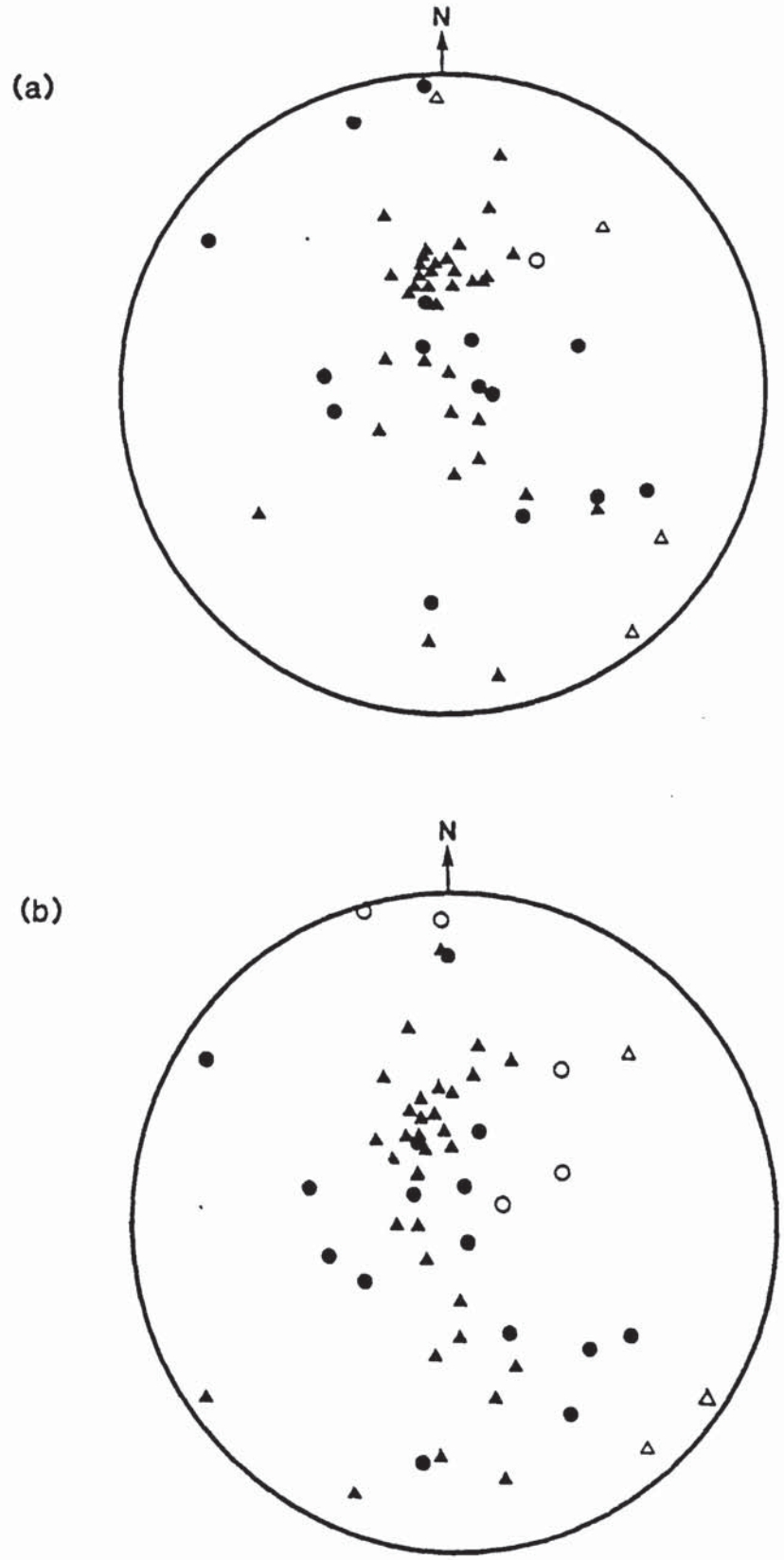

Fig. 6.13 Directions passing 10° linearity test for Upper Buntsandstein samples (a) before and (b) after correction for bedding. For key to symbols see Fig. 6.2.

TABLE 6.4 BULK DEMAGNETIZATION RESULTS FOR THE UPPER BUNTSANDSTEIN

Sample	Height (m)	F Dec(°)	F Inc(°)	P Dec(°)	P Inc(°)	Pole Long(°)	Pole Lat(°)	N	R	α95(°)	α95(°) Pole	Intensity (mAm^{-1})	Susceptibility ($mAm^{-1}nT^{-1}$)	Temp (°C)
MA1	12	313.2	8.8	310.5	12.4	244.0	34.0	5	4.84	15.2	13.5	0.07	4.40	400
MA2	18	6.3	57.3	3.4	70.2	6.7	76.3	3	2.99	7.3	12.4	0.04	-	60 mT
MA3	30	173.3	19.9	179.5	12.9	358.7	-42.6	1	1.00	-	-	0.09	14.36	600
MA4	50	329.3	39.2	315.4	46.3	266.4	55.6	6	5.39	24.8	22.9	0.17	-4.46	400
MA5	64	296.6	28.4	287.6	28.3	268.6	22.9	3	2.96	16.6	16.4	0.06	-	600
MA6	74	166.0	57.0	170.0	60.0	-	-	3	-	5.4	-	0.47	-	600
MA7	102	253.9	1.9	254.4	-7.6	275.2	-14.2	3	2.86	33.2	30.6	0.09	3.40	675
MA8	110	106.3	30.4	114.8	32.0	57.1	-5.5	4	3.67	32.1	25.6	0.47	-	630
MA9	122	330.5	49.1	314.1	55.2	289.2	60.1	3	2.39	84	87.8	0.24	-	630
MA11	152	341.0	68.0	346.0	66.0	-	-	7	-	5.2	-	3.41	-	640
MA12	156	304.0	69.0	301.0	70.0	-	-	6	-	2.5	-	4.70	-	650
MA13	157	349.0	72.0	351.0	77.0	-	-	6	-	10.8	-	6.11	-	640
MA41	182	117.8	75.4	151.0	74.1	14.4	17.3	4	3.81	23.5	36.6	0.30	-	580
MA42	192	218.9	33.4	218.6	24.4	315.6	-25.5	2	1.99	-	-	0.09	-	660
MA43	195	300.2	31.2	294.9	29.9	265.1	31.2	4	3.61	35.3	31.2	0.07	98.11	580
MA44	-	99.9	28.0	104.7	30.3	67.0	1.4	3	2.63	59.4	61.9	0.05	-1.60	580
MA45	-	151.9	13.6	151.9	13.6	33.1	-35.7	1	1.00	-	-	0.03	1.11	300
MA46	221	157.0	70.0	162.0	68.0	194.0	15.0	4	3.69	39.3	51.1	0.06	58.04	300
MA48	234	357.0	47.0	349.0	54.0	254.0	78.0	6	5.90	11.9	10.1	0.81	14.80	630
MA49	241	366.5	59.0	298.0	64.0	313.0	59.0	6	5.35	21.0	30.9	0.29	1.60	630
MA50	246	347.2	47.9	333.7	57.7	290.3	69.8	6	5.32	26.6	31.0	0.26	3.47	630
MA51	252	-	-	316.0	70.0	-	-	4	-	17.3	-	3.54	-	640
MA52	256	-	-	333.0	68.0	-	-	6	-	4.1	-	12.18	-	600
MA53	260	71.6	32.5	79.6	41.8	72.3	23.7	4	2.83	73.1	77.6	0.08	-	675
MA54	262	271.4	33.2	264.4	26.3	282.4	4.8	2	1.98	-	-	0.06	-6.60	675
MA55	171	259.2	40.9	256.4	33.6	291.4	4.7	3	2.79	42.8	33.3	0.16	11.95	675
MA57	-	133.5	53.9	144.6	54.1	23.2	-7.3	4	2.91	19.1	84.7	0.53	-	400

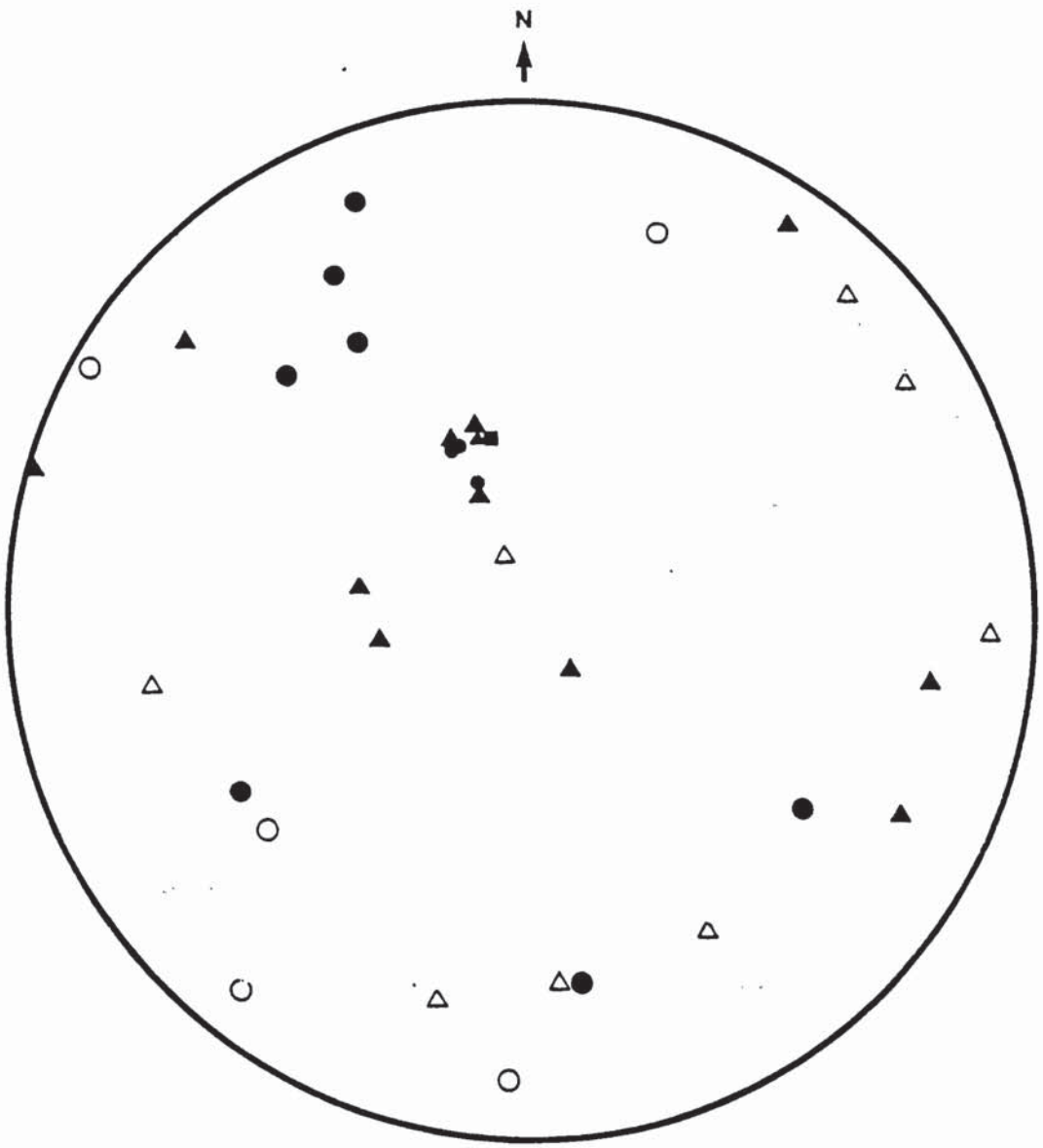

Fig. 6.14 Mean bedding corrected directions isolated during bulk thermal demagnetization of the Upper Buntsandstein. For key to symbols see Fig. 6.2.

6.4.4 Chemical Demagnetization Results

Two specimens were selected from the Upper Buntsandstein units to undergo chemical demagnetization by immersion in dilute HCL acid (MA74.2.1 and RA7.1.1, Table 6.3). Fig. 6.15 shows the results of this chemical demagnetization of the latter together with results of thermal cleaning of specimen RA7.2.1.

The two demagnetization techniques show very similar results. The chemically cleaned specimen shows a steep, positive initial direction which remains unchanged up to 150 hours and has a most stable direction of D=351.1°, I=40.6° after correction for bedding over the range 2-150 hours. Longer immersion in the acid results in movement of the direction towards a more northerly position with a shallow inclination. The normalized intensity decay curve (Fig. 6.15a(ii)) shows a rapid loss in intensity after fairly short immersion times, after 33 hours 75% of the original remanence has been removed. This is followed by a more gradual loss intensity between 33 and 150 hours. At 150 hours 3% of the original remanence remains. Between 150 hours and 250 hours the last fragment of remanence is removed and is accompanied by the northerly movement in direction previously mentioned.

6.4.5 Discussion of Palaeomagnetic Results

Initial intensities for the Rio Arandilla sandstones are similar to those recorded in the Lower Buntsandstein units, ranging from 0.09 mAm^{-1} up to 1.68 mAm^{-1} (with the exception of MA62 (11.60 mAm^{-1}). The Rillo mudstones and sandstones show a greater range in N.R.M. intensities (0.04 mAm^{-1} (MA76), up to 39.44 mAm^{-1}(MA71)). The Torete mudstones and sandstones have higher initial intensities than the underlying units (13.74 mAm^{-1} (mean)). The samples with highest initial intensities have N.R.M. directions very close to the present-day local geomagnetic field. A streaking of directions towards the northwest and southeast quadrants suggests that older components are still present in some samples.

I.R.M. results indicate that haematite is the predominant remanence carrier in these sediments, although it seems likely that a second, low coercivity mineral is also present in many samples, especially those from the Rillo mudstones and sandstones.

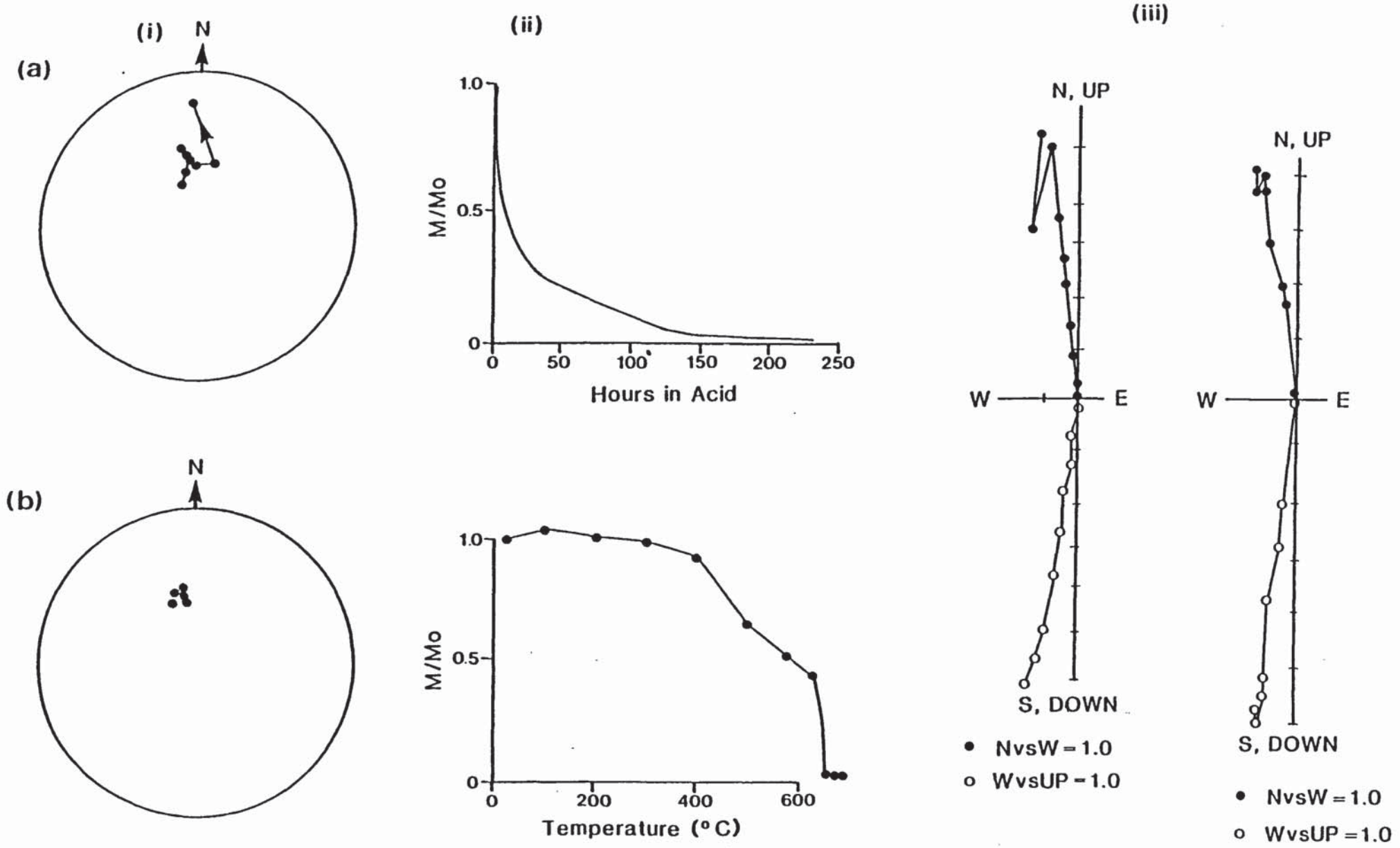

Fig. 6.15 Results of (a) Chemical demagnetization of specimen RA7.1.1 with those of (b) Thermal demagnetization of specimen TA6.5.2, (i) Stereographic projections, (ii) Normalized intensity decay curves, (iii) Orthogonal vector plots.

Partial thermal demagnetization of the Upper Buntsandstein specimens reveals four characteristic types of behaviour. All specimens show a recent magnetization which has a direction close to the present-day local geomagnetic field direction. A few specimens have been totally remagnetized with no indication of an older component of remanence remaining at all. The majority of the specimens show a second older component older with either a Triassic normal, reversed or mixed direction of remanence which is only revealed after heating to higher temperatures.

The thermally demagnetized specimen is a good example of Type D behaviour (see section 6.4.3.4). One component of magnetization is present, having a blocking temperature at 630°-660°C. the direction is again close to the present-day local geomagnetic field direction. These results show that chemical demagnetization can be a useful method in the determination of remanence components not always revealed using thermal demagnetization techniques.

Different blocking temperatures are seen in different specimens, although the majority show a secondary Triassic component which is only revealed after heating to temperatures in excess of 630°C. This suggests that the older component is carried by crystalline haematite. Chemical demagnetization of specimen RA7.1.1 shows a rapid removal of remanence intensity after only a short time in the acid, although the direction remains unchanged. But after prolonged immersion a Triassic normal is revealed. It is thought that fine grained pore filling iron oxide is removed first during chemical demagnetization (Collinson, 1967 Park, 1970) coarser grained detrital haematite being dissolved only after more prolonged acid attack. This suggests that the initial remanence component is carried by fine grained diagenetic haematite and the Older, Triassic component is carried by coarse detrital haematite.

Table 6.5 shows previously published pole positions for Stable Europe (A-E) and Iberia (1-4) (these are also plotted on the stereographic projection in Fig. 6.16), together with the mean pole positions calculated for each of the Upper Buntsandstein units.

Pole positions for individual specimens are also shown in Fig. 6.16. The majority of specimens show a close grouping of palaeopole directions close to that of the present-day pole position but consistantly different to the Triassic poles of Stable Europe and Iberia.

TABLE 6.5 PREVIOUSLY PUBLISHED LOWER TRIASSIC DIRECTIONS AND POLES FOR STABLE EUROPE AND IBERIA, TOGETHER WITH THOSE FOUND IN THIS STUDY FOR THE UPPER BUNTSANDSTEIN OF MOLINA DE ARAGON

Letter/ No.	Locality (formation)	D(°)	I(°)	N	α_{95} (°)	Pole Position Lat	Pole Position Long	Reference
STABLE EUROPE								
A	Triassic sediments, USSR	-	-	-	-	51°N	159°E	Irving (1964)
B	Arran sandstone, Scotland	-	-	-	-	54°N	118°E	Irving (1964)
C	Buntsandstein, Germany	-	-	-	13	55°N	169°E	Irving (1964)
D	Vosge sandstone, France	-	-	-	-	28°N	143°E	Irving (1964)
E	Vosge sandstone, France	-	-	-	-	62°N	167°E	Irving (1964)
IBERIA								
1	Rio Aragon C. Pyrenees (andesites)	152.0	-22.5	14	6	51°N	133°W	Schwarz (1962)
2	Anayet C.Pyrenees (andesites and sandstones)	164.0	-14.0	11	10	52°N	154°W	Van der Lingen (1960)
3	Serra del Cadi E.Pyrenees (redbeds)	169.5	-3.0	41	4	48.5°N	163°W	Van Dongen (1967)
4	Alcazar de San Juan, Central Spain (redbeds)	359.5	23.0	36	6	63°N	177.5°E	Van der Voo (1967)
UPPER BUNTSANDSTEIN OF MOLINA DE ARAGON (MEANS)								
	Rio Arandilla sandstone	272.0	47.0	16	45	43°N	137°E	This Study
	Rillo de Gallo mudstones and sandstones	297.5	49.0	25	23	42.5°N	95°E	This Study
	Torette mudstones and sandstones	320.0	55.0	3	19	-	-	This Study

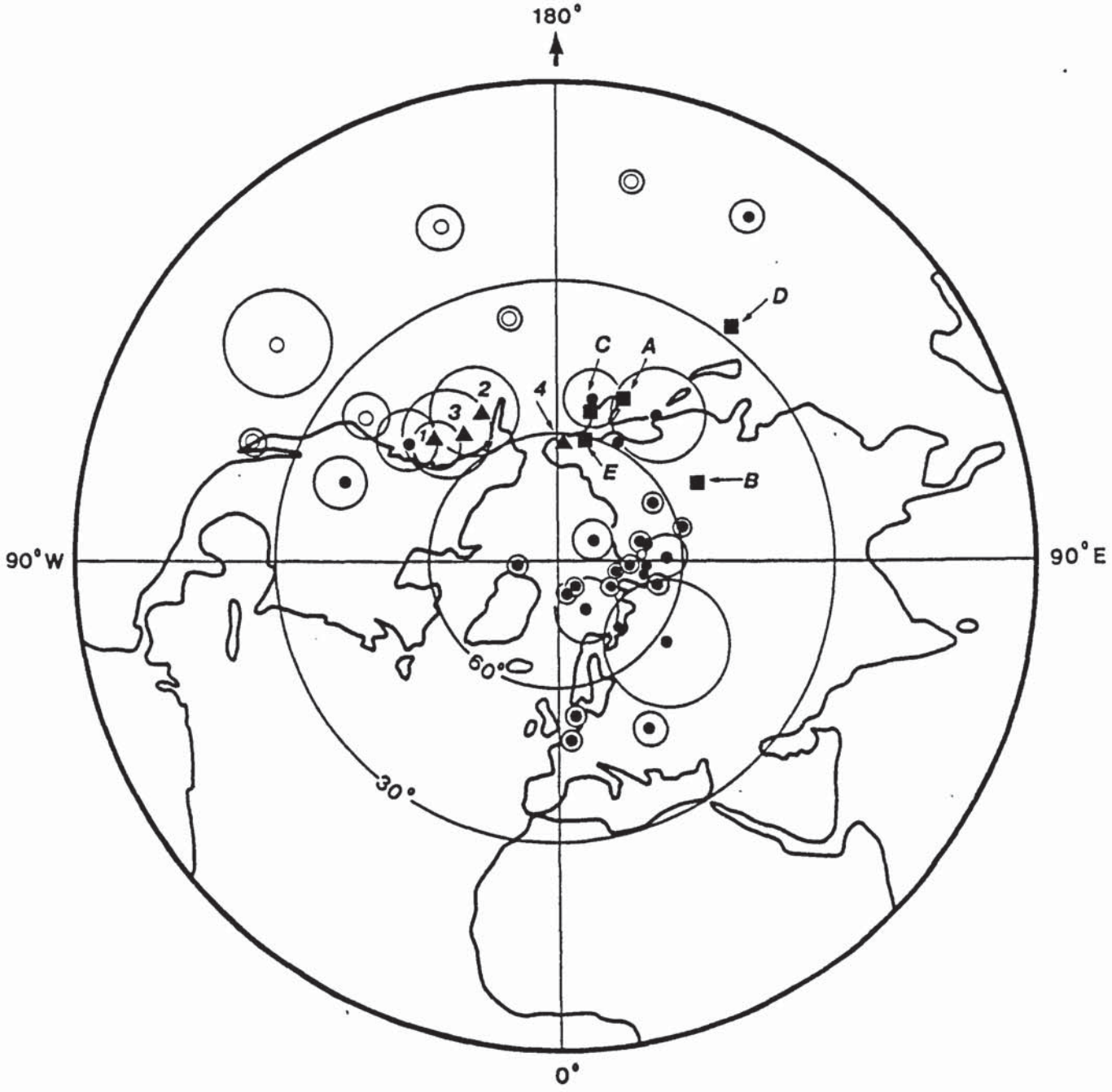

Fig. 6.16 Palaeopole positions for the Upper Buntsandstein. ■ Previously described Triassic poles for stable Europe (Letters A-E refer to Table 6.5). ▲ Previously described Triassic pole positions for the Triassic of Iberia (Numbers 1-4 refer to Table 6.5). ● Pole positions calculated from the most stable directions found in this study (see Table 6.5).

The pole positions plotted are derived from the most stable directions isolated for each specimen. Since, in the majority of cases, this is the lower temperature recent component, the poles plotted for the Upper Buntsandstein reflect the remagnetized directions and not the original remanence directions and thus cannot be compared with previously published results for the Upper Buntsandstein.

6.5 RELATIONSHIP BETWEEN DIAGENESIS AND PALAEOMAGNETISM

Initial intensities and N.R.M. intensity values correlated well for samples from the Upper Buntsandstein. Samples with the highest initial intensities contain the largest amounts of point counted iron oxide and those with the lowest initial intensities contain the smallest amounts of iron oxide. Since amounts of coarse detrital haematite are fairly uniformly distributed through the sequence it is the variation in amounts of fine grained pore filling iron oxide which affect the intensities the most. The largest amounts of fine grained heamatite are found in the middle part of the Rillo mudstones and sandstones from both sections studied (MA80-MA90 and RA6-RA10) and in the Torete mudstones and sandstones. These are finer grained deposits than those of the lower Rio Arandilla sandstone unit and were deposited in a lower energy environment.

Reflected light analysis on these deposits shows that although detrital haematite grains are present in the sediments, they are usually very altered and commonly have a skeletal appearance. Many also show marginal replacement by fine grained iron oxide or goethite.

Early diagenetic haematite in the form of parallel crystals in biotite traces and as a microcrystalline replacement of rock fragments has a much fresher appearance. It is probable that this haematite associated with the replacement of framework grains during early diagenesis, carries a component of remanence which is of Triassic age. If this were the case it would explain why some specimens show a 'mixed' or immediate Triassic polarity e.g. MA85.5.1 and MA86.2.2. Growth of the authigenic haematite during a period of polar reversal would result in the acquisition of a

component of magnetization intermediate between a Triassic normal and Triassic reversed direction.

Fine-grained pore filling haematite is the most abundant phase of haematite in these deposits. It almost certainly carries the component of remanence which is nearly coincident with the present-day local geomagnetic field direction. Evidence for the dissolution of a carbonate cement is abundant in many samples (eg. 'V' shaped notches (Burley and Kantorowicz, 1986)) and it is likely that iron oxide precipitated in secondary pores when Fe ions, held in the carbonate lattice, were released into solution during dissolution of the cement.

CHAPTER SEVEN

THE MUSCHELKALK AND KEUPER

7.1 INTRODUCTION

Rocks of the Upper Triassic Muschelkalk facies were sampled at four localities within the Province of Guadalajara, Central Spain (Fig. 7.1): Castellar de la Muella (01° 46' 12"W, 40° 49' 12"N), Hoz del Gallo (01° 59' 24"W, 40° 49' 48"N), Rillo de Gallo (02° 42' 36"W, 40° 48' 00"N) and Riba de Santiuste (02° 43' 00"W, 41° 12' 20"N). The overlying Keuper facies was sampled at one locality, Teroleja (01° 57' 36"W, 40° 48' 00"N).

The samples collected from Castellar de la Muella are prefixed by the letters CM, those from Riba de Santiuste by MQ and those from Teroleja by T. Samples from the sections at Hoz del Gallo and Rillo de Gallo are both prefixed by the letters MA. Samples MA96-MA103 were collected from Hoz del Gallo and samples MA104-MA111 from the section at Rillo de Gallo.

7.2 STRATIGRAPHY AND SEDIMENTOLOGY

Three different lithostratigraphic classifications exist for the Upper Triassic of these areas (Fig. 7.2). In the most easterly section, Castellar de Muella, Hinkelbein (1965, 1969), divided the Muschelkalk into two units. The "Dolomias de Tramacastilla" (Tramacastilla dolomites) and overlying these the "Dolomias Maries y Calizas de Royuella" (Royuella dolomites, marls and caliches). Samples CM1-CM5 were taken from this upper unit (Fig. 7.3).

Further west, close to the town of Molina de Aragon, Hinklebein (1965, 1969) again divided the Muschelkalk into two units, the "Capas dolomiticas" (Dolomitic cap) and overlying this, the "Capas de Royuella" (Royuella cap). Samples MA96-MA103 were collected from the lower unit and MA104-M111 from the upper unit (Fig. 7.3).

Close to the margin of the Iberian Cordillera with the Central System, Sopena (1979) named the sediments of the Muschelkalk facies the "Dolomias y Areniscas de Riba de Santiuste" (Riba de Santiuste dolomites and sandstones, TM2). He further divided this unit into three subunits, TM2.1, TM2.2 and TM2.3. Samples MQ1-MQ5 were taken from subunit TM2.1, MQ6 and MQ7 from TM2.2 and MQ8 and MQ9 from TM2.3 (Fig. 7.3).

Fig. 7.1 Geological sketch map showing the location of the Muschelkalk and Keuper sections.

Fig. 7.2 Lithostratigraphic units of the Upper Permian and Triassic of the Central System (after Sopena, 1979), west of Molina de Aragon (after Ramos, 1979) and in the Sierra de Caldereros and Sierra Menera region (after Perez-Arlucea, 1985).

Fig. 7.3 Sedimentological columns showing horizons from which Muschalkalk and Keuper samples were taken. Castellar de Muella and Teroleja columns compiled by Perez-Arlucea (1985); Hoz del Gallo and Rillo de Gallo columns compiled by Ramos (1979); and Riba de Santiuste column compiled by Sopena (1979).

The Spanish Muschelkalk is a diachronous facies which youngs towards the west due to the gradual transgression over this area by the Muschelkalk Sea. In the most easterly section, that of the Castellar de Muella, the Muschelkalk facies is of late Ladinian age (Perez-Arlucea, 1985; Fig. 7.2). In the Molina de Aragon area it is of early Karnian age (Ramos 1979) and in Riba de Santiuste in the west, it is of Karnian age (Sopena, 1979).

The Keuper facies was sampled at a section near to the town of Teroleja, 10 km southeast of Molina de Aragon (Fig. 7.1) Hinklebein (1965, 1969) divided the Keuper in this area into five units (Fig. 7.2) "Lutites y yesos de Noguera" (Noguera mudstones and gypsum). "Lutite de Teroleja" (Teroleja mudstone), "Yesos y Lutites de Teroleja (Teroleja gypsum and mudstones), "Yesos y Margas de Teroleja" (Teroleja gypsum and marls) and overlying these the "Formation de dolomias tableadas de Imon". (Imon dolomite formation). Samples T1-T4 were taken from the Imon dolomite formation (Fig. 7.3).

7.2.1 Castellar de la Muella

The section of Castellar de la Muella is situated in a road cutting near the town of the same name (Plate 7.1). The Royuela dolomites, marls and caliches comprise 51m of grey, white and ochre dolomites with interbedded green marls and dark grey limestones. The predominant lithology is fine grained recrystallized dolomite. Some horizons contain a poorly preserved fauna of bivalves, brachiopods, ostracods, gastropods, forams, bryozoa and algal laminations (Perez-Arlucea, 1985).

Limestones are not common except in the upper part where they often contain dessication cracks, 'tepee' structures, ooid fragments and the trace fossil Rhizocorallium (Perez-Arlucea, 1985).

The deposits are interpreted as lagoonal carbonates. The upper part of the unit being
deposited in a moderately hypersaline lagoonal environment. The presence of ooid shoals and diverse species of bivalves and forams indicates that periods of lower salinity also occurred (Perez-Arlucea, 1985).

7.2.2 Hoz del Gallo and Rio de Gallo

The Dolomite cap and overlying Royuela cap were sampled at the sections of Hoz del Gallo and Rillo de Gallo respectively.

The Dolomite cap consists of 36m of fine to medium grained, grey and yellow crystalline dolomites. Most of the original sedimentary structures have been lost due to recrystallization during dolomitization. Occasionally, horizons containing gravel, gastropods, bivalves and algae can be seen, as well as, algal lamination structures. The rocks are also silicified in places. These beds are interpreted as being intertidal deposits (Ramos, 1979).

Conformable over the last unit is the Royuela cap. This is composed of an irregular alternation of muds and dolomites in beds of up to 10cm thickness (Plate 7.1b). The dolomites are crystalline and some contain bivalves gastropods and algal laminations. At this locality 28m of the sediments are exposed. The top of the beds are often bioturbated and some are composed exclusively of the trace fossil Rhizocorallium. In the upper part, brecciated dolomites occur. Many have iron stained tops, others show 'tepee' structures and dessication cracks.

The lower and middle part of this unit were probably deposited in an intertidal-subtidal zone. The upper part of the Royuela cap shows much evidence of emergence and the sediments were probably laid down in an uppermost intertidal to supratidal zone (Ramos, 1979).

7.2.3 Riba de Santiuste

The Riba de Santiuste section is located approximately 3 km west of the town of Riba de Santiuste in a small gorge cut by a tributary of the Salado river (Fig. 7.11).

Unit TM2 (Riba de Santiuste dolomites and sandstones) has a very heterogeneous composition. It is divided into 3 subunits TM2.1 (predominantly dolomites) TM2.2 (predominantly sandstones) and TM 2.3 (predominantly sandstones and mudstones) Fig. 7.3.

Subunit TM2.1 is composed of very fine grained grey dolomites with intercalations of marls, sandstones and mudstones. Intraclasts and fossils are present in some of the dolomites. Algal laminations are also common and the beds are well bioturbated.

Subunit TM2.2 is composed of red and ochre sandstones with frequent interbeds of mudstones, siltstones and sandy dolomites. The sandstones are arkosic, and predominantly fine to very fine grained. Small scale cross-stratification, adhesion ripples and oscillation ripples are also present and evidence of bioturbation is abundant.

Subunit 2.3 consists of grey, fine grained dolomites and dolomitic marls. Overlying these is a sandstone facies showing parallel lamination, large-scale trough cross-bedding and small scale oscillation ripples. Convolute bedding and flute casts are also seen.

These deposits were probably laid down in a complex intertidal-supratidal regime (Ramos, 1979).

At this locality subunit TM2.1 is approximately 12m thick, subunit TM2.2 is 18m thick and subunit TM2.3 is 14m thick.

7.2.4 Teroleja

The Keuper column of Teroleja is exposed in a south facing cliff section approximately 1 km north of the town of Teroleja (Plate 7.1c, Fig. 7.1).

The Imon dolomite formation is 34m thick in the section at Teroleja (Fig. 7.2). At the base of the unit is a dolomitic breccia. This probably originated from the collapse of dissolved evaporites which are interstratified with the dolomites. Above the breccia, bedded dolomites containing algal laminations and evaporite molds exist.

These deposits were probably laid down in an intertidal-supratidal zone (Perez-Alucea, 1985).

7.3 DIAGENESIS

7.3.1 Castellar de la Muella

The Royuela dolomites marls and caliche consist, predominantly, of very fine grained non-ferroan dolomites which have been completely recrystallized. Little of their original structure remains but 'ghost' structures are sometimes preserved within them, for example ellipsoid features are seen in Sample CM1 (Plate 7.2a), and probably represent compacted ooids. The interiors of these ellipsoids are composed of non-ferroan calcite cement.

Another type of 'ghost' structure seen in these samples consists of slightly coarser grained dolomite crystals which form curvilinear features (Plate 7.2b). These are typically 1cm-2cm in length and probably represent recrystallized shell fragments. Gypsum is also found in samples from Castellar de la Muella. It most commonly occurs as fibrous tabular crystals which infill small fractures (Plate 7.2b). The dolomites, when viewed under the S.E.M., (Plate 7.2c) consist of euhedral crystals approximately 10-15μm in length. This is typical for a recrystallized carbonate.

7.3.2 Hoz del Gallo and Rillo de Gallo

The Muschelkalk of the Molina de Aragon area consists predominantly of micritic non-ferroan dolomites which contain occasional quartz grains. Veinlets of much coarser, later dolomite, cut across the 'dirty' fine grained dolomite (Plate 7.2d). The dark coloration of these dolomites is probably due to abundant organic material trapped within the sediment. Dark organic pellets, algal laminations and recrystallized microfossils (Plate 7.2e) are all common in these deposits.

Coarse grained, irregular, non-ferroan veinlets cut across the dolomite (Plate 7.2f). These appear to lie parallel with bedding and are often lined with fine grained iron oxides. Irregular patches of non-ferroan calcite are also seen in some samples e.g. MA101 and iron oxide is sometimes associated with these.

In the upper unit (Royuela cap), lozenge shaped patches of coarse grained dolomite exist (Plate 7.3a). These range in size from about 0.2 mm up to 0.5 mm and probably represent relict evaporite nodules. In some cases small amounts of relict anhydrite still exist (Plate 7.3b).

In sample MA97 abundant rhombic shaped features composed of coarse grained ferroan dolomite exist (Plate 7.3c). These show a slight zoning from non-ferroan dolomite at the margins to ferroan dolomite in the core which suggests precipitation in a geochemically evolving pore water regime.

7.3.3 Riba de Santiuste

The Muschelkalk deposits of Riba de Santiuste contain a small proportion of clastic sediments in addition to the dolomites. The results of point count analysis on two clastic samples (MQ5 and MQ7) are shown in Appendix VII.

Both samples are fine grained Arkosic sandstones, containing considerable amounts of feldspar (MA5: 12.8%, MQ7: 18%). Quartz grains are predominantly mono-crystalline although strained quartz is also common. Rock fragments are rare but micas, especially muscovite are abundant.

Clay minerals comprise about 3%-10% of the total volume of these clastic sediments. X-ray diffraction analysis was carried out on sample MQ5 and the diffractograms produced are shown in Fig. 7.4. The results of semi-quantitative analysis are also shown below.

TABLE 7.1 Results of semi-quantitative analysis on <2μm clay fraction of Muschelkalk sample MQ5.

	Illite	Kaolinite	Mont.	Chlorite	Total
MQ5	94.5	1.0	0	4.5	100%

The results show that illite is the dominant clay in the sample. Chlorite and kaolinite are also present in minor amounts although kaolinite was not actually recognised from petrographic analysis. Illite and chlorite occur mainly as replacement minerals.

Authigenic quartz and potassium feldspar are common in the deposits (Plate 7.3d) occurring as authigenic overgrowths on detrital grains. Authigenic feldspar, in particular, forms non-syntaxial euhedral overgrowths which are much fresher appearance than the original grain.

Carbonate (non-ferroan dolomite) forms a pore filling cement in MQ5, amounting to almost 13% of the total volume of the rock.

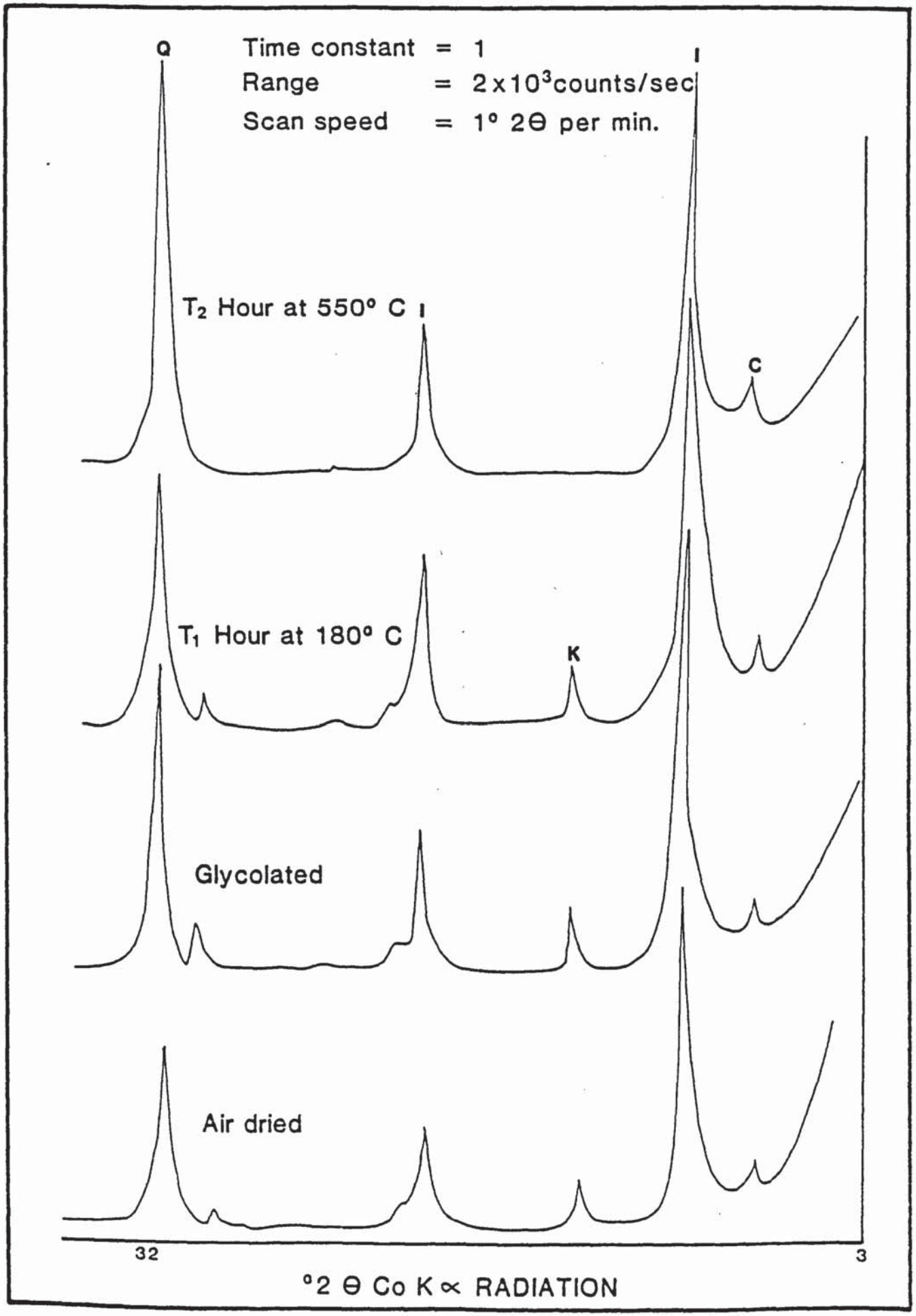

Fig. 7.4 X-ray diffractograms for the <2μm clay fraction of sample MQ5.

Visible porosities are 13.6% in MQ5 and 5.6% in MQ7 and opaques range from 5%-10% of the total in these deposits.

The majority of the samples collected from the Muschelkalk of Riba de Santiuste are micritic dolomites. They frequently contain organic material which mainly occurs in fine laminations (Plate 7.3e) and is probably of algal origin. Small rounded aggregates of organic matter are also seen in some samples (Plate 7.3f). These probably represent faecal pellets. In sample MQ8 a small recrystallized, chambered microfossil is present (Plate 7.4a). Also found within this sample is a lozenge shaped vug which is partially infilled with coarse grained non-ferroan dolomite (Plate 7.4b). At the margins of the infilled vug, small euhedral voids rimmed by fine grained iron oxide are present.

7.3.4 Teroleja

The Keuper deposits of Teroleja show many diagenetic features similar to those of the underlying Muschelkalk facies. Four samples (T1-T4), were collected from this locality, all are dolostones. Fine, organic-rich laminations are seen in T1 together with small lensoid patches of coarser grained non-ferroan dolomite (Plate 7.4c). These probably represent algal laminations and early evaporite nodules respectively. Vugs are a common feature in these deposits. They are quite variable in shape and size (0.1 mm-5 cm) and probably originate by the dissolution of evaporite nodules or skeletal debris (Plate 7.4d). Many show partial infilling by coarse grained euhedral, non-ferroan dolomite. The crescent shaped vug shown in Plate 7.4d also contains a small amount of non-ferroan calcite and may formed by the dissolution of a shell fragment.

Barite is also found in these deposits. It is usually associated with the coarser grained lensoid patched of dolomite which appear in places to replace it (Plate 7.4e).

Sample T4 has a brecciated appearance (Plate 7.4f). Coarse dolomite crystals are cemented by a non-ferroan dolomite. This breccia may have formed by the collapse of dissolved evaporitic horizons.

7.3.5 Magnetic Mineralogy

The Muschelkalk and Keuper sediments contain very few iron oxides of either detrital or authigenic origin. Small amounts of framboidal pyrite are present in many samples (Plate 7.5a). In the Muschelkalk of the Hoz del Gallo section, irregular patches of coarse grained calcite, occur These often have fine grained iron oxide around their margins (Plate 7.5b). As mentioned in section 7.2.3, iron oxide is also found lining euhedral voids in samples from Riba de Santiuste (Plate 7.4b).

Clastic deposits from this section do contain small amounts of detrital iron and titanium oxides (Plate 7.5c and d). These are usually subhedral in shape and fairly fresh in appearance. Dissolved veinlets also show a lining of fine grained iron oxide in many instances (Plate 7.5e).

The Keuper facies of Teroleja contain even fewer magnetic minerals than the underlying Muschelkalk. Fine grained haematite is found, however, lining a few secondary voids (Plate 7.5f).

7.3.6 Paragenesis

7.3.6 1 Dolomitization

There has been much debate as to the origin and timing of the dolomitization of these rocks e.g. Virgili (1958), Freeman (1972), Pena (1972), Pena and Yebenes (1977).

Virgili (1985) suggested that dolomitization was contemporaneous with sedimentation i.e. that these are primary dolomites. Freeman (1972), disagreed with this view postulating that dolomitization was controlled by structure and suggested that chlorites from the overlying Keuper provided the magnesium necessary for dolomitization.

Pena (1972) and Pena and Yeberes (1977) identified three different types of dolomitization in the Muschelkalk.

Type 1: **Penecontemporaneous or very early diagenetic dolomitization.** This dolomitization was selective, primarily affecting the micritic matrix. Dolomites formed in this manner are of minor importance volumetrically in these rocks.

Type 2: **Eogenetic limpid dolomitization.**
This resulted in the formation of a xenotopic mosaic of crystals containing numerous inclusions. This type of fabric is shown by the oolitic dolomites and probably originated by the mixing of descending meteroic waters with marine waters rich in magnesium.

Type 3: **"Freeman type" dolomitization** i.e. Structurally controlled telogenetic dolomitization.
The mixing of meteoric waters perculating through the Keuper whose pore water composition is similar to that of sea water, would provide favourable conditions for the local precipitation of dolomite adjacent to fractures in the underlying Muschelkalk.

7.3.6.2 Other Diagenetic Processes

The earliest diagenetic processes in the Muschelkalk and Keuper deposits were probably controlled by organic activity.

Many of the sediments were intensively bioturbated and organic debris, such as faecal pellets and algal laminations were deposited. Subaerial erosion of the sediments led to the formation of dessication cracks and the arid hypersaline conditions resulted in the development of evaporite nodules. Framboidal pyrite formed in the near surface sulphate reduced zone due to the reaction between iron oxides and H_2S.

$$2Fe_2O_3 + 8SO_4^{2-} + 15CH_2O \rightarrow 4FeS_2 + 15HCO_3^- + 7H_2O + OH^-$$

In the clastic sediments authigenic quartz and potassium feldspar precipitated and labile grains such as rock fragments, amphiboles etc. were replaced or removed.

Burial of the sediments led to a change in the pore water geochemistry. The evaporites became unstable and were removed creating 'vuggy' secondary porosity. Many of the vugs were then filled by a coarsely crystalline non-ferroan dolomite cement. Some samples show a zoning of this vug filling dolomite. The vug margin (earliest) dolomites appear to have been slightly ferroan. The brecciated dolomite (Plate 7.4f) was probably cemented at this time.

The lithified rocks were compacted upon further burial, as indicated by ellipsoid shape of the relict ooids (Plate 7.2a). Fractures also developed, and many were subsequently annealed by coarse grained dolomite (Plate 7.2d).

Uplift of the sequence resulted in another change in pore water chemistry and caused the dissolution of unstable minerals. The ferroan dolomite which lines some of the vugs was, preferentially leached at this time (Plate 7.4b). Fe ions were released into solution, they combined with free oxygen and precipitated as iron oxide pore linings. Weathering of the sequence led to the conversion of some of the iron oxide to goethite.

7.4 PALAEOMAGNETISM

7.4.1 Natural Remanent Magnetization (N.R.M.) Results

The results of N.R.M. analysis are summarized in Table 7.2.

Mean initial intensities prior to thermal demagnetization of the samples were $0.12mAm^{-1}$ for the Castellar de la Muella section, $0.13mAm^{-1}$ for the two Molina de Aragon sections and $0.14mAm^{-1}$ for the Riba de Santiuiste section.

Mean initial susceptibility values were $61.14mAm^{-1}nT^{-1}$ for the CM samples, $21.53mAm^{-1}nT^{-1}$ for the MA samples and $79.50mAm^{-1}nT^{-1}$ for those from Riba de Santiuste.

The Keuper samples had a mean N.R.M. intensity of only $0.06mAm^{-1}$. Susceptibility values were all negative and had a mean value of -10.08.

Mean initial N.R.M. directions for the Muschelkalk and Keuper samples are shown in Fig 7.5.

There is a strong grouping of steep positive directions close to the present-day local geomagnetic field direction, although some degree of scatter is shown. α_{95} values for the samples are generally high with only five samples recording α_{95} values of less than 10°.

TABLE 7.2 N.R.M. RESULTS FOR THE MUSCHELKALK AND KEUPER

Sample	Height (m)	F Dec(°)	F Inc(°)	P Dec(°)	P Inc(°)	Pole Long(°)	Pole Lat(°)	N	R	α95(°)	α95(°) Pole	Intensity (mAm^{-1})	Susceptibility ($mAm^{-1}nT^{-1}$)
CM1	156	34.6	54.3	291.7	79.0	337.8	40.8	7	5.96	27.3	40.2	0.16	79.28
CM3	142	67.5	60.3	174.7	79.6	359.2	25.6	6	4.96	34.1	50.4	0.21	83.97
CM4	128	51.2	41.3	71.5	67.1	51.3	40.7	5	4.95	8.8	13.7	0.05	44.35
CM5	112	26.2	57.6	18.1	76.9	14.3	62.9	6	5.88	10.5	18.6	0.06	36.94
MA96	576	336.1	85.0	224.2	79.8	347.4	25.6	5	4.36	33.4	55.8	0.43	-
MA98	587	80.2	-78.5	50.2	-68.5	154.4	-15.5	5	4.54	27.3	41.0	0.08	2.23
MA99	591	193.8	-47.6	190.4	-60.4	255.8	-81.6	3	2.86	33.4	46.8	0.20	-
MA100	595	65.1	67.2	97.4	74.4	31.6	31.1	5	4.95	8.9	14.8	0.08	1.18
MA101	601	362.6	50.6	341.0	61.1	289.7	75.7	4	3.89	18.0	21.0	0.09	5.29
MA102	605	10.3	64.4	358.4	76.8	356.4	65.9	1	-	-	-	0.06	3.08
MA103	611	38.7	58.1	48.2	70.3	47.2	55.9	4	3.97	8.4	13.2	0.19	15.91
MA104	557	333.7	71.9	289.0	76.3	325.4	43.5	3	2.95	19.8	32.4	0.18	22.11
MA105	566	336.6	45.4	324.5	53.3	267.6	62.2	6	5.82	13.0	14.4	0.03	27.09
MA106	569	120.1	59.3	139.7	55.4	28.3	-3.4	5	4.83	16.2	21.1	0.02	30.05
MA107	570	84.8	71.7	126.9	73.4	22.0	20.8	7	6.78	11.9	19.7	0.08	37.51
MA108	571	346.1	64.7	319.9	73.3	319.7	58.6	5	4.90	12.0	20.7	0.48	26.73
MA109	573	100.5	43.6	113.2	45.0	53.1	1.8	6	5.95	6.8	6.2	0.02	37.21
MA110	577	338.9	41.3	328.8	49.9	256.6	65.3	4	3.76	26.8	30.3	0.02	50.02
MA111	580	351.0	24.5	346.8	35.3	209.1	66.6	4	3.90	17.2	15.0	0.04	-
MQ2	826	313.5	-44.2	315.1	22.5	242.7	42.1	3	2.69	53.3	52.6	0.35	49.8
MQ3	827	14.1	41.1	91.8	44.7	66.3	20.3	3	2.70	51.7	60.2	0.07	35.21
MQ4	830	296.0	51.4	168.8	55.7	6.8	-9.6	5	4.80	17.3	20.4	0.02	55.91
MQ8	856	305.6	50.0	161.2	60.4	12.1	-4.9	3	2.93	23.5	32.5	0.05	67.04
MQ9	865	285.1	44.0	186.6	53.9	351.1	-12.1	6	5.73	16.1	19.2	0.21	189.56
T1	97	287.8	21.2	294.9	15.3	257.3	23.9	3	2.99	10.5	7.1	0.03	-9.65
T2	104	324.7	78.9	318.7	51.0	267.5	56.5	7	6.80	11.2	13.3	0.11	-9.09
T3	111	333.2	60.3	338.7	24.7	217.8	56.6	7	6.98	4.1	3.0	0.06	-11.01
T4	117	263.4	64.9	298.0	38.4	268.4	35.3	6	5.83	13.2	12.5	0.02	-10.55

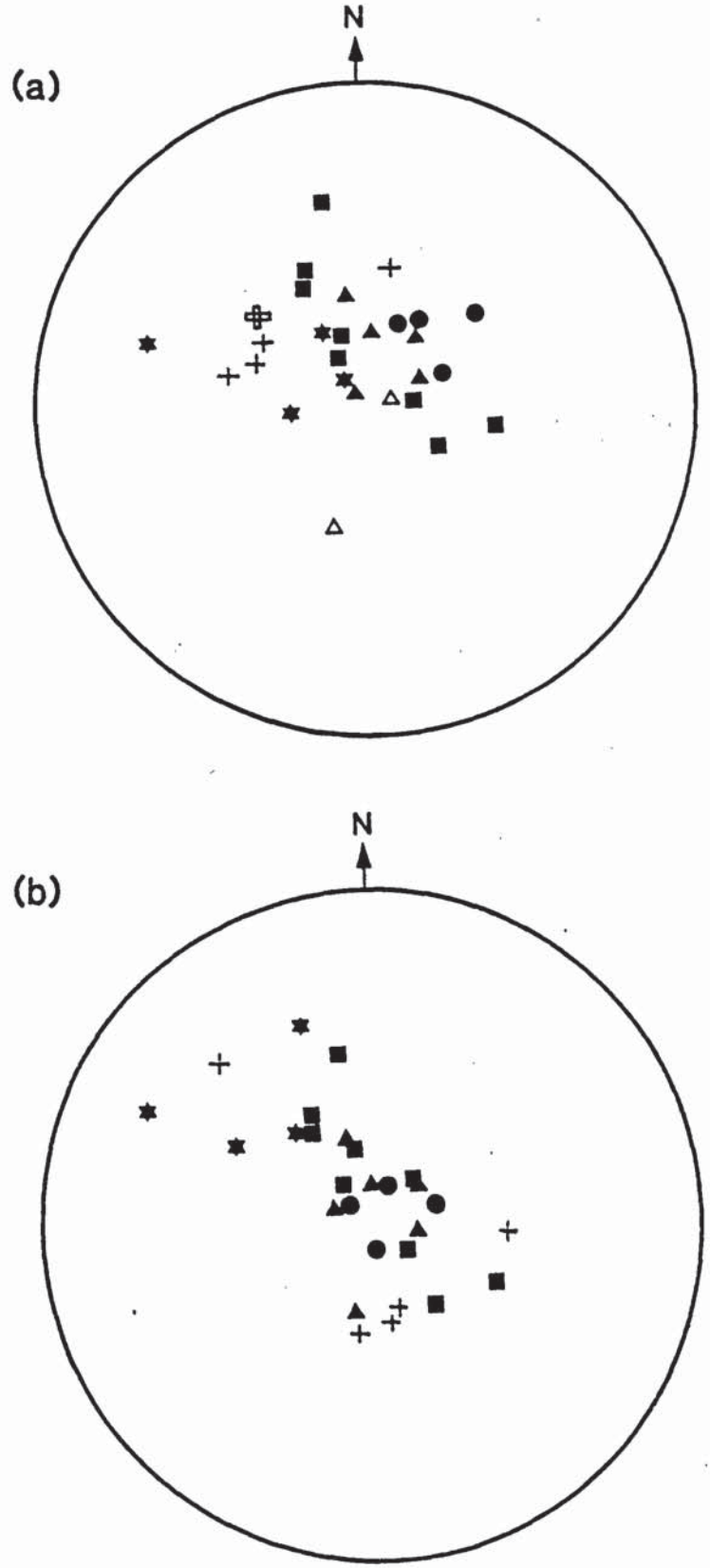

Fig. 7.5 Initial mean N.R.M. directions for the Muschelkalk and Keuper (a) before and (b) after correction for bedding. ● Castellar de Muella samples, ▲ Hoz del Gallo samples, ■ Rillo de Gallo samples, + Riba Santiuste samples, ✱ Teroleja samples.

In the field position, samples from Castellar de la Muella show mean directions which lie in the northeast quadrant (Mean D = 44.9°I = 53.4°).

Samples from the Rillo de Gallo section show a streaking of directions between the northwest and southeast quadrants. This is more clearly shown by the bedding corrected directions (Fig 7.5b). Teroleja directions lie in the northwest quadrant and have shallower inclinations than the Muschelkalk samples. The majority of initial Riba de Santiuste directions lie in the southeast quadrant.

7.4.2 Isothermal Remanent Magnetization (I.R.M.) Results

Nine samples underwent I.R.M. analysis, the results of which are shown in Fig 7.6.

Three different types of behaviour can be identified.

Type 1: Samples CM4, MA111 and MQ4 all show a rapid acquisition of remanence at very low applied field strengths. This is followed only minor remanence acquisition occurs at higher field strengths. Samples showing this type of behaviour characteristically all have very low Peak I.R.M. values (CM4 = 24mAm^{-1}, MA111 - 26mAm^{-1} and MQ4 = 9mAm^{-1}).

Type 2: Samples showing this type of behaviour are CM1, MA98, MA103 and Tw. These samples show a rapid acquisition of remanence at low fields followed by a more gentle rise at applied fields greater than 400mT. Samples CM1 and Tz do not quite reach full saturation but MA98 and MA103 do level off. Peak I.R.M. values ranged between 51mAm^{-1} (CMI) and 282mAm^{-1} (MA98).

Type 3: Two samples (MA96 and MQ9) show slower acquisition of remanence at low fields. The curves are initially concave downwards. At higher field strenghts I.R.M. intensity values also increase. Full saturation is not reached. Peak intensity values are higher than those showing Types 1 and 2 behaviour, MA96 reached 8.25mAm^{-1} and MQ9 392mAm^{-1}.

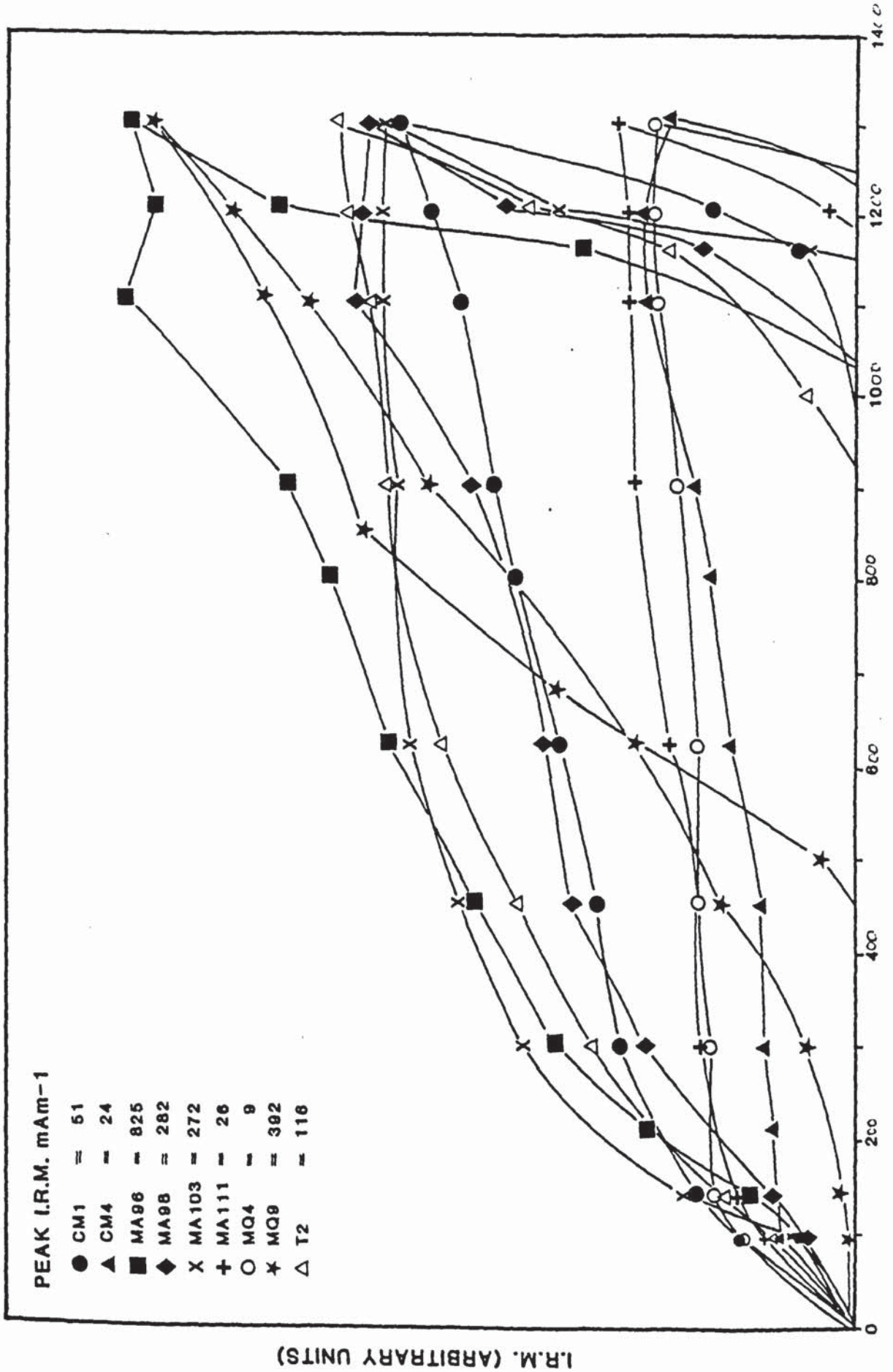

Fig. 7.6 I.R.M. acquisition and reverse field curves for Upper Triassic samples.

7.4.3 Thermal Demagnetization Results

7.4.3.1 Intensity and Susceptibility Changes

The normalized intensity and susceptibility decay curves for the Muschelkalk and Keuper specimens are shown in Figs 7.7 and 7.8.

The intensity decay curves from the different localities exhibit many similarities. Between room temperature and 100°C, the majority of specimens show a marked drop in magnetic remanence. This feature is most pronounced in specimens from Castellar de la Muella (Fig 7.7a). Between 200°C and 400°C intensities remain fairly stable and at temperatures between 400°C and 500°C many of the specimens show a sharp rise in normalized intensity. Above 580°C intensities once again drop towards zero.

The normalized susceptibility curves for specimens from the four different Muschelkalk sections also show similar trends. A small drop in initial susceptibility is recorded by the majority of specimens between room temperature and 100°C. Specimens from Castellar de la Muella and Hoz del Gallo also show a drop in susceptibility between 100°C and 400°C whilst specimens from Rillo de Gallo and Riba de Santuiste remain stable or show a slight increase in susceptibility. At temperatures above 400°C virtually all the specimens demonstrate a sharp rise in susceptibility.

The Keuper specimens from Teroleja (Fig 7.8c and d) show similar normalized intensity decay curves to those of the Muschelkalk. An initial drop in intensity between room temperature and 100°C or 200°C is followed by a period of more stability. Above 500°C the specimens show a sharp rise in intensity.

All initial susceptibility values for the Keuper specimens were negative, so increases in normalized susceptibility represent decreases in measured susceptibility values. The specimens show a drop in normalized susceptbility between room temperature and 100°C and also between 400°C and 600°C (i.e. a rise in actual susceptibility).

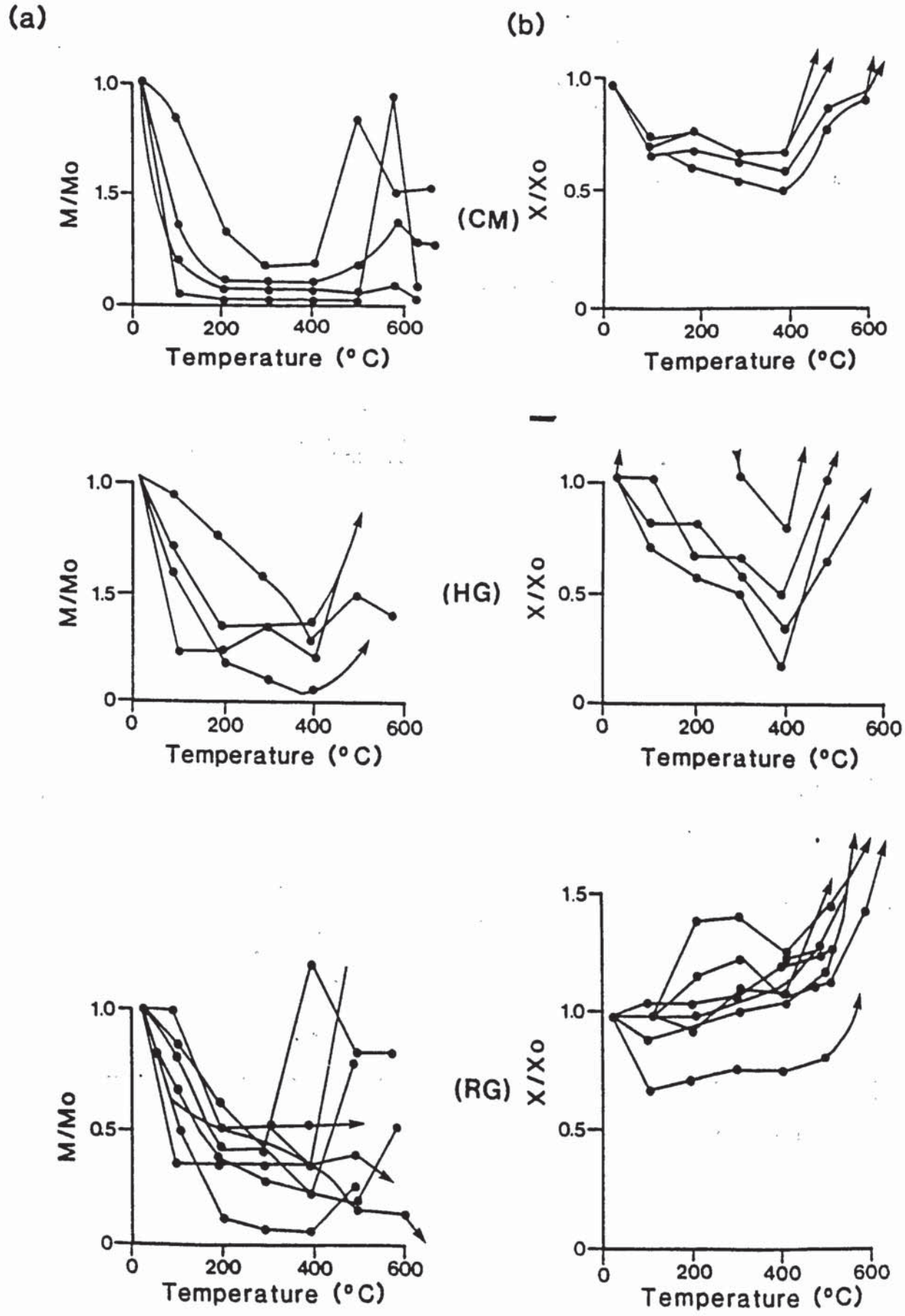

Fig. 7.7 Normalized intensity (a) and susceptibility (b) decay curves for specimens from (CM) Castellar de Muella, (HG) Hoz del Gallo and (RG) Rillo de Gallo.

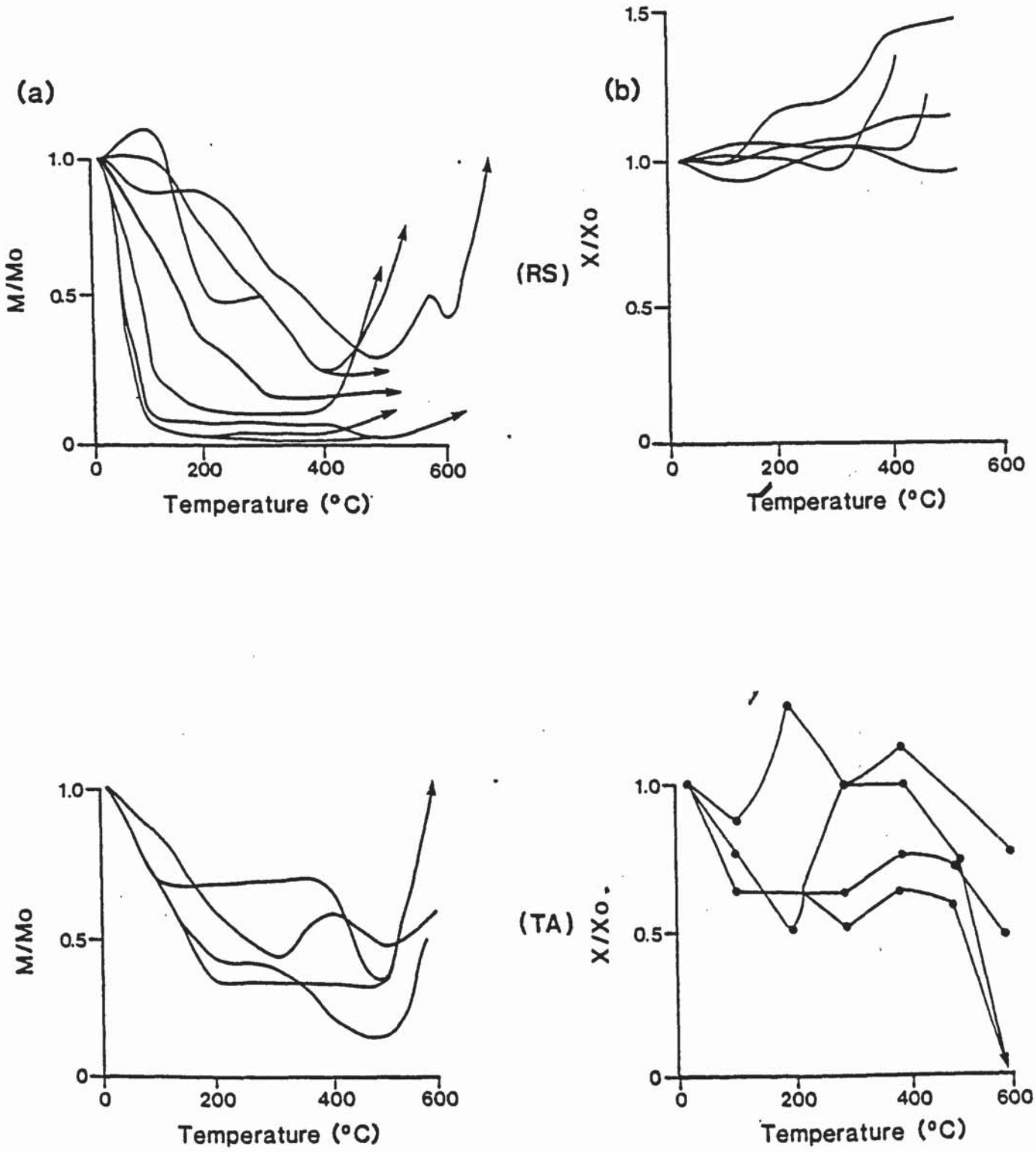

Fig. 7.8 Normalized intensity (a) and susceptibility (b) decay curves for specimens from (RS) Riba de Santiuste and (TA) Teroleja.

7.4.3.2 Discussion of Intensity and Susceptibility Results

Intensity and susceptibility values for these deposits are very low. The rapid drop in remanence intensity at low temperatures suggests that a very low blocking temperature component is present in these deposits.

The sharp rise in susceptibility at about 400°C accompanied in some specimens by a rise in intensity, almost certainly reflects the conversion of pyrite to magnetite (Turner, 1975). The drop in intensity shown by many of the specimens between 500°C and 600°C is due to the demagnetization of the magnetite.

I.R.M. results for these deposits suggest the presence of a low coercivity mineral such as magnetite. The presence of a high coercivity mineral is also seen in some of the samples eg MA96 and MQ9. Many of the intensity decay curves show that a small amount of remanence is retained at temperatures in excess of 600°C. Thus it is likely, that small amounts of haematite are also present in some of these specimens.

7.4.3.3 Directional Changes

Figure 7.9 (CM 5.2.2) shows a typical example of palaeomagnetic behaviour demonstrated by Muschelkalk specimens from Castellar de la Muella. The initial direction is steep and positive and lies in the northern part of the stereogram. During thermal demagnetization, this direction first moves slightly south and then moves towards shallower inclination in the northwest quadrant (Fig 7.9a). The normalized decay intensity curve shows a rapid drop upon heating to 100°C (less than 5% of the original remanence remains). The specimen is totally demagnetized by 400°C.

A typical example of a Muschelkalk dolostone from the Hoz de Galoo section is shown in Fig 7.10 (MA101 2.2). The N.R.M. direction remains close to the local geomagnetic field direction until above 400°C when it moves towards a shallower inclination in the northwest quadrant. Most of the samples behave consistently in this manner enabling the estimation of

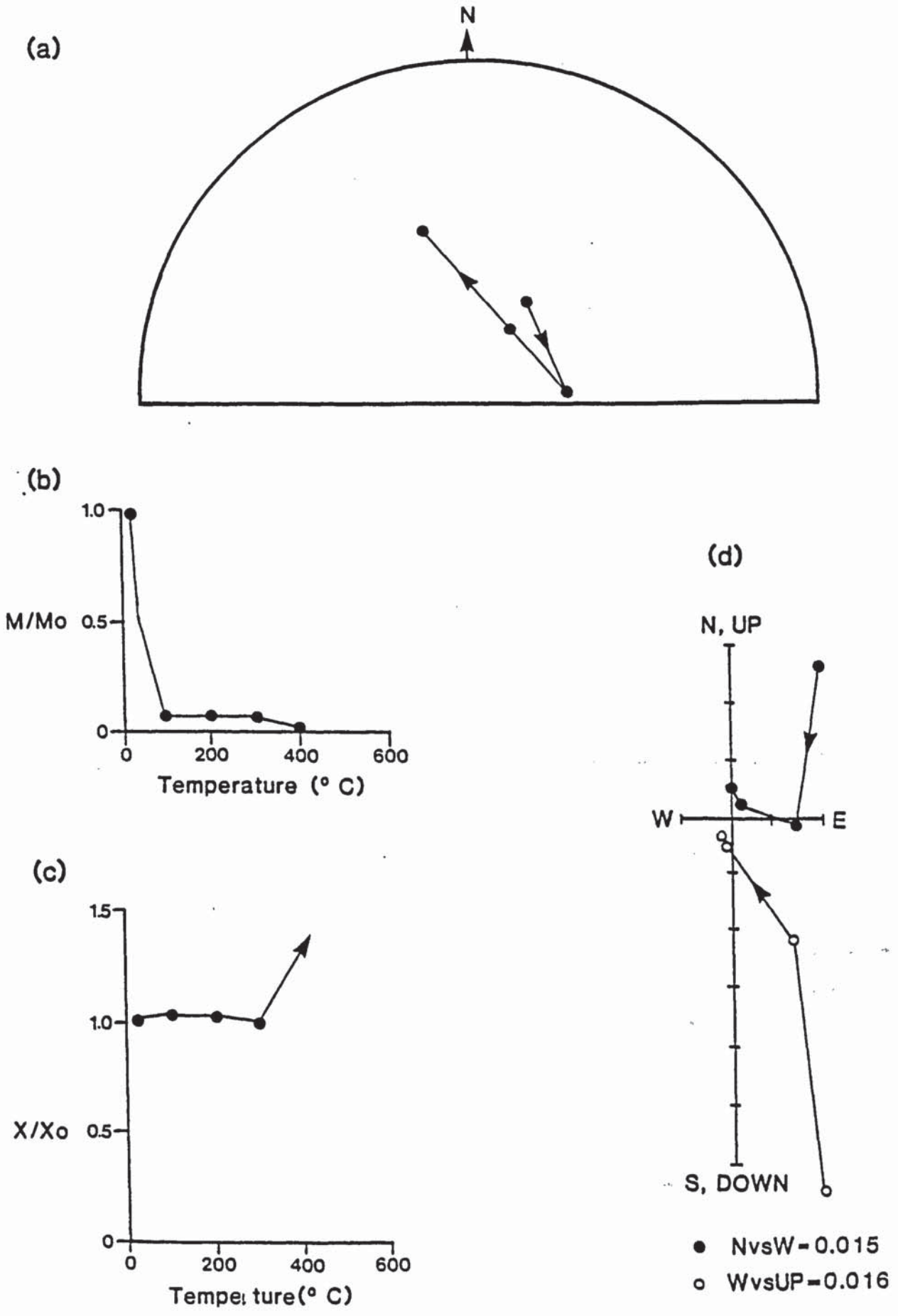

Fig. 7.9 Palaeomagnetic behaviour demonstrated by specimen CM 5.2.2 during partial thermal demagnetization, (a) Stereographic projection, (b) Normalized intensity decay curve, (c) Normalized susceptibility decay curve, (d) Orthogonal vector plot.

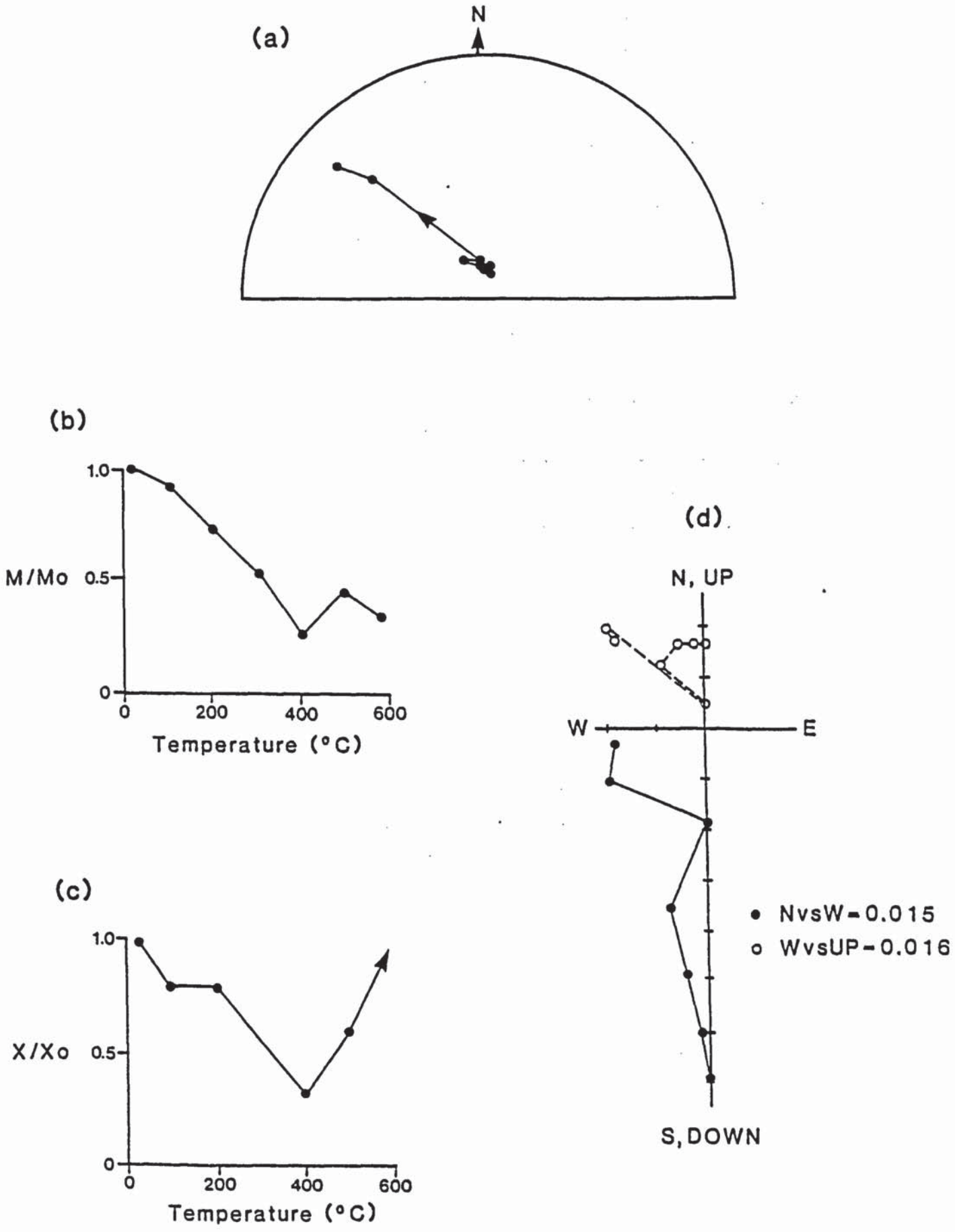

Fig. 7.10 Palaeomagnetic behaviour demonstrated by specimen MA101.2.2 during partial thermal demagnetization, (a) Stereographic projection, (b) Normalized intensity decay curve, (c) Normalized susceptibility decay curve, (d) Orthogonal vector plot.

characteristic components. These components are usually isolated between 500 and 580°C. Above 580°C the specimens are too weak for measurement with the cryogenic magnetometer (intensity 0.01mAm^{-1}).

Figure 7.11 shows an example of the palaeomagnetic behaviour demonstrated by specimens from Riba de Santiuste (MQ8.1.1). This shows an initial direction which lies in the southeast quadrant and is very steep (Fig 7.11a). During thermal demagnitization the direction remains virtually unchanged. A steady loss of remanence is observed up to 300°C (Fig 7.11b). Between 300°C and 500°C the remanence has a fairly constant intensity which is about 10% of its original value.

The Keuper deposits of Teroleja show quite complicated palaeomagnetic behaviour during thermal demagnetization. Fig 7.12 shows typical behaviour demonstrated by one of these specimens (TA4.2.2). The N.R.M. direction is steep and normal and lies in the northwest quadrant. Above 100°C the direction moves first towards the northeast and then towards the west before moving southwards to a shallow negative position with a declination of D=183°. The normalized intensity curve (Fig 7.12b) shows an initial drop in intensity between 20°C and 100°C. No further loss in intensity is recorded between 100°C and 400°C. Between 400°C and 500°C the intensity again drops but above 500°C it rises sharply.

The normalized susceptibility curve (Fig 7.12c) shows an initial drop in susceptibility between room temperature and 100°C. No significant changes in susceptibility are recorded between 100°C and 500°C, but between 500°C and 600°C, however, another drop in susceptibility is seen.

7.4.3.4 Thermal Demagnetization Summary

The results of stepwise partial thermal demagnetization of the Muschelkalk and Keuper are shown in Table 7.3. Fig 7.13 shows the most stable directions isolated during the demagnetization for these Upper Triassic specimens.

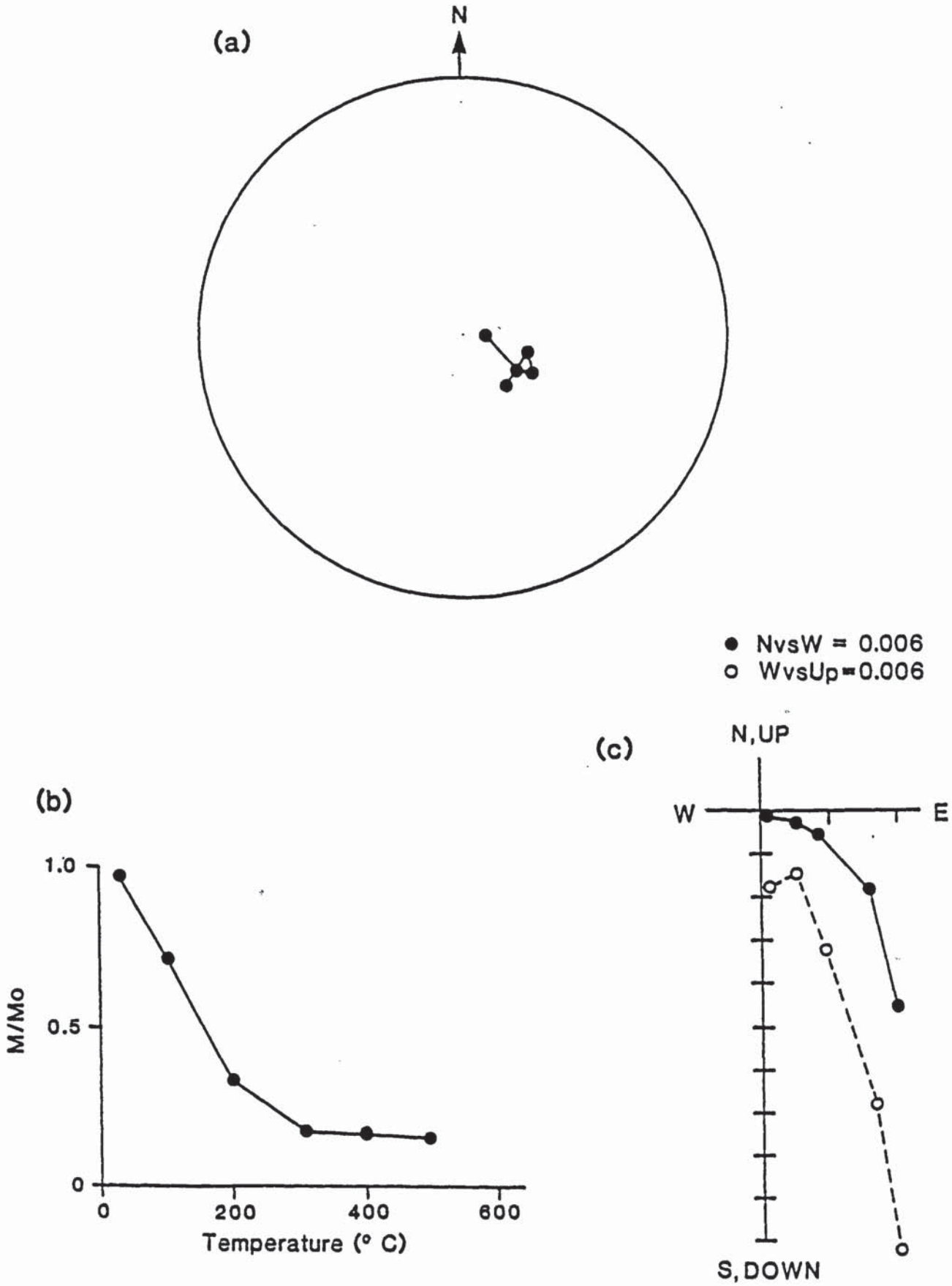

Fig. 7.11 Palaeomagnetic behaviour demonstrated by specimen MQ8.1.1 during partial thermal demagnetization, (a) Stereographic projection, (b) Normalized intensity decay curve, (c) Normalized susceptibility decay curve.

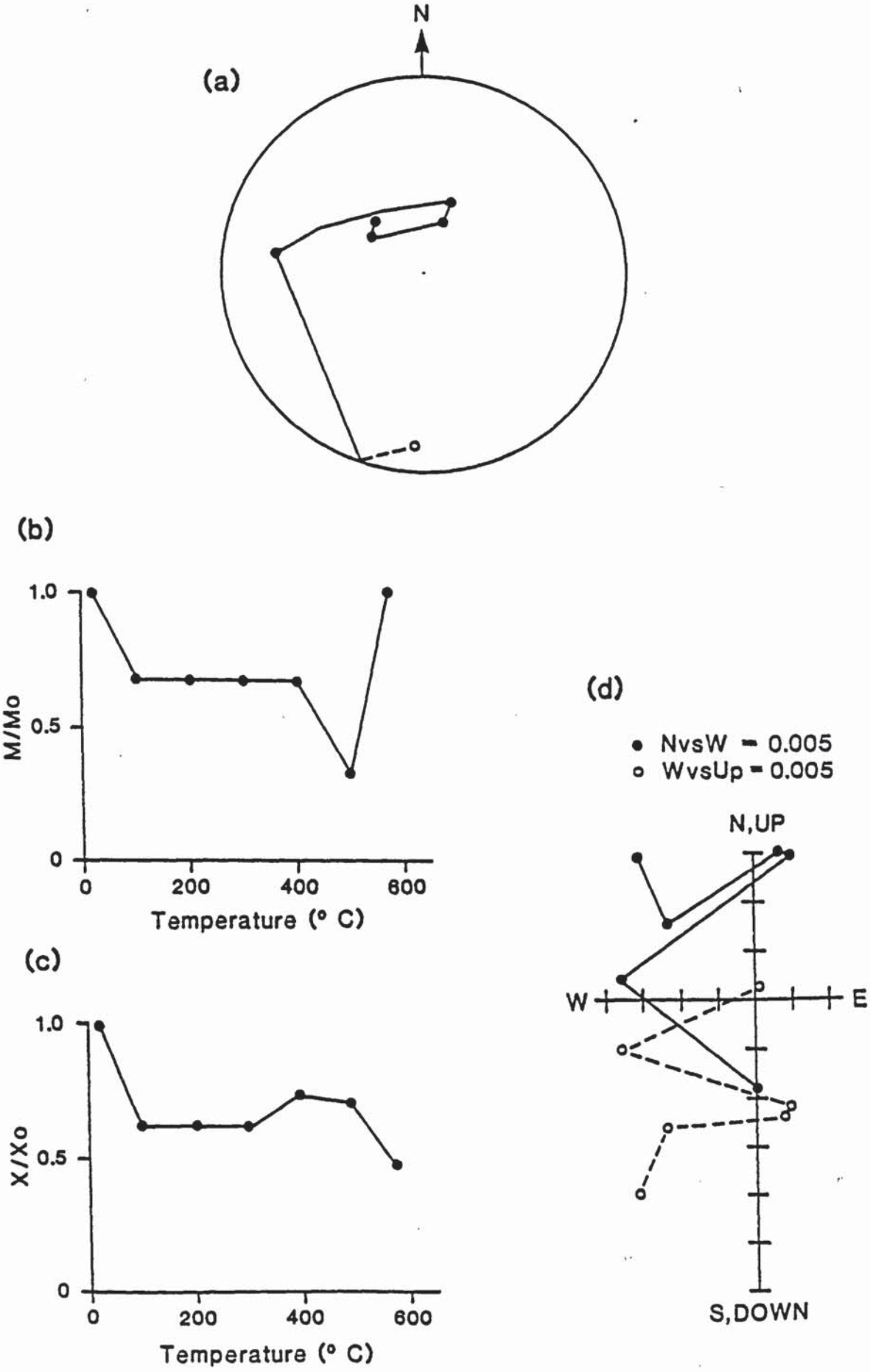

Fig. 7.12 Palaeomagnetic behaviour demonstrated by specimen T4.2.2 during partial thermal demagnetization, (a) Stereographic projection, (b) Normalized intensity decay curve, (c) Normalized susceptibility decay curve, (d) Orthogonal vector plot.

TABLE 7.3 STEPWISE THERMAL DEMAGNETIZATION RESULTS FOR THE MUSCHALKALK AND KEUPER

		Most stable directions				Pole					Range	Directions passing 10° linearity test				
		F		P									F		P	
Specimen	S.I.	Dec(°)	Inc(°)	Dec(°)	Inc(°)	Long(°)	Lat(°)	N	R	α95(°)	(°C)	Range(°C)	Dec(°)	Inc(°)	Dec(°)	Inc(°)
CM1.5.2	0.4	2.7	-24.3	7.9	4.3	165.7	50.7	8	4.69	51.5	20-630	580-660	322.6	4.4	319.4	4.3
												100-500	141.7	-5.1	138.3	-4.4
CM3.5.1	5.7	354.2	61.4	385.2	61.1	296.3	35.9	3	2.99	3.8	200-400	300-500	298.8	38.3	281.4	20.5
CM4.2.1	1.0	54.1	42.5	77.8	67.2	50.3	37.1	3	2.95	20.0	20-200	300-500	263.7	-10.2	271.9	-26.8
CM5.2.2	0.7	48.2	51.4	61.8	69.5	49.7	47.5	3	2.90	28.7	20-200	300-500	297.7	-15.2	303.1	-15.7
												100-300	97.2	44.5	117.8	49.5
MA96.1.1	0.6	255.7	82.8	221.5	71.8	336.0	13.6	5	4.22	37.4	20-400	None				
MA97.5.1	1.6	349.4	53.7	335.4	63.7	290.4	71.6	5	4.90	12.2	20-400	400-580	331.0	52.0	315.0	58.0
												300-500	343.0	51.0	329.0	60.0
MA98.4.3	1.7	222.9	-53.4	232.0	-65.3	240.1	-52.8	3	2.98	12.8	200-400	200-500	52.6	26.0	57.0	37.0
MA99.2.1	0.3	297.7	79.0	245.9	73.7	327.8	24.1	8	2.84	88.2	100-660	300-500	220.0	79.5	222.0	-32.0
												100-300	305.0	81.0	241.0	76.0
MA100.1.1	2.9	321.0	68.1	286.4	70.7	311.0	42.2	4	3.98	6.8	100-400	100-300	330.0	59.0	308.0	65.0
MA101.2.2	4.4	2.3	62.3	346.8	73.8	339.1	69.3	3	2.99	4.6	20-200	500-630	318.0	12.3	315.0	17.0
												100-300	33.0	62.0	41.0	75.0
MA102.1.1	4.3	4.9	62.4	350.9	74.3	345.3	69.5	3	2.99	4.7	20-200	500-630	318.0	-2.0	318.0	4.0
												400-580	143.0	11.0	145.0	5.0
												20-200	16.0	66.0	9.0	79.0
MA103.2.1	1.1	10.6	58.8	2.7	71.3	3.9	74.9	3	2.96	18.1	20-200	100-300	0.4	57.0	348.0	69.0
MA104.2.2	0.7	273.4	68.4	249.4	61.4	312.7	14.3	3	2.89	29.9	20-200	300-500	86.0	14.0	89.0	20.0
												100-300	271.0	67.0	249.0	60.0
MA105.3.1	7.2	337.7	49.2	323.9	57.2	273.7	62.1	3	2.99	2.8	20-200	20-400	339.0	50.0	325.0	59.0
MA106.1.2	2.1	330.3	44.5	318.0	51.3	266.9	55.4	3	2.98	10.4	100-300	200-400	134.0	-26.0	128.0	-30.0
MA107.1.1	3.5	6.9	42.1	2.3	54.4	160.4	83.8	4	3.99	5.6	100-400	500-630	348.0	20.0	345.0	30.0
MA108.2.1	7.3	342.5	58.9	322.6	67.3	300.4	62.5	4	3.99	2.7	200-500	20-500	332.0	65.0	303.0	70.0
MA109.4.1	0.6	345.7	49.5	333.0	59.0	273.9	69.6	3	2.85	34.9	100-300	200-400	86.0	70.0	125.0	72.0
MA110.2.1	2.7	294.4	25.5	288.3	25.1	266.4	22.3	3	2.99	7.9	100-300	100-300	302.0	28.0	295.0	30.0
MA111.2.2	3.9	326.2	25.6	320.0	32.2	245.8	48.5	4	3.99	5.1	100-400	300-500	316.0	20.0	311.0	24.0
MQ1.3.1	0.3	344.5	43.1	102.5	62.1	46.2	19.5	3	2.99	6.8	100-300	200-400	1.0	64.1	119.1	41.2
MQ2.1.1	0.4	256.7	-28.4	267.5	9.5	272.5	1.3	4	3.09	60.2	100-400	100-300	287.1	-2.5	264.1	48.3
												20-200	345.2	-25.0	356.9	32.2
MQ3.1.1	0.9	359.7	36.5	88.6	56.7	58.2	24.5	3	2.93	24.3	20-200	300-500	176.3	10.9	191.1	-45.0
												20-400	27.6	43.1	93.1	34.5
MQ4.1.2	2.6	312.0	42.6	159.8	69.0	9.5	5.3	4	3.98	7.2	20-300	None				
MQ6.1.2	0.5	29.0	25.8	68.9	58.8	89.2	25.8	3	2.77	45.2	20-200	None				
MQ8.1.1	4.1	339.6	49.4	116.6	59.8	40.8	10.0	3	2.99	5.3	100-300	100-300	334.5	49.8	122.7	61.2
												20-200	312.1	57.0	149.5	55.4
MQ9.3.1	1.0	6.9	52.8	110.0	50.8	51.1	7.2	3	2.94	21.6	100-300	20-300	289.3	50.3	175.1	53.2
T1.3.1	0.4	114.2	38.9	95.2	42.3	66.0	12.0	3	2.52	70.1	200-400	200-400	226.6	-43.1	217.4	-25.6
												20-200	297.3	10.8	299.4	14.8
T2.3.1	1.0	350.4	67.6	333.1	41.9	239.7	62.1	4	3.87	19.8	20-300	400-580	218.7	-13.6	213.3	-8.5
												100-300	264.9	44.4	278.7	24.5
T3.2.2	0.9	19.6	75.0	356.4	41.0	188.9	72.4	4	3.84	20.0	20-300	200-400	64.5	20.9	54.3	10.5
												100-300	282.3	49.2	304.9	26.5
T4.2.2	0.6	16.9	76.1	341.8	44.0	228.8	68.7	4	3.59	36.6	20-300	200-400	66.9	10.8	55.6	14.5
												100-300	240.7	8.0	244.7	4.3

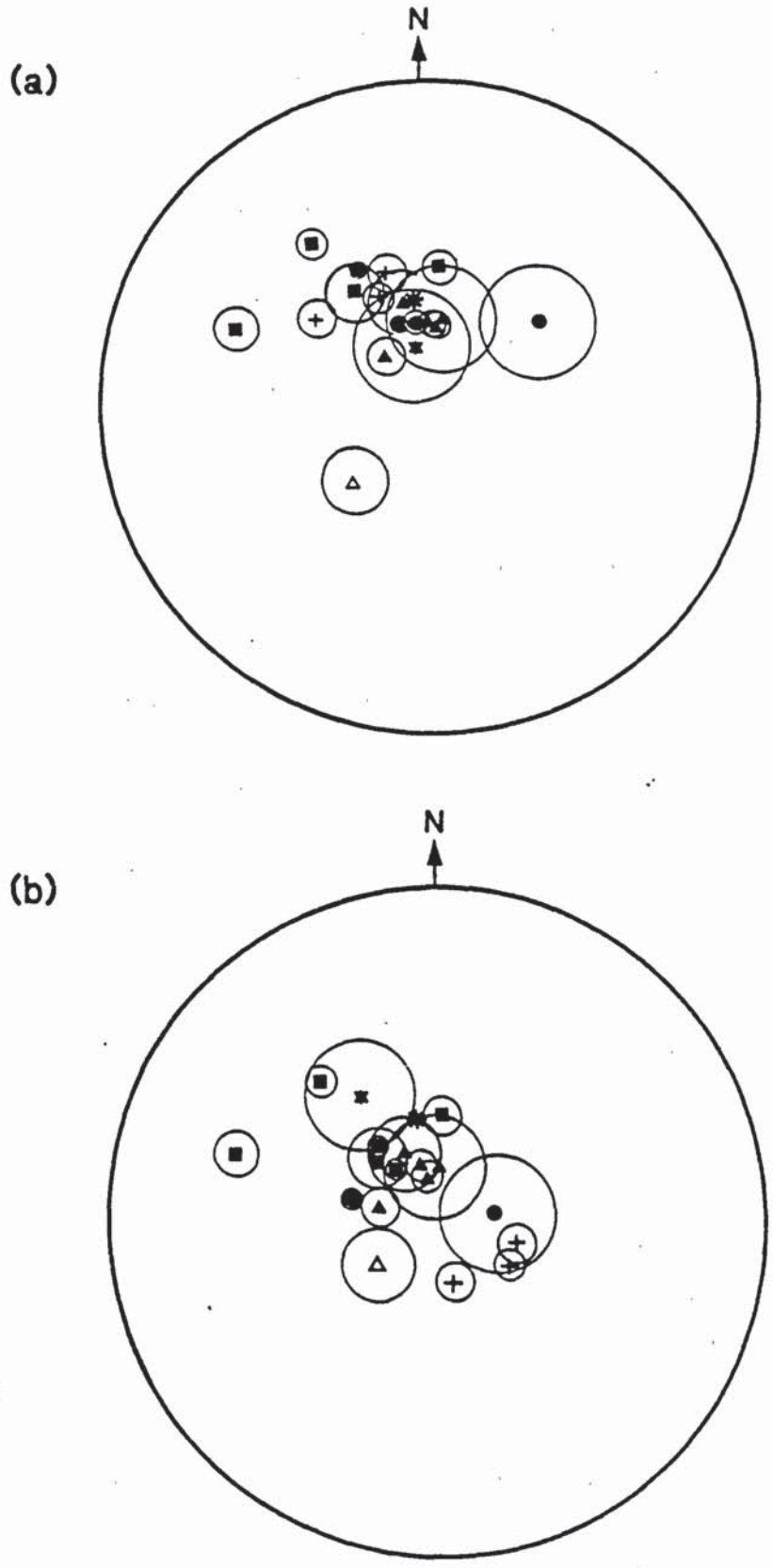

Fig. 7.13 Most stable directions isolated during partial thermal demagnetization for Upper Triassic specimens (a) before and (b) after correction for bedding. Circles represent α_{95} values. Asterisk represents present-day local geomagnetic field position. For key to symbols see Fig. 7.5.

The strong grouping of directions close to the present-day local geomagnetic field direction suggests that these sediment have been remagnetized. Most of these directions were isolated over low temperature ranges.

Fig 7.14 shows directions passing the 10° linearity test. These show much more scatter than the most stable directions. Bedding corrected directions, however do show a streaking effect between shallow directions in the northwest quadrant and shallow directions in the southeast quadrant. Two further groups of directions (in the northeast and southwest quadrants) can also be identified.

Many of these shallow directions have been isolated over a high temperature range which suggests that they may be carried by more coarsely crystalline detrital haematite grains.

7.4.3.5 Bulk Demagnetization Results

The results of bulk demagnetization of the Muschelkalk and Keuper facies are summarized in Table 7.4. Bedding corrected directions (Fig 7.15) show a streaking of directions from the fairly steep directions in the northwest quadrant to shallow directions in the southeast quadrant.

Mean intensity values are very low ranging from $0.01mAm^{-1}$ (CM5, MA106) up to $0.38mAm^{-1}$ (CM3). All the samples were demagnetized at a temperature of 300°C, with the exception of MA97 and MA98, which were bulk demagnetised at 500°C.

Mean susceptibility values ranged from $1.18mAm^{-1}nT^{-1}$ up to $54.57mAm^{-1}nT^{-1}$ for the Muschelkalk samples. Negative susceptibility $-9.09mAm^{-1}nT^{-1}$ and $-8.53mAm^{-1}nT^{-1}$ were recorded for Keuper samples TA2 and TA3 respectively.

7.4.4 Discussion of Palaeomagnetic Results

The N.R.M. intensities for the Muschelkalk and Keuper samples are very low, the mean N.M.R intensity for these sediments being only $0.01mAm^{-1}$.

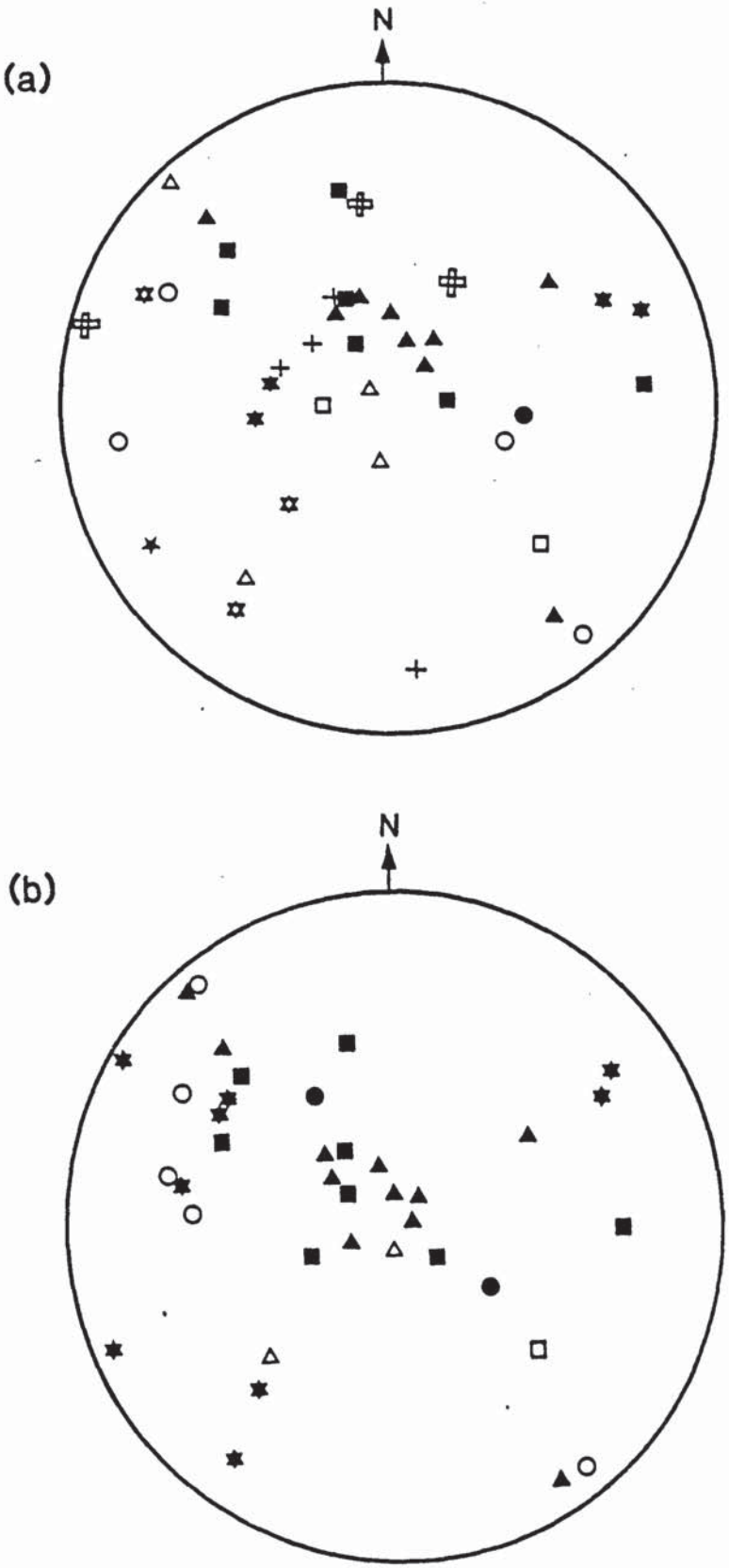

Fig. 7.14 Directions passing 10° linearity test isolated during partial thermal demagnetization for Upper Triassic specimens (a) before and (b) after correction for bedding. For key to symbols see Fig. 7.5.

TABLE 7.4 BULK DEMAGNETIZATION RESULTS FOR THE MUSCHELKALK AND KEUPER

Sample	Height (m)	F Dec(°)	F Inc(°)	P Dec(°)	P Inc(°)	Pole Long(°)	Pole Lat(°)	N	R	α95(°)	α95(°) Pole	Intensity (mAm^{-1})	Susceptibility ($mAm^{-1}nT^{-1}$)	Temp (°C)
CM3	142	128.1	-9.8	124.5	-1.6	54.2	-0.5	4	3.92	15.2	13.8	0.38	48.30	300
CM5	112	321.2	14.7	314.9	20.4	232.2	10.3	4	3.68	31.5	30.6	0.01	25.66	300
MA97	579	326.2	9.7	323.7	16.6	233.1	44.5	5	4.95	9.0	5.8	0.09	-	500
MA98	587	49.2	32.6	54.1	44.0	89.3	43.5	5	4.97	7.0	6.6	0.08	3.40	500
MA100	595	273.2	1.7	273.3	-2.7	264.9	1.6	4	3.99	4.6	3.8	0.04	1.18	300
MA101	601	92.3	48.9	107.7	51.8	52.3	10.2	2	1.97	-	-	0.02	5.29	300
MA102	605	335.5	49.5	321.2	57.1	274.9	60.1	1	-	-	-	0.02	2.05	300
MA103	611	312.4	19.2	307.6	23.0	251.9	36.3	3	2.89	29.9	19.0	0.06	7.96	300
MA105	566	85.6	12.7	88.9	18.4	81.7	7.1	4	3.81	23.8	24.4	0.02	29.18	300
MA106	569	126.5	7.3	127.7	4.1	59.7	-26.0	4	3.97	9.1	5.9	0.01	32.36	300
MA107	570	145.6	9.5	146.7	2.3	42.3	-38.2	5	4.86	14.8	12.0	0.03	28.76	300
MA108	571	327.0	35.6	317.9	42.0	256.7	52.1	4	3.90	17.3	12.8	0.13	33.41	300
MA109	573	119.5	14.7	122.7	12.9	60.2	-19.3	3	2.93	24.0	16.4	0.03	38.33	300
MA110	577	102.6	3.3	103.6	5.5	77.0	-8.4	2	1.99	-	-	0.03	54.57	300
MA111	580	348.0	29.6	342.5	39.9	221.4	67.7	2	1.95	-	-	0.03	36.54	300
TA2	104	341.5	78.6	323.8	51.5	264.3	59.2	6	5.61	19.3	24.8	0.05	-9.09	300
TA3	111	308.1	59.3	324.0	27.6	239.0	49.1	6	5.53	20.3	21.5	0.03	-8.53	300
TA4	117	243.9	22.3	254.9	14.2	284.4	7.1	4	3.78	26.11	27.9	0.05	-	300

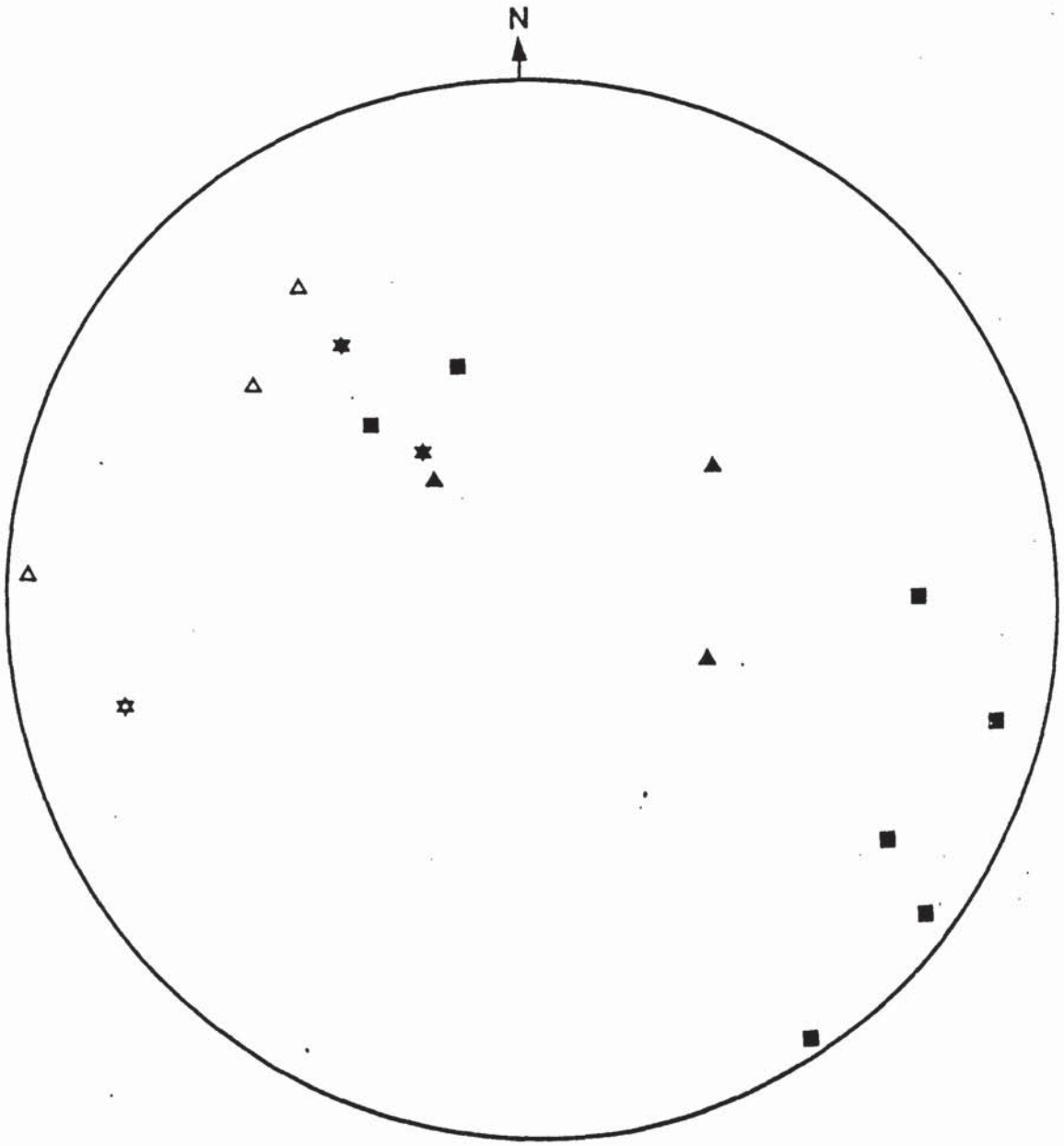

Fig. 7.15 Mean bedding corrected directions isolated during bulk thermal demagnetization of the Upper Triassic. For key to symbols see Fig. 7.5.

Initial N.R.M. directions show a strong grouping close to the present-day local geomagnetic field direction. This suggests that the rocks have been remagnetized in recent times. Intensity and susceptibility decay curves show that there is a significant blocking temperature at about 100°C.

I.R.M. results indicate the presence of a low coercivity mineral in these deposits (probably magnetite or goethite) together with a high coercitivy mineral (haematite). These results suggest that the low blocking component may be carried by goethite, which has a blocking temperature of 110°C.

The sharp rise in susceptibility at 400° shown by many of the specimens, reflects the conversion of pyrite the magnetite. This is supported by an accompanying rise in remanence intensity and followed by a sharp drop at about 580°C (the Neel temperature for magnetite is 575°C).

Directional changes during partial thermal demagnetization are complex. Secondary components similar to those of the Buntsandstein are present (ie steep, normal components in the northwest quadrant) but there is evidence that primary components of both normal and reversed polarity are also present.

Table 7.5 and Fig 7.16 show previously published Triassic pole positions for stable Europe (A-C) and Iberia (1-4) together with Poles calculated from the current study. These show that the majority of samples have Poles (calculated from most stable directions) which do not represent primary components of remanence but instead reflect secondary components acquired during remagnetization of the sediments.

7.5 RELATIONSHIP BETWEEN DIAGENESIS AND PALAEOMAGNETISM

The very small amount of magnetic minerals in the Muschelkalk and Keuper deposits is reflected in the very low N.R.M. intensities shown by the samples.

TABLE 7.5 PREVIOUSLY PUBLISHED UPPER TRIASSIC DIRECTIONS AND POLES FOR STABLE EUROPE AND IBERIA, TOGETHER WITH THOSE FOUND IN THIS STUDY

Letter/ No.	Locality (formation)	D(°)	I(°)	N	α_{95}(°)	Pole Position Lat	Pole Position Long	Reference
STABLE EUROPE								
A	Siberian traps, combined, USSR	-	-	-	-	60°N	133°E	Irving (1964)
B	Arran sandstone, Scotland	-	-	-	-	54°N	118°E	Irving (1964)
C	Keuper marls, England	-	-	-	12	43°N	131°E	Irving (1964)
IBERIA								
1	Rio Aragon C. Pyrenees (andesites)	152.0	-22.5	14	6	51°N	133°W	Schwarz (1962)
2	Anayet C.Pyrenees (andesites and sandstones)	164.0	-14.0	11	10	52°N	154°W	Van der Lingen (1960)
3	Serra del Cadi E.Pyrenees (redbeds)	169.5	-3.0	41	4	48.5°N	163°W	Van Dongen (1967)
4	Alcazar de San Juan, Central Spain (redbeds)	359.5	23.0	36	6	63°N	177.5°E	Van der Voo (1967)
UPPER TRIASSIC (MEANS)								
	Muschelkalk of Castellar de Muella	18.1	48.5	5	30	45.9°N	151.1°W	This Study
	Muschelkalk of Hoz del Gallo	297.7	71.3	8	23	34.7°N	139.2°E	This Study
	Muschelkalk of Rillo de Gallo	324.0	49.5	8	18	52.3°N	127.5°E	This Study
	Muschelkalk of Riba de Santiuste	130.6	52.4	7	42	13.4°N		This Study
	Keuper of Teroleja	11.6	42.3	4	15	53.8°N	135.8°N	This Study

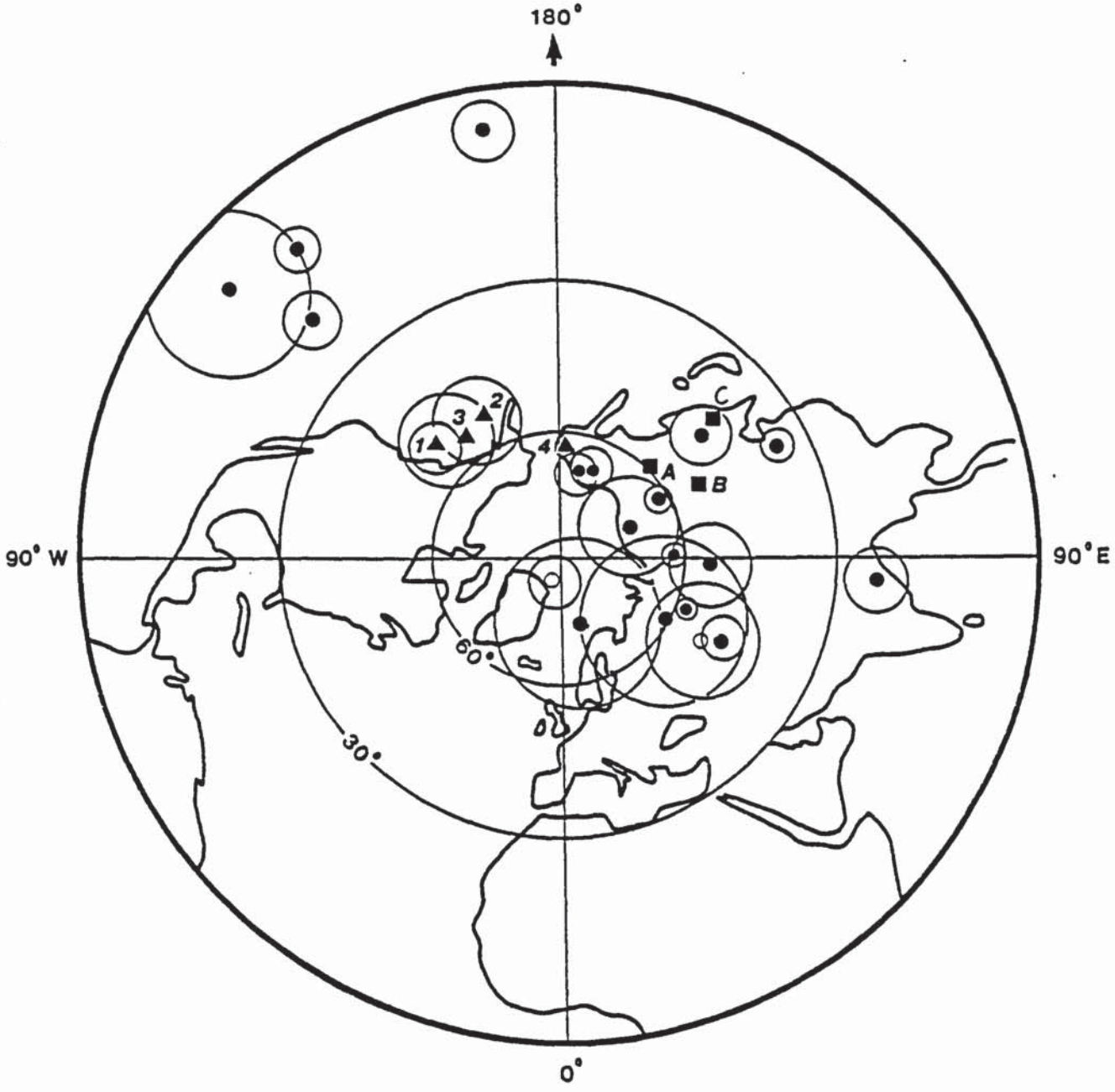

Fig. 7.16 Palaeopole directions for Upper Triassic. ■ Letters A-E represent previously described palaeopoles for Stable Europe (see Table 7.5), ▲ Numbers 1-4 represent previously described palaeopoles for Iberia (see Table 7.5).

The iron oxides which are present may be associated with the oxidation of pyrite or organic matter, which are both fairly common in the deposits. A very small amount of detrital haematite and magnetite may also contribute to the remanence. All of the above types of iron oxide would result in the acquisition of a depositional or early diagenetic remanence of Triassic age.

Weathering of the rocks after inversion, resulted in the formation of goethite and it is this mineral which almost certainly carries the recent, secondary component of magnetization.

CHAPTER EIGHT

CONCLUSIONS.

8.1 SUMMARY OF CONCLUSIONS

1. Detailed palaeomagnetic and diagenetic analysis has enabled the construction of a magnetostratigraphy for the entire Permian and Triassic lithological section of the Molina de Aragon area.

2. Palaeomagnetic results further support the theory of the rotation of Iberia, suggested by Carey, 1958.

3. Palaeomagnetic studies should always be accompanied by relevant rock magnetic and mineralogical studies in attempts to ascertain the age of the remanence.

4. Absolute dating of diagenetic events using palaeomagnetism may be attempted.

5. Further work is needed to fully assess the implications of the current research.

8.2 DETAILED CONCLUSIONS

8.2.1 Magnetostratigraphy

The construction of a magnetostratigraphy for the entire Permian and Triassic lithological section of the Molina de Aragon area has been attempted (Fig. 8.1). (Only samples from the sections of Rillo de Gallo, Hoz del Gallo and Barranco de la Hoz have been used).

Figure 8.1 shows the sampling horizons in relation to a summary of the sedimentological variation. The minimum blocking temperature of components used for polarity determination is indicated and it should be noted that this gives an immediate visual impression of the most intensely remagnetized zones (TB column in Fig. 8.1).

It should be noted that this section is based on higher blocking temperature components which have survived the pervasive Holocene remagnetization seen in these rocks.

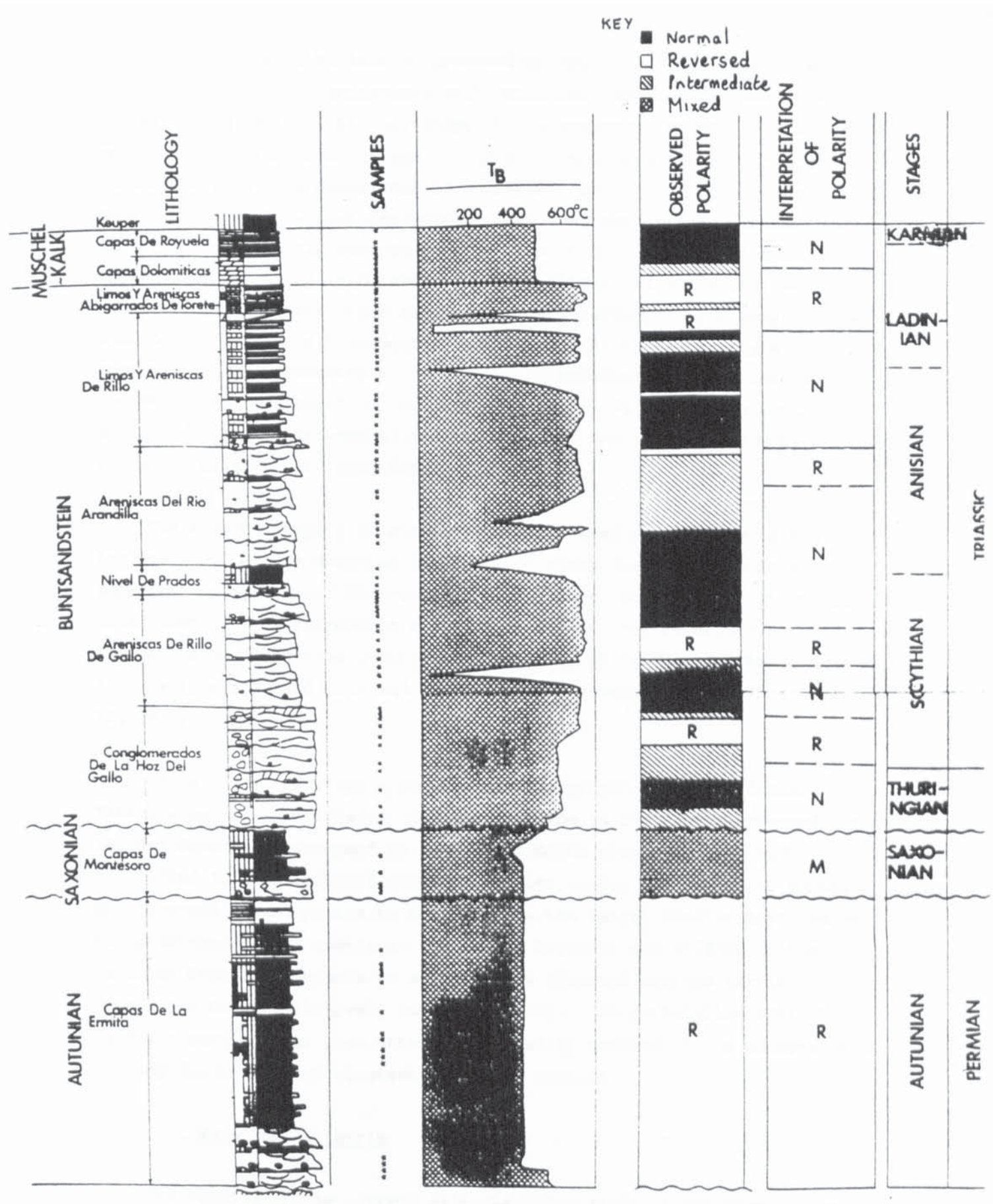

Fig. 8.1 Composite diagram showing the entire Permian and Triassic lithological section exposed in the Molina de Aragon area, the horizons from which samples were taken, the blocking temperatures at which the 'original' remanence was revealed, the observed polarity of the sample and finally an interpretation of that polarity giving a complete magnetostratigraphy for these Permo-Triassic deposits of this region.

For each sample horizon an observed polarity has been determined on the basis of isolated components or directional trends (observed polarity column in Fig. 8.1). At this stage of the analysis, no implications are made regarding the absolute age of the remanence (polarity). Four categories have been used: Normal, reversed, intermediate and mixed. Sample horizons have been designated, normal or reversed only when directions are clearly defined on the basis of declination and inclination. Intermediate polarity is determined with declinations and/or inclinations which lie in quadrants other than normal or reversed. No attempt has been made for discriminate intermediate components which may be single components and representative of genuine intermediate field direction (assuming they may exist in the data) and those which comprise resultant directions of combined normal and reversed components (which almost certainly do exist in these data).

The fourth category of mixed polarity is used exclusively in Fig. 8.1 for the rocks of the Saxonian facies. In every specimen from this unit superimposed normal and reversed components were identified. It is not clear whether this represents a series of short-lived reversals so that discrete zones cannot be identified or whether it is due to overlap between a normally magnetized zone and the underlying reversed Kiaman zone (see Fig. 8.1).

Using these criterion a member of stratigraphically significant features can be identified. Autunian section is completely reversed; it is considered to correspond to the Kiaman Epoch which has been widely identified in late Carboniferous and Permian rocks. A period of normal and reversed zones appears to characterize the latest Permian Scythian with two prominent normal events in the latest Scythian and Anisian. The Ladinian Stage corresponds to an important reversal and the Karnian appears to be of exclusively normal polarity. No correlation with other Triassic sections has been attempted primarily because of the uncertainties arising due to lack of biostratigraphical control.

8.2.2 Rotation of Iberia

The results of the current palaeomagnetic study on the Permo-Triassic rocks of Central Spain are consistent with the previously postulated theory that Iberia has undergone an anticlockwise rotation of approximately 35° about a pivot point in the western Pyrenees (see Section 1.5.3.1).

Poles calculated from Lower Permian directions and higher blocking temperature Upper Permian and Triassic components, carried predominantly by

detrital haematite, are certainly pre-Cretaceous since they are rotated relative to stable Europe (Van der Voo, 1969) and by comparison with other data from Iberia.

Poles calculated from Upper Permian and Triassic, lower temperature components (carried by haematite of diagenetic origin) are, however, consistent with poles calculated for recent deposits of Stable Europe.

8.2.3 Palaeomagnetic Studies Should Always be Accompanied by Diagenetic Studies

Not all magnetic remanence is of primary origin. In many cases the rocks carry a secondary remanence or, may even be, totally remagnetized. It is therefore essential that palaeomagnetic studies should always be accompanied by relevant rock magnetic, mineralogical and diagenetic studies in attempts to ascertain the age of the remanence. Geological criteria such as structural and burial history may provide crucial clues to remanence acquisition.

8.2.4 The Absolute Dating of Diagenetic Events Using Palaeomagnetism

The possibility of dating diagenetic events using palaeomagnetism has been suggested previously (Turner, 1979, Elmore et al., 1985, Turner 1986).

If the magnetic direction carried by a ferromagnetic authigenic mineral such as haematite can be determined, the corresponding pole position can be compared to the apparent polar wander path, hence the time of remanence acquisition and presumably that of formation of the authigenic phase may be determined. In addition, if the authigenic phase can be texturally related to other diagenetic features then the timing of those features can also be constrained.

It is not, however, a straight forward matter to date asbsolutely the secondary porosity generation seen in the Buntsandstein of Central Spain using the remanence directions. The authigenic haematite may have formed recently, perhaps in association with the present ground water zone. Alternatively the haematite may have formed at deeper burial depths and remained in the superparamagnetic state until the thermal remanence was blocked in, possibly as a result of structural uplift in recent times.

8.2.5 Future Work

A number of suggestions for areas of future work identified during the course of this research are listed below:

a) The geochemical nature and timing of the dehydration of iron hydroxides, such as goethite, to haematite and their effect on palaeomagnetism.

b) Examination of relationships between diagenesis and palaeomagnetism in a wide variety of sedimentological facies in many different regions. Is there a facies effect?

c) Improvement of the magnetostratigraphical record back into the early Mesozoic and Palaeozoic (especially in red beds where biostratigraphical control is poor).

d) Assessment of the validity of absolute dating of diagenetic events using palaeomagnetism and its practical applications in, for example, dating secondary porosity generation in a hydrocarbon reservoir.

References

Al-Khafaji, S.A. and Vincenz, S.A. (1971). Magnetization of the Cambrian Lamotte Formation in Missouri, Geophys. J., 24, 175-205.

Arribas, J. and Soriano, J. (1984). La Porosidad en las areniscas Triasicas (Rama Aragonesa de la Cordillera Iberica). Estud. Geol., 40, 341-353.

As, J.A. (1960). Instruments and measuring methods in palaeomagnetic research. Med. Verh., Kon. Ned, Meteorol. Instit. No. 78, 56pp.

Baag, C.G. and Helsley, C.E. (1974). Evidence for penecontemporaneous magnetization of the Moenkopi Formation. J. Geophys. Res., 79, 3308-3320.

Banda, E. Pares, J.M., Freeman, R. (In press). La tecnica del paleomagnetismo estudio piloto en los bordes de la cuenca Balear.

Berner, R.A. (1984) Sedimentary pyrite formation; an update. Geochim. Cosmochim. Acta., 33, 267-273.

Boles, J.R. and Coombs, D.S. (1975). Mineral reactions in zeolitic Triassic tuff, Hokonui Hills, New Zealand. Geol. Soc. A. Bull., 86(2) 163-173.

Bullard, E., Everett, J. and Gilbert Smith, A. (1965). A synmposium on continental drift. Phil. Trans. Roy. Soc. London. Ser. A, 258, 41-51.

Burek, P.J. (1968). Korrelation reversmagnetyisiertar Gestein folgen als stratigraphisches Hilfsmittelanfgezeigt am Beispiel liner palaeomagnetischen Studie im Buntsandstein SW-Deutchlands, XXIII Int. Geol. Congr., 5, 23-36.

Burley, S.D. and Kantorowicz, J.D. (1986). Thin section and S.E.M. criteria for the recognition of cement-dissolution porosity in sandstones. Sedimentology, 33, 587-604.

Burley, S.D., Kantorowicz, J.D. and Waugh, B. (1985). Clastic diagenesis in: Sedimentology: Recent developments and applied aspects (eds. Brenchley, P.J. and Williams, B.P.J.). Geol. Soc. Spec. Pub., 18, pp.189-226.

Burst, J.F., (1969). Diagenesis of Gulf Coast clayey sediments and its possible relation to petroleum migration. Am. Ass. Pet. Geol. Bull., 53, 73-93.

Calderon, S. (1898). Existencia del terreno Carbonifero en Molina de Aragon. Act. R. Soc. Esp. Hist. Nat., 26, 147-150.

Carey, S.W., (1958). A tectonic approach to continental drift. Symp. Continental Drift, Hobart, pp. 177-355.

Chilingar, G.V. and Bissell, H.J. (1963). Is dolomite formation favoured by high or low pH? Sedimentology, 2, 171-172.

Chilingar, G.V., Zenger, D.H., Bissell, H.J. and Wolf, K.H. (1979). Dolomite and dolomitization (written communication with Langmuir, D, 1973) in: Diagenesis in sediments and sedimentary rocks. (eds. Larsen, G. and Chillingar, G.V.), Elselvier, Amsterdam, pp. 513-515.

Clegg, J.A., Almond, A. and Stubbs, P.H.S. (1954a). Remanent magnetism of some sedimentary rocks in Great Britain. Phil. Mag., 45, 583-598.

Clegg, J.A., Almond, A. and Stubbs, P.H.S. (1956b). Some recent studies of the pre-history of the earth's magnetic field. J. Geomagn. Geoelect., 4, 194-199.

Clegg, J.A., Deutsch, E.R., Everitt, C.W.F. and Stubbs, P.H.S. (1977). Some recent palaeomagnetic measurements made at Imperial College, London. Phil. Mag. Suppl. Advan. Phys., 6(22), 219-231.

Clegg, J.A., Deutsch, E.R. and Griffiths, D.H. (1956). Rock magnetism in India. Phil. Mag., Ser. 8, 1, 419-231.

Clegg, J.A., Radakrishnamurty, C. and Sahasrabudhe, P.W. (1958). Remanent magnetism of the Rajmahal traps of northeastern India. Nature, 181, 830-831.

Collinson, D.W. (1967). Chemical demagnetization in methods of palaeomagnetism. In (eds. Creer, K.M. and Runcorn, S.K.),Developments in Solid Earth Geophysics,Volume 3,Elsevier, Amsterdam, pp.306-310.

Collinson, D.W. (1968). Ferrous and ferric iron in red sediments and their magnetic properties. Geophys. J.R. astr. Soc., 16, 531-542.

Collinson, D.W. (1983). Methods in Palaeomagnetism and Rock Magnetism, Chapman and Hall, London, 500pp.

Collinson, D.W. and Molyneux, L. (1967). An instrument for the measurement of isotropic initial susceptibility of rock samples. In : Methods in Paleomagnetism (eds. Collinson, D.W., Creer, K.M. and Runcorn, S.K.), Elsevier, Amsterdam, pp368-371.

Creer, K.M. (1957). Palaeomagnetic investigations in Great Britain -IV. The natural remanence magnetization for certain stable rocks from Great Britain. Phil. Trans. Roy. Soc. Lond. Ser. A 250, 111-129.

Curtis, C.D. (1978). Possible links between sandstone diagenesis and depth related geochemical reactions occurring in enclosing mudstones. J. Geol. Soc. London, 135, 107-117.

Curtis, C.D. and Spears, D.A. (1971). Diagenetic development of kaolinite. Clays Clay Miner., 19, 219-227.

Curtis, C.D. (1983). Link between aluminium mobility and destructions of secondary porosity. Am. Ass. of Pet. Geol., 67, 3, 380-393.

Dott, R.L., Jr. (1964). Wacke, graywacke and matrix - What approach to immature sandstone classification? J. Sed. Pet., 34, 625-632.

Du Toit, A.L. (1937). Our Wandering Continents. Oliver and Boyd, Edinburgh, 366pp.

Elmore, R.D., Dunn, W. and Peck. (1985). Absolute dating of dedolomitisation by means of palaeomagnetic techniques. Geology, 13, 558-561.

Elston, D.P. and Purucker, M.E. (1979). Detrital magnetization in red beds of the Moenkopi Formation (Triassic), Gray Mountain, Arizona. J. Geophys. Res., 84, 1653-1665.

Fisher, R.A. (1953). Dispersion on a sphere. Proc. R. Soc., A217, 295-305.

Folk, R.L. (1968). Petrology of Sedimentary Rocks. Hemphills Bookstore, Austin, Texas. 91pp.

Freeman, T. (1972). Sedimentology and dolomitization of Muschelkalk Carbonates (Triassic), Iberian Range, Spain. Am. Ass. Petrol. Geol. Bull., 56, 434-453.

Garcia-Palacios, M. and Lucas, J. (1977). Le bassin Triassique de la branch Castellane de la chaine Iberique. II. Geochime Cuad. Geol. Iberica, 4, 355-368.

Garrels, R.M. and Christ, C.L. (1965). Solutions, Minerals and Equilibria. Harper and Row, New York, 450pp.

Girder, R.W. (1968). A plaaeomagnetic investigation of some late Triassic and early Jurassic volcanic rocks from the Northern Pyrenees. Ann. Geophy., 24, 695-708.

Glennie, K.W. (1970). Desert sedimentary environments. Elsevier, Amsterdam 222pp.

Glennie, K.W., Mudd, G.C. and Nagtegaal, P.J.C. (1978). Depositional environment and diagenesis of Permian Rotliegendes sandstones in Leman Bank and Sole Pit areas of the U.K. Southern North Sea. J. Geol. Soc. London, 135, 25-34.

Goree, W.S. and Fuller, M. (1976). Magnetometers using R.F. - driven squids and their application in rock magnetism and paleomagnetism. Revs. Geophys. Spec Phys, 14, 591-608.

Griffin, G.M. (1971). Interpretation of X-ray diffraction data in: Procedures in sedimentary petrology (ed. Carver, R.E.), Wiley-Interscience pp. 541-569.

Hay, R.L. (1966). Zeolites and zeolite reactions in sedimentary rocks. Geol. Soc. A., spec. pap., 85-130.

Helsley, C.E. (1969). Magnetic reversal stratigraphy of the Lower Triassic Moenkopi Formation of western Colorado. Geol. Soc. Amer. Bull., 80, 2431-2450.

Helsley, C.E. and Steiner, M. (1974). Paleomagnetism of the lower Triassic Moenkopi Formation. Geol. Soc. Amer. Bull., 85, 457-464.

Hernando, S. and Hernando, J. (1976). Los minerales pesados como criterio de diferenciacion entre Permico y Triasico. Est. Geol., 32, 265-273.

Hernando, S. Schott, J.J., Thuizat R. and Montigny, R. (1980). Age des Andesites et des sediments interstratifies de la region d'Atienza (Espagne); Etude Stratigraphique, geochronologiqu et paleomatnetique. Sci. Geol. Bull., 33, 2, 119-128.

Hinkelbein, K. (1965). Der Muschelkalk der zentralen Hesperischen Ketten (Prov. Tervel, Spanien). Mit ein Beitrag von O.Geyer. Oberrhein. Geol. Abh., 14, 55-95.

Hinkelbein, K. (1969). El Triasico y el Jurasico de los alrededores de Albarracin. Teruel, 41, 35-75.

Hoblitt, R.P., Larson, E.E. and Walker, T.R. (1974). Chemical remagnetization of Miocene red beds in southern New Mexico (abstract), Eos Trans. AGU., 55, 1110.

Iijima, A. (1970). Present day zeolitic diagenesis of the Neogene geosynclinal deposits in the Niigata oilfield, Japan. Amer. Chem. Sco. 2nd Int. Zeolite Conf. 540-546.

Iijima, A. (1975). Effect of pore water to clinoptilolite-analcime-albite reaction series. J. Fac. Sci. Uni. Tokyo, 19, 133-147.

Irving, E. (1957). The origin of the palaeomagnetism of the Torridonian Sandstones of northwest Scotland. Phil. Trans. Roy. Soc. Lond., Ser. A, 250, 110.

Irving, E. (1964). Palaeomagnetism and its application to geological and geophysical problems. Wiley, New York, 399pp.

Irving, E., Stott, P.M. and Ward, M.A. (1961). Demagnetization of igneous rocks by alternating magnetic fields. Phil. Mag., 6, 225-241.

Jacquot, E. (1866). Sur la composition et sur l'age des assises qui, dans la Peninsule Iberique separent la formation Carbonifere des depots Jurassiques. Bull. Soc. Geol. France., 24, 132-147.

Johnson, A.H. (1976). Paleomagnetism of the Jurassic Navajo Sandstone from southwestern Utah, Geophys. J., 44, 161-175.

Kantorowicz, J.D. (1984). The origin, nature and distribution of authigenic clay minerals from Middle Jurassic Ravenscar and Brent Group Sandstones. Clay Miner., 19, 359-375.

Kessler, L.G. (1978). Diagenetic sequence in ancient sandstones deposited under desert climatic conditions. J. Geol. Soc. London, 135, 41-49.

Khramov, A.N. (1967). The Earth's magnetic field in the late Palaeozoic. I z v. Earth Phys., 86-108.

Kirschvink, J.L. (1980). The least-squares line and plane and the analysis of palaeomagnetic data. J.R. astr. Soc., 62, 699-718.

Krynine, P.D. (1949). The origin of red beds. Trans. N.Y. Acad. Sci.(2) 11, 60-68.

Larsen, G. and Chilingar, G.V. (1979). Diagenesis in Sediments and Sedimentary Rocks (Developments in Sedimentology, 25A) Elsevier, Amsterdam. 579pp.

Larsen, G. and Chilingar, G.V. (1967). Diagenesis in Sediments (Developments in Sedimentology, 8). Elsevier, Amsterdam, 453pp.

Larson, E.E. and Walker, T.R. (1975). Development of C.R.M. during early stages of red bed formation in late Cenozoic sediments, Baja, California, Geol. Soc. Am. Bull., 86, 639-650.

Marfil, R. and Buendia, E. (1980). La evolution diagenetica de los sedimentos detriticos del Permico y Triasico del sondeo de Siguenza (Guadalajara). Rev. Inst. de Investigaciones Geologicas. Univ. de Barcelona, 34, 59-74.

Marfil, R. and Pena, J.A. de la (1980). Diagenetic aspects of Permian sandstones in Central Spain : Implication for graywacke genesis. Internat. Assoc. Sedimentologists 1st Europ. MTG. Bochum. Abstr., 158-160.

Marfil, R., Alonso, J.J. and Garcia, M.C. (1971). Estudio del material cementante de Trias inferior de la Cordillera Iberica. Estudios Geologicos Vol. XXVII, Instituto Lucas Mallada, CSIC, pp.427-439.

Marfil, R., Arribas, J., Arribas, M.E. and Pena, J.A. de la (1984). Sedimentacion lacustre (carbonato-salina) en las facies Autuniense de la Cordillera Iberica. Publicaciones de Geol., 20, Univ. Autonoma de Barcelona, 73-83.

Marfil, R., Cruz, B. de la and Pena, J.A. de la. (1977). Processos diageneticos en las areniscas de Buntsandstein de la Cordillera Iberica. Cuad. Geol. Iberica, 4, 411-422.

Marfil, R., Pena, J.A. de la and Soriano, J. (1980). Aplicion de la microscopia electronica de barrido al estudio de los procesos diageneticos de rocas volcanoclasticas. Rev. Inst. de Investigaciones Geologicas. Univ. de Barcelona, 34, 75-88.

McElhinny, M.W. (1973). Palaeomagnetism and Plate Tectonics, Cambridge University Press, 358pp.

McGlynn, J.C., Hanson, G.N., Irving, E. and Park, J.K. (1974). Paleomagnetism and age of Nonacho Group Sandstones and associated Sparrow Dikes, District of Mackenzie, Can. J. Earth Sci., 11, 30-42.

Molyneux, L. (1971). A complete result magnetometer for measuring the remanent magnetization of rocks. Geophys. J.R. astr. Soc., 24, 429-433.

Munoz, M., Ancochea, E., Sagredo, J., Pena, J.A., Hernan, F., Brandle, J.L. and Marfil, R. (1984). Vulcanismo Carbonifero de la Cordillera Iberica. C.R. X Int. Carboniferous Congress. 3, 27-52.

Nijenhuis, G.H.W. (1961). A palaeomagnetic study of the Permian volcanics in the Nahe region (SW Germany). Geol. Mijnbouw, 40, 26-30.

Park, J.K. (1970). Acid leaching of red beds and the relative stability of the red and black components. Can. J. Earth. Sci., 7, 1086-1092.

Pena, J.A. de la (1972). Estudio Petrogenetico del Muschelkalk de la Cordillera Iberica. Estud. Geol., 31, 513-530.

Pena, J.A. de la and Yebenes, A. (1977). Procesos diageneticos en las rocas carbonaticas del Muschelkalk de la Cordillera Iberica. Cuad. Geol. Iber., 4, 437-446.

Perex-Arlucea, M. (1985). Estratigrafia y sedimentologia del Permico y Triasico en el sector Molina de Aragon-Albarracin (Provincias de Guadalajara y Tervel). Ph.D thesis (unpubl.), Universidad Complutense, Madrid, 322pp.

Perry, S.P.G. (1979). Palaeomagnetic studies of British carbonate sediments. Ph.D. thesis (unpubl.), Univeristy of Newcastle-upon-Tyne, 391pp.

Pettijohn, F.J. (1957). Sedimentary Rocks. Harper and Row, New York, N.Y., 2nd ed., 718pp.

Pettijohn, F.J., Potter, P.E. and Siever, R. (1973). Sand and Sandstone. Springer Verlag, Berling, 618pp.

Ramos, A. (1979). Estratigrafia y Paleogeografia del Permico y Triasico al Oeste de Molina de Aragon (Prov. de Guadalajara). Ph.D thesis (unpub.) Universidad Complutense, Madrid. Seminarios de Estratigrafia. Serie monografias, 6, 313 pp.

Ramos, A. and Doubinger, J. (1979). Decoverte d'une microflore Thuringienne dans le Buntsandstein de la Cordilliere Iberique (Espagne) C.R. Acad. Sc. Paris, 289, 525-528.

Ramos, A., Sopena, A. and Perez-Arlucea, M. (1986). Evolution of Buntsandstein fluvial sedimentation in Northwest Iberian Ranges (Central Spain). J. Sed. Pet., 56, 862-875.

Reeve, S.C., Leyhaeuser, D. Helsley, C.E. and Bay, K.W. (1974). Palaeomagnetic results from the Upper Triassic of East Greenland. J. Geophys. Res., 79, 3302-3307.

Riba, A. (1959). Estudio Geologico de la Sierra de Albarracin. Ph.D. Thesis (unpubl.). Instituto Lucas Mallada, CSIC, Monografia, b, 283pp.

Riba, O. (1983). Sierra de Albarracin. XVII Curso de Geologia Practica. Teruel, 58-80.

Roche, A., Saucier, H. and Lacaze, J. (1962). Etude paleomagnetique des roches volcaniques Permiennes de la regiona. Nideck-Donon. Bull. Serv. Carte Geol. Alsace-Lorraine, 15(2), 59-68.

Roy, J.L. and Park, J.K. (1972). Red beds DRM or CRM?, Earth Plant. Sci. Lett., 17, 211.

Runcorn, S.K. (1956a). Palaeomagnetic survey in Arizona and Utah : Preliminary results. Bull. Geol. Soc. Amer., 67, 301-316.

Sacher, L. (1966). Stratigraphie und tecktonik der Norwestlichen Hesperischen Kitten bei Molina de Aragon (Spanien). Teil. 1. Stratigraphie (Palaeozoikum). N.J. Geol. und Palaont., 124(2), 151-167.

Schmidt, V. and MacDonald, D.A. (1979). The role of secondary porosity in the course of sandstone diagenesis. In : Aspects of Diagenesis (eds. Scholle, P.A. and Schuger) SEPM Spec. Publ., 26, 175-207

Schwarz, E.J. (1962). Geology and palaemagnetism of the valley of the Rio Aragon Subordan north and east of Oza (Spanish Pyrenees, Heusca province). Estud. Geolog., Invest. Geol. "Lucas Mallada" Madrid, 18, 193-240.

Sentchordi, E. and Marfil, R. (1983). Estudio petrologio de las facies Saxon Saxoniense y Buntsandstein de la zona de El Pobo de Duenas. (Cordillera Iberica) Boletin Geologico y Minero, 94-5, 448-471.

Shaw, H.F. (1972). The preparation of oriented clay mineral specimens for X-ray diffraction analysis by a suction-onto-ceramic-tile method. Clay Miner., 20, 349-350.

Shoemaker, E.M. and Purucker, M. (1974). Gray Mountain magnetozone in the Moenkopi Formation of Arizona and Utah, Eos Trans. AGU, 55, 1107-1109, 1974.

Shoemaker, E.M., Elston, D.P. and Helsley, C.F. (1973). Depositional history of the Moenkopi Formation in light of its magnetostratigraphy. (abst.) Geol. Soc. Am. Abstr. Progr. 5, 807-808.

Sopena, A. (1979). Estratigrafia del Permico y Triasico del Guadalagara. Ph.D. thesis (unpubl.), Universidad Complutense, Madrid. Seminarios de Estratigrafia. Serie monografias, 5, 329pp.

Sopena, A., Virgili, C., Hernando, S., and Ramos, A. (1977). Permico Continental en Espana. Cuad. Geol. Iberica. 4. 11-34.

Steiner, M.B. and Helsley, C.E. (1972). Jurassic polar movement relative to North America, J. Geophys. Res., 77, 4981-4993.

Steiner, M.B. and Helsley, C.E. (1974a). Magnetic polarity sequence of the Upper Triassic, Kayenta Formation, Geology. 2, 191-194.

Steiner, M.B. and Helsley, C.S. (1974b). Reproducible Anomalous Upper Triassic Magnetization. Geology, 2, 195-198.

Surdam, R.C. and Sheppard, R.A. (1978). Zeolite in saline, alkaline-lake deposits. In (eds. Sand, L.B. and Mumpton, F.A.) Natural Zeolites - Occurrences, Properties. Pergamon Press, New York N.Y., pp145-174.

Tarling, D.H. (1983). Palaeomagnetism (Principles and Applications in Geology, Geophysics and Archaeology). Chapman and Hall, London, 379pp.

Tarling, D.H. and Symons, D.T.A. (1967). Research Note: A stability of remanence in palaeomagnetism. Geophys. J.R. Astr. Soc., 12, 443-448.

Tricalinos, J. (1928). Untersuchungen uber den Ban dr Keltiberishen Ketten des nordostlichen Spaniens. Zeitoder. Dutsch. Geol. Gessel., 80, 409-482.

Turner, A.R. (1986). Dating diagenetic events using palaeomagnetism. 12th International Sedimentological Congress Abstracts, p.308.

Turner, P. (1975). Depositional magnetisation of Carboniferous Limestone from the Craven basin of northern England. Sedimentology, 22, 563-581.

Turner, P. (1979). The paleomagnetic evolution of continental red beds, Geol. Mag., 116, 289-301.

Turner, P. (1980). Continental red beds (Developments in Sedimentology, 29). Elsevier, Amsterdam, 562pp.

Turner, P. and Archer, R. (1975). Magnetization history of the lower Old Red Sandstones from the Gamrie Outlier, Scotland, Earth Planet. Sci. Lett., 27, 240-250.

Turner, P. and Ixer, R.A. (1977). Diagenetic development of unstable and stable magnetizations in the St. Bees Sandstone (Triassic) of North England. Earth Planet. Sci. Lett., 34, 113-124.

Turner, P., Ramos, A. and Sopena, A. (1984). Datos paleomagneticos del Permico y Triasico de la Cordillera Iberica. I Congreso Espanol de Geologia III, 289-301.

Turner, P., Turner, A.R., Ramos, A. and Sopena, A. (in press). Diagenetic processes and remagnetization in red beds. J. Geol. Soc. London.

Vandenberg, J. (1979). Palaeomagnetic data from the Western Mediterranean : A review. Geol. Mijnb., 58, 161-174.

Vandenberg, J. (1980). New palaeomagnetic data from the Iberian Peninsula. Geol. Mijnb., 59, 49-60.

Van den Ende, C. (1970). Secular variation in Permian red beds from the Dome de Barrot (France) in : Palaeogoephysics (ed. Runcorn, S.K.). Academic, New York, pp101-116.

Van der Lingen, G.J. (1960). Geology of the Spanish Pyrenees, north of Canfranc, Huesca province. Estud. Geol., 16, 205-242.

Van der Voo, R. (1967). The rotation of Spain : paleomagnetic evidence from the Spanish meseta. Palaeogeog. Palaeoclim. Palaeocol., 3, 393-416.

Van der Voo, R. (1968). Geology and paleomagnetism of lower Triassic sediments in an anticlinal structure east of Atienza (Guadalajara prov., Spain). Geol. Mijnbouw, 47(3), 186-190.

Van der Voo, R. (1969). Palaeomagnetic evidence for the rotation of Iberian peninsula. Tectonophysics, 78(1) 5-56

Van Dongen, P.G. (1967). The rotation of Spain : Palaeomagnetic evidence from the eastern Pyrenees. Palaeogeog., Palaeoclim., Palaeoecol., 3, 417-432.

Van Houten, F.B. (1961). Climatic significance of red beds, in : Descriptive Palaeoclimatology (ed. Nairn, A.E.M.). Interscience, New York, N.Y. pp.89-139.

Van Houten, F.B. (1964). Origin of red beds - some unsolved problems in : Problems in Palaeoclimatology (ed. Nairn, A.E.M.). John Wiley, New York, pp.647-661.

Van Houten, F.B. (1973). Origin of red beds : A review 1961-1972. Ann. Rev. Earth. Planet. Soc., 1, 39-61.

Virgili, C. (1954). Algunas consideraciones sobre el trazado de las costas espanolas durante el Triasico. R. Soc. Esp. Hist. Nat. Tomo Homenaje al Prof. E. Hernandez-Pacheco, 697-716.

Virgili, R. (1958). El Triasico de los Catalanides. Bol. Inst. Geol. Min. de Espana, 69, 1-856.

Virgili, C., Sopena, A., Ramos, A., Hernando, S. and Arche, A. (1980). El Permico en Espana. Revista Espanda de Micropaleontologia, 12, 255-262.

Walker, T.R. (1967). Formation of red beds in modern and ancient deserts. Geol. Soc. Am. Bull., 78, 353-368.

Walker, T.R., (1976). Diagenetic origin of continental red beds. In : The Continental Permian in Central, West and South Europe. (ed. Falke, H.). D. Reidel, Dordrecht, Holland, pp.240-282.

Walker, T.R. and Honea, R.M. (1969). Iron content of modern deposits in the Sonoran Desert : A contribution to the origin of red beds. Geol. Soc. Am. Bull., 80, 535-544.

Walker, T.R., Larsen, E.E. and Hoblett, R.P. (1981). Nature and origin of hematite in the Moenkopi Formation (Triassic), Colorado Plateau : A contribution to the origin of magnetism in Red Beds. J. Geophys. Res., 86, 317-333.

Walker, T.R., Waugh, B. and Crone, A.J. (1978). Diagenesis in first cycle desert alluvium of Cenozoic age, southwestern United States and northwestern Mexico. Bull. Geol. Soc. Am., 89, 19-32.

Waugh, B. (1978). Authigenic K-feldspar in British Permo-Triassic sandstones. J. Geol. Soc. London. 135, 51-56.

Westcott-Lewis, M.F. and Parry, L.G. (1971). Thermoremanence in synthetic rhombohedral iron-titanium oxides. Aust. J. Phys., 24, 735-752.

Zijderveld, J.D.A. (1967). The NRM of the Exeter volcanic traps (Permian, Europe). Tectonophysics, 4(2) : 121-153